Thèse n° 8620

District heating and cooling systems to integrate renewable energy in urban areas

Présentée le 28 octobre 2021

Faculté des sciences et techniques de l'ingénieur
Groupe SCI STI FM
Programme doctoral en énergie

pour l'obtention du grade de Docteur ès Sciences

par

Francesca BELFIORE

Acceptée sur proposition du jury

Dr J. Van Herle, président du jury
Prof. F. Maréchal, Prof. J. Page, directeurs de thèse
Prof. N. Nord, rapporteuse
Prof. N. Shah, rapporteur
Prof. D. Khovalyg, rapporteuse

École
polytechnique
fédérale
de Lausanne

2021

Alla mia piccolina,
che ha reso la scrittura di questa tesi
un periodo emozionante ed indimenticabile.
Non vedo l'ora di conoscerti...

Acknowledgements

At the end of this exciting journey, I would like to express my gratitude to all the people who, in different ways, contributed to this result, supporting me until this point.

First of all I would like to thank my supervisors, Prof. François Maréchal and Prof. Jessen Page, for giving me the opportunity of carrying out this work and showing to me the two sides of the complicated world of research: one more academical and visionary, the other more applied and pragmatic. Even though my constant search for an equilibrium among the two was very demanding, now I feel grateful for getting to know both the aspects. I would also like to extend my gratitude to all the members of my jury, Prof. Dolaana Khovalyg, Prof. Natasa Nord, Prof. Nilay Shah and the president Dr. Jan Van Herle, for accepting this difficult and onerous work and taking the time of revising my thesis. I had pictured the moment of my oral exam over and over in my mind before that day, but none of the potential outcomes resembled the engaging and relaxed discussion we had. I would also like to thank the members of the energy management team of the airport that represented the case study of my work, for providing data, support and information essential to carry out my studies. Many thanks also to the problem-solvers, who assisted me during my journey. On the administrative side to Sylvie and Véronique, for always finding a solution to all the very last minute requests. On the IT side, to Cyrille and Michel, for putting in place the first IPESE IT-support team and never laughing at my requests even when the answer was "just look in your trash bin".

Even if the PhD is a very personal battle, having people fighting their own next to you is always a great help. I could have never won mine, without the support of all the members of this large and evolving family at IPESE. Thanks to the "*old generation of PhDs*", Dylan, Sophia, Elfie, Mazi, Victor, Nils, Stefano, Sébastien, Raman, for always representing an example of those who made it. Thanks to Jean-Loup for his kindness and patience in answering all my Osmose-related questions. Thanks to Alberto, the first IPESE member I met, for first encouraging me to apply and then always trusting the quality of my work. Thanks to Hür, for his humble attitude in explaining to me over and over the same MILP constraints and his support up to the HES office. Thanks to Raluca, a sweet personality behind a warrior mask, whose determination and hard working attitude makes her the role model of a PhD candidate. Thanks to Alessio, for the great playlists during our trips to Italy, which usually revealed some summer-hits I had never heard about. Your presence in the lab made me feel less a "pesce fuor d'acqua", probably because of our common origins or our similar starting time in the lab. Little matters the reason, it was nice to share this long journey with you. Many thanks to the "*new generation of PhDs*", as well. To Julia, always joyful and full of energy, a valuable scientist and a strong

woman, much more than what she is aware of. To Rafael, for always bringing a comforting smile and for your constant fight to sugar. I think you know by now that I am a lost cause, but I really appreciate your trying. To Xiang for showing that learning French is possible and to Dorsan and Jonas for recently deciding of starting this experience, full of motivation, despite the challenging times. I would like to thank Ivan, for being the rock of our lab, from both the scientific and the social perspectives. Thank you for helping me in the revision of this manuscript, for never judging the poor English skills of not-native people, for always joining all the social events, for warmly welcoming newcomers and for being a constant source of precious advice. Thanks to Luc, the "*evergreen of IPESE*". The speed of your thoughts is often difficult to follow and requires training. After a first learning period, I could appreciate your widespread view, your ability to connect topics in fractions of a second and especially your kindness and humble attitude. Thanks to TiVi, the non plus ultra of a researcher, for all the nice discussions over a glass of wine. The care and the passion that you devote to coaching your students make them really lucky for having you! Thanks to Francesco, for making my starting phase in the lab easier and much more fun. Thanks for sharing with me the duty of completing the Osmose tutorial, for all your support inside and outside the lab and for opening my eyes towards the topic of gender equality. If today I am a stronger and emancipated woman is also thanks to you. Thanks to Luise, for the constant support and advice, which helped me to go through the most difficult moments. Thanks for introducing me to the 1/3-2/3-3/3 counting, that became a constant in my daily life. Thanks for all the precious moments shared in these past years: the exhausting and rewarding running sessions, the summer schools, the visit to Rome in probably the hottest day of the century, the million aperos and Pizza-Taxi, the trip to Munich, the pasta making sessions, the lake-side walks and of course the endless chatting.
Thanks to the HES family, who warmly welcomed me despite my first reluctance to the change. Thanks to Pablo, the coding expert, always available to help anyone regardless his own work load. Thanks to Fred, for sharing with me the challenging experience of having a real case study and being an example of success in applied research. Thanks to Tristan, the symbol of multitasking, working on thousand projects and still finding the energy to climb the highest mountains in his free time.
Many thanks to the members of our twin lab, GEM. To Guillaume, the most peaceful person I have ever met, for being a reminder that feeling upset is never helping in finding a solution and to Katie, always cheerful and smiling, for helping me during the revision of this thesis and all the nice spontaneous aperos on the lake side. Thanks to Giorgio and Cecilia, for being an example of elegance, the kind of elegance that always reminds me of my country. Thanks to Priscilla, for showing up at my desk on my very first day in the lab and supporting me all the way since then. I feel lucky for having met a friend like you during this journey. Thanks for always being an example of a strong, determined and successful woman at the work place and a sweet, generous and caring person outside. Thanks also to Manuel, for teaching me the Italian grammar rules I had never learnt and for always bringing a spicy touch with his humor.
I would also like to express my gratitude to my "amiche di sempre", Alessandra and Chiara, the friends who, no matter what, have always been there. Those that the geographic distance kept physically away, but never affected our relationship. Thanks for keeping calling me "Inge",

even if I am the problems-maker of the group, always over-thinking about all the potential outcomes and creating problems before they even exist. Thanks to Chiara, the problems-intensifier, whose "ci penso io" is never going to work, but often turns out in a "chiarata", a pearl enlightening the greyest days. Thanks to Alessandra, the pragmatic problems-solver, real engineer of the group, for being at my side since our very first day at the kindergarten. And thanks to the other members of this extended family, Giusta, Nazzareno, Federico, Francesca, Cesare, for all the moments shared together, all the dinners in the garden, simple events of inestimable value. I am extremely glad of being part of this family.

Thanks to "Les Demoiselles d'Avignon": I have never seen a group of friends as diverse and yet united as ours. During the high school, our different personalities fused together creating this unbreakable bond, which nothing and nobody could now dissolve. Thanks to Klizia, whose Italian soul, influenced by the German culture, is the symbol of a restless attitude, supported by a perfect mix of organizational skills and attention to details. Thanks to Michela for being an example of determination, the living proof that "wanting" means "achieving" and for always reminding us of living in the moment and enjoy the present. Thanks to Paoletta, for her commitment to sustainability causes. If we all did 1% of what you do everyday, we would live in a better world. Thanks to Ludovica, for always bringing sensitivity and profoundness to the group, mitigated by a fine sense of humor and a contagious smile. Also thanks for always taking the duty of choosing the wine!

I would also like to take the opportunity to thank my recently acquired family, Richard, Susanne, Sabine, Christian and Tiffany, for having warmly welcomed me since the very first days. Thanks for making me feel at home here in Switzerland, for your constant support and the valuable example of multicultural environment you represent.

Many thanks to my parents, for always encouraging me and my brother to study, even if that meant for us to leave our warm nest. Thanks for always supporting me in all my decisions, for helping me all the time I had to change an apartment, for simply giving me all the tools to build up my own future. Thanks to my brother, Guido, for encouraging me to apply for the PhD. Even if my experience turned out to be a bit more challenging than how you firstly described a PhD to me, I am grateful that I have always had you as a role model. Thanks to Angeliki for your pragmatic and modest attitude, which always helps me in focusing on what really counts the most and forgetting about useless worries. And thanks to you both for my sweet nephew Lukas, in the worst moments of my PhD, looking at his warm smile always calmed me down and helped me deal with all problems.

Finally I would like to express all my gratitude to Paul, who from one of the many colleagues became my life companion. Without you at my side, amore mio, I would have never achieved this result. You have been silently the post-doc that I never had in the lab, offering to me all the technical help at any time of the day and of the night. Most importantly, thanks for always believing in me, for balancing out my constant-worrying attitude, for boosting my self-esteem, for coping with all my emotional crises, for simply being always there.

Francesca Belfiore

Vevey, August 26, 2021

Abstract

The building sector plays a crucial role in the ongoing energy transition due to its significant share of global energy consumption and carbon dioxide emissions, especially when combined with the estimation that 70% of the world's population will be living in urban areas by 2050. District heating and cooling (DHC) systems have been widely recognized among the viable options as an effective solution for achieving the challenging mid-century targets. In the context of decarbonizing and electrifying the thermal energy requirements in urban areas, this thesis provides a methodology for optimally designing district energy systems (DES).

The thermal demand of existing non-residential buildings was first estimated through the development and calibration of grey-box models. Despite challenges and limitations of relying on measured data, doing so allows the definition of optimal operating temperatures for a future energy system. Comparing models calibrated with measurements obtained over different time resolutions revealed the poor performance of heating signature approaches when reconstructing hourly profiles and the potential of the clustering process of balancing modelling errors at the annual level.

A flexible mixed-integer linear programming superstructure was then developed to systematically investigate optimal DHC configurations, including the sizing and operation of conversion technologies, as well as the type, layout, diameter, and operating temperatures of the thermal network. Comparing different solutions under economic, environmental and exergy-based key-performance indicators, demonstrated the potential of the anergy network to reduce investment costs without deteriorating systems performance. Additionally, a sensitivity analysis revealed that hybrid configurations with an intermediate degree of decentralization are the most robust to cost uncertainties.

Finally, given that 90% of the existing DES worldwide are based on fossil fuels, the developed methods were further enhanced to address the optimal retrofit and expansion of existing systems. Particular focus was given to network expansion, replacing fossil-based technologies with more sustainable heat pumps, and synergies between heating and cooling requirements. Applying the developed methods to a case study further demonstrated both the sustainability and improved economics of the multi-temperature level configuration compared with the fossil-based, high temperature option.

The work presented was carried out in collaboration with an international airport to assist their transition towards a fossil-free energy system based on a low temperature network.

Keywords: District energy systems, District heating and cooling, Mixed-integer linear programming, Heat pump integration, Multi-objective optimization, Building thermal models.

Résumé

Le secteur bâti joue un rôle crucial dans la transition énergétique en raison de sa part significative dans la consommation d'énergie et les émissions de CO_2 globales, surtout si l'on tient compte du fait que 70% de la population mondiale vivra dans des zones urbaines d'ici 2050. Les systèmes de chauffage et de refroidissement à distance représentent, parmi les options viables identifiées, une solution efficace pour contribuer aux objectifs climatiques. Dans le contexte de la décarbonisation et de l'électrification des besoins en énergie thermique dans le milieu urbain, cette thèse fournit une méthodologie pour la conception optimale des systèmes énergétiques.

Dans un premier temps, la demande thermique des bâtiments non-résidentiels existants a été estimée en développant et calibrant des modèles de type *grey-box*. Malgré les défis et les limites liés à l'utilisation des données mesurées, ceux-ci permettent de définir des températures de fonctionnement optimales pour le futur système énergétique. La comparaison des modèles calibrés avec les mesures disponibles à de différentes résolutions temporelles a révélé la faible performance de l'approche de la courbe de chauffe lors de la reconstruction des profils horaires et le potentiel du processus de *clustering* pour compenser les erreurs de modélisation au niveau annuel.

Une superstructure flexible basée sur une programmation linéaire mixte en nombres entiers a ensuite été développée pour étudier systématiquement les configurations optimales des systèmes de chauffage et de refroidissement à distance, y compris le dimensionnement et le fonctionnement des technologies de conversion, ainsi que le type, la disposition, le diamètre et les températures de fonctionnement des réseaux thermiques. La comparaison des différentes solutions à l'aide d'indicateurs de performance économiques, environnementaux et exégétiques a démontré le potentiel du réseau anergie pour réduire les coûts d'investissement sans détériorer les performances des systèmes. En outre, une analyse de sensibilité a révélé que les configurations hybrides avec un degré intermédiaire de décentralisation sont les plus robustes aux incertitudes de coûts.

Enfin, étant donné que 90% des système énergétiques urbaines existants dans le monde sont basés sur des combustibles fossiles, les méthodes développées ont été approfondies pour traiter la rénovation et l'expansion optimales des systèmes existants. Une attention particulière a été accordée à l'expansion du réseau, au remplacement des technologies fossiles par des pompes à chaleur et à l'exploitation de potentielles synergies entre les besoins de chauffage et de refroidissement. L'application des méthodes développées à une étude de cas a permis de démontrer la durabilité et les avantages économiques de la configuration à plusieurs niveaux

de température par rapport à l'option haute température à base de combustibles fossiles.
Le travail présenté a été réalisé en collaboration avec un aéroport international afin de le soutenir durant sa transition vers un système énergétique renouvelable basé sur un réseau basse température.
Mots-clefs : Systèmes énergétiques urbains, Systèmes de chauffage et de refroidissement à distance, Programmation linéaire mixte en nombres entiers, Intégration de pompes à chaleur, Optimisation multi-objectif, Modélisation thermique de bâtiments.

Sommario

Il settore edilizio riveste un ruolo cruciale nella transizione energetica in corso, a causa della sua quota significativa di consumo energetico e di emissioni di anidride carbonica, sopratutto se si tiene in considerazione la stima che il 70% della popolazione mondiale vivrà in aree urbane entro il 2050. Tra le diverse opzioni, i sistemi di teleriscaldamento e teleraffreddamento sono stati universalmente riconosciuti come una soluzione efficace per raggiungere gli impegnativi obiettivi di metà secolo. Nel contesto della decarbonizzazione ed elettrificazione dei fabbisogni termici in ambienti urbani, questa tesi fornisce una metodologia per la progettazione ottimale dei sistemi energetici urbani.

Il fabbisogno termico di edifici non-residenziali esistenti è stato prima stimato attraverso lo sviluppo e la calibrazione di modelli *grey-box*. Utilizzare i dati di misura, nonostante le difficoltà e le intrinsiche limitazioni, permette di definire le temperature ottimali di funzionamento per il futuro sistema energetico. Il confronto di modelli calibrati con misurazioni ottenute su diverse risoluzioni temporali ha rivelato le scarse prestazioni dell'approccio della *heating signature* nel ricostruire i profili orari e il potenziale ruolo del processo di *clustering* nel bilanciare gli errori dei modelli a livello annuale.

Una superstruttura flessibile, basata su di una programmazione lineare intera mista è stata successivamente sviluppata per indagare sistematicamente le configurazioni ottimali di sistemi di teleriscaldamento e teleraffreddamento, inlcudendo il dimensionamento e il funzionamento delle tecnologie di conversione, così come la tipologia, il layout, il diametro e le temperature operative della rete termica. Confrontando diverse configurazioni rispetto ad indicatori di performance economici, ambientali e basati sull'exergia, è stato dimostrato il potenziale della rete anergia di ridurre i costi di investimento senza deteriorare le prestazioni del sistema. Inoltre, un'analisi di sensibilità ha rivelato che le configurazioni ibride con un grado intermedio di decentralizzazione sono le più robuste alle incertezze dei costi.

Infine, dato che il 90% dei sistemi esistenti in tutto il mondo è tuttora basato sull'utilizzo di combustibili fossili, i metodi sviluppati sono stati ulteriormente ampliati per gestire il retrofit ottimale e il miglioramento delle reti esistenti. Particolare attenzione è stata dedicata all'espansione della rete, alla sostituzione di tecnologie basate su combustibili fossili con le più sostenibili pompe di calore e alle sinergie tra i fabbisogni di riscaldamento e climatizzazione. L'applicazione dei metodi sviluppati ad un caso studio ha ulteriormente dimostrato le migliori prestazioni sia ambientali che economiche della configurazione a più livelli di temperatura rispetto all'opzione ad alta temperatura basata sui combustibili fossili.

Il lavoro di tesi presentato è stato svolto in collaborazione con un aeroporto internazionale per assistere la loro transizione verso un sistema energetico privo di combustibili fossili e basato su di una rete a bassa temperatura.

Parole chiave: Sistemi energetici urbani, Sistemi di teleriscaldamento e teleraffreddamento, Programmazione lineare intera mista, Integrazione di pompe di calore, Ottimizzazione multi-obiettivo, Modelli termici degli edifici.

Contents

Acknowledgements **i**

Abstract (English) **v**

Résumé (Français) **vii**

Sommario (Italiano) **ix**

List of Figures **xv**

List of Tables **xxi**

Glossary **xxi**

Introduction **1**

1 Thermal energy requirements of existing, non-residential buildings **11**
1.1 Introduction . . . 11
1.2 State of the art and contributions . . . 18
1.3 Application . . . 23
1.4 Space heating requirements . . . 25
1.4.1 Hourly measurements . . . 26
1.4.2 Monthly measurements . . . 39
1.4.3 Yearly measurements . . . 40
1.4.4 Definition of the users' operating temperatures . . . 41
1.4.5 Comparison of different time resolutions . . . 50
1.5 Other thermal requirements . . . 52
1.5.1 Domestic hot water requirements . . . 52
1.5.2 Space cooling requirements . . . 53
1.6 Conclusion . . . 56

2 Optimization of district energy systems equipped with thermal networks **61**
2.1 Introduction . . . 61
2.2 State of the art and contributions . . . 63
2.3 Modelling framework . . . 67
2.3.1 Primary objects . . . 68

2.3.2 Linking constraints 69
2.3.3 Technologies 75
2.3.4 Objective function 85
2.3.5 Problem solving strategy 86
2.4 Application 87
2.4.1 Results 91
2.4.2 Sensitivity analysis 97
2.5 Conclusion 108

3 Retrofit of district energy systems to integrate renewable energy 115
3.1 Introduction 115
3.2 State of the art and contributions 117
3.3 Application 122
3.3.1 Estimating the thermal energy requirements 122
3.4 Modelling framework 123
3.4.1 Existing pipelines 123
3.4.2 The central plant 124
3.4.3 Chillers 125
3.4.4 Thermal storage 126
3.4.5 Model superstructure 128
3.5 Problem solving strategy 130
3.6 Results 132
3.6.1 Definition of a reference case 132
3.6.2 Identification of the Pareto frontier 132
3.6.3 Network layout optimization 132
3.6.4 Definition of the most interesting solutions 135
3.6.5 Improved problem decomposition 142
3.6.6 Definition of alternative scenarios 144
3.6.7 Decision support tool 145
3.7 Conclusion 151

Conclusion 157

Appendices 163

A Chapter 1: Thermal building models additional information 165
A.1 Application 165
A.2 Defining potential exergy savings by optimal operation 167
A.3 Results of the building thermal models 168
A.3.1 Substations with outliers in monthly measurements 168
A.4 Definition of the typical and extreme periods of operation 169
A.5 Estimation of the users installed heating capacity 173

A.6 Estimation of the cooling demand 174
A.6.1 Shifting the profile of the number of passengers to the reference year . . 174
A.6.2 Cooling thermal building model error 177
A.6.3 Operating temperatures 177

B Chapter 2: Optimal DES design additional information 181
B.1 Modelling assumptions and parameters 181
B.1.1 Water-water heat pump 181
B.1.2 Air-water heat pump 183
B.1.3 Chillers 183
B.1.4 Electrical heaters 184
B.1.5 Natural gas boilers 185
B.1.6 Photovoltaic panels 186
B.1.7 Cost functions coefficients 187
B.2 Linearization of product among binaries 187
B.2.1 Definition of network temperatures 188
B.3 Definition of thermal losses 189
B.3.1 Above ground piping 189
B.3.2 Under-ground piping 192
B.4 Additional results 194
B.4.1 Pareto frontiers for network temperatures enabling DHW supply 196
B.4.2 Results for the configuration equipped with the anergy network 197

C Chapter 3: Optimal DES retrofit additional information 203
C.1 Modelling assumptions and parameters 203
C.1.1 Definition of network temperatures 203
C.1.2 Chillers 203
C.1.3 Thermal storage 204
C.2 Additional results 204

Bibliography 207

Curriculum Vitae 217

List of Figures

1 Breakdown of worldwide energy consumption and related emissions in 2019 [8]. 2
2 Schematic of a HP based on a vapor-compression thermodynamic cycle. 6

1.1 Passenger occupancy profile for a terminal building at Birmingham airport [30]. 12
1.2 Heating and cooling signature for a building of administrative type, constructed in the period 1980-2005 and renovated. Values adapted from [33]. 13
1.3 Supply temperature in different locations of the distribution system. 16
1.4 Potential exergy savings by better exploiting the heat exchange surfaces to minimize exergy losses. 17
1.5 Map of the international airport. 24
1.6 Schematic representation of a generic substation including two end-users: a ventilation unit and a radiator. 25
1.7 Generic building schematic with main contributions to the heat balance. 26
1.8 Flowsheet of the proposed method for the development and calibration of thermal models based on hourly measurements. 28
1.9 Pearson coefficient between heat load profiles of each substation (SS1 to SS18) and different potential influencing parameters. 29
1.10 Daily profile of the internal set-point temperature 31
1.11 Amount of surface devoted to the different activities in each building. Values normalized with respect to the largest building surface. 32
1.12 Share of surface devoted to the different activity in each building. 33
1.13 Weekly normalized profile of the electricity consumption for building B3 over one year of operation. 34
1.14 Normalized average daily profile of the electricity consumption for building B3. 34
1.15 MAPE and APE errors calculated for each model and substation and weighted average values. 36
1.16 Comparison of MAPE errors of different thermal models applied to 5, 6, 7 and 8 typical days. 37
1.17 Sequence of typical operating periods over the representative year and daily mean ambient temperature profile. 38
1.18 Results of “Model 7” for substation SS3 and the 5th typical operating period . . 39
1.19 Results of “Model 7” for substation SS14 and the 4th typical operating period . . 40
1.20 Flow sheet of the proposed method for the development and calibration of thermal models based on monthly measurements. 41

1.21 Piecewise linear interpolation of normalized monthly data to estimate the threshold temperature and coefficients of the heating curve 42
1.22 Flow sheet of the proposed method for the development and calibration of thermal models based on yearly measurements. 43
1.23 Normalized heat load supplied by the static appliances and the ventilation units during the 5th typical operating period for substation SS3. 44
1.24 Normalized measured heat delivered and installed capacity of one radiator (on the left) and one ventilation unit (on the right). 45
1.25 Supply and return temperature to a radiator during the measuring period. . . . 46
1.26 Normalized daily energy supplied by each end-user as a function of the degree day. 46
1.27 Normalized measured power delivered by substation SS9 compared to the heat exchangers available capacity. 48
1.28 Simplified model of a generic ventilation unit (on the left) and radiator (on the left). 48
1.29 Comparison between the MAPE and APE errors relative to models calibrated on data with different time resolution, including and excluding the clustering process. 51
1.30 Normalized measured daily profiles of DHW mass flow rate. 53
1.31 Normalized profile of daily average cooling power supplied by substation SS8 and results of the calibrated model. 55

2.1 Compressor isentropic efficiency at varying evaporating and condensing temperatures. 77
2.2 Carnot efficiency for varying source and sink temperatures. 79
2.3 Carnot efficiency for varying source temperature and ΔT_{lift}. 80
2.4 Interpolation of the maximum isentropic efficiency curve as a function of the temperature lift. 81
2.5 COP calculated with varying and constant exergy efficiency for a potential central plant. 82
2.6 Deviation of simple and advanced COP calculation and relative number of hours of occurrence over the reference year for a potential central plant. 82
2.7 COP calculated with varying and constant exergy efficiency for a potential decentralized heat plant. 83
2.8 Deviation of simple and advance COP calculation and relative number of hours of occurrence over the reference year for a potential decentralized heat pump. . 83
2.9 Schematic of the case study. 88
2.10 Heating and cooling signature for a building of type administrative, constructed in the period 1980-2005 and renovated. 89
2.11 Electricity and domestic hot water consumption profiles for all building types. Source: adjusted from [52] and [33]. 90
2.12 Potential supply and return temperature profiles for the HN. 91
2.13 Pareto-optimal and fully centralized solutions in CAPEX-OPEX domain. 92
2.14 Pareto-optimal and fully centralized solutions in CAPEX-KPI^{env} domain. . . . 94

2.15 Pareto-optimal and fully centralized solutions in the CAPEX-Ex_{loss} domain. . . 95
2.16 Evolution of investment decisions at increasing capital allowance for the configuration with the HN at 40°C. 95
2.17 CAPEX breakdown for configurations with the HN at 40°C. 96
2.18 Heating and cooling breakdown for configurations with the HN at 40°C. 96
2.19 Layout of the HN for configurations with the HN at 40°C. Capital cost expressed in kCHF/y. 98
2.20 Layout of the CN for configurations with the HN at 40°C. Capital cost expressed in kCHF/y. 99
2.21 TOTEX breakdown for the Pareto-optimal configurations (and the fully centralized one) related to the HN at 40°C. 100
2.22 Sensitivity analysis on cost of resources for configurations relative to the HN at 40°C. 100
2.23 Sensitivity analysis on electricity tariff for configurations relative to the HN at 40°C.101
2.24 Sensitivity analysis on investment cost parameters of technologies for configurations relative to the HN at 40°C. 102
2.25 Sensitivity analysis on investment cost parameters of network for configurations relative to the HN at 40°C. 102
2.26 Sensitivity analysis on the interest rate for configurations relative to the HN at 40°C. 103
2.27 Sensitivity analysis on cost parameters for configurations relative to the HN at 40°C. 104
2.28 Sensitivity analysis on cost parameters for all the Pareto frontiers at different network temperatures. 104
2.29 Probability of each solution of having the lowest TOTEX. 105
2.30 Sensitivity analysis on investment cost parameters of technologies for configurations relative to the AN. 106
2.31 Recomputed Pareto optimal solutions for different HN temperatures and the AN. Centralized solutions represent designs excluding standalone units. 107
2.33 Recomputed Pareto-optimal solutions (and fully centralized configurations) for different HN temperatures and the AN plotted in the CAPEX-Ex_{loss} domain. . . 107
2.32 Recomputed Pareto-optimal solutions (and fully centralized configurations) for different HN temperatures and the AN plotted in the CAPEX-KPI^{env} domain. . 108

3.1 Distribution of the typical operating periods over the reference year and trend of the ambient temperature. 124
3.2 Scheme of the temperature levels assigned to the two central HPs in the case only one temperature couple is defined for each of the two HNs. 126
3.3 Model schematic representation 129
3.4 All solutions in the OPEX-CAPEX domain and highlighted Pareto frontier. TOTEX in colormap. Values normalized with respect to the TOTEX of the reference case. 133

3.5 Effect of the networks layout optimization on the Pareto optimal solutions in the OPEX-CAPEX domain. 134
3.6 Effect of the networks layout optimization on investment decisions. 135
3.7 TOTEX breakdown of the solutions identified as interesting including the optimization of the networks layout. 136
3.8 Energy breakdowns of resources employed to supply the heating (on the left) and the cooling (on the right) demand. 137
3.9 Networks topology of solution 5. 139
3.10 Networks topology of solution 6. 139
3.11 Comparison of economic performance indicators for three different operations in cooling mode. 141
3.12 All solutions in the OPEX-CAPEX domain and highlighted Pareto frontier achieved with advanced solving strategy. 143
3.13 Comparison of the two solving strategies in terms of computational time. On the left results achieved without optimizing the networks investment cost upper bound, whereas results on the right include the latter as a variable at the master level. 143
3.14 Load duration curve of users' temperature requirements. 146
3.15 Load duration curve of users' temperature requirements after the two temperatures reduction stages. 146
3.16 Screenshot of the results visualization platform. 150

A.1 Schematic of the case study. 166
A.2 Piecewise linear interpolation of normalized monthly data to estimate the threshold temperature and coefficients of the heating curve for substation SS6. 170
A.3 Piecewise linear interpolation of normalized monthly data to estimate the threshold temperature and coefficients of the heating curve for substation SS7. 171
A.4 Piecewise linear interpolation of normalized monthly data to estimate the threshold temperature and coefficients of the heating curve for substation SS9. 171
A.5 Piecewise linear interpolation of normalized monthly data to estimate the threshold temperature and coefficients of the heating curve for substation SS14. . . . 172
A.6 Pearson coefficient between daily number of passengers (PAX), profile of week-end days (WE), profile of holidays (Holidays), ambient temperature (Tamb) and solar irradiation (Irr). 175
A.7 Normalized profile of daily number of passengers, week-end days, holidays, ambient temperature and solar irradiation. 176
A.8 Normalized profile of daily average cooling power supplied by substation SS14 and results of the calibrated model 178
A.9 Normalized profile of average daily cooling power supplied by substation SS4 and results of the calibrated model. 178
A.10 Normalized profile of average daily cooling power supplied by substation SS20 and results of the calibrated model. 179

B.1 Deviation of simple and advance COP calculation and cumulative frequency of occurrence over the reference year for a potential central plant. 183
B.2 Deviation of simple and advance COP calculation and cumulative frequency of occurrence over the reference year for a potential decentralized heat pump. . . 184
B.3 Chillers Carnot efficiency at varying source and sink temperatures (source: [54]). 185
B.4 Chillers COP at varying source and sink temperatures (source: computed from [54]). 186
B.5 Example of heating network temperature profiles for the coverage of DHW demand. 188
B.6 Thermal losses coefficients for above-ground pipes. 191
B.7 Effect of flow velocity on thermal losses. 192
B.8 Effect of flow temperature on thermal losses. 192
B.9 Thermal losses coefficients for buried pipes. 194
B.10 Heating and cooling signature for a building of commercial usage, constructed in the period 1980-2005. 195
B.11 Heating and cooling signature for a building of residential usage, constructed in the period 2005-2020. 195
B.12 Heating and cooling signature for a building of educational usage, constructed in the period 1980-2005 196
B.13 Heating and cooling signature for an hotel building, constructed in the period 1980-2005 and renovated. 196
B.14 Pareto-optimal and fully centralized solutions for DHW coverage in the CAPEX-OPEX domain. 197
B.15 Pareto-optimal and fully centralized solutions for DHW coverage in the CAPEX-KPI^{env} domain. 198
B.16 Pareto-optimal and fully centralized solutions for DHW coverage in the CAPEX-Ex_{loss} domain. 199
B.17 Evolution of investment decisions at increasing capital allowance for the configurations with the AN. 199
B.18 CAPEX breakdown for configurations with the AN. 200
B.19 Heating and cooling coverage breakdown for configurations with the AN. 200
B.20 Layout of the distribution network for configurations with the AN. Capital cost expressed in kCHF/y. 201

C.1 Results of the Pareto optimal solutions listed in Table 3.6. 205
C.2 Installed capacity of conversion technologies for Pareto optimal solutions listed in Table 3.6. 206

List of Tables

1.1 Review of studies on model-based estimation of buildings' TER in the field of system design. 22
1.2 List of thermal models and calibration strategies adopted. 35

2.1 Review of studies on district energy systems optimization. 66
2.2 List of buildings included in the case study and their details. 89

3.1 Review of studies on optimal retrofit of district energy systems. 120
3.2 Variables of the master level optimization. 130
3.3 Variables of the slave level optimization. 131
3.4 Solutions on the Pareto frontier and fully decentralized configuration. 133
3.5 Cost breakdown for solutions identified as interesting. 136
3.6 Solutions of the Pareto frontier achieved with advanced solving strategy. 144
3.7 Scenarios. 145

A.1 Errors of thermal model based on hourly measurements. 169
A.2 Thermal model based on monthly measurements: errors and estimated threshold temperature. 169
A.3 Errors of thermal model based on yearly measurements. 170
A.4 Representative days of the typical operating periods of operation 170
A.5 Errors in cooling demand estimation 177

B.1 Coefficients of Eq. B.1 with validity range $T_e \in [-20;25]$ and $T_c \in [20;70]$ 182
B.2 Water-water heat pump modelling parameters. 182
B.3 Air-water heat pump modelling parameters. 184
B.4 Chiller modelling parameters. 185
B.5 Cost function coefficients. 187
B.6 Pipe details. Sources: adapted by extrapolation if needed from [22, 102]. 189

C.1 Chillers operating modes. 204
C.2 Thermal storage model coefficients. 204

Acronyms

5GDHC	5th generation district heating and cooling
AN	Anergy network
ANN	Artificial neural network
APE	Annual percentage error
BAT	Stationary battery
BES	Building energy system
BOI	Boiler
CAPEX	Capital expenses (annualized)
CDA	Conditional demand analysis
CEPCI	Chemical engineering's plant cost index
CFD	Computational fluid dynamics
CHI	Chiller
CHP	Combined heat and power
CN	Cooling network
COP	Coefficient of performance
DC	District cooling
DCN	District cooling network
DES	District energy systems
DH	District heating
DHC	District heating and cooling
DHCN	District heating and cooling network
DHN	District heating network
DHW	Domestic hot water
DI	Dummy index
EHPA	European Heat Pump Association
ELH	Electrical heater
FC	Fuel cell
GA	Genetic algorithm
GHI	Global horizontal irradiation
HEX	Heat exchnager
HN	Heating network
HP	Heat pump
HVAC	Heating ventilation and air conditioning

IEA	International Energy Agency
IQR	Inter quartile range
KPI	Key performance indicator
LNG	Liquified natural gas
LTH	Low-temperature heat
LTN	Low-temperature network
MAPE	Mean absolute percentage error
MILP	Mixed-integer linear programming
MINLP	Mixed-integer non linear programming
MLTD	Mean logarithmic temperature difference
NG	Natural gas
OPEX	Operating expenses (annual)
PV	Photovoltaic
RES	Renewable energy sources
RMSE	Root Mean Squared error
STC	Solar thermal collector
TEN	Thermal energy network
TER	Thermal energy requirements
TES	Thermal energy storage
TOTEX	Total expenses (annualized)

List of Symbols

Greek Letters

η_{II}	Carnot efficiency	[-]
η	First law efficiency	[-]
k	Heating/cooling signature parameter	[-]
π	Thermal model parameter	[-]
σ	Storage self discharge rate	[-]

Variables (MILP)

$CAPEX$	Annualized investment cost	[kCHF/y]
$\dot{Ex}$	Exergy flow	[kW]
$\dot{E}$	Electricity flow	[kW]
$\dot{M}$	Resource flow	[kW]
$OPEX$	Annual operating cost	[kCHF/y]
$\dot{Q}$	Heat flow	[kW]
$\dot{R}$	Heat cascaded	[kW]
V	Storage state of charge	[m^3]
f	Multiplication factor	[-]
$\dot{m}$	Mass flow rate	[kg/s]
y	Binary activation decision	[-]

Parameters (MILP)

$\mathrm{C}^{inv,1}$	Fixed investment cost parameter	[kCHF]
$\mathrm{C}^{inv,2}$	Variable investment cost parameter	[kCHF/size]
C^{m}	Maintenance cost parameter	[kCHF/y]
C^{op}	Operating cost parameter	[kCHF/size/h]
F	Unit size factor bound	[-]
T	Temperature	[K]
ΔT	Temperature difference	[K]
$\Delta\dot{\mathrm{H}}$	Heat load (stream)	[kW]
dp	Pressure losses coefficient	[Pa/m]
d	Duration	[h]
f	Frequency of occurance	[-]
h	Specific enthalpy	[J/kg]

L	Manatthan distance	[m]
p	Pressure	[Pa]
q^{loss}	Thermal losses factor	[kW/m/K]
s	Specific entropy	[J/kg/K]
v	Flow velocity	[m/s]
x	Steam quality	[-]

Sets

A	Activity
BOI	Boiler utilities
B	Buildings
CH	Chiller utilities
CS	Cold streams
C	Evaporator/condenser streams couples
DN	Pipes diameters
D	Days
ELH	Electrical heater utilities
HC	Heat cascade layers
HP	Heat pump utilities
HS	Hot streams
LC	Locations
LY	Layers
NCU	Network cold utilities
NHU	Network hot utilities
NU	Network utilities
N	Networks
PU	Process units
PV	Photovoltaic panel utilities
SS	Substations
TS	Thermal storage utilities
$\mathbf{T^{f/r}}$	Temperature couples
UL	Thermal losses utilities
UP	Circulation pump utilities
UU	Utilities units
U	Units
T	Timesteps

Accents

$\bar{}$	Averaged
$\dot{}$	Power
$\tilde{}$	Measured

Subscripts/superscripts

$+/-$	Input/Output
0	Design conditions
H/C	Heating/cooling
ON/OFF	Switching-on/-off
PAX	Passengers
SH	Superheating
amb	Ambient
dhw	Domestic hot water
e/c	Evaporator/condenser (refrigerant side)
el	Electricity
env	Environment
$evap/cond$	Evaporator/condenser (source/sink side)
f/r	Feed/return
frg	Refrigeration
gr	Ground
hs/cs	Heating/cooling signature
in/out	Ingoing/outgoing
int	Internal
irr	Solar irradiation
$loss$	Thermal losses
ng	Natural gas
pl	People
rad	Radiator
ref	Reference
set	Set-point
tr	Threshold (cut-off)
$vent$	Ventilation
w/a	Water/air
yr	Yearly

Introduction

"We are at war with nature. If we win, we are lost."
Hubert Reeves

Chapter overview

- General context overview
- The importance of the building sector
- The potential of district energy systems and heat pump integration
- Thesis contributions and structure

In 2020, global energy demand experienced a drastic and sudden reduction by 3.8% in the first quarter [1], demanding an adjustment of the prediction to the 2050 by 8% [2]. Following a similar trend, carbon dioxide emissions, which had been steadily increasing by 1% per annum over the previous decade, registered a sudden drop of up to -17% by early April [3]. Unfortunately, these trends were not caused by the successful implementation of polices, designed to reduced global warming, but by the global health crisis of the COVID-19 pandemic that has led to over 4.4 million deaths. The efforts to slow down the COVID-19 spread included restrictions on most of the social and economical activities, resulting in entire countries being in partial or full lockdown. As the crisis evolved from its outbreak in December 2019 to having half of the total population in confinement by the end of April 2020, the inevitable effects on the economy culminated in a global shock, unprecedented in peacetime. The long-lasting effects of the worldwide pandemic on economies and emissions will depend heavily on the duration of the confinement policies and the speed of recoveries. However, what is already clear is that despite the sudden drop of emissions experienced during 2020, the ongoing energy transition is not fast enough to achieve the Paris Agreement's objective of limiting global warming within 2°C of pre-industrial levels [2]. To reach this challenging target we would need to repeat the decline experienced in 2020 every year from now on [2]. Therefore, now more than ever, investments speeding the energy transition are vital to reduce air pollution, limit its related health impacts and create jobs and opportunities providing a durable economic recovery from the COVID-19 crisis [4]. To be effective, efforts in this direction should involve all parties, from individuals to governments, and implicate all sectors: energy conversion and distribution, industry, transportation, buildings, agriculture, etc. In this thesis, particular focus is given to the building sector and its energy consumption.

The building sector

Since ancient times humans have tended to aggregate in *nucleated settlements*. Doing so has allowed participants to share resources and manpower, contribute to social activities and duties, trade with other communities and strengthen their own against enemy attackers. Whereas the first settlements mainly relied on farming and agricultural activities, the Industrial Revolution of the late 18th and early 19th centuries drastically impacted village life. Urbanization thus began at this time in most of nowadays developed countries with settlements building up around factories. Before spreading around the world, this trend began in Great Britain after rail lines opened in the 1860s with the rapid expansion of the small village of Hampstead, which remains a major neighborhood in London [5]. The United Nations have estimated that in 1950, 30% of the world's population lived in urban areas. This share has increased to 55% in 2018 and is expected to reach nearly 70% by 2050 [6]. This growth is driven by the overall increase of global population, as well as the movement of people from rural to urban areas, nowadays mainly affecting Asia and Africa [6].

Following the steady growth of urban areas, the global final energy demand and emissions of the building sector have continuously increased with the expansion of population and floor area, despite some marginal efficiency improvements. Emissions allocated to the sector increased by 2% between 2017 and 2018 [7], reaching their highest level at around 10 $GtCO_2$ in 2019, representing 28% of the global energy-related CO_2 emissions [8]. The construction and operation of this sector were responsible for 130 EJ in 2019, comprising the 35% of the worldwide energy use and 55% of worldwide electricity consumption [8], as highlighted in the breakdown of the final energy and emissions shown in Fig. 1.

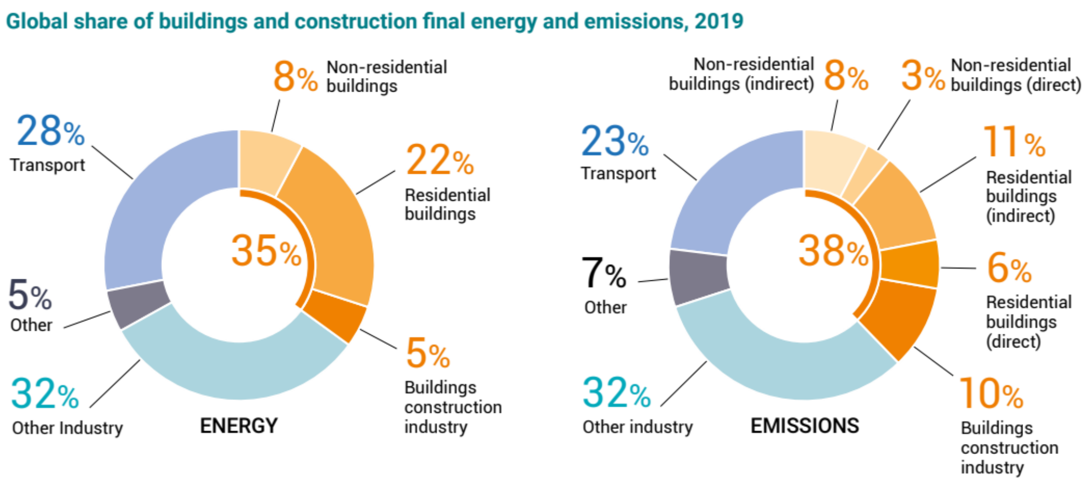

Figure 1: Breakdown of worldwide energy consumption and related emissions in 2019 [8].

The International Energy Agency (IEA) has estimated that direct and indirect building emissions must be reduced by 50% and 60% by 2030, respectively, to achieve the challenging target of a net-zero carbon building stock by 2050. Thus, emissions from this sector should decrease by 6% each year between 2020 and 2030 [8]. Despite the enhanced global awareness of the effects of increased emissions and the correlated global warming, very little has been done to reverse the current emissions trends. In particular, new buildings constructed by 2050 under inadequate energy policies are estimated to be equivalent to 2.5 times the current building stock of China [9].

However, the relevance of the building sector in both energy consumption and emission reduction render it a key actor in the on-going energy transition. Decarbonizing this sector, by reducing direct and indirect emissions appears essential to meet the global ambitions of limiting global warming within 2°C of pre-industrial levels. The IEA has provided recommendations to create a sustainable built environment, including imposing urban planning policies, the construction of new low-emission efficient and resilient buildings, improving existing buildings' energy efficiency through renovation or better energy management, decreasing the overall energy demand, and promoting a clean energy transition in the sector [7].

District heating and cooling systems

The heating and cooling sector is responsible for half of the final energy consumption and 40% of the energy-related CO_2 emissions worldwide [10]. In Europe, the heating and cooling of residential buildings account for nearly 45% of the final energy demand, followed by the industrial and tertiary sectors. Therefore, the decarbonization of society cannot be achieved without promoting energy efficiency and the use of renewable energy sources (RES) in heating and cooling. Many political challenges remain regarding modifying the current legislative framework governing the heating and cooling sector towards fossil-free solutions by 2050 [11], despite the availability of technically proficient, sustainable technologies in this field. Indeed, although the well-known benefits, policy-makers have given limited attention to accelerating the transition to cleaner and more efficient heating and cooling services.

one of the available options to promote energy efficiency and renewable sources in the heating and cooling sector is to switch from individual systems to district energy in urban areas [12]. The Heat Roadmap Europe studies [13] have shown that increasing the share of heat demand supplied by district heating (DH) in 14 European countries from 12% (the current value) to 50% brings, not only improvements in efficiency when compared with conventional decentralized solutions, but higher shares of RES at a lower cost, as well. Moreover, DH enables the valorization of excess heat sources that would be otherwise wasted since not accessible by the single buildings, as well as geothermal and solar thermal heat. Today, European countries vary in terms of their level of integration of residential DH; at the highest end of the spectrum, Central, Eastern and North Europe have reached around 50% [12]. Further, despite the energy mix in the sector varies regionally, 70% of the fuels in 2017 were still of fossil origin, mainly burnt in combined heat and power (CHP) facilities, offering a large margin for improvements.

Several practices, used during the operation of the existing systems, must also be revised to improve energy efficiency. At the distribution level, system operators often define the supply and return temperatures as a function of the external conditions, without considering the consumers' needs and apply margins of safety to avoid users' complaints [14]. A more dynamic approach based on digital solutions could allow the operating temperature to be decreased, benefiting both the production and distribution processes [14]. Similarly, the pressure and flow rate are often maintained at a constant value regardless of consumption, using unique set-points designated at the pumping station, that are changed only between summer and winter operations [14]. However, adjusting the operation with respect to the requirements of the most critical users could bring significant savings in pumping cost [12]. At the building level, the supply temperature is often controlled using a set-back function to save energy during periods of lower required comfort (e.g., at night) [15]. While this strategy works well for poorly insulated buildings, it results in minimal savings in new ones, which are characterized by large inertia. Moreover, set-back functions might have negative impacts on the system efficiency, especially for systems that are highly dependent on the supply temperature, such as heat pumps (HP). Set-back functions cause greater peak demands during buildings reheating, higher heat losses, poorer operation of the heat source, due to the increased temperature, and higher pumping costs, induced by the higher flow rate [16].

The operating temperature of DH systems greatly affects the production and distribution efficiencies. A trend toward lower-temperature networks has been registered during the evolution of such systems, as pointed out by Lund et al. [17], who discussed the progression of DH since it was introduced in 1880s. Four generations were identified, with an inversely proportional relationship between efficiency and operating temperature [17]. The advantages of lower operating temperatures have been highlighted in several studies, such as [12, 18–21], and can be summarized by the following aspects:

- reduced network heat losses;
- use of more effective material for pipelines due to lower thermal stress;
- possible integration of additional heat sources, such as solar thermal collectors, geothermal heat and low temperature waste heat;
- improved efficiency of conversion technologies (such as CHP power plants and HPs);
- increased security of energy supply and expected higher price stability due to the use of local resources.

Following the trend of reducing network operating temperatures, the latest configuration of networks (defined as 5^{th} generation based on the terminology introduced by [17]) aims at operating networks at conditions closer to the ambient, supplying both heating and cooling requirements through district heating and cooling (DHC) systems. Such systems could be operated with water as a transfer fluid or adopt refrigerants. Pioneering work in refrigerant-based networks was carried out by Henchoz [22], who investigated their potential in the city of Geneva (CH), and then by Suciu [23], who integrated such systems into the analysis of zero- or negative-emission, autonomous district energy systems (DES).

When needing to design new DHC systems or expand an existing infrastructure, decisions are commonly left to the personal preference of individual stakeholders, influenced by targets defined by political tendencies and boundary conditions [14]. Decentralized sources are still not accounted for during the design process; the resulting configuration is traditionally chosen using a "rule of thumb", causing sub-optimal solutions. However, involving optimization at the design stage could bring benefits to all actors [14], including:

- the consumers: optimum planning improves the security of the supply and might result in lower costs if benefits are passed on to users;
- the energy sector: optimization provides means to improve both economic and ecologic system performance, reducing investment and operating costs, promoting the share of RES and enhancing system performance, all resulting in higher consumers' satisfaction and thus connection rates;
- society at large: promotion of sustainable solutions in urban areas at lower costs.

Even if the optimum planning, design and adaptation of new and existing DHC systems is a challenging problem, the potential benefits highly encourage gathering efforts in this direction, both at research and at decision making levels.

Heat pump integration

The switch from fossil fuels to high-efficiency HPs for heating and cooling demand is expected to be the main driver in reducing greenhouse gases emission in the building sector [24]. In 2019, however, HPs were only used for a minor share of the residential heat demand (around 5% as estimated by [4]). HPs are a well-established technology that can not only facilitate the decarbonization of the heating and cooling sector but also bring several economic, environmental, and societal benefits for a sustainable future [11].

A HP can simultaneously supply heating and cooling demands and is used to upgrade the exergy content of a heat flow by exploiting different principles, the simplest (and most commercially available) being the use of electricity in a vapor-compression thermodynamic cycle. The final effect is the transfer of heat from a low temperature heat source to a higher-temperature heat sink. In this alternative, the machine includes: 1) an evaporator in which the transfer fluid is exposed to the cold source (ambient air, water, ground) and evaporates, 2) a compressor to increase the vapor temperature and pressure, 3) a condenser in which the inner fluid cools down and condenses releasing heat to the sink, and 4) an expansion valve to bring the transfer fluid back to the initial conditions. A schematic of this type of HP and its operating principle is shown in Fig. 3.2.

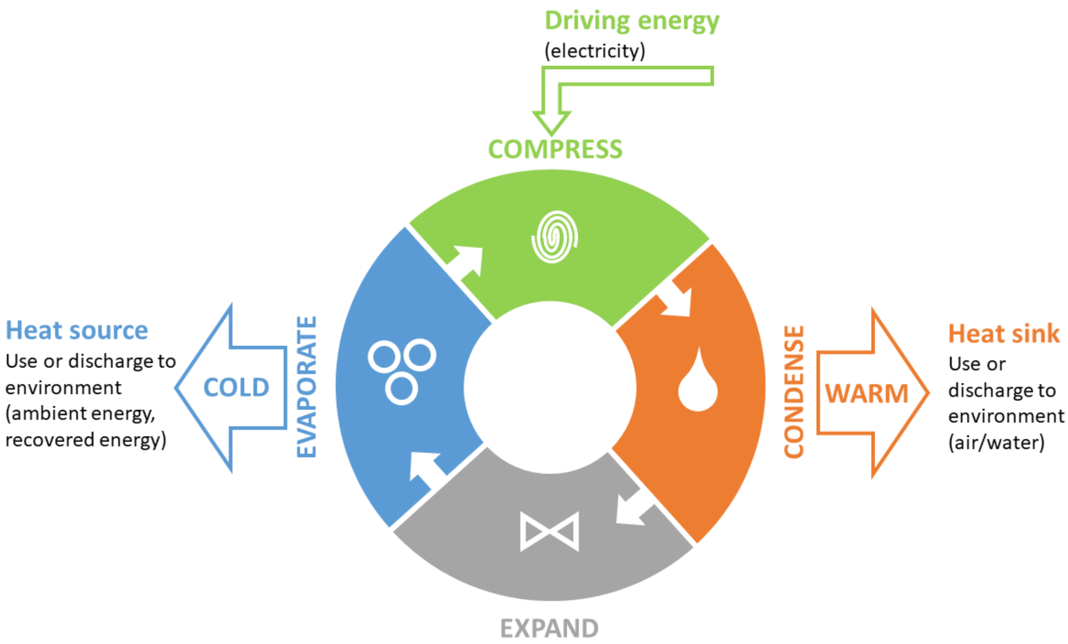

Figure 2: Schematic of a HP based on a vapor-compression thermodynamic cycle.

The ratio between the beneficial effect (i.e., the heat supplied to the sink or cold released to the source) and the electricity consumption is defined as the coefficient of performance (COP), which is dependent on the temperature of evaporator and condenser and the efficiency of each component. Consider a HP delivering heat at 70°C while connected to a source at 10°C with a COP of 3; from one unit of electricity, the HP delivers 3 units of heat. If the 2 units of energy provided by the low-temperature source are of renewable origin (ambient air, ground water, etc.) and considering an average efficiency of power generation of 40% ([25]), the HP consumes 2.5 units of primary energy. The latter would increase to 3.5 units if the same heat is delivered by a conventional fossil-fired boiler (BOI). Moreover, if sustainable resources (e.g., photovoltaic (PV) or wind energy) are used to provide electricity to the compressor, the heating supplied by the HP becomes 100% renewable and emission-free.

An additional benefit of HP penetration in urban areas is the possibility of offering demand response services to the grid. With the increasing share in electricity production of intermittent renewable sources such as wind and solar, operating the grid by modifying the supply to match the demand becomes difficult, if not impossible. The potential of HPs in offering grid flexibility in the residential sector has been investigated recently by Amblard [26]. HPs could be coupled with thermal storage or batteries or exploit the building thermal capacity to provide load shifting and peak shaving. With these systems, heat production can be optimized to maximize the self-consumption of electricity generated by PV.

Moreover, local RES can be exploited, thereby improving the security of supply and reducing dependence on imports. Today, more than 50% of all fossil fuels used in Europe are imported, mainly from Russia and the Middle East [11]. Beyond local energy, the HP industry also promotes local employment: in 2020, the European Heat Pump Association (EHPA) estimated that 87,000 full-time jobs would be necessary to produce, install and maintain the annual sale of HPs in Europe [27].

The options to integrate HPs in urban areas are various [11, 13]:

- in old residential buildings, equipped with limited exchange surfaces, HPs can be coupled with conventional systems, allowing the HP to efficiently meet heating demands during the milder seasons, whereas conventional systems can be used as a backup solution for the coldest periods;
- in new or refurbished residential buildings with sufficient distribution surfaces that allow a relatively low-temperature supply (below 55°C), HPs can fully replace conventional BOIs;
- in non-residential buildings (e.g., hospitals, offices, educational campuses, airports), large HPs can supply both heating and cooling requirements by exploiting the synergies among the different services and
- in rural areas with limited access to DHC, HPs can be installed as standalone options.

The number of HPs sold in Europe in the past decade has constantly increased, reaching 1.3 million units in 2018 for a total useful energy of 250 TWh and representing an energy saving of 203 TWh over conventional gas BOIs, as documented by EHPA [27]. Despite these positive trends, the penetration of HPs in the heating and cooling sector remains marginal, with fossil fuels covering the major share. HPs are today already the most cost-effective solution for new buildings, which are subjected to stricter emissions regulations and are designed for low-temperature supply. On the other hand, government policies and incentives should encourage retrofitting existing buildings by replacing conventional BOIs with HPs.

Contributions and structure

Given the urgent need to accelerate the ongoing energy transition, the key role played by the building sector, and the potential of DHC systems, this thesis aims at developing methods for optimizing DES. Particular focus is given to the estimation of the thermal energy requirements (TER) in existing, non-residential buildings, the comparison of different thermal energy networks (TEN) configurations and the HP integration to promote the share of RES in urban areas. Three major research questions are formulated and addressed in the respective chapters, as follows.

Chapter 1: Thermal energy requirements of existing, non-residential buildings

1st Research question:

"How can the thermal energy requirements of existing, non-residential buildings be modelled for the integrated energy system design?"

The first question arises from the challenges identified in estimating the demand of existing, non-residential buildings. In this chapter issues to be tackled in the field are presented; methods to develop simple thermal building models making the best use of available measurements are then proposed. Particular focus is given to space heating demand estimation, by developing grey-box models and calibrating them using hourly, monthly and yearly data. In the first case, different models with varying levels of detail are compared and tested on different numbers of typical periods to represent the operating conditions during the project life time. Simplified models following a heating signature approach are also developed when monthly and yearly data are available. Models calibrated on measurements obtained over different time resolutions are then compared. Finally, a method to define optimal operating temperatures, by exploiting the available heat exchange surfaces to reduce exergy losses in view of HP integration, is proposed; suggestions for estimating the domestic hot water (DHW) and space cooling demand, based on the available measurements, are also provided. All the developed models are applied to a case study of an international airport.

Chapter 2: Optimization of district energy systems equipped with thermal networks

2nd Research question:

How can optimal design solutions for district energy systems equipped with thermal networks be defined, and how can the best configuration be selected?

The second question originates from the proven potential of DES toward a more sustainable building sector. Methods to optimally size equipment and infrastructure are proposed in this chapter, focusing on solutions to promote the share of RES in urban areas. A flexible optimization framework based on a mixed-integer linear programming (MILP) superstructure is presented that includes layout, type, and operation of TENs and can be used to investigate the optimal degree of centralization/decentralization of heat and cold production. To promote the electrification within the sector, particular attention is given to HP integration. Finally, a method to generate and investigate different design solutions is proposed, based on the definition of Pareto-optimal configurations for various operating temperatures of the TENs. The generated design solutions are consequently compared under economic, environmental, and exergy-related key performance indicators (KPI). The robustness of the proposed solutions is assessed through a sensitivity analysis on the resources tariffs, investment cost of networks and technologies, and interest rate. As a case study, the proposed method is applied to a fictitious neighborhood comprising six buildings of different usage and construction periods.

Chapter 3: Deep energy retrofit of district energy systems to integrate renewable energy

3rd Research question:

How can existing district energy systems be retrofitted to optimally integrate renewable energy sources and exploit synergies between heating and cooling requirements?

Most existing DES are supplied by fossil fuels and thus often require retrofit and expansion to increase the penetration of DHC systems and promote the share of RES. A strategy to combine and further improve the methods previously presented is therefore proposed in this chapter to allow optimal energy retrofits of current systems. Particular importance is given to exploiting the existing infrastructure and synergies between heating and cooling requirements. The proposed MILP framework and resolution strategy are at first adapted to cope with the system complexity. The methods are then applied to the international airport case study to assist the transition from a fossil-based energy system to the connection to a low-temperature network, and results are discussed. Finally, an online visualization platform based on parallel coordinates is developed as a decision-support tool.

1 Thermal energy requirements of existing, non-residential buildings

Chapter overview

- Development and calibration of grey-box models for the estimation of the thermal energy requirements of existing, non-residential buildings
- Comparison of models calibrated with measurements obtained over different time resolutions
- Definition of optimal operating temperatures for future energy systems in existing buildings

The work presented in this chapter is the result of a collaboration with an international airport aiming at assisting their transition to a more sustainable energy system.

1.1 Introduction

In view of improving energy efficiency and promoting the share of RES in the building sector this thesis focuses on the optimal design of DES. The latter is a complex problem which includes multiple challenges, among which the estimation of the buildings' TER, topic of this first chapter. Models development and calibration of buildings' TER is a wide field of research, shared among different applications, such as accessing the buildings energy performance, investigating measures to decrease the building TER (i.e., the effect of thermal insulation or other refurbishment actions), studying the contaminant distribution, assessing the performance of the heating ventilation and air conditioning (HVAC) system, analyzing natural and artificial ventilation, forecasting the energy consumption, defining inputs for the design of the building energy system. It is evident that each application requires a different complexity and level of accuracy. In particular this chapter addresses the challenges of estimating the TER of existing, non-residential buildings with the final aim of defining the optimal integrated energy system design.

Estimating the demand of existing and complex buildings greatly differs from dealing with newly constructed residential ones for various reasons. In the following paragraphs the most relevant challenges in this field are gathered, based on studies in the literature and the experience of the author gained during this work.

Residential vs. non-residential buildings The demand estimation of residential buildings often relies on standard building characteristics, as suggested by norms, and assigned according to the building usage and year of construction [28]. When dealing with complex buildings, the particular structural characteristics are often not available and only accessible through an extensive and expensive measuring campaign on site. In case the technical information is available from the buildings design plans, the structures, which deteriorate in time and could be subject to retrofit actions, might behave differently. In addition, the estimation of occupants' behavior in the non-domestic sector is a difficult and often impossible task [29]. As an example, the occupants' profile in an airport greatly varies according to the building's usage and highly differs from the standard profiles suggested by the norms. As an example, Fig. 1.1 shows the passenger occupancy profile in the departure and arrival sides of the terminal building at Birmingham airport, respectively.

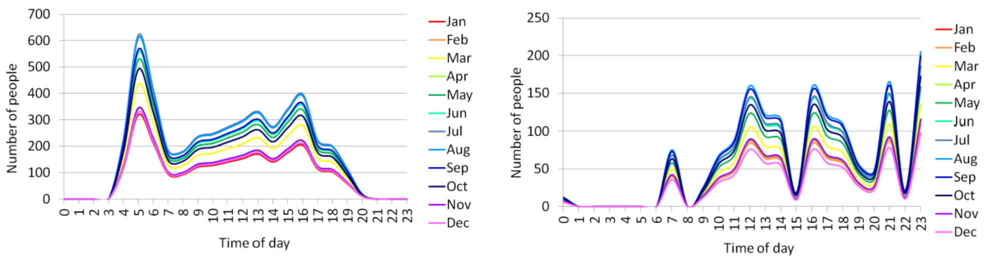

(a) Departure side

(b) Arrival side

Figure 1.1: Passenger occupancy profile for a terminal building at Birmingham airport [30].

Most of the studies in the literature focused on modelling non-residential buildings cope with the building complexity either by adopting detailed dynamic thermal models [30] or by resorting to machine learning techniques [31, 32]. In both cases, such models are not suitable within an holistic optimization framework aimed at the integrated energy system design: in the first case due to the difficulty of gathering all the parameters required and in the second due to the non-predictive nature of the models, which are mainly employed for short-term predictions. Moreover, the relevant amount of measured data required is often not available for existing buildings.

A simplified approach consists in assessing the heating (and cooling) signature at building scale and the aggregation of the different demands through a bottom-up approach. Indeed, to express the TER as a function of the difference between the external and room temperatures is a common practice, especially at district level [33, 34]. The main assumption in this approach is that a unique set-point temperature over the whole year is considered and the change in energy demand is driven by a variation of the outdoor temperature, whereas heat losses/gains such as those from occupants, lighting appliances and infiltration are considered constant [35]. Figure 1.2 shows an example of heating and cooling signatures relative to an administrative building, constructed in the period 1980-2005 and renovated.

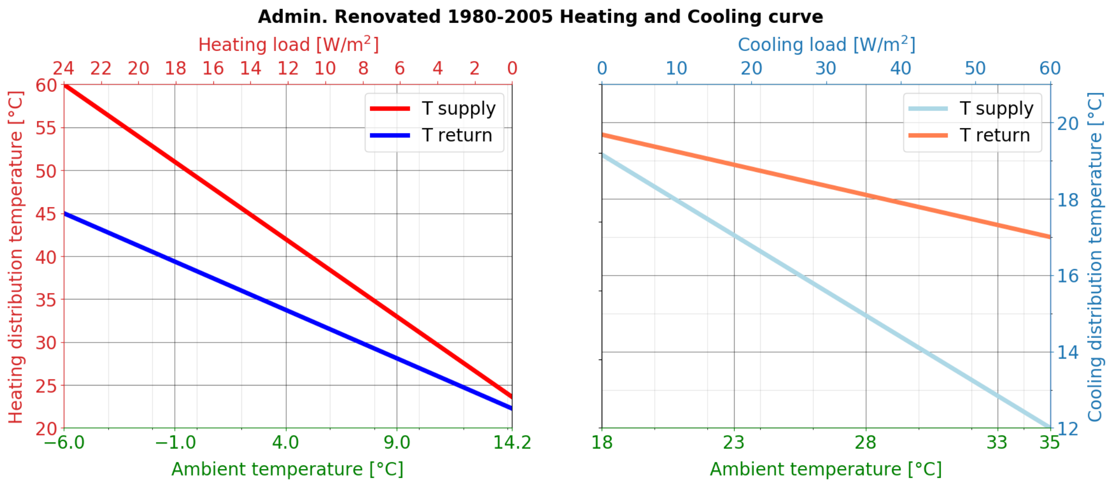

Figure 1.2: Heating and cooling signature for a building of administrative type, constructed in the period 1980-2005 and renovated. Values adapted from [33].

Even if widely adopted, especially due to the simplicity of the model, the heating/cooling signature approach shows some drawbacks. Andrić et al. [35] explored in their study the feasibility of adopting the heating signature method to estimate future demand under different weather conditions and renovation scenarios. Results were compared with the output of a dynamic heat demand model. The authors concluded that whereas the approach could be considered accurate enough for the reference year and under different weather scenarios, the error increased up to almost 60% after introducing the renovation scenarios. The study solely focused on residential buildings. Moreover, the heating and cooling signatures fail at capturing the impact of internal gains at an intra-daily basis, which for complex non-residential buildings is proven to highly effect the thermal demand. However, the use of the heating (and cooling) signature approach remains the only alternative if the measurements available are very limited (i.e., data measured on a yearly basis).

Scaling up to buildings blocks An additional challenge is encountered when passing from an individual to an aggregated level (e.g., building stocks, district, city). Simulating the TER in this case is more complex mainly due to three reasons [36]:

- the determination of all information about built structures needs expensive and time consuming surveys and measurements due to the large size of the domain studied;

- the maximal demand appears different from the sum of the individual maximal power demands, due to the temporal variability of occupants' behaviors;
- buildings can no longer be assumed to be standalone because of the influence of neighboring structures.

When dealing with building stocks models, the largest amount of published literature is on residential buildings, due to the relevant role of the residential sector in the total energy consumption in urban areas [37]. Swan and Ugursal [38], Kavgic et al. [39], Lim and Zhai [40] and Koulamas et al. [41] all provided reviews on existing building stock models for residential applications. At the building stock level two different modelling approaches can be identified [36–40]:

- the top-down approach which is based on data-driven models and does not investigate individual building models, but rather studies the building stock as a whole at an aggregated level;
- the bottom-up approach which starts at a disaggregated level, such as the building one and resorts to statistical or deterministic aggregation methods and techniques to represent the entire building stock.

Bottom-up models are usually classified in sub-categories according to the building model approach adopted [41].

Lim and Zhai [40] investigated the role of uncertainties in shifting from a building to an aggregated level. The authors explained that errors at the individual building level are higher than those at an aggregated one, such as city or national scale, since the inaccuracies tend to average out. However, the same cannot be claimed if the case study is a small neighborhood or a limited complex of buildings.

In the field of non-residential buildings, Borgstein et al. [42] reviewed methods to evaluate energy performance. Whereas the same classification as for residential building stocks holds, the authors pointed out the crucial role of model calibration, uncertainty analysis and impacts of users' behavior to minimize the performance gap between simulated and measured results.

Existing buildings and quality of available measurements According to Heo et al. [43] the use of building simulation software has recently become the mainstream approach to estimate the building energy consumption (e.g., to identify the benefit of retrofit actions). However, the authors also highlighted how such a procedure is effective for yet-to-built projects, in which the building properties and its systems parameters can be assumed to follow engineering design specifications. On the contrary measurements from existing buildings include the effect of the current operation, which is often difficult to represent in a building energy model. Moreover, Legorburu and Smith [44] pointed out that while adopting building energy software is widely accepted by the building design community, it requires substantial engineering labor to provide all the necessary information parameters and risks to produce poor predictions if the latter are not accurate. Therefore, especially in the case of existing buildings, the development of simplified models and their calibration on historical measured data becomes essential.

The calibration of building thermal models relies on the availability of historical data, but when dealing with existing, complex buildings the type and quality of the measurements available is often insufficient. For example, in old buildings the operation of the energy system is often controlled based on the heating/cooling signature principle, that is by a linear correlation between the external temperature and the TER. This approach does not include a feedback on the internal state of the building, which thus lacks sensors to measure the internal temperature. Moreover, the existing measuring devices used to control the current operation might be placed at an aggregated level, losing information about the single final users (radiators or ventilation units). In this case the measurements available include different users placed in various zones of the building, both in terms of power and supply/return temperatures to the space conditioning technologies.

To know the temperature requirements of the building's space conditioning technologies is very important to properly size and operate sustainable heat and cold production systems. Indeed, assessing the building's TER in terms of power with the aim of improving the efficiency of the underlying energy system is not enough. While the efficiency of fossil-based technologies is not greatly affected by the delivered temperature, the latter plays a major role in the case of a HP, largely influencing the amount of electricity needed per unit of heat delivered. Therefore, given the heat surfaces in place and the maximum flow constraints, knowing the minimum temperature requirements to be able to provide the required comfort level is a critical aspect to properly size the equipment.

In the case of newly built distribution systems the temperature requirements can be easily estimated, once the exchanging surfaces and the technical constraints are identified. On the contrary for existing buildings the tendency is to assign the equipment design temperatures without considering eventual changes in operation with respect to the design conditions. In reality, the actual building demand is often much smaller than the installed capacity. This mismatch can be due to renovation actions, a natural evolution of the building usage or the over-sizing procedure common in the past decades. Even if measurements of the operating temperatures are available, they turn out to solely reflect the current control strategy and not of the real requirements. For example, a fossil-based systems is never controlled to minimize the operating temperature, since the latter influences little the efficiency of the heat production. Often the control strategy relies on exergy destruction by mixing hot and cold water through three-way valves to adjust the temperature at the final users and if sensors are positioned before that stage the real requirements remain unknown.

Figure 1.3 shows the recorded temperature in the distribution system of an existing building stock at an airport. Particularly each measurement refers to an aggregation of different space conditioning technologies (radiators and ventilation units) serving zones of the buildings with distinct usage and activity pattern and supplied by the respective substations (indicated as "SS" and a cardinal number throughout this chapter). The dots represent the measured temperature, the black line shows the trend line of the cloud and the red one the system set-point.

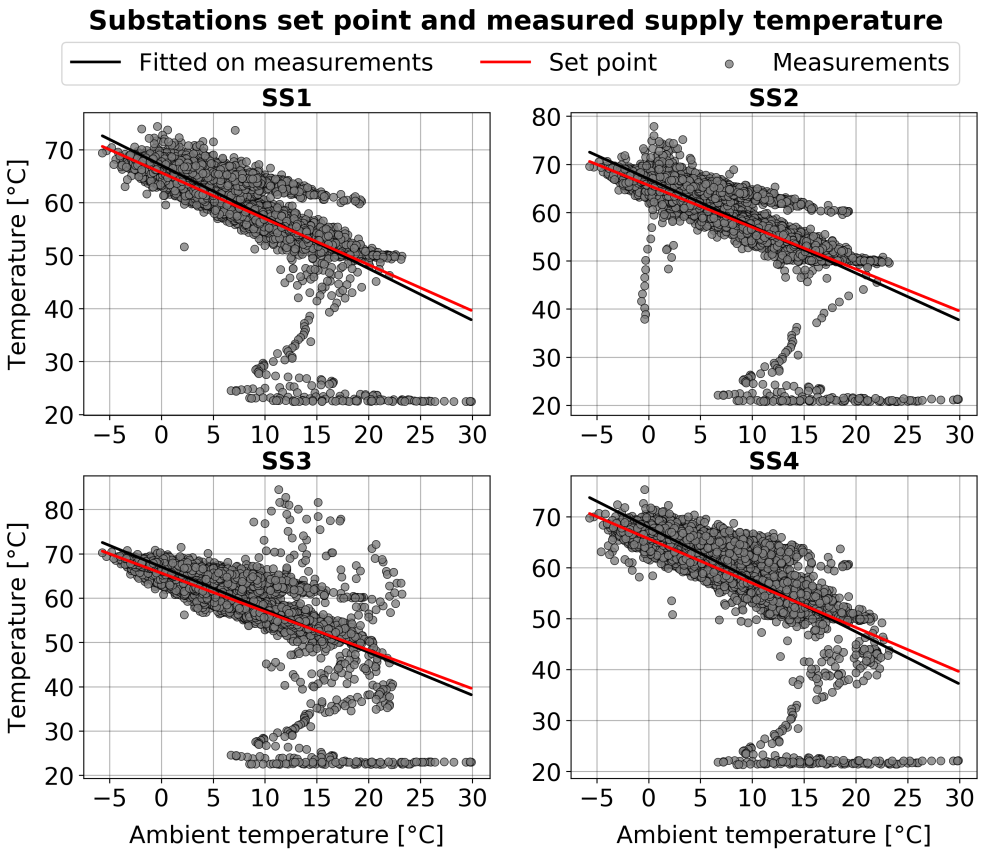

Figure 1.3: Measured supply temperature in different locations of the distribution system (grey dots) with corresponding trend lines (black line) and relative set-points (red line).

As visible in Fig. 1.3 the supply temperature is governed by the same heat curve (red line) and as a result the temperature arriving at the final end-users shows a very similar trend. To satisfy the end-users' requirements the temperature level is finally adjusted by three-way valves. Since the temperature measuring sensors are positioned before that stage, the real requirements stay unknown.

Moreover, as previously mentioned, an additional aspect to take into account when using measurements in terms of operating temperature for the future operation is that existing buildings might have undergone refurbishment actions and thus might be equipped with oversized heat exchange surfaces with respect to the current TER. The latter situation allows to reduce the operating temperature to favor the performance of the heat generation system in the case of a

HP. To estimate the potential benefit of exploiting the existing heat exchange surfaces and reducing the operating temperatures, a preliminary analysis can be carried out. Considering all the end-users supplied by the different substations as aggregated in an hypothetical heat exchanger, by means of the measurements of heat load delivered, operating temperatures, mass flow and comfort temperature in the room, the characteristic (UA), product of the heat transfer coefficient and heat exchange surface, can be estimated for this hypothetical heat exhanger. Thus, the minimum temperature required by the installation to guarantee the level of comfort within the building zone, while respecting the technical constraints (i.e., maximum flow, available surface), can be predicted. More insight on how this analysis can be conducted are given in Section A.2, whereas Figure 1.4 shows the potential exergy saving in different substations over 2 years of operation in an airport complex.

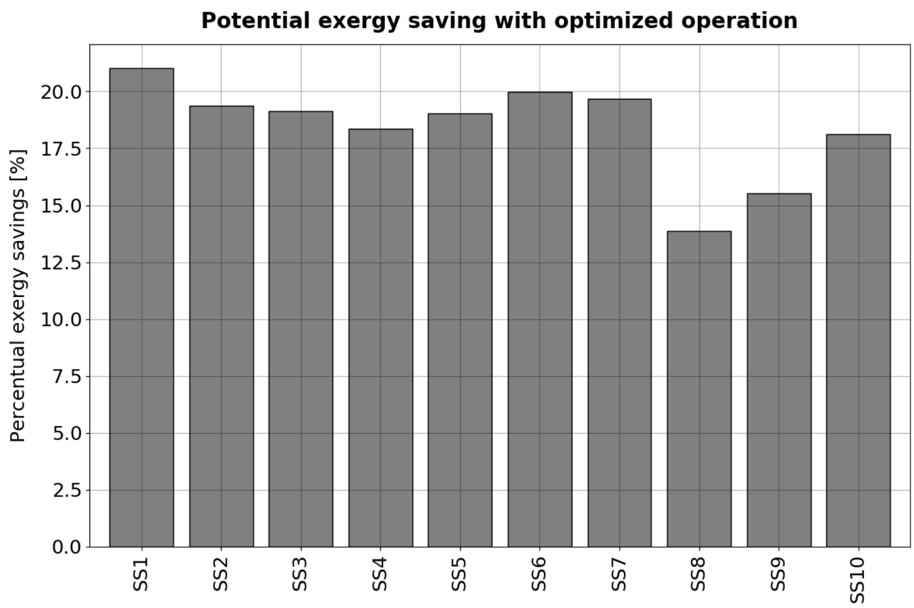

Figure 1.4: Potential exergy savings by better exploiting the heat exchange surfaces to minimize exergy losses.

The exergy content defines the “quality” of a heat flow and represents the amount of electricity theoretically consumed by an ideal HP (i.e., a Carnot machine) to supply it. Despite the disadvantages of relying on data recorded by the existing control system, to perform new measuring campaigns in large public buildings is often difficult and expensive, and given the strict constraints on the quality of services provided, any result would still be based on the current operation. Therefore, this chapter focuses on ways to exploit the measurements available, while coping with their limitations.

1.2 State of the art and contributions

The most common classification among building thermal models identifies three main modelling approaches [45]:

- **"white-box" approaches** based on physical models, which may be further divided into three sub-categories corresponding to a gradual increase of details level in the building model: the multizone (or nodal) technique, the zonal method and the computational fluid dynamics;
- **"black-box" approaches** based on statistical analysis of large database of measured data (e.g., energy consumption and meteorological data) and including different techniques such as conditional demand analysis, genetic algorithm, artificial neural network, etc;
- **"grey-box" approaches** also called hybrid for coupling characteristics of the statistical and physical ones.

Foucquier et al. [45] and Koulamas et al. [41] offered in their reviews a detailed explanation for each of the aforementioned approaches, specifying the underlying principle, advantages, field of application, limitations and offering some examples from the literature. In short, *white-box* methods assume that all thermal and geometric building characteristics are well-known and that all physical mechanisms can be described with high accuracy. Whereas this information can be easily extracted from design data in the case of new buildings, it becomes less obvious for existing structures. However, there is no need of modelling training data and the results can be interpreted in physical terms. On the contrary, *black-box* approaches are based on machine learning techniques, deducing functions from samples of training data to describe the behavior of a specific system. Therefore, no information on the building is required, but large amount of measured data is necessary to achieve satisfactory results. Another main difference among the two categories is that *white-box* models can be applied generally and exploited to estimate future demand, while *black-box* are building-specific and might fail to predict the behavior under circumstances different from those employed for the calibration. *Grey-box* methods combine physics and statistics, overcoming the limitations of the other two groups. Since a partial physical interpretation is included, the amount of measured data required is reasonable and results are more easily interpreted. Such methods may be appreciated in particular when a building physical model is available, but it is incomplete or does not offer enough details. An interesting application is the parameters identification. In this case the model calibration process allows to estimate a set of input values, such as the thermal properties of the walls, corresponding to given outputs (e.g., a target consumption level) [45]. Examples of this application are the coupling between nodal techniques for the thermal and geometrical representation and genetic algorithm (GA) for the parameters identification, or also between regression techniques and thermal models.

Koulamas et al. [41] introduced in their review the use of slightly different terminology to define the same underlying principles when classifying building modelling approaches: 1) physical/statistical/hybrid, 2) white/black/gray, 3) calculation/measurements/hybrid and 4) engineering/statistical/hybrid approaches. The authors also reported an extensive list of studies focusing on different kinds of building thermal models, highlighting field of application, contributions, type of buildings included and methods applied.

Table 1.1 gathers some examples of studies in the field of building thermal modelling, all characterized by the final aim of designing the energy system of non-residential buildings. In the following a brief explanation for each of study is given.

Bornand et al. [46] estimated the space building demand of an existing hospital site by minimizing the square of the residuals between the hourly measured profile and the results of a grey-box model. At first parameters for the thermal losses, fresh air flow and internal gains were estimated according to the standards, based on the buildings' usage and year of construction. Then tuning factors were used for each parameter to catch the building's specific behavior. Finally the calibrated parameters were employed for other buildings on the site for which the hourly measured profile was not available. The resulting R^2 coefficient of the calibration averaged over the 5 buildings included in the analysis was of 0.778. The final goal of the study was the optimal investment planning strategy to replace the current equipment by more sustainable options.

Wen et al. [47] investigated the optimal design and operation strategies in shopping malls, hotels and office buildings equipped with DES. Seven different operating strategies were compared. The authors employed a multi-criteria genetic algorithm to simultaneously maximize energetic, environmental and economic system performances, by acting on the installed capacity of the gas-fired power generation unit and the share of cooling demand met by refrigeration units. The method is applied to three hypothetical commercial buildings of 60.000 m^2 each, supposed to be located in China. The energy demand (heating, cooling and electricity) was estimated with the use of the simulation software EnergyPlus. The hourly trend over the reference year of heating, cooling and electricity demand was shown, but not much information was given on the parameters chosen for the building model. Since the buildings were fictitious a model calibration process was not required.

Pagliarini and Rainieri [48] modelled the TER of the University of Parma, in Italy, to assess the feasibility of coupling a CHP facility with a thermal energy storage (TES) to supply the demand. The authors calibrated a simple grey-box model taking into account the only losses through the building envelope by matching the annual consumption for the reference year. The authors concluded their study by suggesting an optimal storage size to reduce both the use of the auxiliary boiler and of the heat produced by the CHP and wasted to the environment. Since the annual heat demand was the only datum available to the authors, the performance of the presented building model on an hourly base could not be assessed.

Legorburu and Smith [44] combined physical and data-driven models to represent buildings' internal loads and thermal losses in a university campus. The authors relied on physical models to simulate the space conditioning technologies and used measured data to estimate the loads associated to the occupancy profiles and to the thermal losses through the building envelope. The scope of the method was to estimate the building performance allowing decision-makers to choose the best option for the HVAC system configuration. The collected data were gathered by building types to develop a design framework valid for similar buildings. The authors highlighted the challenges of using historical data (missing measurements, building specific information) as well as the benefits with respect to the whole-building energy model approach in forecasting the campus growth. Despite that the models employed to simulate the mechanical equipment were widely described, little information was given about the data-driven ones employed to estimate the building thermal loads. The performance of the latter was also not reported in the study.

Safaei et al. [49] proposed a method to identify the optimal investment planning and operating strategies of energy systems within commercial buildings. The aim was to propose solutions including cogeneration, solar and conventional energy sources with the constraint of satisfying all the energy demands (electricity, heating and cooling). The latter were estimated as a load duration curve calibrated on measured data. Electricity and thermal energy consumption profiles, available at respectively 15-minutes and hourly intervals, were employed to calibrate a model, representing the operation of the building during the project lifetime. Seven block-loads were defined for three seasons (high, mild and cold) meant to reproduce the reference year. The optimized variables included the different units size and their output for each season/block-load for cogeneration, thermal and cooling systems. The approach was verified on a hotel complex located in Coimbra, Portugal. The authors concluded that the long-term optimization model proposed was particularly effective for scenario analysis to minimize life-cycle costs while meeting the energy demand, but did not discuss the performance in estimating the latter.

Beccali et al. [50] developed a decision support tool for the selection of energy retrofit actions for non-residential buildings in South Italy. The approach consisted in combining extensive energy audits of 151 existing public buildings and gathering the information in a large data set. The latter was used to identify the best architecture and subsequently train an artificial neural network (ANN) model. The first model aimed at providing the current performance of non-residential buildings making use of a wide range of collected parameters related to climate, building structure and usage, type of HVAC system and energy consumption. The model was validated on 15% of the data which was neglected for the calibration phase. Results showed that the model reached a mean average error of 1.99 kWh/m^{3}year, which translates to 7% of the average value measured for the buildings (28.40 kWh/m^{3}year). The second ANN focused on assessing key economic indicators of different retrofit actions, based on obtainable energy performance, economic feasibility and payback time of different options. The output of the network was the cost of the retrofit action normalized per heated volume. An error of 0.012 €/m^3 was registered while the cost of the considered actions on average was of 5.681 €/m^3. The authors concluded that the most relevant retrofit actions to implement were the upgrade of the HVAC system, the improvement of transparent envelopes and lighting performances and the promotion of more advanced building management and automation systems. Both the ANN models showed very good performance at estimating demand and potential savings on an annual basis.

Table 1.1: Review of studies on model-based estimation of buildings' TER in the field of system design.

Study	Type of building	Aim of the work	Type of model	Calibration method[a]	Real case study	Data available[a]
Bornand et al. [46]	Hospital	Optimal energy system design	Grey-box	Linear regression	✓	Hourly energy consumption
Wen et al. [47]	Shopping malls, hotels, office	Optimal energy system design and operation	White-box	Simulation software	✗	NA
Pagliarini and Rainieri [48]	University campus	Simulation of CHP and optimal TES design	Grey-box	Direct comparison	✓	Annual energy consumption
Legorburu and Smith [44]	University campus	Best choice of HVAC	Black-box	NA	✓	Hourly heating, cooling and electricity consumption
Safaei et al. [49]	Hotels	Energy system design and operation	Black-box	NA	✓	Hourly heating and cooling demand and 15-min electricity consumption
Beccali et al. [50]	Non-residential[b]	Optimal retrofit action selection	Black-box	ANN	✓	Annual primary energy consumption
This work	Airport	Optimal energy system design	Grey-box	Linear regression/GA	✓	Hourly heating and electricity consumption

[a] NA: not available (not specified)
[b] Including schools, offices, sport, library, museum, university and research laboratories

To summarize, in the field of building thermal demand estimation, good results have been reached in modelling single residential buildings for which a deep knowledge of the design can be provided or for large cities, where errors and uncertainties often balance out. The current work aims at tackling the challenges of estimating the thermal power and temperature requirements of existing non-residential small and medium scale building blocks by developing and analysing different grey-box models. The latter are calibrated on measurements available. The presented literature review highlighted a scarcity of studies focusing on estimating the TER of complex buildings, within the scope of system design. In this case, most of the authors either rely on fictitious case studies or offer very little detail on the modelling approaches and the errors committed. Given the current gaps in the literature this chapter aims at answering the following research question:

How can the thermal energy requirements of existing, non-residential buildings be modelled for the integrated energy system design?

To tackle the latter challenge this chapter proposes different grey-box models, with increasing level of details, whose parameters are estimated through calibration, using linear regression techniques and GA. Given the quality of the data available, which aggregates different distribution systems (radiators and ventilation units), and the importance of the temperature requirements in sizing the future energy system, an effort is made to distinguish between the heat load supplied by static appliances and the one supplied by the ventilation units. Moreover, the possibility of reducing the supplied temperature to each space conditioning technology is assessed. Finally, modelling errors arising from the calibration with measurements obtained over different time resolutions are compared. Moreover, the additional error generated by relying on the clustering process to represent the system operation is also assessed. In addition, suggestions on how to estimate the thermal demand for DHW and space cooling, still based on the available measurements, are included.

The work presented in this chapter has been carried out in collaboration with an international airport, during the wider project framework of offering assistance during their transition from a fossil-based energy system to a low-temperature network (LTN). Due to confidentiality clauses all results showed throughout the chapter are normalized.

1.3 Application

As reported in the previous section, the methods presented in this chapter aim at estimating the TER of complex buildings. An international airport, located in Central Europe, is chosen as case study to validate the proposed models. Since modelling choices depend on the type and quality of the data available, before presenting the methods, for the sake of clarity and to introduce the nomenclature later used in this chapter, a brief explanation of the application is offered in this section.

The site, represented in Fig. 1.5, accounts for 20 buildings, spread across a distance of 4 km, for a total of 500’000 m^2 of surface.

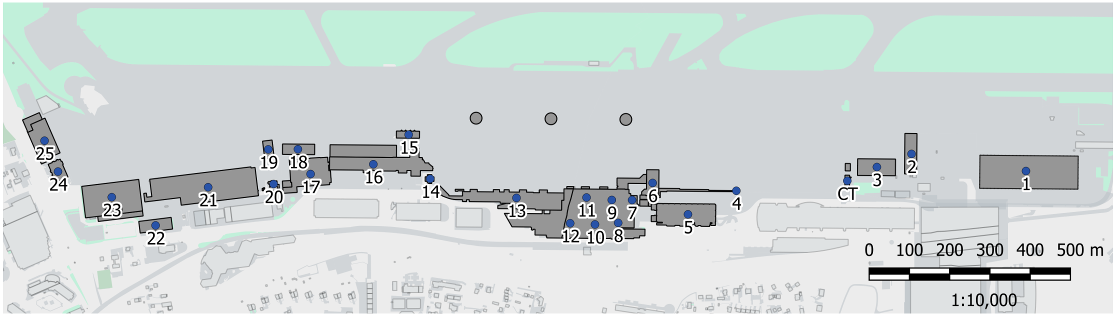

Figure 1.5: Map of the international airport. Buildings are represented in grey, substations are shown in blue and defined by cardinal numbers, central heating station labeled as “CT”.

The current energy system on the site relies on oil-fired BOIs combined with a bi-level distribution network to supply the buildings’ heating demands. The primary network delivers water at around 80°C from the central heating station to the multiple substations on the site, represented as blue dots in Fig. 1.5. Two-way valves, controlled by the principle of a heat curve, govern the mass flow rate delivered to the substations, whereas the circulating pump and pressure sensor on the primary network ensure that the pressure difference remains around the predefined set-point. The substations represent the link between the primary network and the secondary side, comprising the different space conditioning technologies supplying the various buildings’ zones. Figure 1.6 represents an example of a substation, where two heat exchangers (HEX), positioned in parallel deliver the heat to the final end-users thorough a collector. The latter, supplies the space conditioning technologies with the same temperature, which is finally adjusted by a three-way valve, following the principle of a heat curve.

Measurements at the substations, when available, refer to the conditions at the collector and include the delivered heat load, supply and return temperatures and mass flow rate. These measurements were recorded in the platform currently used for the control of the network and relative infrastructure and were made available by the company in charge of the network operation. In this chapter, substations are treated as standalone buildings, neglecting the influence that each zone naturally has on the neighboring ones. In reality, exchanges of air flow and people’s movements among buildings’ zones impact the heat loads. Aggregating the substations at the building level would ease the calibration process. However, this approach would not provide enough detail for the energy system design: equipment, such as decentralized HPs, are likely to be installed at the substation level and therefore their sizing and operation depends on the heat loads of the substation.

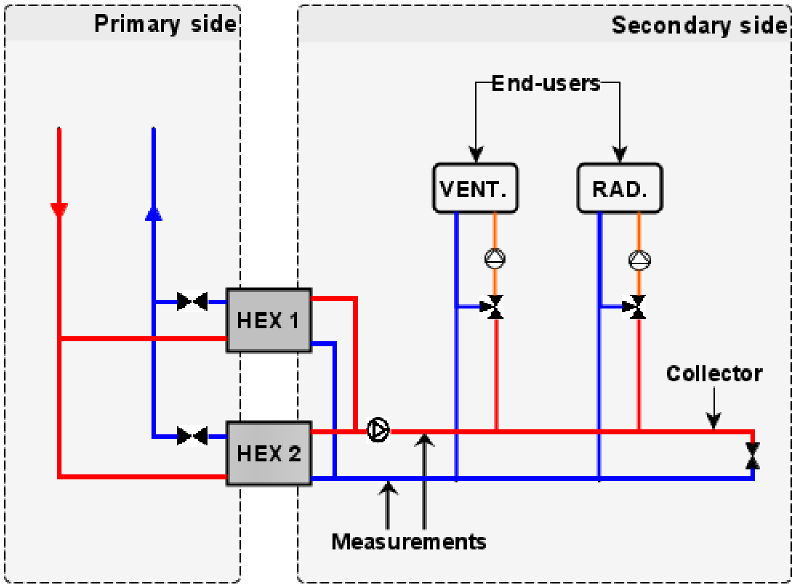

Figure 1.6: Schematic representation of a generic substation including two end-users: a ventilation unit and a radiator.

1.4 Space heating requirements

Figure 1.7 shows a schematic of a building with the main contributions to the heat balance. The latter, in a single nodal approach, can be written as reported in Eq. 1.1:

$$C \cdot \frac{\mathrm{d}T^{int}}{\mathrm{d}t} = \dot{Q}_t^{rad} + \dot{Q}_t^{vent} + \dot{Q}_t^{pl} + \dot{Q}_t^{el} + \dot{Q}_t^{irr} - \dot{Q}_t^{loss} \tag{1.1}$$

where:

- C is the building thermal capacity;
- $\mathrm{d}T^{int}/\mathrm{d}t$ is the variation of the internal temperature inside the room;
- $\dot{Q}_t^{rad}$ is the heat load supplied by the radiation units;
- $\dot{Q}_t^{vent} = \dot{m}_t^{air} \cdot c_p^{air} \cdot (T_t^{int} - T_t^{air})$ is the heat load supplied by the ventilation units to compensate the losses due to the air renewal, dependent on the mass flow rate of air $\dot{m}_t^{air}$ and the difference between the internal temperature and the one af the air flow T_t^{air}, which might be greater than the external ambient temperature due to heat recovery on the air flow extracted from the building zone;
- $\dot{Q}_t^{pl}$ represents the internal gains generated by the occupants.
- $\dot{Q}_t^{el}$ stands for the internal gains due to the use of lights and other electric appliances;

- $\dot{Q}_t^{irr}$ represents the solar gains due to the global horizontal irradiation (GHI) and to the transmittance of the glazed surfaces;
- $\dot{Q}_t^{loss} = U \cdot A_e \cdot (T_t^{int} - T_t^{amb})$ includes the thermal losses through the building envelope, driven by the difference between the internal temperature T_t^{int} and the external one T_t^{amb}, depending on the heat transfer coefficient U and the envelope surface A_e.

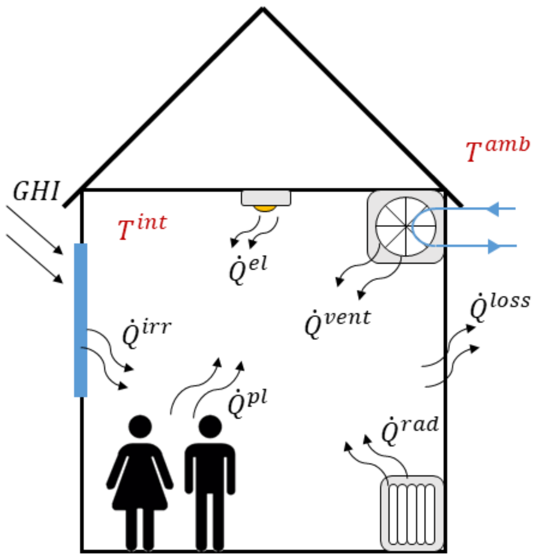

Figure 1.7: Generic building schematic with main contributions to the heat balance.

In steady state, which implies no changes in the internal temperature, the balance shows the equivalence between the load supplied by the heating systems and the contribution of internal gains with the losses through the building envelope.

In this chapter, first different grey-box steady state models, taking into account gradually each of the contributions to the building thermal balance, are developed and compared. The validity of those models is verified on the hourly measurements, when available. Secondly, for the buildings for which measurements are available at monthly and yearly time intervals, simplified models are developed and tested.

1.4.1 Hourly measurements

If hourly measurements of the heat loads are available, the developed method to estimate the heat loads at the substations comprises different steps: 1) identification of the influential parameters, 2) cleaning of the measurements, 3) definition of the grey-box models, 4) calibration process, 5) identification of the typical periods of operation, 6) estimation of the errors. The inputs to the methods are represented by the hourly measurements and the attributes used in the thermal models and for the clustering process: ambient temperature, GHI, buildings' electric consumption, buildings' occupancy profiles, daily number of passengers, summer/winter and day/night operation. The outputs of the process are the tuned parameters for the thermal model chosen and the typical periods of operation. Figure 1.8 shows a schematic of the method.

Identifying the influencing parameters

To identify the parameters influencing a specific trend is never a straight forward process. In this study, the Pearson coefficient is employed to assess the linear correlation between two time series. In particular, as shown in Eq. 1.2, the coefficient expresses the ratio between the covariance of the two variables divided by the product of their standard deviation. Therefore the resulting parameter is a normalized covariance bounded between -1 and 1.

$$\pi_{X,Y} = \frac{\mathrm{cov}(X,Y)}{\sigma_X \sigma_Y} \tag{1.2}$$

In the above formulation $\pi_{X,Y}$ represents the Pearson coefficient among the two variables X and Y, while σ_X and σ_Y are respectively the standard deviation of the first and second variable. A positive value of the Pearson coefficient underlines a direct linear correlation between the two variables, while a negative one shows an inverse correlation. The closer the value is to -/+ 1, the stronger the correlation. Figure 1.9 shows the Pearson coefficient calculated for each substation between the measured heat load profile and different potential influencing parameters.

Fig. 1.9 highlights that the attribute influencing the most the heat demand is the ambient temperature and as expected the two profiles are inversely correlated, meaning that the higher the temperature the lower the building heat demand. Another parameter showing the same effect for all the substations is the solar irradiation, responsible of the generation of solar gains. All the other parameters are correlated to the heat load in different ways depending on the usage of the associated buildings (e.g., hangars, offices, waiting halls, etc.). Electricity profiles and internal gains (estimated as reported in Eq. 1.7), contrarily to what expected, seem to be directly correlated with the heat demand for most of the buildings, while the number of passengers[1] seems not having any influence. Due to the different behaviors showed by each substation, all the parameters are gradually taken into account in different building models. The choice of including each parameter is finally the result of the calibration process.

Pre-processing the measurements

The first common step when employing measured data for model calibration is to pre-process the measurements making sure that measuring errors do not affect the calibration process. The following actions are performed on the measurements:

[1] To correlate the heat load profiles available at an hourly time interval and the number of passengers defined for each day, consumption data have been re-sampled in a daily time resolution.

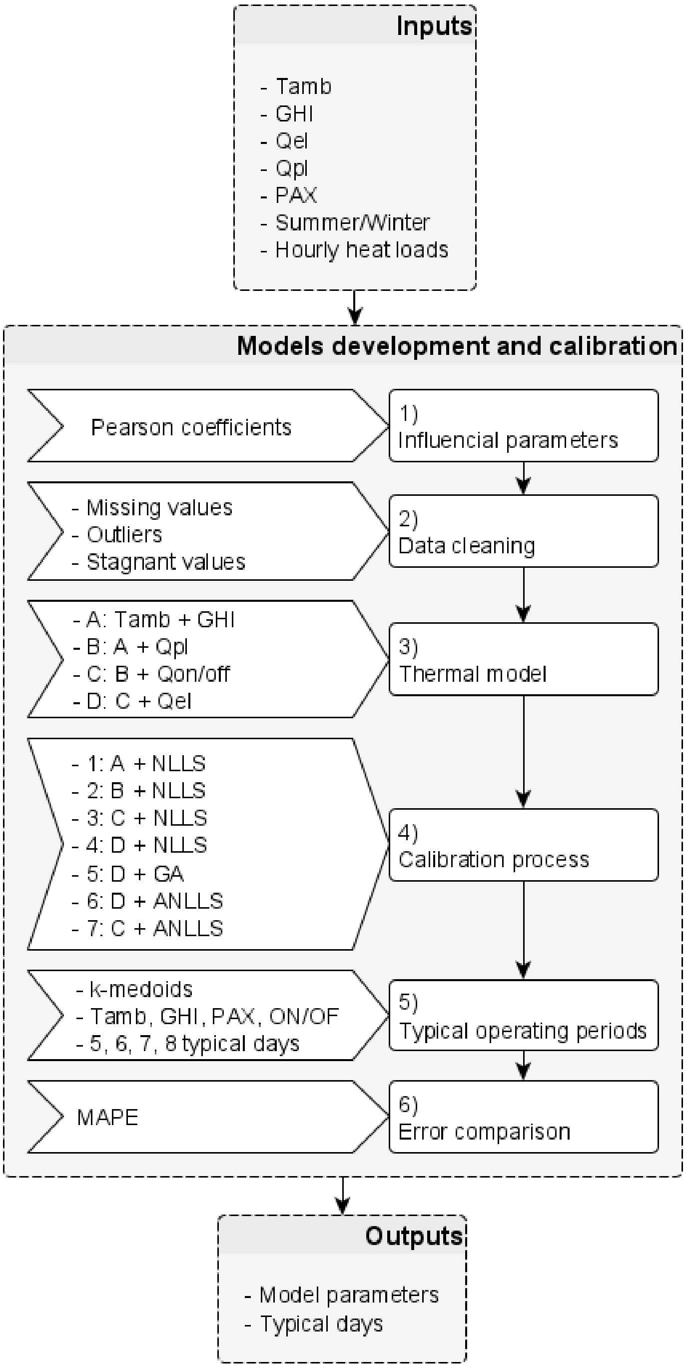

Figure 1.8: Flowsheet of the proposed method for the development and calibration of thermal models based on hourly measurements. NLLS: non-linear least square, GA: genetic-algorithm, ANLLS: advanced non-linear least square.

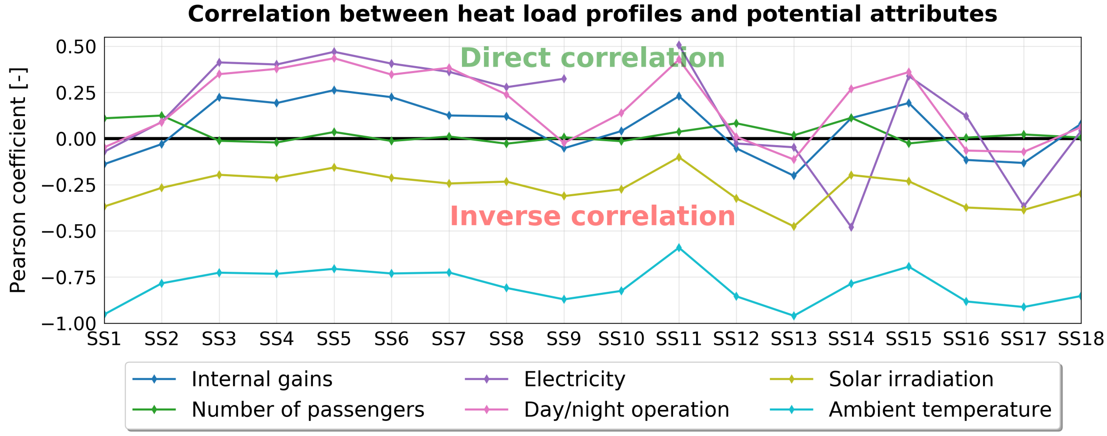

Figure 1.9: Pearson coefficient between heat load profiles of each substation (SS1 to SS18) and different potential influencing parameters.

- missing values are replaced by linear interpolation;
- stagnant values for more than a day are removed;
- values during summer (period in which the heating system is switched-off) are removed and not considered during the calibration;
- outliers are removed (see below for definition) and replaced by a rolling average with 24 hours time window;
- to calibrate the model, the longest sequence of consecutive measurements, not including any missing value, is employed. Errors reported in this chapter for the model validation refer to the overall profile, including both the calibration and validation sets. In this way the errors include the performance of the model in both reproducing the original demand under the same conditions used during the calibration process and estimating the output under new circumstances. Moreover, this choice allows to ease the comparison between the errors generated by including the clustering process.

Outliers are detected using the Tukey's definition [51], based on the inter quartile range (IQR), that is the difference between the upper and lower quartile ($IQR = Q_3 - Q_1 = P_{75} - P_{25}$). Following the original definition, the IQR is enlarged by a factor 1.5, as reported in Eq. 1.3.

$$Q_3 + 1.5 \cdot IQR < \tilde{y}_i < Q_1 - 1.5 \cdot IQR \tag{1.3}$$

Building thermal models formulation

All the models presented in this section to estimate the space heating demand as a function of different input parameters are developed as linear models. The calibration of the models' parameters is based on the minimization of the error between the output of the model and the measured power profile. Equation 1.4 represents a generic formulation of the minimization function for the calibration process:

$$\min_{\pi_i} \frac{\sum_{t=1}^{N_t} |\tilde{y}_t - \sum_i \pi_i x_i|}{N_t} \tag{1.4}$$

where:

- N_t is the number of observations;
- $\tilde{y}_t$ is the measured heat load during the timestep t;
- π_i are the model's parameters tuned by the calibration process;
- x_i are the model's attributes

Model A The simplest model includes a linear dependency on the ambient temperature and solar irradiation, as shown in Eq. 1.5:

$$\dot{Q}^{H}_{s,t} = \pi^{loss}_s \cdot (T^{set}_t - T^{amb}_t) + \pi^{vent}_s \cdot (T^{set}_t - T^{amb}_t) \cdot y^{day}_t \cdot (1 - \eta^{vent}) - \pi^{irr}_s \cdot GHI_t \qquad \forall\ t \in \mathbf{T}, \forall\ s \in \mathbf{SS} \tag{1.5}$$

where:

- $\mathbf{T}$ is the set of the time steps t;
- $\mathbf{SS}$ is the set of the substations s;
- T^{set}_t, shown in Fig. 1.10 is the set point for the internal temperature, assumed as a step function: 21°C during the day (5:00 - 22:00) and 16°C at night (23:00-4:00)[2];
- T^{amb}_t is the external ambient temperature in [°C];
- y^{day}_t is a parameter equal to 1 during daily hours and to 0 in the night;
- η^{vent} is the heat recovery rate of the ventilation units, assumed as 70%;
- GHI_t is the GHI expressed in [W/m^2].

The coefficients π^{loss}_s, π^{vent}_s and π^{irr}_s are estimated by minimization of the error between the measured data and model results in each substation. They represent the parameters to tune respectively the losses through the building envelope, the losses due to the air renewal and the solar gains.

[2]The internal temperature at steady state is considered to be equal to the one defined by the set-point, assuming an ideal operation of the control system.

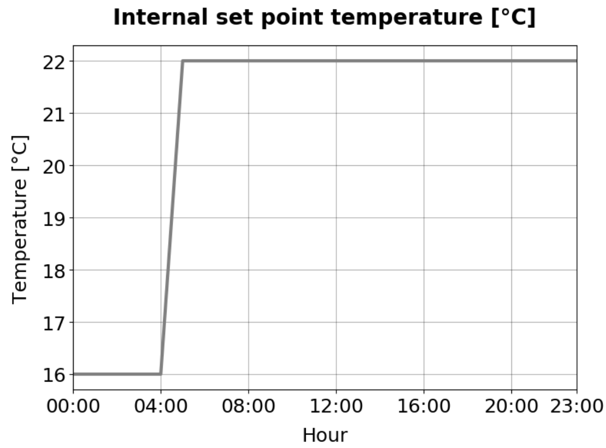

Figure 1.10: Daily profile of the internal set-point temperature

Model B The first extension to the model consists in taking into account the internal gains due to the occupants, modifying Eq. 1.5 into Eq. 1.6 as follows:

$$\dot{Q}^{H}_{s,t} = \pi^{loss}_{s} \cdot (T^{set}_{t} - T^{amb}_{t}) + \pi^{vent}_{s} \cdot (T^{set}_{t} - T^{amb}_{t}) \cdot y^{day}_{t} \cdot (1 - \eta^{vent}) - \pi^{irr}_{s} \cdot GHI_{t} - \pi^{pl}_{s} \cdot \dot{Q}^{pl}_{t,b}$$
$$\forall\ t \in \mathbf{T}, \forall\ b \in \mathbf{B}, \forall\ s \in \mathbf{SS} : s \in \mathbf{S_b} \quad (1.6)$$

where:

- $\mathbf{B}$ represents the set of buildings b and $\mathbf{S_b}$ the set of substations belonging to the building b;
- π^{pl}_{s} is an additional parameter subject to the calibration to take into account the internal gains due to the presence of the people;
- $\dot{Q}^{pl}_{t,b}$ represents a normalized daily profile estimated for each building to account for the people's presence.

The daily profile $\dot{Q}^{pl}_{t,b}$ is estimated for each building relying on the information of the activities thereby carried on and the occupancy profiles defined by the national standards [52]. Fourteen types[3] of activities are selected among the typical ones proposed by the standards and the final occupancy profile is evaluated as a weighted average, in which the weights are the percentages of building surface devoted to each activity as reported in Eq. 1.7.

$$\dot{Q}^{pl}_{t,b} = \sum_{a} w^{a}_{b} \cdot \dot{q}^{a}_{t} \cdot \phi_{a} \qquad \forall\ t \in \mathbf{T}, \forall\ b \in \mathbf{B}, \forall\ a \in \mathbf{A_b} \quad (1.7)$$

[3] In case of mismatch between the value of the total surface for each building and the sum of the surfaces for which a type of activity is specified, the difference is labeled as "Unknown" and neglected during the weighted average to estimate the occupancy profile.

In Eq. 1.7, w_b^a represents the share of the surface of building b devoted to the activity a, ϕ_a is the modified normalized occupancy profile assigned to the activity a and $\dot{q}_t^a$ is the generated heat load per unit of surface associated by the standards to the relative activity. The original standard profiles are slightly modified to take into account specific characteristics of the application (e.g., change in opening and closing hours with respect to standard activities).

Figure 1.11 shows the amount of surface in each building devoted to the different activities. The values are normalized with respect to the total surface of the largest building. Due to the

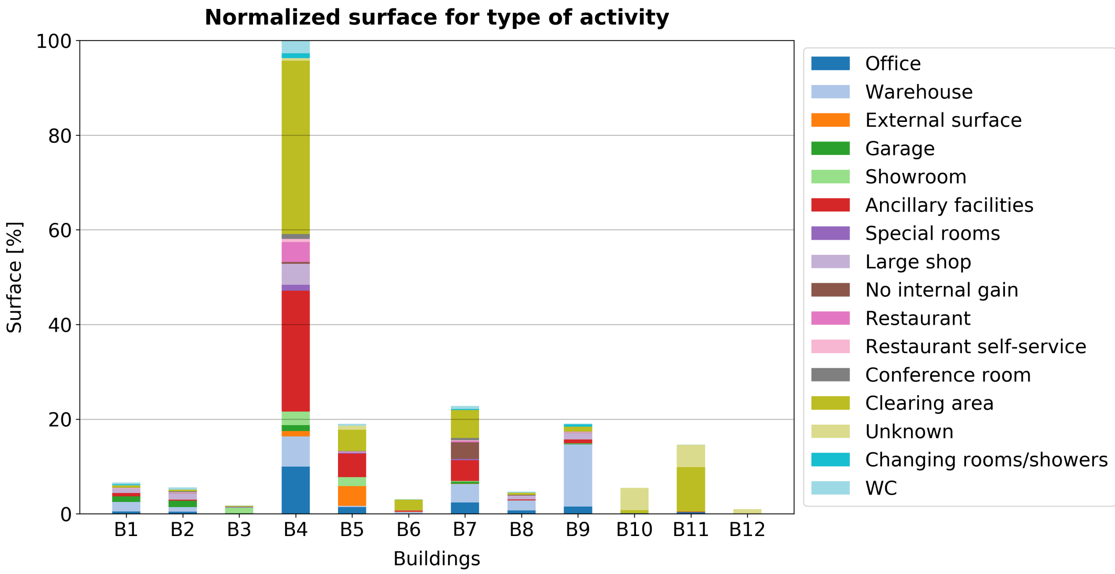

Figure 1.11: Amount of surface devoted to the different activities in each building. Values normalized with respect to the largest building surface.

significant difference in buildings size, to better visualize the share of the different activities in each building, Fig. 1.12 shows the same values reported in the previous figure, but normalized with respect to the total surface in each building.

Substations belonging to the same building are assigned the same occupancy profile since no information is available on which zone of the building is covered by each substation. The daily profile due to the presence of people is supposed to be the same for each day of the year.

Model C The following extension to the model aims at catching the effects of the building inertia, mostly visible at the ramp-up and ramp-down during the opening and closing hours.

$$\dot{Q}_{s,t}^{H} = \pi_s^{loss} \cdot (T_t^{set} - T_t^{amb}) + \pi_s^{vent} \cdot (T_t^{set} - T_t^{amb}) \cdot y_t^{day} \cdot 1 - \eta^{vent} - \pi_s^{irr} \cdot GHI_t - \pi_s^{pl} \cdot \dot{Q}_{t,b}^{pl} + \sum_{h=5:00}^{h=6:00} \pi_{s,h}^{ON} \cdot y_t^{ON} - \sum_{h=22:00}^{h=00:00} \pi_{s,h}^{OFF} \cdot y_t^{OFF}$$

$$\forall\ t \in \mathbf{T}, \forall\ b \in \mathbf{B}, \forall\ s \in \mathbf{SS} : s \in \mathbf{S_b} \quad (1.8)$$

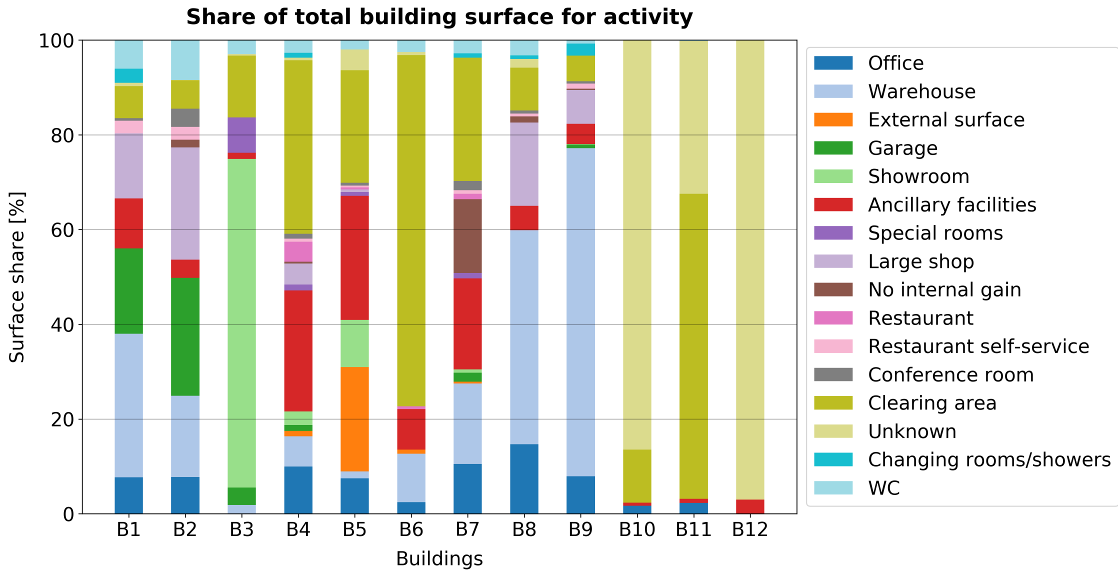

Figure 1.12: Share of surface devoted to the different activity in each building.

To do so, five new parameters are introduced: $\pi^{ON}_{s,h=5:00}$ and $\pi^{ON}_{s,h=6:00}$ to take into account the ramp-up in the morning due to the shift between the night and daily operation and three in the night ($\pi^{OFF}_{s,h=22:00}$, $\pi^{OFF}_{s,h=23:00}$, $\pi^{OFF}_{s,h=00:00}$) to catch the opposite behavior. The different contributions are activated by a parameter equal to 1 only during the respective hour. The choice of the hours is the result of analyses on the measured data. The observed behavior is due to the presence of a set-back at night for the internal set-point temperature and the switch-off of the ventilation units, combined with the building inertia.

Model D This model includes the electricity consumption profiles, available at the building level, to take into account the internal gains due to the electric equipment as well as an alternative solution to include the presence of the people (which is highly correlated to the usage of electric equipment [53]). The underlying equation is reported in Eq. 1.9.

$$\dot{Q}^{H}_{s,t} = \pi^{loss}_{s} \cdot (T^{set}_{t} - T^{amb}_{t}) + \pi^{vent}_{s} \cdot (T^{set}_{t} - T^{amb}_{t}) \cdot y^{day}_{t} \cdot (1 - \eta^{vent}) - \pi^{irr}_{s} \cdot \dot{Q}^{irr}_{t} - \pi^{pl}_{s} \cdot \dot{Q}^{pl}_{t,b} + \sum_{h=5:00}^{h=6:00} \pi^{ON}_{s,h} \cdot y^{ON}_{t} - \sum_{h=22:00}^{h=00:00} \pi^{OFF}_{s,h} \cdot y^{OFF}_{t} - \pi^{el}_{s} \cdot \dot{E}^{el}_{b}$$

$$\forall\ t \in \mathbf{T}, \forall\ b \in \mathbf{B}, \forall\ s \in \mathbf{SS} : s \in \mathbf{S_b} \quad (1.9)$$

The additional parameter subject to the calibration π^{el}_{s} aims at estimating the internal gains due to the use of the electric equipment while $\dot{E}^{el}_{b}$ is the daily profile of the electricity consumption in each building. The latter is estimated from the hourly profile of electric consumption, averaged to get a daily trend applied to each day of the year. Figure 1.13 shows the measurements of the electricity consumption over one year, for the largest building, while Fig. 1.14 reports the average daily profile (solid black line), together with the IQR of the distribution for each hour (grey zone). In the legend the mean absolute percentage error (MAPE) error is reported (definition in Eq. 1.10).

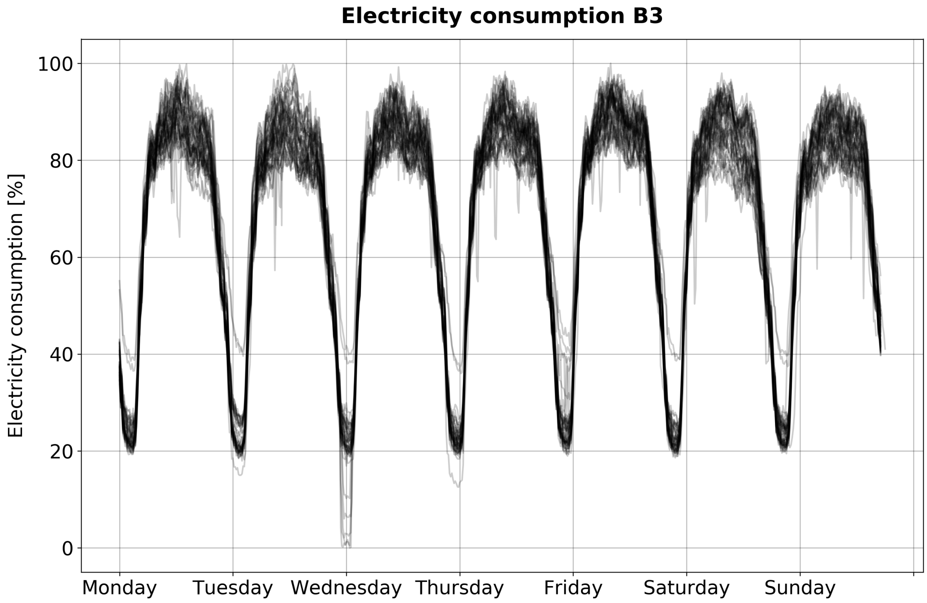

Figure 1.13: Weekly normalized profile of the electricity consumption for building B3 over one year of operation.

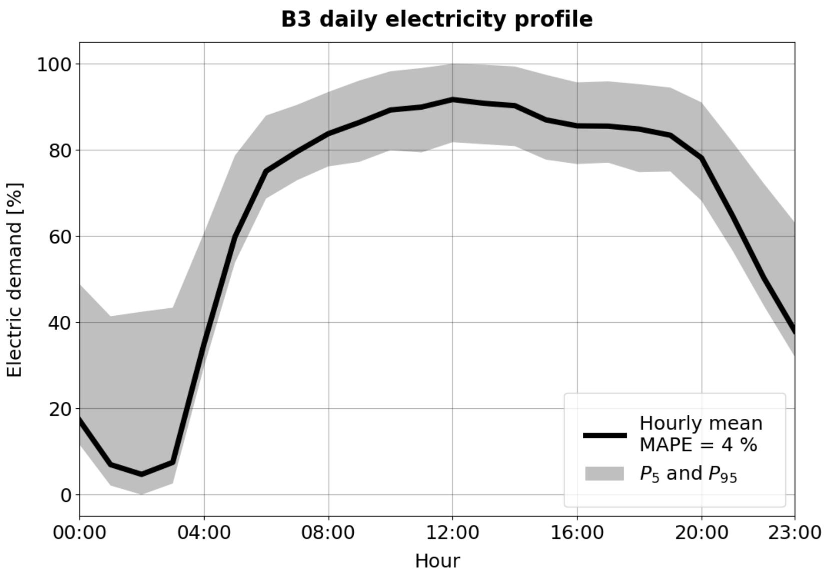

Figure 1.14: Normalized average daily profile of the electricity consumption for building B3 (black line) and IQR for each hour (grey zone) over one year of operation.

As previously done for the profile of the internal gains, given that the electricity consumption is only available at the building level, the same profile is assigned to all substations belonging to the same building.

Calibration strategy and choice of the thermal model

The model parameters are calibrated by minimizing the error between the model results and the original profiles. Different Python libraries are employed to tune the model parameters, as reported in Table 1.2.

Table 1.2: List of thermal models and calibration strategies adopted.

Model identifier	Thermal model	Fitting strategy	Python library
Model 1	Model A	Non-linear least squares	*scipy.optimize.curve_fit*[a]
Model 2	Model B	Non-linear least squares	*scipy.optimize.curve_fit*[a]
Model 3	Model C	Non-linear least squares	*scipy.optimize.curve_fit*[a]
Model 4	Model D	Non-linear least squares	*scipy.optimize.curve_fit*[a]
Model 5	Model D	Genetic algorithm	*platypus.NSGAII*[b]
Model 6	Model D	Advanced non-linear least square	*LMFIT.minimize*[c]
Model 7	Model C	Advanced non-linear least square	*LMFIT.minimize*[c]

[a] Further information available at https://docs.scipy.org/doc/scipy/reference/generated/scipy.optimize.curve_fit.html
[b] Further information available at https://platypus.readthedocs.io/en/latest/index.html
[c] Further information available at https://lmfit.github.io/lmfit-py/index.html

Two types of errors are investigated to define the performance of the models. The MAPE, reported in Eq. 1.10 aims at defining the capability of the model in reproducing the hourly profile[4], whereas the annual percentage error (APE), shown in Eq. 1.11, defines the difference in terms of yearly values (energy consumption).

$$MAPE = \frac{\sum_{t=1}^{N_t} |\tilde{y}_t - \sum_i \pi_i x_i|}{\sum_{t=1}^{N_t} \tilde{y}_t} \tag{1.10}$$

$$APE = \frac{|\sum_{t=1}^{N_t} \sum_i \pi_i x_i - \sum_{t=1}^{N_t} \tilde{y}_i|}{\sum_{t=1}^{N_t} \tilde{y}_t} \tag{1.11}$$

The errors are calculated on the entire yearly profile, to investigate the performance of each model in both 1) reproducing the original demand under the same conditions used to train the models (the calibration set) and 2) estimating the demand under different circumstances (validation set). Figure 1.15 shows the MAPE and APE errors for each model and substation. In each graph the weighted average among substations is also calculated by using as weights the measured annual energy demand.

The graph shows similar errors between the different thermal models and calibration proce-

[4]To avoid errors due to null measurements, the original definition of the MAPE is slightly modified into a weighted mean absolute percentage error.

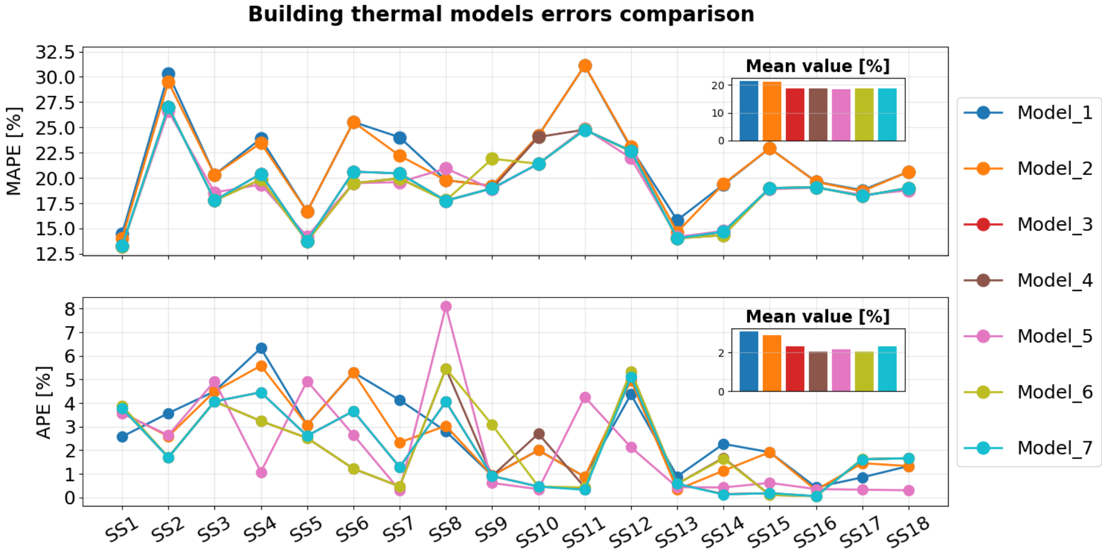

Figure 1.15: MAPE and APE errors calculated for each model and substation and weighted average values.

dures. The only remarkable improvement is registered by including parameters to take into account the thermal inertia of the building and the set-back during the night. In terms of MAPE all models show an averaged error below 22%, with *Model 3*, *Model 4*, *Model 5*, *Model 6* and *Model 7* having the same performance. In relation to the APE, all models are characterized by an average error below 3% and *Model 4* appears as the most efficient.

Definition of typical periods of operation

Due to the intrinsic complexity of problems dealing with the design and operation of urban energy systems, it is common practice to apply techniques aimed at reducing the problem size, hence the number of variables involved. Therefore, a set of typical and extreme periods of operations are defined to represent the conditions that the system will face during the project lifetime.

As reported by Stadler [54], a first reduction is justified by the dominant importance of the seasonal and daily cyclicity over the variation among consecutive years, which allows the use of a single yearly profile over the entire equipment lifetime, passing from $20^{\text{year}}\text{x}8760^{\text{hour}}$ to $1^{\text{year}}\text{x}8760^{\text{hour}}$ time steps. In this study, the year 2018 is taken as the reference, period for which most of the measurements are available. To further reduce the problem complexity an additional data clustering is performed on the yearly profile, aiming at defining the final typical periods of operation. In this study the k-medoid approach presented by Stadler [54] is applied. The method consists in first identifying the attributes influencing the system operation the most (i.e. ambient temperature), then normalizing their yearly profiles and finally selecting specific days from the original data set based on an objective function and attributing to them the remaining observations. The objective is chosen such as to minimize the intra-clusters distance and maximize the inter-clusters one, that means having clusters as compact as possible and as distinct as possible. In a nutshell, this method allows to identify clusters of days, having similar values for each attribute and to define for each cluster the representative day. If, for example, 7 typical days are chosen, then the number of time steps is reduced from $1^{year}x356^{day}x24^{hour}$ to $1^{year}x7^{day}x24^{hour}$. To each of the typical days, a frequency of occurrence is assigned, equal to the number of days represented by the cluster medoid.

In this study four options for the number of clusters are investigated: results based on 5, 6, 7 and 8 typical operating periods are compared. The upper and lower bounds are chosen, based on experience, to allow an effective representation of the yearly profile, but at the same time, to limit the complexity of the arising system design problem. All the options are compared in terms of the performance of the thermal model in reproducing the original hourly profile when applied to the different k-medoids. Figure 1.16 shows the MAPE error generated by applying the different models to the 5, 6, 7 and 8 typical days. The latter are found by the k-medoid approach including among the attributes ambient temperature, solar irradiation, daily number of passengers and winter/summer operation. The weighted average among the different substations for seven typical periods is also shown in the graph.

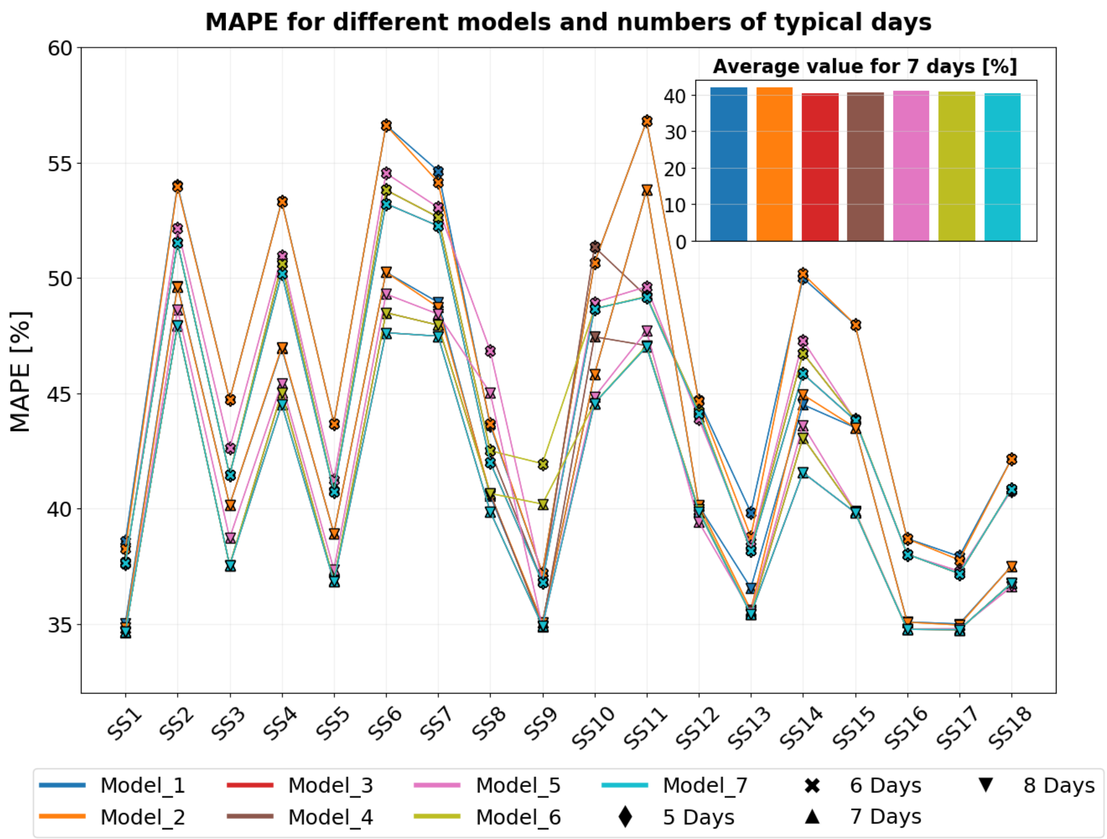

Figure 1.16: Comparison of MAPE errors of different thermal models applied to 5, 6, 7 and 8 typical days.

The comparison between Fig. 1.15 and Fig. 1.16 highlights that the clustering approach deteriorates, as expected, the MAPE, by doubling its value. An improvement is registered by using 7 typical periods with respect to 6, whereas adding a new one does not bring any benefit in terms of error. As previously, all the models show similar performance, with *Model 3* and *Model 7* achieving the lowest average error of 40.3%.

Therefore, seven typical days are finally adopted to represent the system operation. Figure 1.17 shows the sequence over the year of the operating typical periods and the daily mean ambient temperature profile. The list of days of the year chosen as representative of each cluster (k-medoids) is reported in Table A.4, whereas Table A.1 lists the error generated by *Model 7*, taken as the representative one, including the clustering process.

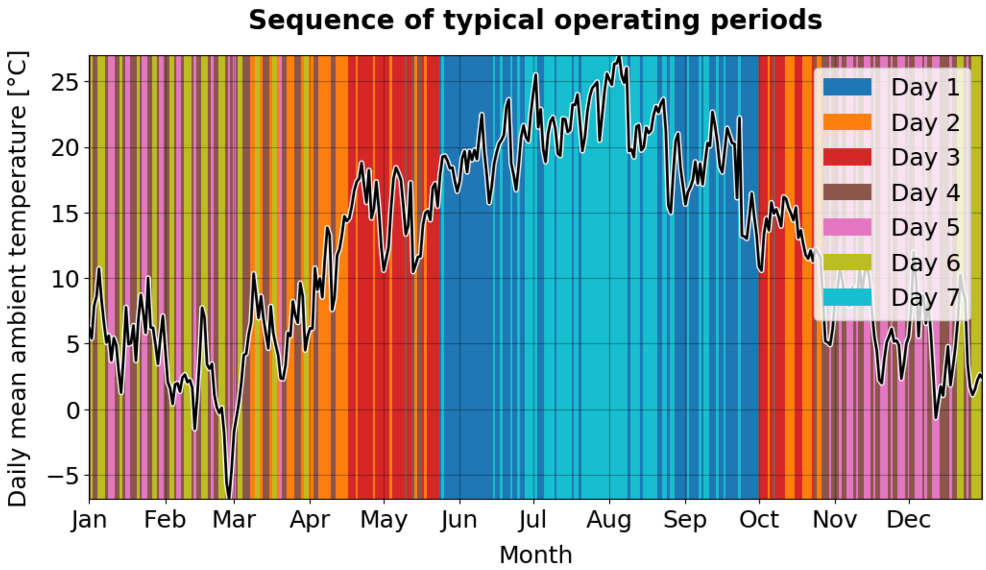

Figure 1.17: Sequence of typical operating periods over the representative year and daily mean ambient temperature profile.

An additional analysis to estimate the performance of the thermal model is to compare the result of the model applied to the original medoids of the attributes with the distribution of the original days belonging to the same cluster. Figure 1.18 shows the results of this analysis for *Model 7* relative to one substation and one typical day. The graph highlights how the result of the model for this specific substation and typical operating period perfectly falls within the distribution of the original profiles belonging to the same cluster (the light grey lines represent the original measured power profiles in all the days of the year represented by the 5th typical operating period). The dark green surface shows the area defined by one standard deviation from the median (median +/- σ), while the light green area the IQR. The solid black line is the original profile of the k-medoid (the power recorded during the day representative of the 5th cluster). Figure 1.19 shows the same representation for substation SS14 and the 4th typical operating period.

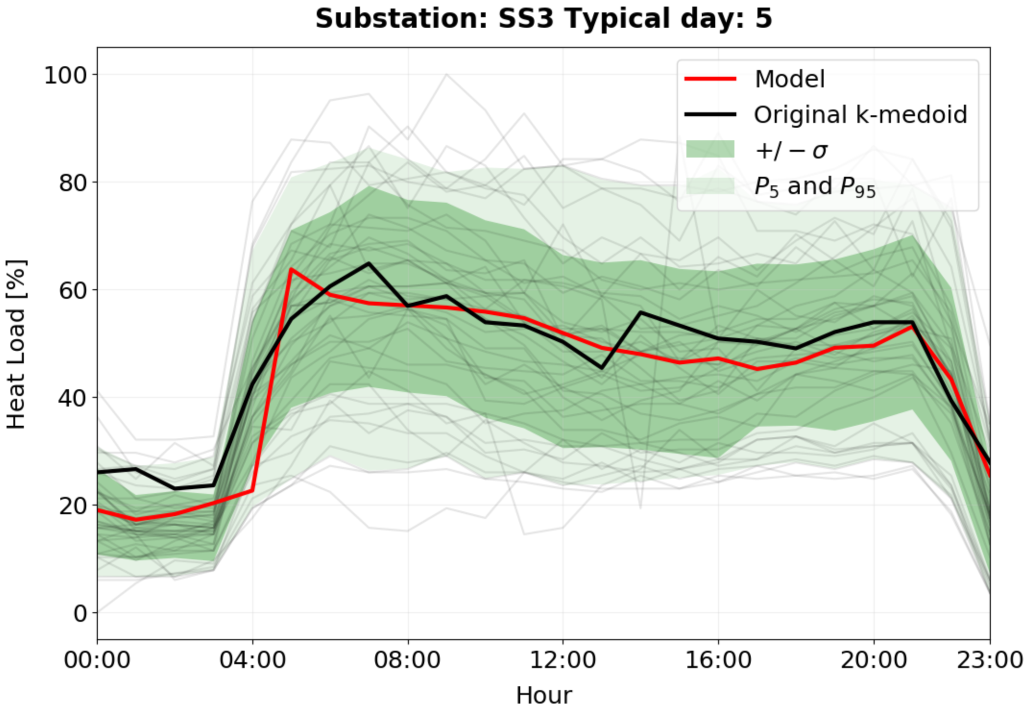

Figure 1.18: Results of "Model 7" for substation SS3 and the 5th typical operating period (red line) compared to the original k-medoid (black line) and original profiles corresponding to the days belonging to the cluster (single profiles in light grey and statistics of the distribution in green). All values normalized.

This latter case shows an example in which the result of the model perfectly falls within the distribution of the original profiles it is meant to represent, whereas the original k-medoid has null values, due to missing measurements. This example shows a case in which reconstructing the original profile by relying on the original measurements of the k-medoid would generate large errors, since all the underlying grey lines would be represented by a null profile. The use of a thermal model in this case allows to cope with measuring errors.

1.4.2 Monthly measurements

In the case that the recorded measurements of power delivered by the substations are available with a monthly frequency instead of the hourly resolution, the thermal model employed must be modified. Thus, a simpler heating signature is fitted on the monthly data to estimate the threshold temperature ($T_s^{tr,H}$) and the curve parameters ($k_s^{1,H}$, $k_s^{2,H}$). The former, also defined as cut-off temperature, is the value of ambient temperature beyond which the heating system is switched-off. Figure 1.20 shows a schematic of the developed method. Inputs to the process are the monthly heat loads, the ambient temperature and the typical periods of operation. The outputs comprise the models parameters and the cut-off temperature for each substation. Figure 1.21 shows the piecewise linear interpolation for substation SS20.

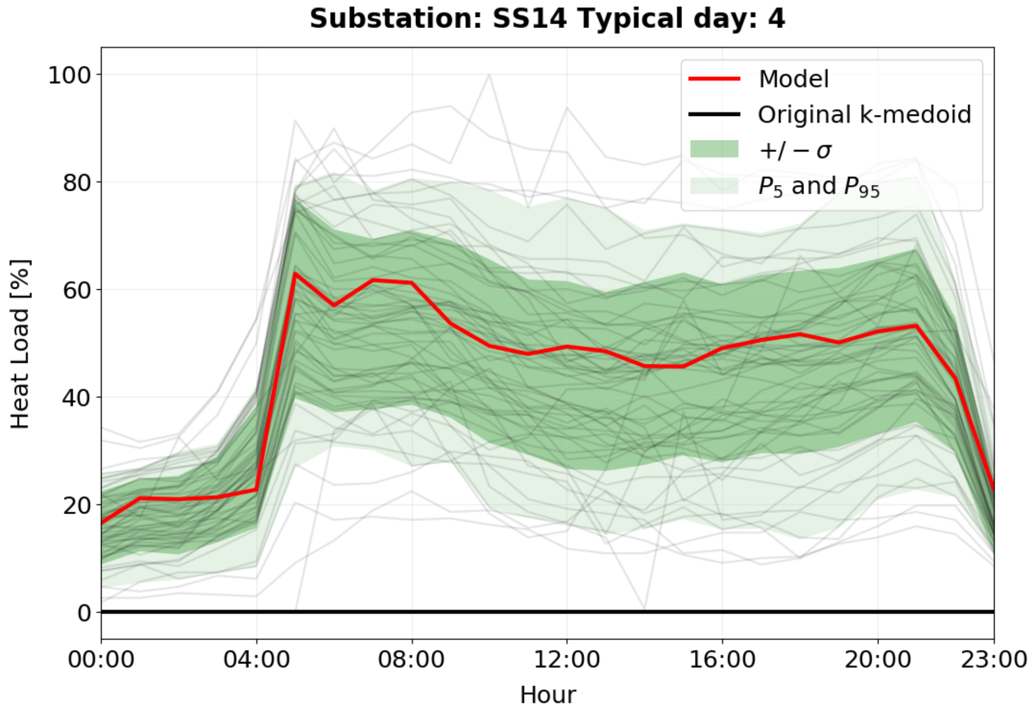

Figure 1.19: Results of “Model 7” for substation SS14 and the 4th typical operating period (red line) compared to the original k-medoid (black line) and original profiles corresponding to the days belonging to the cluster (single profiles in light grey and statistics of the distribution in green). Values normalized.

Once the heating signature parameters are estimated, to define the hourly profile of the heat load, Eq. 1.12 is employed.

$$\dot{Q}^{H}_{s,t} = \begin{cases} k^{1,H}_{s} \cdot T^{amb}_{t} + k^{2,H}_{s} & \text{if } T^{amb}_{t} < T^{tr,H}_{s} \\ 0 & \text{otherwise} \end{cases} \qquad \forall t \in \mathbf{T}, \forall s \in \mathbf{SS} \quad (1.12)$$

The errors committed by estimating the demand based on the monthly measurements and the corresponding threshold temperatures are reported in Table A.2.

1.4.3 Yearly measurements

In the case that the recorded measurements are solely available on a yearly basis, as for the previous case, a heating signature approach is applied. However, with a unique measurement the threshold temperature must be assumed. Figure 1.22 shows the schematic of the process, very similar to the previous one, with the difference that the calibration process is based on the equivalence of the yearly heat load ($Q^{H,yr}_{s}$), as suggested by Girardin [33] and reported in

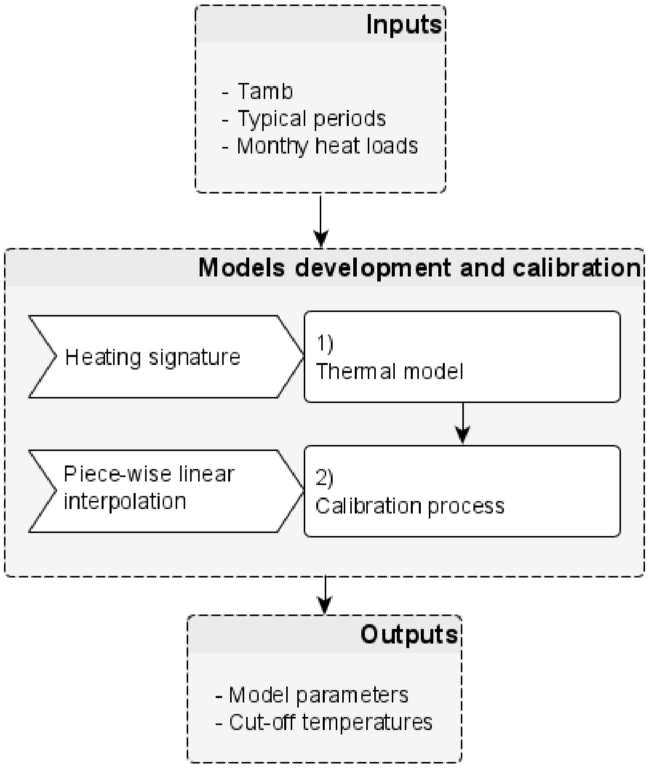

Figure 1.20: Flow sheet of the proposed method for the development and calibration of thermal models based on monthly measurements.

Eq. 1.13:

$$\begin{cases} k_s^{1,H} & = \dfrac{Q_s^{H,yr}}{\int\limits_{yr:T_t^{amb}<T_s^{tr,H}} (T_t^{amb} - T_s^{tr,H})\mathrm{d}t} \\ k_s^{2,H} & = -k_s^{1,H} \cdot T_s^{tr,H} \end{cases} \qquad \forall s \in \mathbf{SS} \quad (1.13)$$

To afterwards reconstruct the hourly profile, Eq. 1.12 is employed. The errors made by estimating the demand based on the annual measurements are reported in Table A.3.

1.4.4 Definition of the users' operating temperatures

As previously mentioned, the challenge of estimating the demand of an existing building arises from the difficulty of assessing its parameters (i.e., information on the buildings structure and usage). To overcome this problem, calibration techniques can be implemented aiming at tuning the model parameters such as to represent the measured data. However, an additional challenge arises from the estimation of the operating temperature. In this regard, measurements might be not detailed enough: recorded data might refer to aggregated users or reflect the current control strategy, optimized for the existing energy system. Therefore, the measure-

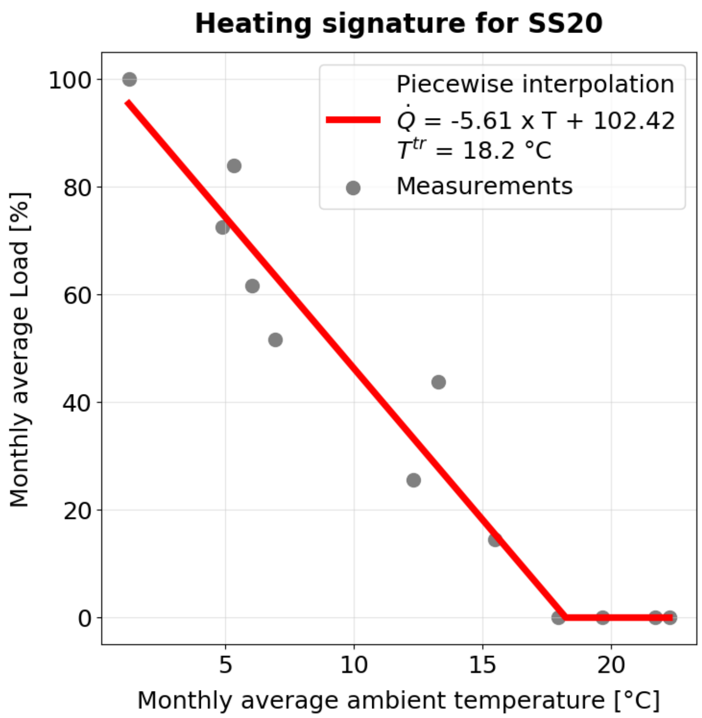

Figure 1.21: Piecewise linear interpolation of normalized monthly data to estimate the threshold temperature and coefficients of the heating curve

ments available might not show the real temperature requirements of the final end-users, but rather the set-point defined by the current control system. In this work, due to the final goal of designing the new energy system and the importance of the operating temperature in view of the use of HPs, an effort is made to estimate the temperature requirements of each user. The goal is to exploit the current infrastructure to minimize the exergy loss and thus decrease the temperature needs.

From the substation to the end-users

The first step to assign the operating temperatures is to distinguish the different types of end-users. Static appliances and ventilation units usually present different temperature requirements. In particular, due to the lower heat transfer coefficient of the latter, to limit heat transfer surfaces, ventilation units usually require higher temperatures. Therefore, it would be beneficial to differentiate the thermal needs associated to the air renewal. This is solely possible if the model offers enough details. Indeed, in the case of the models calibrated on monthly and annual measurements, the distinction must rely on assumptions. On the contrary, in the case of the thermal model calibrated on the hourly profile, the information provided by tuned parameters can be exploited. Hence, the total heat demand is divided in two main contributions (Eq. 1.14), which in the case of the model calibrated on the hourly

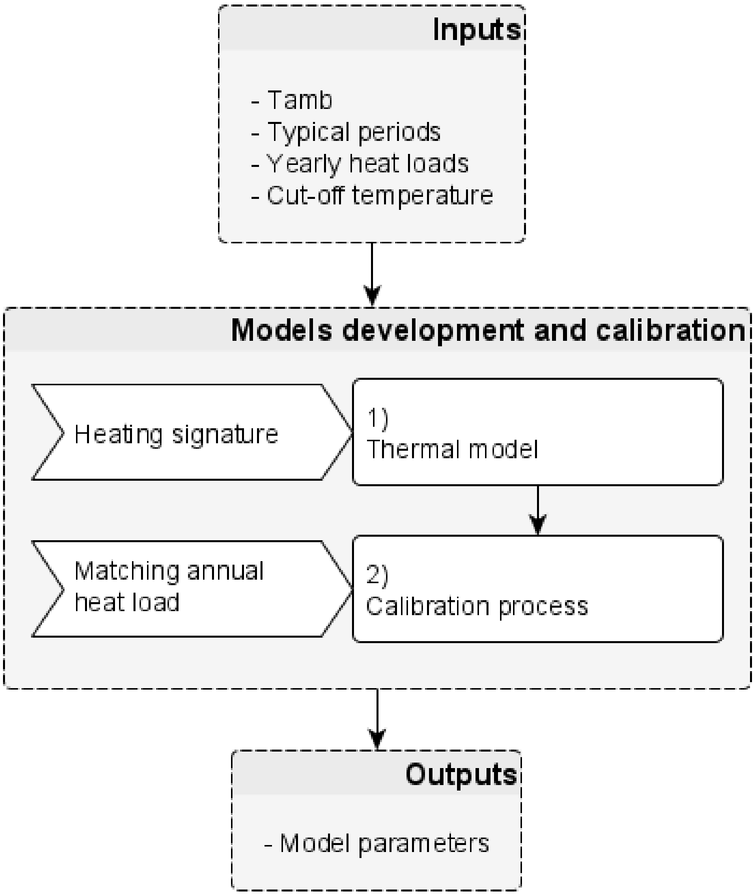

Figure 1.22: Flow sheet of the proposed method for the development and calibration of thermal models based on yearly measurements.

measurements are estimated as in Eqs. 1.15 and 1.16:

$$\dot{Q}^{H}_{s,t} = \dot{Q}^{H,vent}_{s,t} + \dot{Q}^{H,rad}_{s,t} \tag{1.14}$$

$$\dot{Q}^{H,vent}_{s,t} = \pi^{air}_{s} \cdot (T^{set}_{t} - T^{amb}_{t}) \cdot y^{day}_{t} \cdot (1 - \eta^{vent}) \tag{1.15}$$

$$\dot{Q}^{H,rad}_{s,t} = \pi^{loss}_{s} \cdot (T^{set}_{t} - T^{amb}_{t}) - \dot{Q}^{int}_{t} \tag{1.16}$$

where:

- $\dot{Q}^{H,vent}_{s,t}$ represents the contribution to the heat demand due to the air renewal and supplied by the ventilation units;
- $\dot{Q}^{H,rad}_{s,t}$ represents the contribution to the heat demand associated to the static appliances;
- $\dot{Q}^{int}_{t}$ includes all the internal gains and ramp-up(-down) at the opening and closing

hours as reported in Eq. 1.8.

Following this procedure or relying on assumptions for substations with solely monthly or yearly measurements available, the profile of each substation is split in the two contributions.

Figure 1.23 shows how the total demand of substation SS3 during the 5th typical operating period is split between the contribution assigned to the ventilation units (area in pink) and the one associated to the static appliances (area in blue). The grey line shows the original profile of the k-medoid. The available measurements used for the calibration of the thermal model

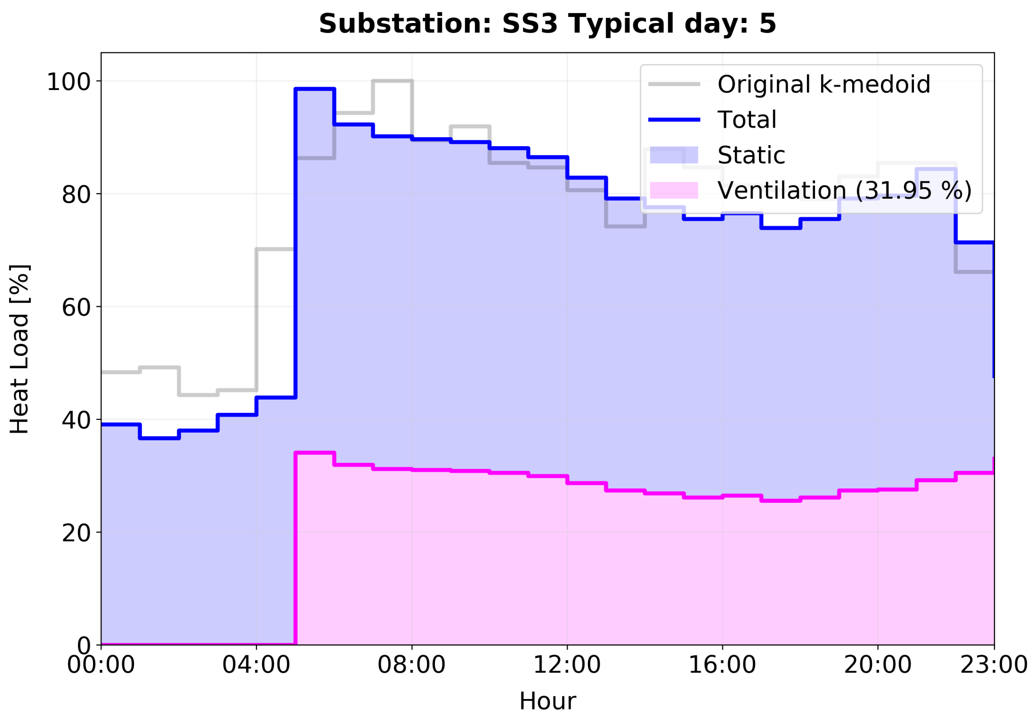

Figure 1.23: Normalized heat load covered by the static appliances (blue area) and the one associated to the ventilation units (pink area) during the 5th typical operating period for substation SS3. The grey line represents the original profile of the k-medoid. In the legend the share of daily energy covered by the ventilation units is reported.

do not provide enough information to validate the result of such analysis. For this reason, further measuring campaigns were carried out, as reported in the following section.

Further investigation of final end-users for model validation

Due to lack of data associated to the final end-users and the complexity of the case study, one particular substation is taken as the representative one. This substation is associated to a building used as a passengers' terminal and equipped with two radiators (later in this section, defined as *STATIC 1* and *STATIC 2*) and two ventilation units (*VENT. 1* and *VENT. 2*). For this substation additional measuring campaigns were carried out: the operating temperatures (supply and return), mass flow rate and pressure losses are registered during a period ranging from 5 to 6 days at the final end-users. The goal of this additional measuring campaign is to 1) validate the results of the model in terms of defining the heat load covered by the static appliances and the one by the ventilation units, 2) estimate the over-capacity factor of the substation[5], 3) investigate the operating temperatures of the final end-users.

The first observation based on the data newly available is that, as previously assumed, the ventilation units are switched-off during the night, while the radiators operate over the entire period, as visible in Fig. 1.24.

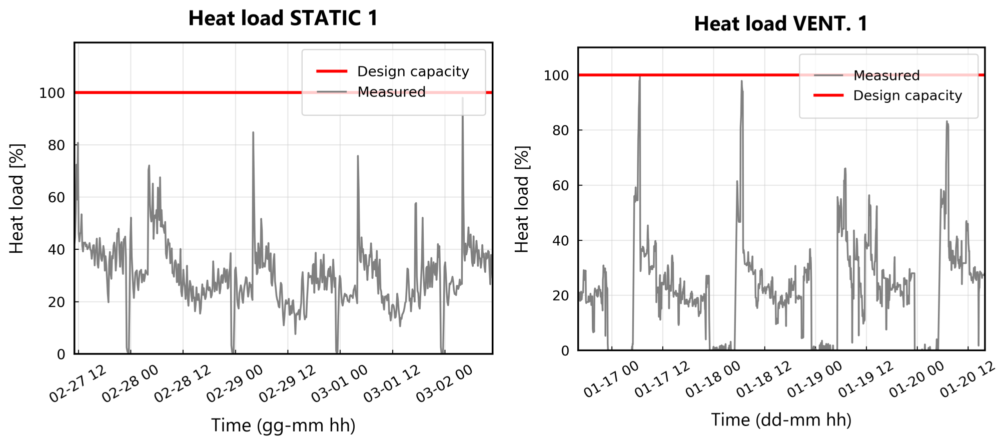

Figure 1.24: Normalized measured heat delivered and installed capacity of one radiator (on the left) and one ventilation unit (on the right).

Moreover, from the trends of the operating temperatures it can be noticed how the radiators are operated at a lower set-point during the night (due to the decrease of the set-point of the internal temperature), which together with the switching-off of the ventilation systems create the ramp-up/-down effect visible on the aggregated profile. Figure 1.25 shows the supply and return temperature to a static user during the day (5:00-22:00, on the left) and the night (23:00-4:00, on the right) operation.

Figure 1.24 also highlights that the users are operated at a much lower load then the installed capacity. Since the measurements refer to different periods, to be able to define the factor to split the heat load supplied by the substation between the static appliances and the ventilation units all the measurements must be reported to the same conditions. To do so the observations are compared in terms of daily energy supplied per degree day, as shown in Fig. 1.26. The daily energy takes into account only the operation during the day (between 5:00 and 23:00), while the degree day is calculated as the difference between the internal set-point temperature (21°C) and the mean ambient temperature over the daily operation.

[5]The study reported in Section A.2 and relative results shown in Fig. 1.4 are solely based on the current operation and assume that extreme working conditions are encountered during the measuring period.

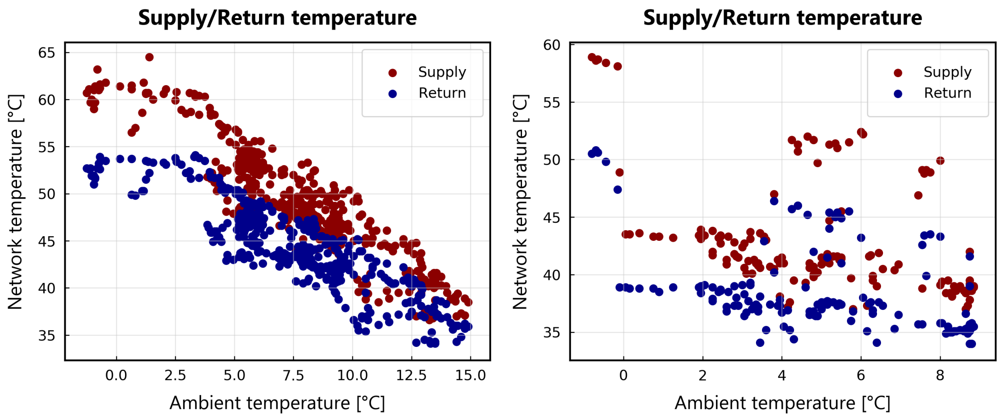

(a) Daily operation (b) Night operation

Figure 1.25: Supply and return temperature to a radiator during the measuring period.

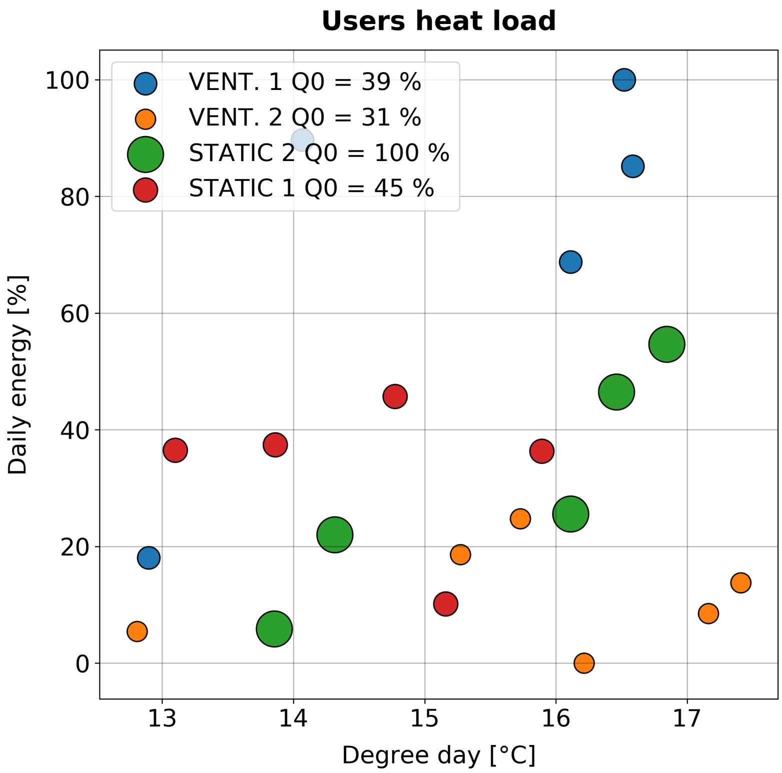

Figure 1.26: Normalized daily energy supplied by each end-user as a function of the degree day. In the legend the heat transfer capacity of each user is reported normalized with respect to the largest one.

Figure 1.26 highlights that there is no correlation between the capacity of the end-users and their operation, meaning that smaller end-users appear to supply, in the respective building zones, more energy than bigger ones. Moreover, not all the end-users show a clear trend with the degree days. Therefore, a unique factor to split the heat load between the static appliances and the ventilation units, valid for the whole operation, cannot be estimated based on the information available. On the other hand, the fact that the space conditioning technologies appear to be operated at partial load encourages to look for a procedure to estimate the minimum operating temperatures at which the end-users can be operated, while still being able to guarantee the required comfort level.

The over capacity of the substation under study is also proven by comparing the measurements with the information from the technical sheets. Figure 1.27 shows the power delivered by the substations during 2 years of operation. The square indicates the power extrapolated to the conditions that were used for the design of the substation, while the cross indicates the substation capacity. Therefore, not only the design conditions used to define the capacity of the substation are never encountered during the 2 years of operation, but also even at the extreme conditions the heat exchanger appears double the size needed. Figure 1.4 already showed the potential benefit in terms of exergy achieved by reducing the operating temperatures. However, such a study relied on measured data to estimate the installed heating capacity, assuming that during the measuring period the system encountered the extreme operating conditions, employed for the design. On the other hand, the current analysis reveals that the area estimated in that way might be highly underestimated with respect to the installed capacity. Therefore, the aim is to fully exploit the surface available to decrease the operating temperatures.

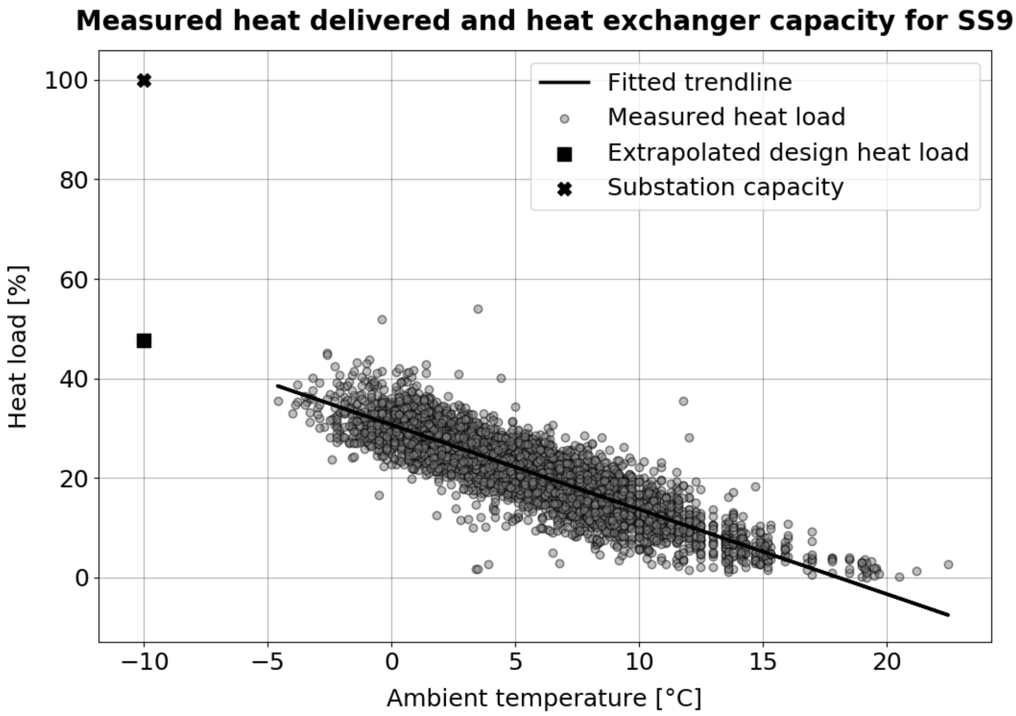

Figure 1.27: Normalized measured power delivered by substation SS9 (grey dots) with relative trend line (solid black line) and extrapolated power at design condition (black square), compared to the heat exchangers available capacity (black cross).

Estimation of the optimum operating temperatures

To estimate the new operating temperatures, ventilation units and radiators are modelled as represented in Fig. 1.28.

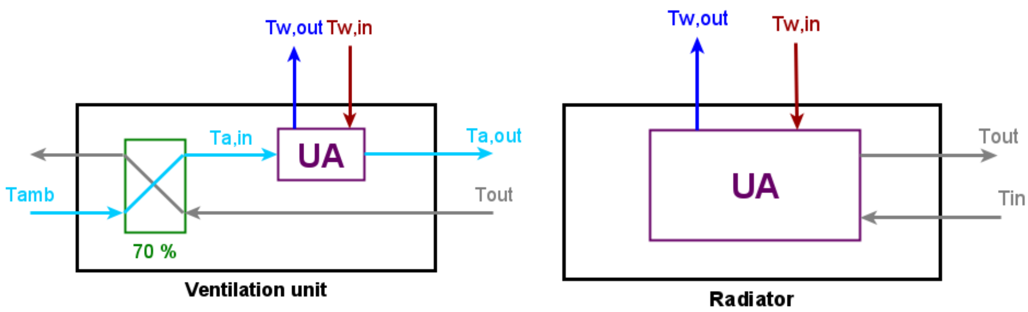

Figure 1.28: Simplified model of a generic ventilation unit (on the left) and radiator (on the left).

The modelled ventilation units include a heat recovery system, in which the fresh ambient air is pre-heated by the one sucked from the building. Additionally, a counter-current heat exchanger heats up the air flow until the internal set-point temperature. On the other hand, the radiators are simply modelled as a counter-current heat exchanger, which keeps the internal temperature at the required comfort level, as also reported in [33].

The general characteristic equation of a heat exchanger is the following:

$$\dot{Q} = (UA) \cdot \mathrm{LMTD} \tag{1.17}$$

where U is the overall heat transfer coefficient, A the exchange surface and LMTD the logaritmic mean temperature difference as reported in Eq. 1.18.

$$\mathrm{LMTD} = \frac{(T_{in}^{hot} - T_{out}^{cold}) - (T_{out}^{hot} - T_{in}^{cold})}{\log \frac{(T_{in}^{hot} - T_{out}^{cold})}{(T_{out}^{hot} - T_{in}^{cold})}} \tag{1.18}$$

In both ventilation units and radiators the hot fluid is the hot water of the hydronic distribution system, therefore $T_{in}^{hot} = T_{in}^{w}$ and $T_{out}^{hot} = T_{out}^{w}$. In the case of the ventilation units, the cold side is represented by the fresh air, preheated by the heat recovery system and blown into the building's zone: $T_{in}^{cold} = T_{in}^{a}$ and $T_{out}^{cold} = T_{out}^{a}$. In the radiators, the cold side is the ambient air in the building's zone. Making the simplification that indoor temperature is stable at the required set-point, as also reported in [33], the inlet and outlet temperature of the cold side in the radiator are constant $T_{in}^{cold} = T_{out}^{cold} = T_{in} = T_{out}$.

Equation 1.17 is valid during the whole operation of the heat exchanger. The characteristic (UA) can be estimated at design conditions, making the following assumptions:

- T_0^{amb} = -10°C[6]
- $T_{out}^{a} = T_{out} = T_{in} = 21$°C
- $T_{in,0}^{w}$, $T_{out,0}^{w}$, $\dot{Q}_0$, $\dot{m}_0^{w}$ are respectively supply and return temperatures, heat delivered and water mass flow rate at design conditions that must be known.

Therefore, at design conditions the following holds:

$$(UA)_0 = \frac{\dot{Q}_0}{\mathrm{LMTD}_0} \tag{1.19}$$

Considering that the heat transfer coefficient does not change with the operating temperatures, the HEX characteristic $(UA)_0$ can be then employed to estimate the network temperatures at the maximum power measured for each end-user. For a given difference between the network

[6]The ambient conditions assumed at design are taken from the technical sheets of the equipment.

supply and return temperatures, the former one can be estimated as reported in Eq. 1.20:

$$T_{in}^{w,max} = \begin{cases} \frac{T_{out}^{a} - e^{\alpha}(T_{in}^{a} + \Delta T^{w})}{1-e^{\alpha}} & \text{if the user is a ventilation unit} \\ \frac{T_{in} - e^{\alpha}(T_{in} + \Delta T^{w})}{1-e^{\alpha}} & \text{if the user is a radiator} \end{cases} \tag{1.20}$$

where:

$$\alpha = \begin{cases} \frac{(UA)_0}{\dot{Q}^{max}}(T_{in}^{a} - T_{out}^{a} + \Delta T^{w}) & \text{if the user is a ventilation unit} \\ \frac{(UA)_0 \Delta T^{w}}{\dot{Q}^{max}} & \text{if the user is a radiator} \end{cases} \tag{1.21}$$

For each end-user, at first a ΔT^{w} of 10°C, between the supply and return temperatures is assumed. The new supply temperature, $T_{in}^{w,max}$ can be estimated through Eq. 1.20. Consequently, the new water mass flow rate is calculated and compared with the value at design, as reported in Eq. 1.22.

$$\dot{m}^{w,max} = \frac{\dot{Q}^{max}}{c_p^{w} \cdot \Delta T^{w}} \overset{?}{\geq} \dot{m}_0^{w} \tag{1.22}$$

In case the technical constraint is violated the ΔT^{w} is increased iteratively by 1°C until the calculated mass flow is lower than or equal to the one at design. Further information on how for each user the installed capacity and the maximum operating load are estimated in case of missing information are given in Section A.5.

Once the supply and return temperatures at the conditions of maximum power are defined fo each end-users, for the rest of the operation they are estimated as a linear function of the ambient temperature, until reaching the cut-off. The latter, when not available, is assumed being equal to 18°C. A tolerance of 2°C at the cut-off temperature is taken into account such that a ΔT^{w} greater than 0 is always defined between the supply and return temperatures (as done for the definition of the potential network operating temperatures, shown in Fig. 2.12).

1.4.5 Comparison of different time resolutions

The quality of the measurements available plays a major role in the choice of the thermal model. In this chapter different models are developed according to the time resolution of the measurements available. To check if the model calibrated on the hourly measurements is more accurate with respect to the heating signature approach, the measurements available on a hourly basis, are re-sampled in monthly and yearly time resolutions and the thermal models presented respectively in Sections 1.4.2 and 1.4.3 are applied to reconstruct the hourly profile. The errors generated in reconstructing the original profiles, employing the different models, are then compared.

Figure 1.29 shows the MAPE and APE relative to the models calibrated respectively on hourly, monthly and annual data (in red, blue and green on the graph). The first error shown (solid line) refers to the use of the thermal models on the yearly profile of the attributes. The second one (dashed line) includes also the error due to the clustering process.

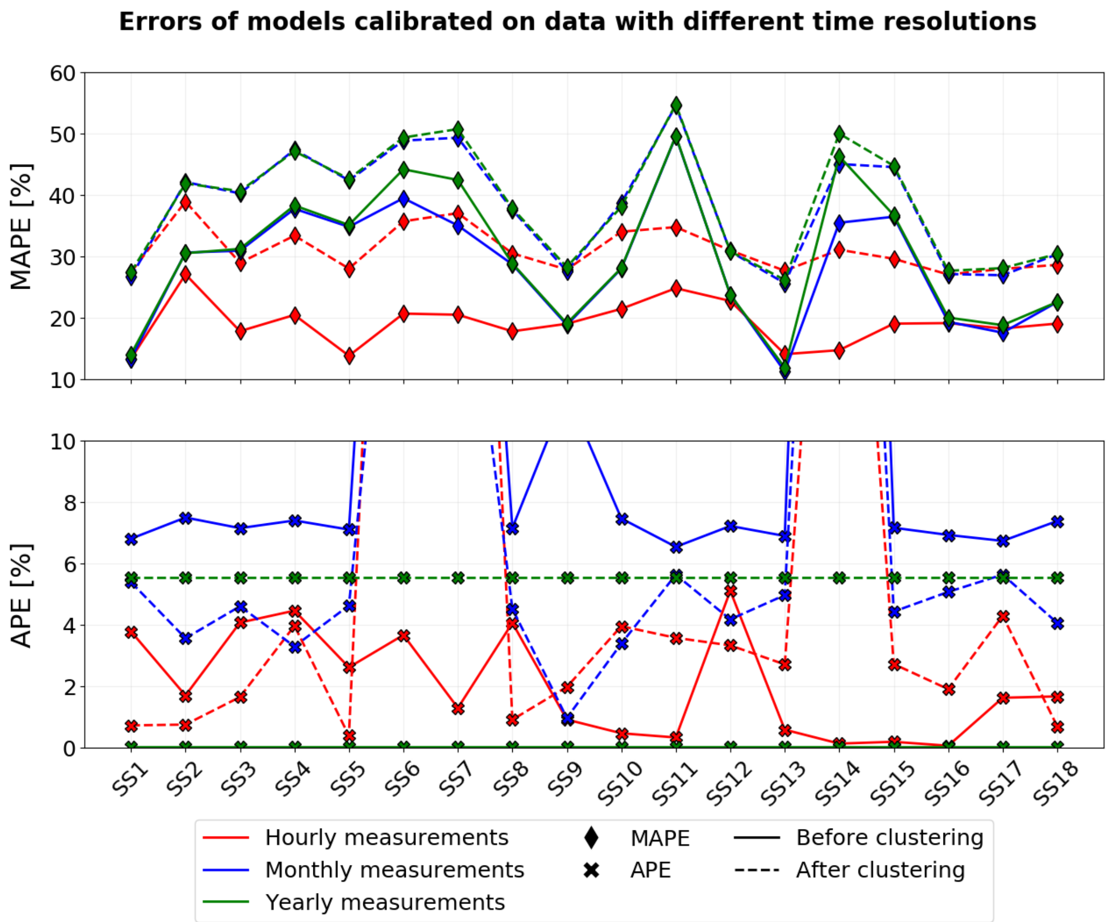

Figure 1.29: Comparison between the MAPE and APE errors relative to models calibrated on data with different time resolution, including and excluding the clustering process.

The comparison of the different models previously introduced in this chapter highlights that in terms of the capability of reproducing the original hourly profile (MAPE error) the monthly and annual models perform equally for most of the substations. The reason is that the two models are based on the same approach, the one of the heating signature, with the only difference that the threshold temperature is estimated in the case of the monthly measurements and assumed for the yearly data. Hence, it can be concluded that the assumption made to calibrate the annual signature is very close to the real value. The advanced thermal model, calibrated on the hourly data overall performs better than the other two, but not for all substations, since for some of them the error is very close. The reason could be that for those substations the attributes chosen might not be the relevant ones in explaining the thermal demand. In terms of estimating the annual energy demand, as expected, the heating signature model calibrated on the annual value has a null error (since the calibration is based on the equivalence of the yearly energy value), whereas the hourly calibrated model performs better than the monthly one. Some of the substations (SS6, SS7, SS9, SS14) show a much larger APE error with respect to the remaining ones. The reason is that in those substations, to achieve a better fit of the piece-wise linear interpolations, some measurements had to be neglected, since they are outliers with respect to the overall trend (the corresponding calibration results are shown in Figs. A.2 to A.5). This procedure improves the MAPE, but not the APE, revealing that either those substations are characterized by higher measuring errors, which cannot be corrected by the data cleaning process on the hourly measurements, or their heat load cannot be solely correlated to the ambient temperature. The effect of the clustering error is much more relevant in the MAPE with respect to the APE and it affects similarly all the models. On the contrary, when estimating the total energy demand, the use of the clustered profile might balance out some modelling errors resulting in a better estimation for the monthly model and for some of the substations when relying on the hourly calibration.

1.5 Other thermal requirements

Within the context of energy system design, all the services provided by the latter should be taken into account. In non-residential buildings, beyond the space heating requirements, the energy system supplies also space and process cooling, and possibly DHW. In the current application, space cooling is required only by four of the buildings and provided by chillers (CHI), placed in five substations. DHW is supplied by a unique substation and distributed to the different building zones with a dedicated infrastructure. Processes needing refrigeration are not present at the site. The following sections present the procedure adopted to estimate the DHW and space cooling needs, based on the measurements available.

1.5.1 Domestic hot water requirements

Estimating the requirements of DHW is important due to the very different temperature profiles with respect to the space heating demand. However, in the current application, DHW requirements constitute only a minor share of the total heating needs (3.5% of the overall yearly demand). The use of hot water is mainly devoted to restaurants and restrooms. Therefore, a simplified approach is followed, based on a single daily profile assumed throughout the whole year. Hourly measurements of the flow rate of DHW delivered by the relative substation are employed to estimate a mean profile over all the recorded days. Figure 1.30 shows the original daily profiles (in grey), statistics of their distribution (in green) and the mean taken as representative (red line). The graph also highlights a very minor variation among the recorded daily profiles, justifying the simplification of adopting a unique trend. To supply DHW requirements, the fresh water is supposedly heated up from 10 to 55°C, neglecting the need of periodically reaching 60°C in order to avoid the formation of Legionella bacteria. By assuming such temperatures and considering the daily average profile of Fig. 1.30 the APE calculated between the estimated power required and the one measured at the relative substation is of 2%. The MAPE generated by adopting a single daily profile to represent the mass flow rate measured throughout the year is of 27%.

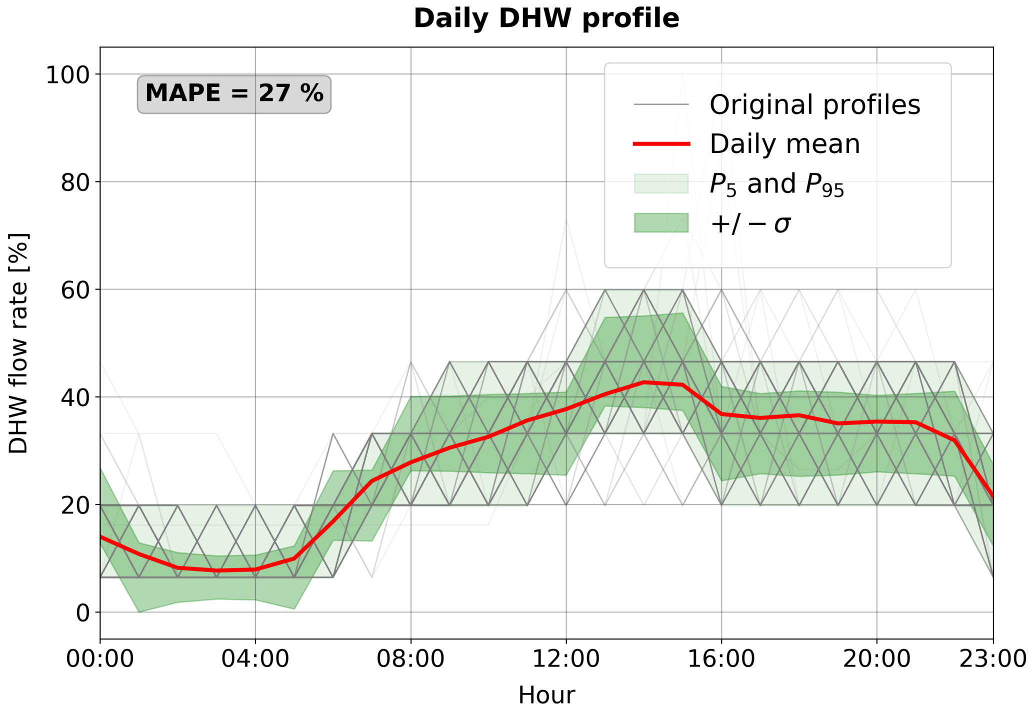

Figure 1.30: Normalized measurements of the daily profiles of DHW mass flow rate (in grey), with first and last quartile in light green, area defined by one standard deviation around the median (green zone) and mean daily profile (red line).

1.5.2 Space cooling requirements

The space cooling demand is estimated based on measurements of the electricity consumption of CHIs. Due to the use of an on-site ice-water storage system, the cold production and distribution are disconnected in time. Therefore, only daily values could be defined, losing the information of the hourly trend.

For each machine the COP is calculated in each time step, considering the evaporator's inlet and outlet temperatures at design conditions and the temperature of the condenser (respectively sink and source sides) as reported in Eq. 1.23:

$$COP_{s,t} = \frac{T_{LM}(T_{s,t}^{evap,in}, T_{s,t}^{evap,out})}{T_{s,t}^{cond} - T_{LM}(T_{s,t}^{evap,in}, T_{s,t}^{evap,out})} \cdot \eta_{II} \tag{1.23}$$

where η_{II} is the CHI Carnot efficiency, $T_{LM}(T_{s,t}^{evap,in}, T_{s,t}^{evap,out})$ is the logarithmic mean temperature between the evaporator inlet and outlet temperatures and the temperature at the condenser is assumed as shown in Eq. 1.24.

$$T_{s,t}^{cond} = \begin{cases} T_t^a & \text{if } T_t^a > T_{s,t}^{evap,in} + \Delta T_{min}^{lift} \\ T_{s,t}^{evap,in} + \Delta T_{min}^{lift} & \text{otherwise} \end{cases} \tag{1.24}$$

A minimum temperature lift ΔT_{min}^{lift} of 5°C is introduced to avoid an unreasonably high COP. Additional parameters employed for the estimation of the CHIs performance are reported in Section B.1.3. The COP calculated for each machine and time step is used to convert the measurements of electric consumption into cooling power delivered. Due to the usage of a night storage, the hourly profile of electricity consumption does not match the one of cooling demand. The time steps over the year are grouped into the original days ($d \in \mathbf{D^{2019}}$), each one constituted by 24 hours ($h = 1..N_h \in \mathbf{D_h}$, $N_h = 24$). An equal cooling demand is assigned to all hours belonging to the same day. The value is estimated as the mean over the ones registered during the respective day, as reported in Eq. 1.25:

$$\widetilde{\dot{Q}}_{s,d}^{C} = \text{mean}\left(\left[\widetilde{\dot{E}}_{s,h}^{C} \cdot COP_{s,h}\right]_{h \in \mathbf{D_h}}\right) \qquad \forall s \in \mathbf{SS}, \forall d \in \mathbf{D^{2019}} \quad (1.25)$$

Where $\widetilde{\dot{E}}_{s,h}^{C}$ is the electricity consumed by the CHI in substation s, during the hour h, whereas $\widetilde{\dot{Q}}_{s,d}^{C}$ is the mean value of the cold provided each hour, taken as the representative for the day d. Since the measurements available refer to a different year with respect to those of the heating demand, a linear model is developed and calibrated to be able to estimate the cooling requirements for the reference year. The linear model is represented by Eq. 1.25:

$$\dot{Q}_{s,d}^{C} = \pi_s^{a} \cdot \overline{T}_d^{amb} + \pi_s^{irr,c} \cdot \overline{GHI}_d + \pi_s^{PAX} \cdot N_d^{PAX} + \pi_s^{C} \qquad \forall s \in \mathbf{SS}, \forall d \in \mathbf{D^{2019}} \quad (1.26)$$

where:

- $\dot{Q}_{s,d}^{C}$ is the estimated average cooling demand supplied by the substation s for each hour of the day d;
- $\overline{T}_d^{amb}$ is the mean value of the ambient temperature over the day d;
- $\overline{GHI}_d$ is the mean value of the GHI during the day d;
- π_s^{PAX} is the daily number of passengers;
- π_s^{a}, $\pi_s^{irr,c}$, π_s^{PAX}, π_s^{C} are the parameters of the model tuned by the calibration process.

Section A.6.1 gives more details on how the number of passengers, available during the year 2018 is extrapolated to the following year, period of the measuring campaign on the CHIs. The model is calibrated by means of the non-linear least squares approach available in the Python library *scipy.optimize.curve_fit*[7]. The error for each substation in estimating the yearly profile of cooling demand is reported in Table A.5. Figure 1.31 shows the original daily averaged cooling profile of substation SS8 (based on the estimation of the chiller COP) and the result of the calibrated model. The same representation for the other substations are reported in Section A.6.2.

[7] Further information available at https://docs.scipy.org/doc/scipy/reference/generated/scipy.optimize.curve_fit.html

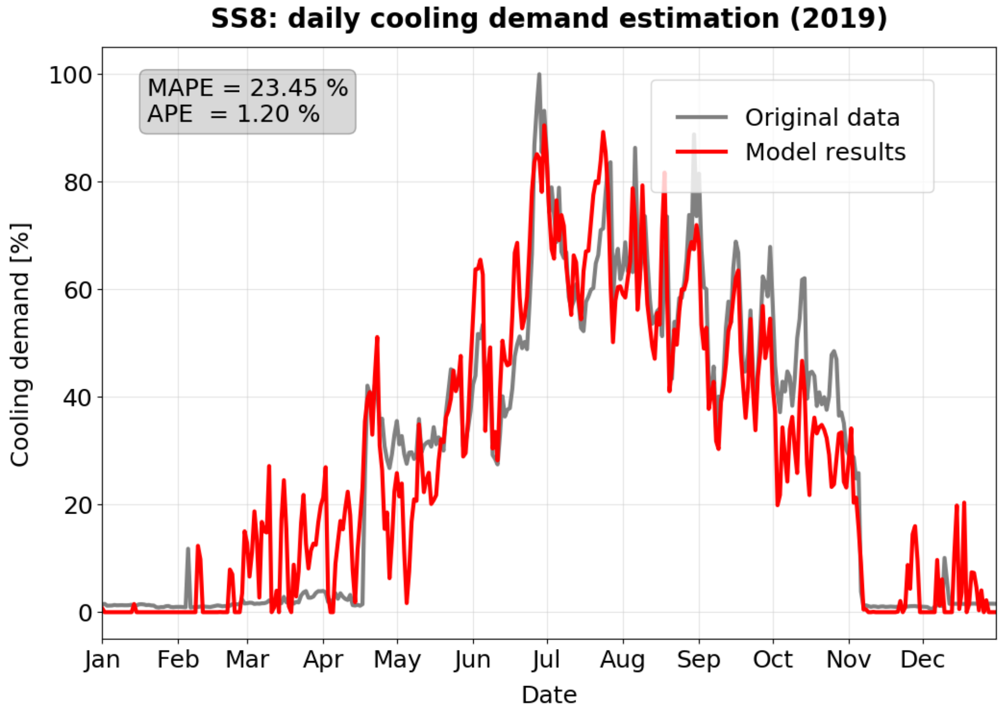

Figure 1.31: Normalized profile of daily average cooling power supplied by substation SS8 and results of the calibrated model.

The calibrated coefficients are employed to estimate the demand during the reference year (2018). To do so the model is applied to the mean daily values of the attributes referring to the year 2018, employing Eq. 1.26 with the set of days of the reference year $d \in \mathbf{D^{2018}}$. Finally to all the time steps belonging to each day (hours) the same value is assigned:

$$\dot{Q}^{C}_{s,t} = \dot{Q}^{C}_{s,d} \qquad \forall t \in [(d-1)\times 24+1 : 24\times d],\ \forall s \in \mathbf{SS}, \forall d \in \mathbf{D^{2018}} \quad (1.27)$$

Annual time resolution

In the current application, one building is under construction and its TER are estimated and made available on a yearly basis. The hourly profile of space heating is reconstructed through the heating signature presented in Section 1.4.3 and a similar approach is used to estimate the cooling hourly profile. Therefore, at first the cooling signature parameters are calibrated to match the yearly annual demand, as reported in Eq. 1.28. Then, the hourly profile is reconstructed by means of Eq. 1.29.

$$\begin{cases} k^{1,C}_{s} &= \dfrac{Q^{C,yr}_{s}}{\int\limits_{yr:T^{amb}_{t}>T^{tr,C}_{s}} (T^{amb}_{t} - T^{tr,C}_{s})\mathrm{d}t} \\ k^{2,C}_{s} &= -k^{1,C}_{s} \cdot T^{tr,C}_{s} \end{cases} \qquad \forall s \in \mathbf{SS} \quad (1.28)$$

$$\dot{Q}^{C}_{s,t} = \begin{cases} k^{1,C}_{s} \cdot T^{amb}_{t} + k^{2,C}_{s} & \text{if } T^{amb}_{t} > T^{tr,C}_{s} \\ 0 & \text{otherwise} \end{cases} \qquad \forall t \in \mathbf{T}, \forall s \in \mathbf{SS} \quad (1.29)$$

The APE relative to the estimation of the cooling demand following the cooling signature approach for this particular substation (SS26) is of 8.53%.

It is supposed that the space cooling services are supplied by two different types of systems: ventilation units and radiant panels. The cooling loads are split in the same manner every hour between the two systems and the operating temperatures are also considered constant. All values are defined based on discussions with experts in the field and reported in Section A.4.

1.6 Conclusion

This chapter tackled the challenge of estimating the TER in existing, non-residential buildings within the context of integrated energy system design. The literature review emphasized the scarcity of studies on this topic, in which very little information on the adopted thermal modelling approaches is usually reported by the authors. The gaps highlighted in the literature combined with the challenges arising from dealing with existing, non-residential buildings and the use of measured data, encouraged further research in this field.

At first, this chapter tackled the estimation of space heating requirements. In this regard, different approaches were suggested in function of the time resolution of the measurements available. In the case of hourly heat loads, four linear grey-box models were developed comprising an increasing level of detail and calibrated with different techniques. The errors arising from the use of each model in estimating the original hourly and yearly demand (MAPE and APE, respectively) were then compared. A k-medoid approach was then applied to represent the system operation by different numbers of typical operating periods. The errors arising from applying the thermal models to the aggregated profiles were computed and compared. The selected thermal model was then employed to suggest, by means of the calibrated parameters, the distribution of the heat load among the different end-users: radiators and ventilation units. This distinction is important in view of defining the operating temperatures, given that, with the goal of designing the heat supply system, specifically promoting the use of RES through HP integration, the operating temperature plays a major role in the equipment sizing. To overcome the lack of measurements in this regard, a strategy was presented to estimate the current supply and return temperature requirements to minimize the exergy losses, while still providing the comfort level. This approach was based on the exploitation of the heat exchange surfaces, which are typically oversized with respect to the current needs, either due to changes in the building's occupation and usage or to retrofit actions carried on in the building. In the case that the measured heat loads were available at monthly or yearly time resolutions, simplified thermal models, based on the heating signature approach, were proposed. Lastly, the thermal models calibrated on measurements obtained over different time resolutions were compared in terms of their performance in reproducing the hourly profile and the annual energy demand, both before and after the clustering process.

The DHW demand was estimated by averaging the recorded mass flow rate profiles to a daily trend. The space cooling requirements were modelled based on measurements of the electricity consumption of CHIs. At first, through the definition of a COP for each machine, the electricity profile was converted into cold supplied and afterwards a linear model was calibrated. This approach allowed to estimate the cooling requirements for the same reference year as that of the space heating, since the CHIs electricity consumption was originally available for a different period.

All the analyses were carried out on a real case study, on an international airport. The analysis of the errors of the different thermal models applied to the specific case study led to the following conclusions.

- Thermal models including different parameters grant similar performance, with an average MAPE lower than 22%. A marginal improvement of 2% is registered by including the effect of the buildings' inertia, especially significant during the ramp-up/-down at opening and closing hours. In terms of APE all models are characterized by an average error lower than 3%.
- The occupancy profiles defined combining the information on the activities carried on in each building and the trends suggested by the standards fail at reproducing the internal gains.
- The clustering process drastically deteriorates the MAPE, increasing the average value to around 40%, affecting all the models in a similar way. From the comparison of different numbers of operating periods, 7 is the best compromise between improved performance and increased problem complexity. The effect of the clustering process is much more relevant on the MAPE with respect to the APE: when estimating the annual energy demand the use of clustered profiles might balance out modelling errors resulting in better estimations.
- The comparison of thermal models calibrated on measurements obtained over different time resolutions (hourly, monthly and yearly) reveals the poorer performance of the heating signature approaches in reproducing the hourly profiles. On the other hand, due to the similarity of the models adopted for monthly and yearly measurements, the two approaches perform equally in terms of MAPE, revealing the successful assumption of the threshold temperatures in the latter. Despite the fact that hourly measurements had been pre-processed, the monthly aggregation in some cases showed outliers with respect to a linear trend with the ambient temperature. In this situation the removal of such measurements improves the MAPE, but deteriorates the APE. A deeper investigation of the system would be necessary to distinguish measuring errors from uncommon building behavior.

- Despite the challenges and limitations of relying on measured data, the latter, combined with information on the system, offers an opportunity to define optimal operating temperatures for the future energy system. Heat exchange surfaces often appear oversized for the current needs, allowing a reduction of the operating temperatures, in view of the replacement of fossil fuel technologies with more sustainable HPs. To fully exploit the infrastructure in place, information on the installed capacity is required, since extrapolations of the measured data might lead to significant underestimation of the available heat exchange surfaces.

- Averaging the DHW requirements to a daily profile provides sufficient precision. After assigning the operating temperatures, an error of 2% is registered between the measured yearly demand and the estimated one. The representation of the yearly mass flow by a daily trend generates a MAPE of 27%.

- The use of a daily storage of iced water and the presence of measurements solely related to the electric consumption of CHIs prevent the definition of an hourly profile for the cooling demand. Moreover, in this situation, the error generated in reproducing the cooling requirements cannot be estimated due to lack of information. However, the use of a thermal model enables to extrapolate the measurements to different periods, particularly important to define all TER for the same reference year.

Limitations and perspectives One of the limitations common in all the models proposed arises from the application itself, in particular the quality of the measurements available on one side, and the level of detail needed to design the integrated energy system on the other. Due to the presence of the substations, the respective building zones were treated as standalone buildings. The aggregation of the different zones might have helped for the model calibration, but would not have provided enough detail to size the relative equipment (e.g., decentralized HPs are installed within each substation and not at the building level). On the other hand, not enough information on the different zones was available as for the type of usage and electricity profiles, specified only at the building level. In addition, two consecutive building zones would inevitably affect each other's demand, due to the exchange of air flow and occupants. All these interactions could not be taken into account. However, the current scope was not to develop a physical building model, but rather represent the TER at the substation level.

Moreover, still due to the quality of measurements available some information provided by the models could not be verified. As an example, due to the lack of any data referring to the ventilation units, the distribution of the overall heat load to the static and ventilation appliances could not be confirmed. The additional measuring campaign devoted to gather more information on one of the substations was also not successful in this regard. During this campaign the same measuring device was used for all the systems, with the result that the collected data referred to different periods. Moreover, the short duration of the measuring periods did not enable the extrapolation to other operating conditions. Last, most of the assumptions made to define the new operating temperatures (i.e., the values assigned to the extreme conditions) were also a result of discussions with experts in the field and due to the complexity of the current application could not be verified. Detailed information on all the HEXs in place, such as design operating temperatures and heat exchange surfaces, would be necessary to better define the new operating temperatures.

The clustering process highly deteriorates the error, doubling its average value. Therefore, the choice of the typical operating periods should be deeper investigated. Kotzur et al. [55] offered in their review study an extensive overview of the various techniques available in time-series aggregation for energy system models, while Bahl et al. [56] and Hoffmann et al. [57] both investigated the impact of the choice of aggregation method on the final system design. Since the performance of time-series aggregation is normally deteriorated by higher number of attributes considered in the process, not only different techniques could be compared but it would also be relevant to define a systematic method to include the measurements available within the clustering procedure. In this direction, the variation to the k-medoids presented by Ma et al. [58] seemed effective not only in determining the typical operating periods but also identifying characteristics of the buildings' daily heating profile such as start and end times, peaks and variations.

Another analysis left to future studies, is the investigation of how the modelling assumptions affect the final investment decisions. Within the larger scope of the energy system design the most important aspect is not how well the thermal model is able to reproduce the current demand but if it is able to catch all the characteristics that would imply changes in decision making. An attempt to check if the temperature assigned to the users affects the decision process is presented in Chapter 3, where the system design optimization is performed after potential optimization of the buildings' control strategies, which implies a reduction of temperature supplied to some of the users. However, a more systematic study in this regard would be required.

The following chapters proceed in the analysis of the complex problem of optimal DES design, by tackling the optimal design and retrofit of the energy system, respectively.

2 Optimization of district energy systems equipped with thermal networks

Chapter overview

- MILP framework for optimal sizing and operation of district energy systems equipped with thermal networks
- Investigation of the optimum degree of centralization/decentralization for heat and cold production
- Exploration of investment decisions at increasing capital investment allowance
- Assessment of solutions' robustness considering uncertainty on cost parameters

This chapter is an extended version of the studies reported in [59, 60].

2.1 Introduction

Heating and cooling represent around half of the global final energy consumption, of which 50% is used in industrial processes, 46% in residential and commercial buildings, and the remaining 4% in agriculture [10]. Currently, most of the resources exploited for providing heating and cooling needs, are still based on fossil fuels, which makes this sector a major source of climate change impact, accounting for over 40% of the global energy-related CO_2 emissions. Concurrently, the demand has been constantly rising, tripling since 1990 and recently rising due to climate change itself, with increasing severity of associated heat waves. In particular, the increase of per capita living area footage and population are not being outstripped by improvements in energy efficiency, yielding a continuous increase of energy use in the building sector [4]. Therefore, reducing the use of fossil fuels in heating and cooling remains a crucial step of the current energy transition, and DES have been widely recognized as crucial elements to achieve the challenging mid-century emission reduction target.

The benefits of the transition to renewable energy sources are now well-established and known to the wider public: the use of cleaner, more affordable and reliable sources not only decreases air pollution and its health impacts, but also strengthens the energy security, improves energy access, reduces energy poverty and acts as a magnet to substantial investments, creating jobs and boosting the economy [4]. The latter aspect has become even more compelling in the recent times to help the recovery from the global COVID-19 crisis. However, despite these benefits, many policy makers have given limited attention to accelerating the transition to cleaner and more efficient heating and cooling services; at the end of 2019 only 49 countries (mostly within the European Union) had implemented national targets for renewable heating and cooling [4].

District heating networks (DHN) represent the most common type of thermal network within DES, while district cooling networks (DCN) remain relevant only in tropical and sub-tropical climates. For example, about 11-12% of the total heat demand in Europe was supplied by around 6000 installations of DHNs in 2017 [61], while DCNs covered only the 2% of the overall cooling demand through 115 systems in place [62]. However, the expertise established in DHNs since the 1930s (year of introduction of such technology) are paving the way for the deployment of DCNs, too [63]. A combination of the two services is also possible through district heating and cooling network (DHCN) systems [64]. The latter configuration enables synergies between heating and cooling sectors representing a promising opportunity to improve energy efficiency in urban areas. Moreover, such systems could represent the sustainable and rational electrification of the thermal sector [65] resulting in deeper interactions with the electricity grid. Despite DHC systems have already proven their effectiveness in countries such as Denmark and Sweden, these configurations currently cover only 12% of the European heat demand [12].

Although DES provide various opportunities for the integration of renewable and low-carbon energy sources, such as geothermal heat, solar energy or biomass, only 8% of the energy used in DH in 2018 was of renewable origin [10], with great variation among countries, from almost 100% in Iceland to the 1% in China [4]. However, the use of flexible technologies such as HPs or TES could offer flexibility to the electricity grid, boosting the penetration of RES, providing benefits at the system level, including those external to the local district [66].

Among the viable conversion technologies HPs are widely recognized as an effective option to promote the electrification and decarbonization of the thermal requirements in urban areas. However, despite the higher efficiency compared to conventional technologies, in 2019, HPs have covered only a minor share of residential heat demand (around 5% as estimated by [4]). As reported by the International Renewable Energy Agency (IRENA) [24], 38 million HPs were installed worldwide in 2019, with the global sales rising by 10% between 2017 and 2018. Further increasing their penetration is considered one of the most effective strategies to reduce the greenhouse gas emissions in buildings; the switch from fossil fuels to high-efficiency HPs is indeed expected to be the main driver in this direction [67].

Buffa et al. [65] recently reviewed and classified existing DHC systems and highlighted the need of clarification and harmonization in terminology employed in the literature to address such systems. The author proposed to address all those systems based on an unique network connected to a low-grade heat source to provide heating and cooling demand in combination with decentralized units as 5$^{\text{th}}$ generation district heating and cooling (5GDHC). Later in this work the definition of anergy network (AN) will be used to refer to the infrastructure employed by such systems. The definition of 5GDHC aims at distinguishing this most recent technology from the previous four generations of heat distribution systems. An extensive explanation of these was given first by Lund et al. [17] and most recently by Suciu [23]. Steam was the most common energy vector of first generation systems, nowadays considered inefficient due to heat losses and maintenance cost [63]. Water has been introduced by the second generation, while the third and forth generations both aimed at reducing the network temperature and introducing more sustainable technologies. The most recent fifth generation implies a radical change, with the introduction of new energy vectors such as refrigerants and the use of an unique network to supply both heating and cooling services.

To fully exploit the benefits of DES, the components involved in the district must be optimized, from the heat source to the final users, including the distribution network. However, the optimization of such complex systems is a challenging task for several reasons: 1) it includes both spatial and temporal aspects, 2) consumption profiles may vary in stochastic manner and 3) it involves a large number of decision variables, both continuous and binary. As reported by Aunedi et al. [66], an intrinsic challenge behind the simultaneous optimization of conversion technologies and network design is the different temporal and spatial resolutions required. Indeed, the optimal design and operation of conversion technologies and thermal storage units requires a fine temporal resolution, whereas decisions on long-term investments in network layout rely on a fine spatial resolution. Combining the two in a simultaneous optimization gives rise to very complex problems, given the large number of variables involved.

The numerous studies in the literature focusing on optimization of DES equipped with TENs is an additional proof of the increasing interest in the topic. Authors cope with the intrinsic problem complexity relying on different strategies. The following section reports some of the studies in this field with their main characteristics.

2.2 State of the art and contributions

Fazlollahi et al. [34] tackled the intrinsic complexity of optimizing DES by decomposing the problem into a master level mixed-integer non linear programming (MINLP) problem and a slave level MILP problem. Additionally, the urban district was clustered into aggregated zones to further reduce the problem complexity. Several conversion technologies were proposed as potential options, including BOI, HP, CHP, PV panels, fuel cell (FC) with the possibility of storage using a TES system. A DHN was included, with the temperature selected by the master level optimization and kept constant throughout the yearly operation.

Harb et al. [68] proposed a MILP-based approach for the optimal design and operation of energy systems for different types of residential buildings (apartment building, multi- and single-family houses), first in a single building configuration and then in a neighborhood configuration with six units connected through a local DHN. Despite the network temperature not being optimized, results showed that the use of the thermal network allowed both cost and emission reductions with respect to the single building scenarios.

Henchoz [22] showed some pioneering work in the field of DHC systems. The author compared refrigerant- and water-based DHCNs to a conventional mix of technologies for a district in Geneva, grouped into several clusters. The temperature, assumed constant during summer and winter operation, was selected by comparing different scenarios. The technologies included were conventional BOI, CHI and a set of central and decentralized HP with different options for the working fluids. Results showed that the use of an AN could reduce the final energy consumption over 80% compared to the current situation, with the CO_2 network being the most profitable alternative, followed by the water-based variant.

Bordin et al. [69] focused on the optimization of large-scale network layouts within the context of DHN expansion. The authors developed a MILP framework taking into account existing and potential new connections as well as essential hydraulic characteristics by means of pressure drop and maximum flow constraints. The method was tested on both real case study and a fictitious one incorporating up to 1000 potential new users and 500 existing ones. The objective function maximized the difference between revenues associated with the connection of new users and the cost required for the connection, over five- and ten-year time horizons.

Kuriyan and Shah [70] extended the method proposed by Bordin et al. [69] to include the selection of the optimal mix of technologies for local energy conversion, imports and exports. They included CHP, BOI and HP as technology options. A limited number of time periods was used, distinguishing minor periods, representing seasonal or diurnal variations, and major periods used to model staged investments. A screening procedure was employed to limit the set of potential supply locations among the original 500 included. The impact of heat prices on the selected layout of the distribution network was also investigated.

Marquant et al. [71] proposed a MILP based framework to optimally design and operate a large-scale urban energy system, while maintaining a satisfactory resolution at the building level. The method was based on solving several sub-problems at the neighborhood level, resulting from different numbers of spatial clusters and network layout options. The optimal solutions were then re-evaluated at the district scale for the design of a larger-scale network. The model was based on the energy hub concept while the optimization was solved in two stages to improve the computational time. The conversion technologies included in the study were CHP, BOI, PV and TES. The main focus of this study was the decomposition strategy and spatial clustering to tackle large-scale urban systems design. For this reason, the authors included only a limited set of conversion technologies. The presence of machines such as HP, whose efficiency is eventually linked to the network temperature, would greatly increase the complexity of the problem and could affect the efficiency of the decomposition.

Stadler [54] extended a method initially proposed for single buildings [72] to a neighborhood level. The work aimed at optimizing the energy system of each building, accounting for their interconnection through the gas network, electricity grid and thermal network, considered at a fixed, unoptimized temperature. The choice of conversion technologies was performed considering a broad set of options, including BOI, HP, FC, PV, CHI, electrical heater (ELH), and storage possibilities using TES and stationary battery (BAT) storage and the option of building refurbishment. Particular attention was devoted to the interaction between the local energy systems and the electricity grid, through different control strategies. The author concluded that a multi-location problem formulation allows for a more cost-efficient use of available energy resources.

Pieper et al. [73] investigated the integration of large-scale HPs into an Estonian DHN, considering the seasonal variation of the heat source temperature and corresponding COP trends as well as capacity limitations and technical constraints. The authors developed a MILP approach to compare different potential locations for the HP with respect to the urban district and various low temperature heat sources, namely: ambient air, groundwater, seawater, lake water, river water and sewage water. The whole existing district was considered as a unique user, with aggregated demand. The solution robustness was tested by considering an increase of electricity price and investment cost.

Jing et al. [74] tackled the complexity of DES optimization by adopting a hierarchical decomposition strategy. The authors employed spatial clustering to simplify the district into several independent neighborhood sub-problems. The network layout was optimized within each cluster separately and used for both a heating and cooling network, whose temperatures were not optimized. Uncertainties on cooling and heating demand were addressed through a scenario-based optimization model, aimed at minimizing the expected value of the objective function for different stochastic scenarios. The technologies included in the study were BOI, CHP, CHI and a TES option.

Aunedi et al. [66] proposed a MILP based framework for optimal planning and operation of district heat production assets, taking into account the interactions with local and national electricity infrastructure. They included CHP, large-scale centralized HP, centralized BOI and a TES system. The DHN used to supply the heat demand was considered to be already existing and therefore not subject to the optimization. Results showed that flexible options such as CHP or TES might provide additional flexibility in the interaction with the electricity grid with additional benefits external to the local district. Therefore, the optimization of such units should be performed through systematic analysis, especially in the context of overall energy system decarbonisation.

Table 2.1 reports the studies mentioned above, highlighting the type of problem formulated, the user scale application, the number of locations and time steps tested, if the authors investigated the effect of the network temperature, the type of TEN included in the study, if the possibility of having hybrid centralized/decentralized solutions was investigated, and which technologies were included in the problem.

Table 2.1: Review of studies on district energy systems optimization.

Study	Problem formulation	User scale[a]	Nr. locations	Nr. time steps	Optimal network T	Type of network[b]	Degree of decentralization	Technologies[c]
Fazlollahi et al. [34]	MINLP	AD	13	8 × 24	✓	DHN	✗	BOI, HP, CHP, PV, glsFC, TES
Harb et al. [68]	MILP	B/N	6	12 × 24	✗	DHN	✓	BOI, HP, CHP, ELH, PV, TES
Henchoz [22]	-	AD	32	8760	✓	DHCN	✓	BOI, HP, CHI,
Bordin et al. [69]	MILP	D	1000	1	✗	DHN	✗	-
Marquant et al. [71]	MILP	AD/N	14	12 × 24	✗	DHN	✓	BOI, CHP, PV, TES
Stadler [54]	MILP	B/N	3	8 × 24	✗	DHN	✗	BOI, HP, CHP, ELH, PV, FC, CHI, TES, BAT
Kuriyan and Shah [70]	MILP	D	500	NA	✗	DHN	✗	BOI, HP, CHP
Pieper et al. [73]	MILP	AD	13	8760	✗	DHN	✗	HP
Jing et al. [74]	MILP	AD/N	6	3 × 24	✗	DHN	✓	BOI, CHP, CHI, TES
Aunedi et al. [66]	MILP	AD	1	3 × 24	✗	DHN	✓	BOI, HP, CHP, TES
This work	MILP	N	14	6 × 24 + 2	✓	DHN, DCN, DHCN	✓	BOI, HP, ELH, CHI, PV

[a] B: building, N: neighborhood (building stock of few single buildings), AD: aggregated district, D: district
[b] DHN: district heating network, DCN: district cooling network, DHCN: district heating and cooling network
[c] BOI: boiler, CHP: combined heat and power, HP: heat pump, CHI: chiller, PV: photovoltaic panels, ELH: electrical heater, FC: fuel cells, TES: thermal energy storage, BAT: stationary battery

The presented literature review highlighted that most of the studies still focus on DHNs and only a few of them include a systematic investigation of the network operating temperature. To the best of the author's knowledge a flexible model and optimization framework to systematically investigate different types of TENs together with the equipment sizing and operation is still missing. This work proposes to fill the gaps in the current literature by answering the following research question:

How can optimal design solutions for district energy systems equipped with thermal networks be defined, and how can the best configuration be selected?

To answer this question the current work proposes a flexible optimization framework for the sizing and operation of DES including the layout, type and operating temperatures of the TENs. The core of this formulation consists of the definition of a flexible set of centralized and decentralized conversion technologies able to cope with any network activation, temperature and layout to investigate the best degree of centralization/decentralization of the heat and cold production. Moreover, with the aim of promoting electrification of the TER in urban areas, this work focuses on HP integration. Particular care is given to the estimation of the performances of water-water HPs. Other technologies included in the superstructure are natural gas BOI, ELH, air-water HP, CHI and PV arrays. Finally, a method to investigate the different solutions is proposed, including the definition of economic, environmental and exergy-based KPIs, the exploration of the different design decisions at increasing capital investment allowance and the inspection of solutions' robustness through sensitivity analyses.

In this chapter, the modelling framework is presented, with the explanation of all the sets, variables and constraints included in the formulation. This framework is then applied to a case study, representing a fictitious neighborhood of six buildings, with different usage profiles and construction periods. Results are then presented and investigated including a sensitivity analysis on the cost of resources, technologies, network and the assumed interest rate. Conclusions and future perspectives are presented at the end of the chapter.

2.3 Modelling framework

The formulation of MILP frameworks for the optimal synthesis of utility systems, firstly introduced by Papoulias and Grossmann [75], is widely adopted in various fields of application, including the optimization of DES. The principles governing the interactions between the different actors involved in the systems (users, conversion technologies and distribution networks) are translated into a set of linear constraints, which represent the core of the model formulation. This section includes a definition of the primary objects involved in the model, followed by an explanation of the linking constraints, the technologies included and finally the objective functions used to identify the optimal set of design configurations.

2.3.1 Primary objects

Units The set of units $u \in \mathbf{U}$ identifies the actors in the system and can be divided in two major subsets: the process units $pu \in \mathbf{PU} \subset \mathbf{U}$, characterized by a fixed demand to be fulfilled (e.g., buildings) and the utility units $uu \in \mathbf{UU} \subset \mathbf{U}$, which include conversion technologies existing or potentially newly installed. The subset **NU** groups all the network utilities, respectively hot ($\mathbf{NHU} \subset \mathbf{NU}$) and cold ($\mathbf{NCU} \subset \mathbf{NU}$), defined to model the potential heat exchange between the thermal network and the units present in a specific location. The subset $hp \in \mathbf{HP} \subset \mathbf{UU}$ includes all units defining a HP, for which a specific set of additional constraints is specified, listed in Section 2.3.3. Additional utility subsets, for which specific constraints are defined, are also presented later in this section.

Locations A list of geographical locations $lc \in \mathbf{LC}$, characterized by a tuple of coordinates, is used to assign a location to any unit involved in the system. The subset $\mathbf{U_{lc}} \subset \mathbf{U}$ is defined to contain all the units located in location lc. The purpose of assigning a location to each unit is to enable potential heat exchanges without the need of a thermal network connection. As reported later, the cost of the latter is also estimated on the basis of the distance covered by the pipeline, resulting from the definition of the locations of its starting and ending points.

Time steps The operational profiles are defined for a set of time steps $t \in \mathbf{T}$. Each time step includes a frequency of occurrence f_t and duration d_t. The time steps are those representing typical operating conditions, selected using a clustering algorithm based on the k-medoids formulation presented in [54], and those defining the extreme conditions, characterized by $\mathrm{f}_t = \mathrm{d}_t = 1$ and included for sizing purposes.

Streams Each unit is constituted by a set of material and/or energy streams $s \in \mathbf{S}$ associated to different layers $ly \in \mathbf{LY}$ (such as thermal, electricity, natural gas, etc.). The set $\mathbf{S_u}$ groups all the streams belonging to the generic unit u, while the subset of units $\mathbf{U_{ly}} \subset \mathbf{U}$ defines those possessing at least one stream in layer ly. Each stream is characterized by a reference flow, which is the value relative to the unit reference size. The concept of layer is used to properly impose mass and energy balances.

A particular type of layer is the one defined as "*heat cascade layer*" and includes thermal streams: $hc \in \mathbf{HC} \subset \mathbf{LY}$. Thermal streams can be assigned to one or more heat cascade layers and are divided into hot ($s \in \mathbf{HS}$) and cold ($s \in \mathbf{CS}$) streams depending on their need of respectively being cooled or heated. A thermal stream is characterized in each time step by a reference heat load ($\Delta\dot{\mathrm{H}}^{ref}_{s,t}$), linked to the unit reference size, a heat capacity $C_{p_{s,t}} = \Delta\dot{\mathrm{H}}^{ref}_{s,t} / |\mathrm{T}^{in}_{s,t} - \mathrm{T}^{out}_{s,t}|$ and eventually a minimum approach temperature $\Delta\mathrm{T}^{\min}_{s}$, employed to define the minimum temperature difference between a hot and cold stream for the heat exchange. Thermal streams assigned to different heat cascade layers cannot exchange heat.

The heat exchange among streams belonging to the same layer is governed by heat cascade constraints, presented in Section 2.3.2.

2.3.2 Linking constraints

Sizing and Scheduling The investment decision for each unit is defined by a binary variable y_u, and the size of the unit by a continuous one, f_u. The purchased size is constrained by the lower ($\mathrm{F_u^{min}}$) and upper ($\mathrm{F_u^{max}}$) bounds through Eq. 2.1.

$$\mathrm{F_u^{min}} \cdot y_u \leq f_u \leq \mathrm{F_u^{max}} \cdot y_u \qquad \forall\ u \in \mathbf{U} \quad (2.1)$$

f_u, $\mathrm{F_u^{min}}$ and $\mathrm{F_u^{max}}$ are all dimensionless. The size of the installed unit is finally defined by the multiplication of f_u by the unit reference size. The optimal operation scheduling is governed by a continuous variable $f_{u,t}$ defined for each time step and representing the operating load of the unit. The use of a unit in each time step is bounded by the installed capacity through Eq. 2.2.

$$f_{u,t} \leq f_u \qquad \forall\ u \in \mathbf{U}, \forall\ t \in \mathbf{T} \quad (2.2)$$

Resource balances Neglecting any possibility of storage, for all resources at each time step the balance within each layer (except the thermal ones), defined by Eq. 2.3 has to be satisfied.

$$\sum_{u \in \mathbf{U_{ly}}} M^{-}_{u,ly,t} - \sum_{u \in \mathbf{U_{ly}}} M^{+}_{u,ly,t} = 0 \qquad \forall\ ly \in \mathbf{LY} \setminus \mathbf{HC}, \forall\ t \in \mathbf{T} \quad (2.3)$$

$M^{+/-}_{u,ly,t}$ represents the energy related to the resource of type ly input/output to the unit $u \in \mathbf{U_{ly}}$ during the time step t, linked to the unit reference size and defined by Eq. 2.4.

$$M^{+/-}_{u,ly,t} = \dot{\mathrm{M}}^{+/-,ref}_{u,ly} \cdot f_{u,t} \cdot \mathrm{f}_t \cdot \mathrm{d}_t \qquad \forall u \in \mathbf{U}, \forall ly \in \mathbf{LY}, \forall t \in \mathbf{T} \quad (2.4)$$

The type of resources subjected to Eq. 2.4 are for example the natural gas and the electricity.

Heat integration A heat cascade formulation, as initially proposed by Papoulias and Grossmann [76] is included in all locations and for each thermal layer, to solve the heat integration problem, while ensuring the feasibility of the heat exchanges (i.e., respecting the first and second law of thermodynamics). This formulation ensures that the balance is closed at the location level (first law) and that heat is transferred (i.e., cascaded) from higher to lower temperature intervals. The thermal streams belonging to each heat cascade layer are ordered by temperatures to define the set of temperature intervals $k \in \mathbf{K}$, with k integer. Equation 2.5 ensures that for each layer, location, time step and temperature interval the heat balance is closed (i.e., the first law of thermodynamic is satisfied).

$$\sum_{\substack{s\in\mathbf{HS_{hc}}\\ \mathrm{T}^{out}_{s,t}\geq \mathrm{T}_k}} f_{s,hc,t}\cdot \mathrm{C}_{\mathrm{p}_{s,t}}\cdot(\mathrm{T}^{in}_{s,t}-\mathrm{T}^{out}_{s,t}) + \sum_{\substack{s\in\mathbf{HS_{hc}}\\ \mathrm{T}^{out}_{s,t}\leq \mathrm{T}_k\leq \mathrm{T}^{in}_{s,t}}} f_{s,hc,t}\cdot C_{p_{s,t}}\cdot(\mathrm{T}^{in}_{s,t}-\mathrm{T}_k)$$
$$-\sum_{\substack{s\in\mathbf{CS_{hc}}\\ \mathrm{T}^{in}_{s,t}\geq \mathrm{T}_k}} f_{s,hc,t}\cdot C_{p_{s,t}}\cdot(\mathrm{T}^{out}_{s,t}-\mathrm{T}^{in}_{s,t}) - \sum_{\substack{s\in\mathbf{CS_{hc}}\\ \mathrm{T}^{in}_{s,t}\leq \mathrm{T}_k\leq \mathrm{T}^{out}_{s,t}}} f_{s,hc,t}\cdot C_{p_{s,t}}\cdot(\mathrm{T}^{out}_{s,t}-\mathrm{T}_k) - \dot{R}_{hc,k,lc,t} = 0$$
$$\forall\ hc\in\mathbf{HC}, \forall\ lc\in\mathbf{LC}, \forall\ t\in\mathbf{T}, \forall\ k=1,\ldots n_{k-1} \quad (2.5)$$

The heat balance in each temperature interval is achieved by cascading the heat residual $\dot{R}_{hc,k,lc,t}$ from higher (k) to lower ($k-1$) temperature intervals. In addition, Eqs. 2.6 and 2.7, respectively ensure that the balance is closed at the location level and the cascaded heat is always positive, therefore respecting the second law of thermodynamics (i.e., cascaded from higher to lower temperature levels).

$$\dot{R}_{hc,k,lc,t} = 0 \qquad \forall\ hc\in\mathbf{HC}, \forall\ lc\in\mathbf{LC}, \forall\ t\in\mathbf{T}, k=0, k=n_k \quad (2.6)$$
$$\dot{R}_{hc,k,lc,t} \geq 0 \qquad \forall\ hc\in\mathbf{HC}, \forall\ lc\in\mathbf{LC}, \forall\ t\in\mathbf{T}, k=1,\ldots n_{k-1} \quad (2.7)$$

$f_{s,hc,t}$ in Eq. 2.5 is the multiplication factor of the thermal stream s in the layer hc, linked to the one of the parent unit by Eq. 2.8:

$$f_{u,t} = \sum_{hc\in\mathbf{HC}:s\in\mathbf{S_{hc}}} f_{s,hc,t} \qquad \forall\ u\in\mathbf{U}\setminus\mathbf{HP}\setminus\mathbf{CH}, \forall s\in\mathbf{S_u} \quad (2.8)$$

which implies that if a thermal stream is assigned to a unique heat cascade layer, it takes the entire multiplication factor of the parent unit, while if assigned to multiple layers the load is redistributed among all the layers. Equation 2.8 is valid for all units except for HPs and CHIs, for which different equations, reported in Section 2.3.3 are employed to distinguish thermal streams associated to the condenser and to the evaporator. The definition of different heat cascade layers allows to intrinsically take into account forbidden matches between thermal streams.

Heat distribution network A set of networks $n\in\mathbf{N}$ = {HN, CN, AN} is defined including heating, cooling and anergy networks. A set of potential couples $T^{f/r}_n \in \mathbf{T^{f/r}_n}$, defined by temperature profiles for the feeding and returning line is assigned to each network. The condition to satisfy for each couple is that in each time step the returning temperature is lower then or equal to the feeding one (Eq. 2.9).

$$T^{f/r}_n = (\mathrm{T}^f_n, \mathrm{T}^r_n) \Leftrightarrow \mathrm{T}^r_{n,t} \leq \mathrm{T}^f_{n,t} \qquad \forall\ t\in\mathbf{T}, \forall\ n\in\mathbf{N} \quad (2.9)$$

From the set $\mathbf{T^{f/r}_n}$, the set of feeding temperatures for each network ($\mathbf{T^f_n}$) can also be defined. A superstructure of network hot and cold utilities ($nu\in\mathbf{NU}\subset\mathbf{UU}$) is defined including one cold and one hot utility for each couple $T^{f/r}_n$ and each network n in any location identified as a potential route of the network n. Network utilities represent heat exchangers and are used to close the heat balance at the location level and to define the temperature profiles of the mass flowing to and from each location. Each unit nu is characterized by one unique thermal stream defined in each time step, as all other thermal streams, by the inlet temperature $\mathrm{T}_{s,t}^{in}$, outlet temperature $\mathrm{T}_{s,t}^{out}$ and reference heat load $\Delta\dot{\mathrm{H}}_{s,t}^{ref}$. For each nu assigned to the generic couple $T^{f/r}$, inlet and outlet temperatures must reproduce the profiles T^{f} and T^{r} (in case of hot utility or vice-versa in case of cold utility). The only exception are the cooling utilities assigned to the anergy and cooling network, for which the network feeding temperature T^{f} represents the stream inlet temperature, while the outlet temperature is defined as $\mathrm{T}_{s,t}^{out} = \mathrm{T}_{t}^{f} + \mathrm{T}_{t}^{f} - \mathrm{T}_{t}^{r}$. This modification is needed to take into account that if a couple of temperatures $T^{f/r}$ is assigned to the anergy or cooling network such as 10/8°C, the corresponding network hot utilities can deliver the heat between 10 and 8°C (in the case of an anergy network), whereas the network cold utilities can supply the cold between 10 and 12°C (considering the same temperature difference in the heat exchanger).

The subset of network utilities assigned to the generic couple $T^{f/r}$ and network n is defined as $nu \in \mathbf{NU^{T_n^{f/r}}} = \{\mathbf{NHU^{T_n^{f/r}}} \cup \mathbf{NCU^{T_n^{f/r}}}\} \subset \mathbf{NU}$. An additional subset of network utilities is defined for each potential feeding temperature of each network ($nu \in \mathbf{NU^{T_n^{f}}} = \{\mathbf{NHU^{T_n^{f}}} \cup \mathbf{NCU^{T_n^{f}}}\} \subset \mathbf{NU}$). The latter are characterized by a fixed ΔT between inlet and outlet temperatures independent from that of the network. These units are employed to take into account that the evaporators of HPs might work at fixed ΔT, different than that of the network. For each network and assigned temperature couple two parallel mass balances are solved, one relative to the ΔT defined between the network feeding and returning temperature and another to the fixed ΔT required at the evaporators of HPs. Further details are reported later in this section.

The existence of a network is governed by a binary variable y_n. All locations are coupled, forming the set of potential connections $(lc_1, lc_2) \in \mathbf{LC^N}$. Any directed arc between two generic locations (lc_1, lc_2) is a potential network pipe. The existence of a network arc (feeding line) for each network is governed by a directional binary variable $y_{lc_1,lc_2,n}$. The existence of a network pipe between two locations is subjected to the installation of the network, by Eq. 2.10.

$$y_{lc_1,lc_2,n} \leq y_n \qquad \forall\ (lc_1, lc_2) \in \mathbf{LC^N}, \forall\ n \in \mathbf{N} \quad (2.10)$$

A parameter $\mathrm{y}_{lc_1,lc_2,n}$ can be specified for each couple of locations to restrict the choice of network arches of type n through Eq. 2.11.

$$y_{lc_1,lc_2,n} \leq \mathrm{y}_{lc_1,lc_2,n} \qquad \forall\ (lc_1, lc_2) \in \mathbf{LC^N}, \forall\ n \in \mathbf{N} \quad (2.11)$$

Equation 2.11 is particularly useful to restrict the choice for the potential connections and consequently reduce the problem size. Equation 2.12 enforces that between two locations only one feeding line can be installed.

$$y_{lc_1,lc_2,n} + y_{lc_2,lc_1,n} \leq 1 \qquad \forall\ (lc_1, lc_2) \in \mathbf{LC^N}, \forall n \in \mathbf{N} \quad (2.12)$$

The network temperatures (feeding and returning line) are assumed to be the same for all the connections belonging to the same network. A binary variable ($y_{n,T_n^{f/r}}$) defines the activation of one of the couples $T_n^{f/r}$ for the network n, while Eq. 2.13 restricts the activation to only one couple.

$$\sum_{T_n^{f/r} \in \mathbf{T^{f/r}}} y_{n,T_n^{f/r}} \leq y_n \qquad \forall\, n \in \mathbf{N} \quad (2.13)$$

Moreover, a set of diameters $dn \in \mathbf{DN}$ is defined to assign a diameter to each type of network n, through the binary variable $y_{n,dn}$ and restrict the choice to only one by Eq. 2.14:

$$\sum_{dn \in \mathbf{DN}} y_{n,dn} \leq y_n \qquad \forall\, n \in \mathbf{N} \quad (2.14)$$

which implies that the same diameter is chosen for all the pipes belonging to the same network. In each feeding pipe of network n and diameter dn, connecting the locations lc_1 and lc_2 and at the temperatures defined by the couple $T_n^{f/r}$, the mass flow rate is defined by three continuous variables:

- $\dot{m}^h_{lc_1,lc_2,n,T_n^{f/r},dn,t}$ is the flow rate from lc_1 towards lc_2 and at the temperature T_n^f in the feeding line
- $\dot{m}^c_{lc_1,lc_2,n,T_n^{f/r},dn,t}$ is the mass flow rate from lc_1 towards lc_2 for cooling purposes
- $\dot{m}^{hp}_{lc_1,lc_2,n,T_n^f,dn,t}$ is the mass flow rate used to enforce a fixed ΔT at the evaporators of the decentralized HPs, independent to that of the network and therefore linked only to the feeding network temperature T_n^f.

A series of constraints (Eqs. 2.16 to 2.18) restricts the mass flow rate in each connection to the choice of the network type, diameter and operating temperatures. The maximum value of mass flow rate is defined by the pipe diameter and corresponding maximum velocity, through Eq. 2.15.

$$\dot{\mathrm{M}}_{dn} = \rho \cdot \mathrm{v}_{dn}^{max} \cdot \pi \cdot \frac{dn^2}{4} \qquad \forall\, dn \in \mathbf{DN} \quad (2.15)$$

Equation 2.16 restricts the mass flow rate to the selection of the network diameter and intrinsically to the network installation.

$$\sum_{T_n^{f/r} \in \mathbf{T_n^{f/r}}} \dot{m}^h_{lc_1,lc_2,n,T_n^{f/r},dn,t} + \dot{m}^c_{lc_1,lc_2,n,T_n^{f/r},dn,t} + \sum_{T_n^f \in \mathbf{T^f}} \dot{m}^{hp}_{lc_1,lc_2,n,T_n^f,dn,t} \leq \dot{\mathrm{M}}_{dn} \cdot y_{n,dn}$$
$$\forall\, (lc_1, lc_2) \in \mathbf{LC^N}, \forall\, n \in \mathbf{N}, \forall\, dn \in \mathbf{DN}, \forall\, t \in \mathbf{T} \quad (2.16)$$

Finally, Eqs. 2.17 and 2.18 restrict the mass flow rate to the choice of the operating temperatures.

$$\dot{m}^h_{lc_1,lc_2,N,T_n^{f/r},dn,t} + \dot{m}^c_{lc_1,lc_2,n,T_n^{f/r},dn,t} \leq \dot{\mathrm{M}}_{dn} \cdot y_{n,T_n^{f/r}}$$

$$\forall\ (lc_1, lc_2) \in \mathbf{LC^N}, \forall\ n \in \mathbf{N}, \forall\ T_n^{f/r} \in \mathbf{T_n^{f/r}}, \forall\ dn \in \mathbf{DN}, \forall\ t \in \mathbf{T} \quad (2.17)$$

$$\dot{m}^{hp}_{lc_1,lc_2,n,T_n^f,dn,t} \leq \dot{\mathrm{M}}_{dn} \cdot \sum_{T^r \in \mathbf{T^r_{T_n^f}}} y_{n,T_n^f}$$
$$\forall\ (lc_1, lc_2) \in \mathbf{LC^N}, \forall\ n \in \mathbf{N}, \forall\ T^f \in \mathbf{T_n^f}, \forall\ dn \in \mathbf{DN}, \forall\ t \in \mathbf{T} \quad (2.18)$$

Where $\mathbf{T^f}_n$ is the set of feeding temperature profiles of network n and $\mathbf{T^r_{T_n^f}}$ is the set of all the return temperatures assigned to the feeding temperature T_n^f. For each location, time step and network type, two types of mass balances are written: Eq. 2.19 depending on the temperature couple $T^{f/r}$ and Eq. 2.20 depending only on the network feeding temperature T^f.

$$\sum_{\substack{nu \in \mathbf{NCU^{T_n^{f/r}}} \cap \mathbf{U_{lc}}, \\ s \in \mathbf{S_{nu}}}} \frac{f_{nu,t}}{\Delta\dot{\mathrm{H}}^{ref}_{s,t}} - \sum_{\substack{nu \in \mathbf{NHU^{T_n^{f/r}}} \cap \mathbf{U_{lc}}, \\ s \in \mathbf{S_{nu}}}} \frac{f_{nu,t}}{\Delta\dot{\mathrm{H}}^{ref}_{s,t}} =$$
$$\sum_{\substack{(lc_x, lc) \in \mathbf{LC^N}: \\ lc_x \neq lc}} \left(\dot{m}^h_{lc,lc_x,n,T_n^{f/r},dn,t} - \dot{m}^h_{lc_x,lc,n,T_n^{f/r},dn,t} \right) + \left(\dot{m}^c_{lc_x,lc,n,T_n^{f/r},dn,t} - \dot{m}^c_{lc,lc_x,n,T_n^{f/r},dn,t} \right)$$
$$\forall\ dn \in \mathbf{DN}, \forall\ n \in \mathbf{N}, \forall\ lc \in \mathbf{LC}, \forall\ t \in \mathbf{T}, \forall\ T_n^{f/r} \in \mathbf{T_n^{f/r}} \quad (2.19)$$

$$\sum_{\substack{nu \in \mathbf{NCU^{T_n^f}} \cap \mathbf{U_{lc}}, \\ s \in \mathbf{S_{nu}}}} \frac{f_{nu,t}}{\Delta\dot{\mathrm{H}}^{ref}_{s,t}} - \sum_{\substack{nu \in \mathbf{NHU^{T_n^f}} \cap \mathbf{U_{lc}}, \\ s \in \mathbf{S_{nu}}}} \frac{f_{nu,t}}{\Delta\dot{\mathrm{H}}^{ref}_{s,t}} + \sum_{\substack{(lc_x, lc) \in \mathbf{LC^N}: \\ lc_x \neq lc}} \dot{m}^{hp}_{lc_x,lc,n,T_n^f,dn,t} -$$
$$\sum_{\substack{(lc_x, lc) \in \mathbf{LC^N}: \\ lc_x \neq lc}} \dot{m}^{hp}_{lc,lc_x,n,T_n^f,dn,t} = 0$$
$$\forall\ dn \in \mathbf{DN}, \forall\ n \in \mathbf{N}, \forall\ lc \in \mathbf{LC}, \forall\ t \in \mathbf{T}, \forall\ T_n^f \in \mathbf{T_n^f} \quad (2.20)$$

Pressure losses Pressure losses are introduced by estimating the losses at the nominal flow rate for each diameter dn, given by dp_{dn}, and scaling them to the current flow rate in each time step. A circulation pump $up \in \mathbf{UP} \subset \mathbf{UU}$ is included to cover the need of electricity resulting from Eq. 2.21.

$$f_{up,t} \cdot \dot{M}^{-,ref}_{up,ly=el} \geq \frac{2\mathrm{dp}_{dn}}{1000\eta_P \rho} \sum_{\substack{(lc_1, lc_2) \in \mathbf{LC^N} \\ dn \in \mathbf{DN} \\ n \in \mathbf{N}}} \mathrm{L}_{lc_1,lc_2} \left(\sum_{T^{f/r} \in \mathbf{T^{f/r}}} \dot{m}^h_{lc_1,lc_2,n,T^{f/r},dn,t} + \right.$$
$$\left. \dot{m}^c_{lc_1,lc_2,n,T^{f/r},dn,t} + \sum_{T^f \in \mathbf{T_n^f}} \dot{m}^{hp}_{lc_1,lc_2,n,T^f,dn,t} \right)$$
$$\forall\ t \in \mathbf{T}, \forall\ up \in \mathbf{UP} \quad (2.21)$$

η_P represents the pump efficiency, ρ the fluid density and L_{lc_1,lc_2} the Manhattan distance between locations lc_1 and lc_2. The nominal pressure drop dp_{dn} is estimated in [Pa/m] through the Darcy-Weisbach equation (2.22):

$$\mathrm{dp}_{dn} = \lambda \frac{\rho}{2} \frac{v_{dn}^2}{dn} \qquad \forall\ dn \in \mathbf{DN} \quad (2.22)$$

with $\lambda = 0.11 \left(\frac{K}{dn} + \frac{68}{Re_{dn}} \right)^{0.25}$, named the Darcy friction factor or flow coefficient (dimensionless), in which K is the relative duct roughness, expressed in [m] and $Re_{dn} = \frac{v_{dn} dn \rho}{\mu}$ the Reynolds number also calculated at maximum velocity.

Equation 2.23 takes into account the limitations of the maximum and minimum mass flow rate, with the latter assumed as 10% of the former.

$$\mathrm{y_{ON}}_t \frac{2\mathrm{dp}_{dn}}{1000\eta_P \rho} \sum_{\substack{(lc_1,lc_2)\in \mathbf{LC^N} \\ dn\in\mathbf{DN} \\ n\in\mathbf{N}}} 0.1 \cdot \mathrm{L}_{lc_1,lc_2} \dot{\mathrm{M}}_{dn} \le f_{u,t} \cdot \dot{M}^{-,ref}_{up,ly=el} \le \frac{2\mathrm{dp}_{dn}}{1000\eta_P \rho} \sum_{\substack{(lc_1,lc_2)\in \mathbf{LC^N} \\ dn\in\mathbf{DN} \\ n\in\mathbf{N}}} \mathrm{L}_{lc_1,lc_2} \dot{\mathrm{M}}_{dn}$$
$$\forall\ t \in \mathbf{T}, \forall\ u \in \mathbf{UP} \quad (2.23)$$

Equation 2.23 ensures a minimum flow rate in the pipelines. The parameter $\mathrm{y_{ON}}_t$ takes value 0 outside the heating season. The presence of this parameter avoids that pumping losses are considered during the summer, when the heating network (HN) is only operated to cover the DHW demand but at the same time neglects the losses in the AN during the same period. Due to the low contribution of the circulating pump to the overall system expenses (see Fig. 2.21), this assumption is considered justified.

Thermal losses Thermal losses are estimated as a linear function of the difference between the network mean temperature (calculated between the supply and return) and the surroundings. For each feeding temperature T^f, to model the thermal losses a unit is defined including a thermal cold stream at the temperature T^f. The operating load of such a unit is linked to the estimated losses by Eq. 2.24:

$$f_{u,t} \cdot \Delta\dot{\mathrm{H}}^{ref}_{s\in\mathbf{S_u},t} = \sum_{\substack{(lc_1,lc_2)\in \mathbf{LC^N} \\ dn\in\mathbf{DN} \\ n\in\mathbf{N} \\ T^r_n \in \mathbf{T^r_{T^f_n}} : T^f_n \in \mathbf{T^f_n}}} 2 \cdot \mathrm{y_{ON}}_t \cdot y_{n,dn} \cdot y_{lc_1,lc_2,n} \cdot y_{n,T_n^{f/r}} \cdot \left(\overline{\mathrm{T}}^{f/r}_{n,t} - T^{\infty}_t \right) \cdot \mathrm{q}^{\mathrm{loss}}_{dn} \cdot \mathrm{L}_{lc_1,lc_2}$$
$$\forall\ t \in \mathbf{T}, \forall\ u \in \mathbf{UL_{T^f}} \quad (2.24)$$

where:

- the product $y_{n,dn} \cdot y_{lc_1,lc_2,n} \cdot y_{n,T_n^{f/r}}$ is linearized by introducing additional variables and constraints, following the procedure reported in Section B.2;

- $\mathrm{q}_{dn}^{\mathrm{loss}}$ is the thermal loss parameter expressed for each diameter in [kW/K/m] and estimated through the procedure reported in Section B.3;
- L_{lc_1,lc_2} is the Manhattan distance between locations lc_1 and lc_2;
- $\overline{\mathrm{T}}_{n,t}^{f/r}$ is the average temperature between supply and return;
- T^{∞} is the temperature of the surroundings;
- $\mathbf{T^r_{T^f_n}} = T^r_n : (T^f_n, T^r_n) \in \mathbf{T^{f/r}_n}$ groups the potential return temperatures associated to the feeding temperature T^f_n;
- $\mathbf{UL_{T^f}}$ is the set linking the units of thermal losses to each temperature of the feeding line, making the assumption that losses for different returning temperature must be both compensated with heat at the same temperature (the one of the feeding line).

The estimation of the coefficient q_{dn}^{loss} for above ground and buried pipes and the justification of using the linear dependency with the temperature are all reported in Section B.3.

2.3.3 Technologies

Heat pumps

HPs can be installed at the central heating station to supply the DHN or at decentralized locations to directly feed the users. The latter machines can either be water-water HPs upgrading heat from the heating or anergy network to the required temperature or air-water HPs connected to the ambient air. The existence, installed capacity, operating profiles and level of temperatures are decision variables in the optimization.

As with all other units, HPs are modelled by means of a set of streams: one resource flow linked to the electricity layer and defining the power needed by the compressor and at least one couple of hot and cold streams identifying the condenser and evaporator, respectively. Since the operation of each HP is subjected to the choice of the network temperatures, for each unit a set of potential couples of evaporator and condenser streams are defined $c^{c/e} = (s_c, s_e)_{hp} \in \mathbf{C_{hp}}$. The activation of one of those couples is governed by the binary variable $y_{c^{c/e}}$ and linked to the purchase of the parent unit $y_{u=hp}$, by Eq. 2.25.

$$y_{c^{c/e}} \leq y_{hp} \qquad \forall\ c^{c/e} \in \mathbf{C_{hp}}, \forall\ hp \in \mathbf{HP} \quad (2.25)$$

Furthermore Eq. 2.26 restricts the choice to only one couple.

$$\sum_{c^{c/e} \in \mathbf{C_{hp}}} y_{c^{c/e}} \leq 1 \qquad \forall\ hp \in \mathbf{HP} \quad (2.26)$$

Equation 2.27 links the multiplication factor of the streams in each couple to the activation of the parent couple, while Eqs. 2.28 and 2.29 bound it to the load of the parent unit $f_{hp,t}$.

$$\sum_{hc \in \mathbf{HC}: s \in \mathbf{S_{hc}}} f_{s,hc,t} \leq y_{c^{c/e}} \cdot \mathrm{F}^{\max}_{hp} \quad \forall\ t \in \mathbf{T}, \forall\ s \in \mathbf{S_{hp}} : s = s_c | s_e, \forall\ (s_c, s_e)_{hp} \in \mathbf{C_{hp}}, \forall\ hp \in \mathbf{HP} \tag{2.27}$$

$$\sum_{\substack{hc \in \mathbf{HC} \\ s \in \mathbf{S_{hp}} \bigcap \mathbf{HS} \bigcap \mathbf{S_{hc}}}} f_{s,hc,t} = f_{hp,t} \quad \forall\ t \in \mathbf{T}, \forall\ hp \in \mathbf{HP} \tag{2.28}$$

$$\sum_{\substack{hc \in \mathbf{HC} \\ s \in \mathbf{S_{hp}} \bigcap \mathbf{CS} \bigcap \mathbf{S_{hc}}}} f_{s,hc,t} = f_{hp,t} \quad \forall\ t \in \mathbf{T}, \forall\ hp \in \mathbf{HP} \tag{2.29}$$

Finally, Eq. 2.30 states that evaporator and condenser belonging to the same couple must have the same multiplication factor.

$$\sum_{hc \in \mathbf{HC}} f_{s_c,hc,t} = \sum_{hc \in \mathbf{HC}} f_{s_e,hc,t} \quad \forall\ t \in \mathbf{T}, \forall\ c^{c/e} \in \mathbf{C_{hp}}, \forall\ hp \in \mathbf{HP} \tag{2.30}$$

As a result, once a HP is installed and its size defined, only one of the couples $c^{c/e}$ assigned to the unit is activated and for each time step t, the reference heat load $\Delta\dot{\mathrm{H}}^{ref}_{s,t}$ of the two streams s_c and s_e belonging to the couple is scaled according to the unit multiplication factor $f_{hp,t}$, eventually distributed among the different thermal layers the stream is associated to.

For each HP, the electricity stream characterizes the size of the unit: the reference electricity required by the unit $\dot{\mathrm{M}}^{+,ref}_{hp,el,t}$ is defined constant for each time step and consequently scaled according to the unit load $f_{hp,t}$. On the other hand, for each couple $c^{c/e}$ belonging to the unit, a COP is associated to each time step, depending on the operating temperatures of the two thermal streams. The reference flow of the latter is determined accordingly as reported in Eqs. 2.31 and 2.32.

$$\Delta\dot{\mathrm{H}}^{ref}_{s_c,t} = \mathrm{COP}_{c^{c/e},t} \cdot \dot{M}^{+}_{hp,ly,t} \quad \forall\ t \in \mathbf{T}, \forall\ c^{c/e} \in \mathbf{C_{hp}}, \forall\ hp \in \mathbf{HP}, ly = el \tag{2.31}$$

$$\Delta\dot{\mathrm{H}}^{ref}_{s_e,t} = (\mathrm{COP}_{c^{c/e},t} - 1) \cdot \dot{M}^{+}_{hp,ly,t} \quad \forall\ t \in \mathbf{T}, \forall\ c^{c/e} \in \mathbf{C_{hp}}, \forall\ hp \in \mathbf{HP}, ly = el \tag{2.32}$$

Particular care is devoted to estimate the performance of water-water HPs. The procedure, based on that presented by Henchoz [22] is hereby reported, while additional parameters assumed for the models are listed in Tables B.2 and B.3.

Water-water heat pump performance estimation Considering the variation of the isentropic compressor efficiency with the pressure ratio, an example of compressor is taken as a reference to model this behavior. For such compressors, the manufacturer has published the results of standardized tests (EN12900), disclosing the mass flow rate, heat evacuated at the evaporator and electric power as a polynomial function of the evaporating and condensing temperatures. Additional information on the chosen compressor and the relative polynomial functions are reported in Section B.1.1. Employing basic thermodynamic laws, and using the information given by the manufacturer, the isontropic efficiency of the compressor can be derived for the whole operating range of the machine. The procedure is reported in Section B.1.1, whereas Fig. 2.1 shows the results.

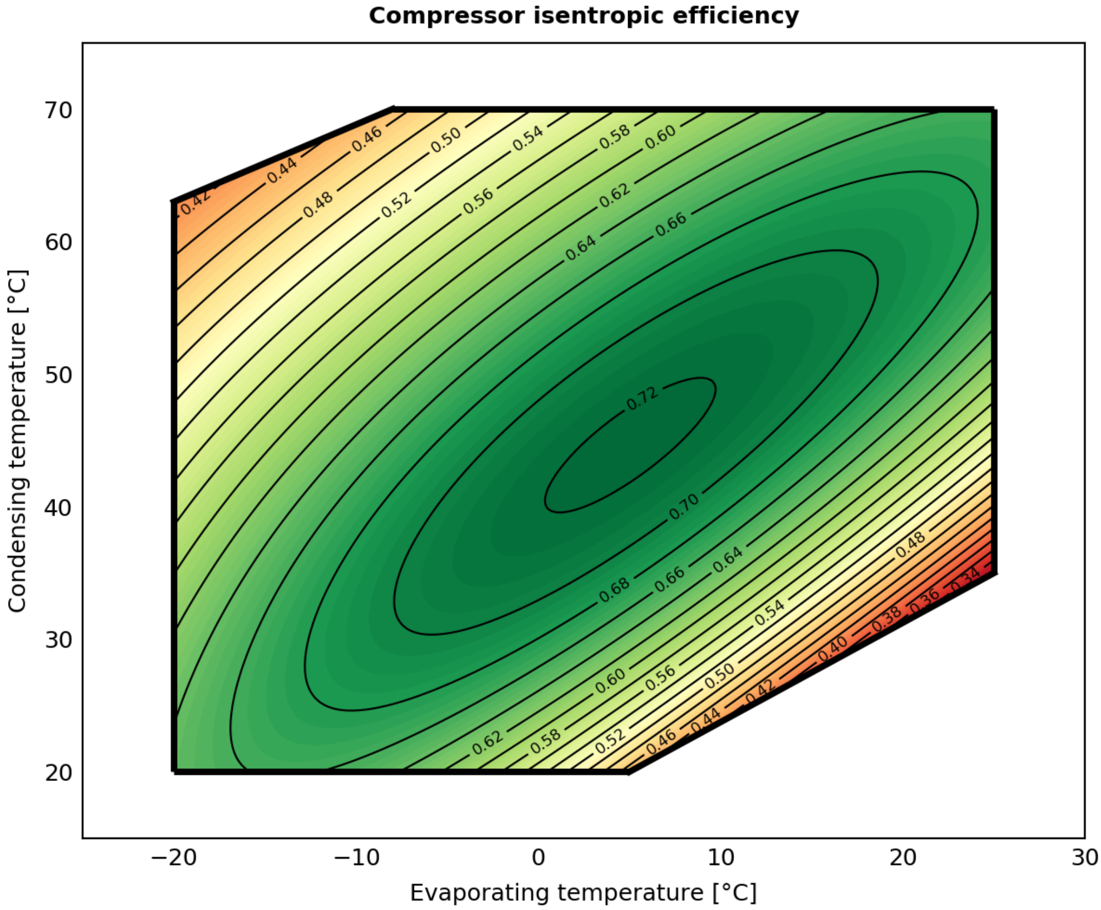

Figure 2.1: Compressor isentropic efficiency at varying evaporating and condensing temperatures.

The isentropic compressor efficiency, as a function of the evaporating and condensing temperatures, can be used for estimating the COP of the considered HPs. Several definitions are required to distinguish conditions and locations in the system. Here, the subscripts $_e$ and $_c$ refer to the conditions of the refrigerant, $_{evap}$ and $_{cond}$ to those of the outer fluid (sink and source), $_g$ and $_l$ to the liquid and gaseous state, respectively.

The efficiency of a HP working between the temperatures T_{evap} and T_{cond} can be estimated based on the compressor map. At the evaporator, a ΔT_e^{min} = 1.5°C is considered[1], while at the condenser the ΔT_c^{min} is neglected, since the temperature of the superheated vapor at the

[1]During the optimisation it is assumed that the AN at the evaporator of the central HP is cooled down by 2°C, while the water network at the evaporators of decentralized HPs by 4°C, therefore in both cases the ΔT_e^{min} is respected also at the evaporator inlet (outlet for the refrigerant).

exit of the compressor is always intrinsically higher. T_{evap} represents the temperature at the exit of the evaporator (water side), while T_{cond} represents the temperature at the exit of the condenser (water side). T_e and T_c are the evaporation and condensation temperatures in the thermodynamic cycle (refrigerant side), linked to the previous ones as follows:

$$T_e = T_{evap} - \Delta T_e^{min} \tag{2.33a}$$

$$T_c = \max(T_{cond}, T_e + 10) \tag{2.33b}$$

ΔT_{SH} = 2°C is taken as a starting point for the superheating at the evaporator exit and iteratively increased by 1°C if the end of the compression falls inside the saturation curve. A minimum ΔT^{lift} equal to 10°C is considered to take into account that, as reported by Gasser et al. [77], HPs currently available on the market do not provide low temperature lift. The value of 10°C is chosen based on the prototype reported in the same study. The thermodynamic points at the inlet and outlet of the compressor can be evaluated as reported in Eqs. 2.34a to 2.34d.

$$h_{e,g} = f(T_e + \Delta T_{SH},\ p_e) \tag{2.34a}$$

$$s_{e,g} = f(T_e + \Delta T_{SH},\ p_e) \tag{2.34b}$$

$$h_{c,g,is} = f(p_c,\ s_{e,g}) \tag{2.34c}$$

$$h_{c,g} = h_{e,g} + \frac{(h_{c,g,is} - h_{e,g})}{\eta_{is}} \tag{2.34d}$$

As previously mentioned, in the case that the compressor outlet falls inside the saturation curve (i.e., $x_{c,g} = f(p_c, h_{c,g}) \leq 1$), the superheating temperature difference is increased ($\Delta T_{SH,new} = \Delta T_{SH} + 1$) and the point at the outlet of the compressor recalculated. The isentropic efficiency is evaluated combining the information from the compressor map of Fig. 2.1 and shifting the values to the current operation as later explained. Potential differences due to the fact that the compressor performance refers to a larger superheating temperature difference ($\Delta T_{SH} = 10K$, as imposed by the norm EN12900) are neglected. Assuming that the condensation ends at the saturated liquid point $h_{c,l}$, the COP can be calculated as:

$$COP = \frac{h_{c,g} - h_{c,l}}{h_{c,g} - h_{e,g}} \tag{2.35}$$

Under the same assumptions of $\Delta T_{e/c}^{min}$ at the condenser and evaporator, the theoretical COP of the same HP can be calculated as follows:

$$COP_{th} = \frac{T_{cond} + 273.15}{T_{cond} - T_{evap} + \Delta T_e^{min}} \tag{2.36}$$

The Carnot efficiency η_{II} is defined as the ratio between the real and the theoretical COP:

$$\eta_{II} = \frac{COP}{COP_{th}} \tag{2.37}$$

In the following, when referring to a simple COP calculation a constant Carnot efficiency of 0.55 is assumed. Figure 2.2 shows the Carnot efficiency curve for varying temperatures at the source and sink. Figure 2.3 shows the Carnot efficiency curve for the same points as the

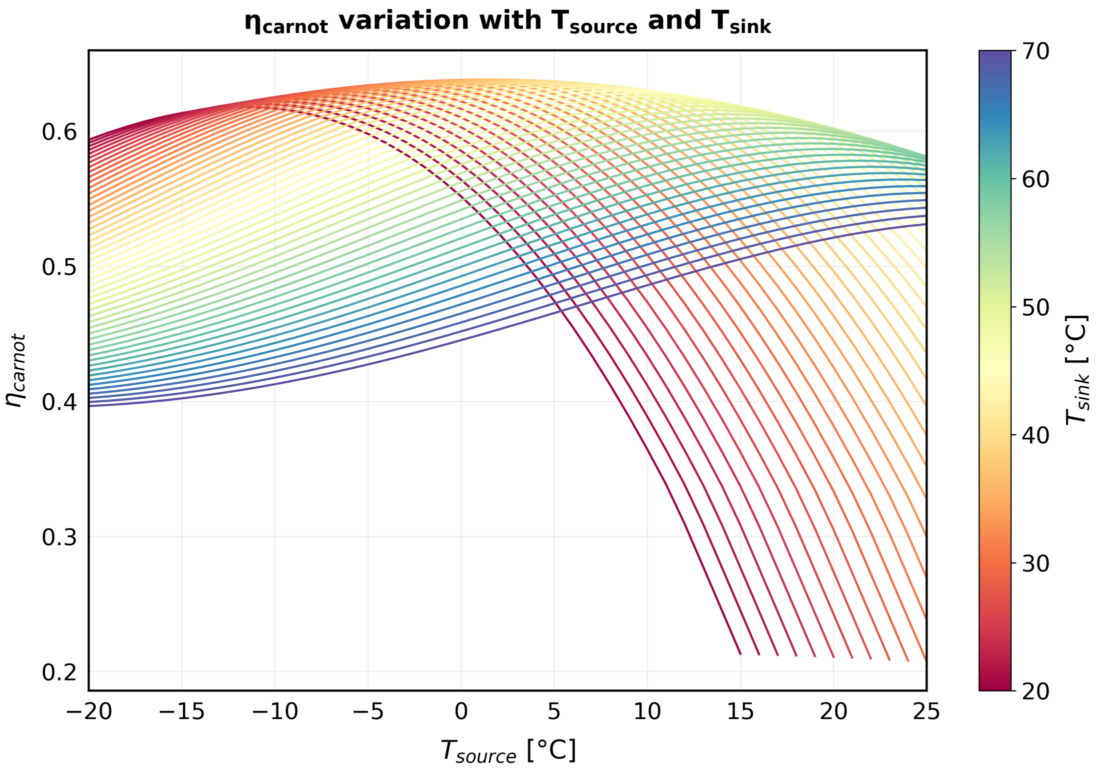

Figure 2.2: Carnot efficiency for varying source and sink temperatures.

previous, but highlights the temperature lift in the colorbar.

Figures 2.2 and 2.3 report the Carnot efficiency of a HP, using the same compressor as the one taken as a reference, which shows the best performance around a ΔT^{lift} of 40°C. Not to penalize potential machines working in a different operating range with respect to the one taken as reference, the trend of the isentropic efficiency with respect to the temperature lift is first interpolated and then shifted such as to always get the best efficiency within the operating range of each HP and keeping the location of the maximum efficiency with respect to the operating bounds as in the reference case. Figure 2.4 shows the map of the values of the isentropic efficiency of Fig. 2.1 plotted against the temperature lift: the upper bound of the area is highlighted in black, while a red line with diamonds markers identifies its interpolation, including the constraint of passing through zero.

Every time that the performance of a HP must be evaluated, the red solid curve in the figure above is taken as reference and translated within the new operating range of the machine. First, in the original curve the relative position of the maximum efficiency $\Delta T_{\%}^{lift}$ with respect

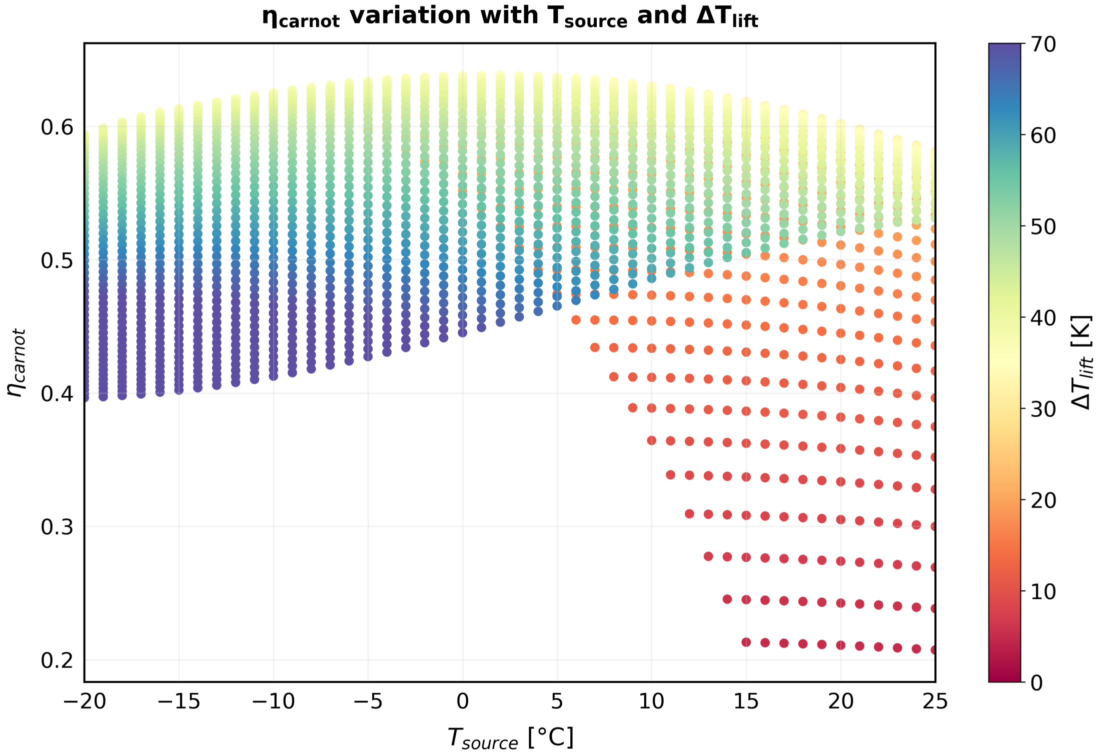

Figure 2.3: Carnot efficiency for varying source temperature and ΔT_{lift}.

to the bounds is evaluated as reported in Eq. 2.38.

$$\Delta \mathrm{T}_{\%}^{lift} = \frac{\Delta \mathrm{T}_{\eta^{max}}^{lift} - \Delta \mathrm{T}_{min}^{lift}}{\Delta \mathrm{T}_{max}^{lift} - \Delta \mathrm{T}_{min}^{lift}} \tag{2.38}$$

$\Delta \mathrm{T}_{\%}^{lift}$ gives the information of where to localize the maximum efficiency if a HP has a new operating range with respect to the reference. Consequently the isentropic efficiency used in Eq. 2.34d, is evaluated as follows:

$$\eta_{is}(\mathrm{T}_e, \mathrm{T}_c) = a \cdot x^3 + b \cdot x^2 + c \cdot x \tag{2.39}$$

Where a, b and c are the coefficients of the polynomial resulting from the fitting of the maximum isentropic efficiency (solid red line with diamonds markers in Fig. 2.4) and x is the temperature lift, including the translation of the curve and the constraint of a minimum $\Delta \mathrm{T}^{lift}$ of 10°C, as reported in Eq. 2.40.

$$\Delta \mathrm{T}^{lift} = \mathrm{T}_e - \mathrm{T}_c \tag{2.40}$$

$$x = \max(\mathrm{T}_e + 10, \mathrm{T}_c) - \mathrm{T}_e + \Delta \mathrm{T}_{\eta^{max}}^{lift} - \left(\min(\Delta \mathrm{T}^{lift}) + \left(\max(\Delta \mathrm{T}^{lift}) - \min(\Delta \mathrm{T}^{lift})\right) \cdot \Delta \mathrm{T}_{\%}^{lift}\right)$$

This procedure is meant to take into account the possibility that another HP in the market

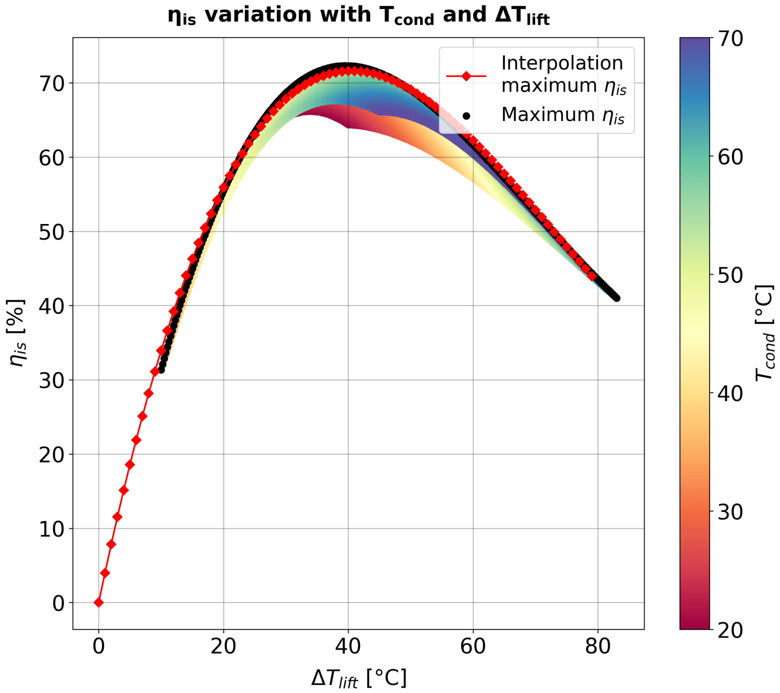

Figure 2.4: Interpolation of the maximum isentropic efficiency curve as a function of the temperature lift (black dots). The red line with diamonds markers represents the interpolation of the black dots curve while the solid red line includes the constraint of passing through the zero point.

would be specifically designed for the new operating range. Figure 2.5 shows the COP calculated with a constant Carnot efficiency of 0.55 and with the procedure presented above (the resulting varying Carnot efficiency is reported in red on the plot). The operating temperatures of the source and sink reflect the temperature profiles during the typical operating periods used for the application reported later in this chapter, related to the source of low-temperature heat (LTH) and a HN designed to work up to 70°C in extreme conditions. Therefore this HP could represent the operating performance of a potential machine in the central plant, coupled with a high temperature network.

Figure 2.6 shows, for the same machine, the deviation between the advanced and simple COP and the respective number of hours of occurrence within the reference year of operation.

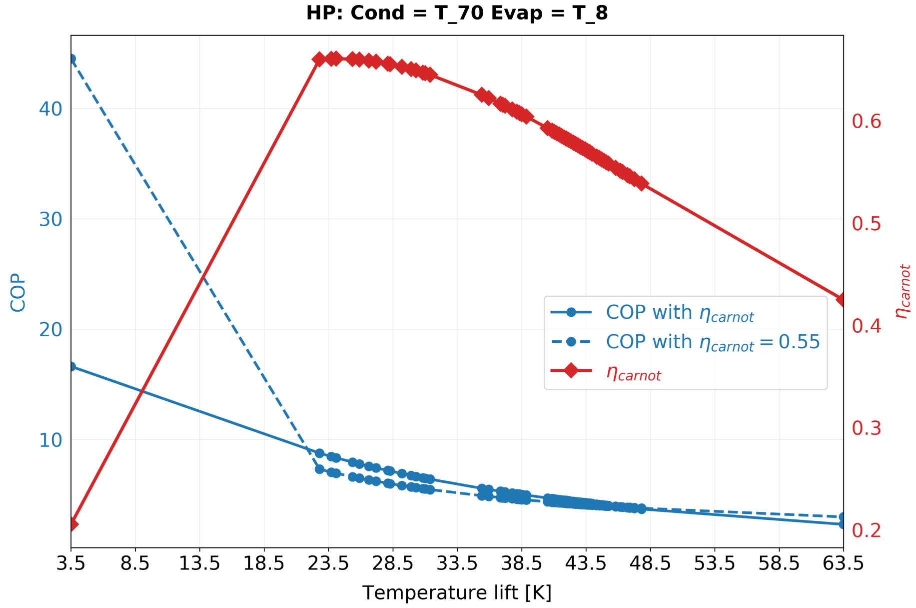

Figure 2.5: COP calculated with varying and constant exergy efficiency for a potential central plant.

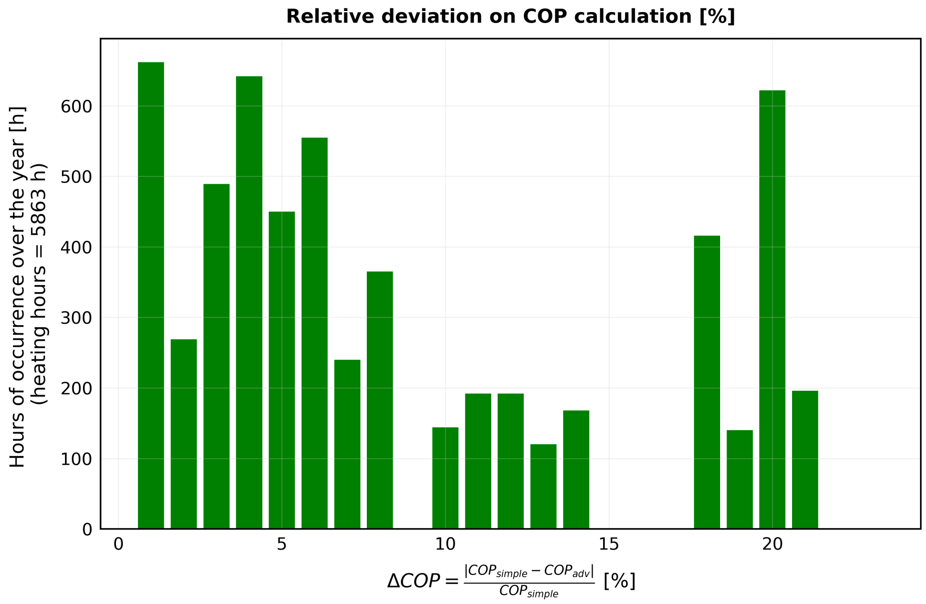

Figure 2.6: Deviation of simple and advanced COP calculation and relative number of hours of occurrence over the reference year for a potential central plant.

Figure B.1, in Section B.1.1, reports the cumulative number of hours of occurrence for different values of deviation between the advanced and simple COP calculation.

The same analyses are made for a potential decentralized HP raising the temperature of the network from 50 to 70°C (at extreme conditions) and the results reported in Figures B.2, 2.7 and 2.8.

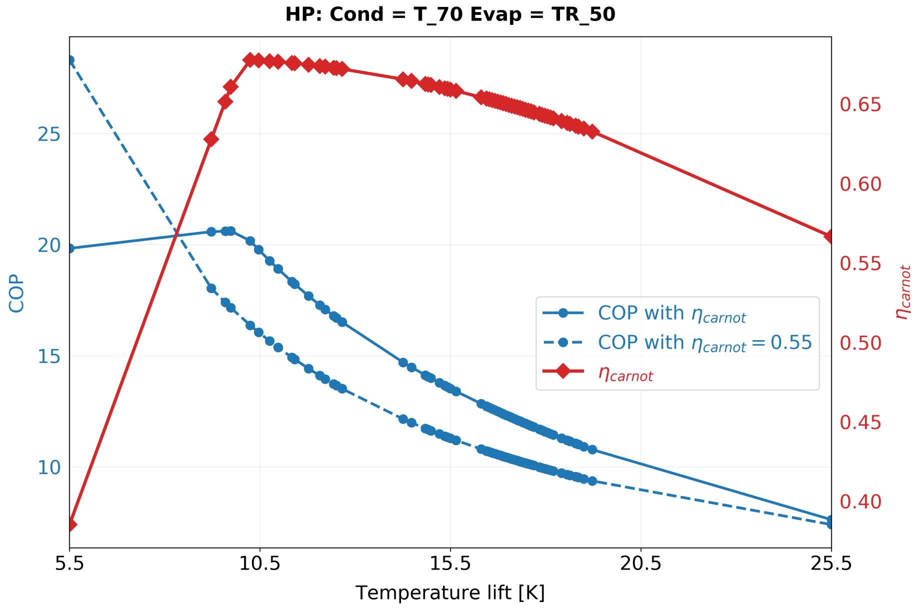

Figure 2.7: COP calculated with varying and constant exergy efficiency for a potential decentralized heat plant.

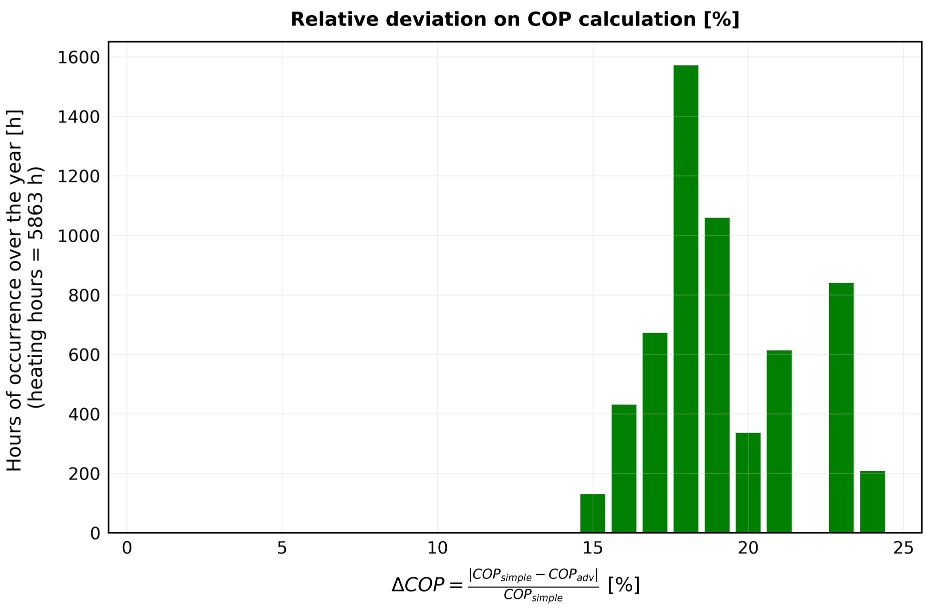

Figure 2.8: Deviation of simple and advance COP calculation and relative number of hours of occurrence over the reference year for a potential decentralized heat pump.

As highlighted by the comparison of the deviation of the COP for a potential centralized and decentralized HP, while in the first case the use of a constant Carnot efficiency seems being a good approximation (the deviation is lower than 15% for almost 80% of the operation), for the decentralized machines, working at a lower temperature lift, the error committed for not taking into account the variation in the compressor isentropic efficiency is between 15 to 25%.

Chillers

CHIs are modelled to be able to supply both space cooling and refrigeration demand. In the first case the condenser is cooled down by ambient air, while in the second one it can be also connected to a LTN (anergy or cooling). As for the HPs, different streams are defined, including one electricity resource stream representing the compressor demand, and couples of hot and cold thermal streams representing the condenser and the evaporator, respectively. The electricity stream defines the size of the unit: the reference flow of electricity input to the unit $\dot{M}^{+,ref}_{ch,el,t}$ is defined constant for each time step and consequently scaled according to the unit load $f_{ch,t}$. Conversely, compressor and evaporator streams are determined in each time step through the COP of the machine, as reported in Eq. 2.41.

$$\mathrm{COP}_{ch,t} = \frac{\mathrm{T}^{e}_{t} + 273.15}{\mathrm{T}^{e}_{t} - \mathrm{T}^{c}_{t}} \cdot \eta_{II} \qquad \forall\ t \in \mathbf{T}, \forall\ ch \in \mathbf{CH} \quad (2.41)$$

The $\mathrm{COP}_{ch,t}$ is used to determine the reference flow in each time step of the thermal streams, as shown in Eqs. 2.42 and 2.43.

$$\Delta\dot{\mathrm{H}}^{ref}_{s_e,t} = \mathrm{COP}_{c^{c/e},t} \cdot \dot{M}^{+}_{ch,ly,t} \qquad \forall\ t \in \mathbf{T}, \forall\ s_e \in \mathbf{C_{ch}} \cap \mathbf{CS}, \forall\ ch \in \mathbf{CH}, ly = el \quad (2.42)$$

$$\Delta\dot{\mathrm{H}}^{ref}_{s_c,t} = (\mathrm{COP}_{c^{c/e},t} + 1) \cdot \dot{M}^{+}_{ch,ly,t} \qquad \forall\ t \in \mathbf{T}, \forall\ s_c \in \mathbf{C_{ch}} \cap \mathbf{HS}, \forall\ ch \in \mathbf{CH}, ly = el \quad (2.43)$$

As for the HPs, the multiplication factors of the streams are linked to that of the parent unit by Eqs. 2.28 and 2.30. Further details on the choice of the model parameters can be found in Section B.1.3.

Heat exchangers

The network cold and hot utilities introduced in Section 2.3.2 represent HEXs. As previously mentioned, they are divided into two groups: 1) those following the temperatures of the network they refer to and representing HEXs used to supply heat or cold to the users directly with the network, and 2) those characterized by a fixed ΔT between inlet and outlet temperature and used to feed the evaporators of HPs and condensers of CHIs. The latter are not costed as this is intrinsically considered in that of the associated machine. All HEXs are defined by a single cold or hot streams, whose reference heat load $\Delta\dot{\mathrm{H}}^{ref}_{s,t}$ is always assumed equal to 1 kW. The load of HEXs is scaled as for all the other units by the variable $f_{u,t}$ and redistributed in each heat cascade layer its stream belongs to, by the multiplication factor $f_{s,hc,t}$. HEX units are also grouped based on the network and the temperature they refer to. In this way, the load of each HEX (e.g., the multiplication factor $f_{u,t}$) can be used in Eqs. 2.19 and 2.20 to determine the mass flow rate entering or exiting in each location.

Others

Other utilities included in the problem are:

- the electricity grid, defining the purchase and possibly selling of electricity to the grid;
- the natural gas grid, defining the purchase of natural gas;
- the resource of LTH, accessible only at the central heating station to either heat up the evaporator of the central plant or to be used to compensate the load on the anergy or cooling network;
- ELHs (more details in Section B.1.4);
- natural gas BOIs (more details in Section B.1.5);
- PV panels (more details in Section B.1.6).

2.3.4 Objective function

The objective is chosen as the simultaneous minimization of the capital expenses (annualized) (CAPEX) (Eq. 2.44) and operating expenses (annual) (OPEX) (Eq. 2.45).

$$CAPEX = \left[\sum_{u \in \mathbf{U}} C_u^{inv,1} \cdot y_u + C_u^{inv,2} \cdot f_u \right] \frac{\mathrm{i}(\mathrm{i}+1)^{\mathrm{n}_u}}{(\mathrm{i}+1)^{\mathrm{n}_u} - 1} + \sum_{n \in \mathbf{N}} C_n \cdot \frac{\mathrm{i}(\mathrm{i}+1)^{\mathrm{n}_n}}{(\mathrm{i}+1)^{\mathrm{n}_n} - 1} \tag{2.44}$$

$$OPEX = \sum_{t \in \mathbf{T}} \left[\sum_{u \in \mathbf{U}} C_u^{op} \cdot f_{u,t} \cdot \mathrm{f}_t \cdot \mathrm{d}_t \right] \tag{2.45}$$

Values for the interest rate i and years of life time for machines and networks $\mathrm{n}_{u/n}$ are reported in Table B.5. For each network type the investment cost is estimated based on the Manhattan distance among the connected locations and the cost per meter of pipe (coefficients are listed in Table B.5).

$$C_n = \sum_{\substack{(lc_1,lc_2) \in \mathbf{LC^N} \\ dn \in \mathbf{DN}}} y_{n,dn} \cdot y_{n,lc_1,lc_2} \cdot \mathrm{L}_{lc_1,lc_2} \cdot C_{dn}^{inv,2} \qquad \forall\ n \in \mathbf{N} \tag{2.46}$$

The product $y_{n,dn} \cdot y_{n,lc_1,lc_2}$ in Eq. 2.46 is linearized by introducing new variables and constraints, following the procedure reported in Section B.2. According to the resolution strategy chosen the two objectives might be possibly combined into a single objective optimization aimed at minimizing the total expenses (annualized) (TOTEX), defined as the sum of the capital and operating expenses ($TOTEX = CAPEX + OPEX$).

2.3.5 Problem solving strategy

The modelling framework is flexible enough to support different solving strategies, to propose a set of optimal system designs, focusing on network temperatures and the degree of decentralization of heat and cold production. The first option relies on an integer-cut constraint on the choice of how to supply the heating demand (i.e. heating or anergy network and corresponding operating temperatures). At each iteration $\mathrm{n_{sol}}$, $(\mathrm{n_{sol}}-1)$ constraints are written as the one reported in Eq. 2.47.

$$\sum_{\substack{n\in\mathbf{N}:n\neq\text{“CN”}\\ T_n^{f/r}\in\mathbf{T_n^{f/r}}}}\left(2\cdot y_{T^{f/r}}^{old,i}-1\right)\cdot y_{n,T_n^{f/r}}\leq\left(\sum_{\substack{n\in\mathbf{N}:n\neq\text{“CN”}\\ T_n^{f/r}\in\mathbf{T_n^{f/r}}}} y_{T_n^{f/r}}^{old,i}\right)-1 \qquad \forall\ i=1..\mathrm{n_{sol}}-1 \quad (2.47)$$

$y_{T^{f/r}}^{old,i}$ represents the activation of the networks temperature couples for each previous solution, whereas the maximum number of iteration (i.e, generated solutions) should not be greater than the potential combinations defined by the predefined temperature couples assigned to the heating and anergy networks. The integer-cut formulation enforces that at each iteration, the optimizer looks for the best solution minimizing a single-objective defined by the system TOTEX, while excluding heating and anergy network temperatures activation from previous solutions. Therefore, for this strategy, a set of potential temperature couples for the heating and anergy networks is specified *apriori*. A superstructure of utilities is automatically included in the problem, ensuring a feasible solution regardless of the network temperature. As an example, the decentralized water-water HPs must include all the potential condensers and evaporators streams to be able to work at any network temperature and upgrade the heat if necessary. This first formulation results in a complex MILP formulation, effective only when the problem size is limited (i.e., limited number of typical operating periods and location, networks layout fixed).

A second strategy relies on problem decomposition, to fix the variables the most responsible for increasing problem complexity at an upper level. Such variables might be, for instance, the choice of the network activation together with the corresponding temperature and diameter. To investigate the solution space, the setting of such variables can be either performed manually (e.g., by iteratively choosing among a set) or attributed to an upper-level heuristic optimization. By fixing these variables, the superstructure of utilities is drastically reduced, resulting in a reduced problem size for the MILP formulation. The choice of the heuristic optimization over the manual choice of the set of network temperatures is preferable when there is a large range of user temperatures. In this chapter, an example of manual temperature selection is presented, while in Chapter 3 an example of the use of the heuristic optimization at the upper level is shown.

Moreover, for each network activation and operating temperature, the single optimal solution resulting from the minimization of the system TOTEX can be generated, as well as, a set of potential configurations, all optimal with respect to the conflicting capital and operating expenses. This latter possibility can be based on an ε-constraint to generate the Pareto-optimal solutions. After finding the extremes of the Pareto frontier through single-objective unconstrained optimization, the mid-points are obtained by solving multiple times the optimization problem using the lexicographic approach presented in [78]. Equation 2.48 reports an example of the resulting optimization problems[2].

$$
\begin{aligned}
&\min_{\boldsymbol{\Sigma}} \ OPEX \\
&\boldsymbol{\Sigma} = \left\{ y_u, y_{u,t}, f_u, f_{u,t}, f_{s,ly,t}, \dot{R}_{hc,k,lc,t}, y_{lc_1,lc_2,n}, y_{n,dn}, y_{c^{c/e}}, \dot{m}^{h/c/hp}_{lc_1,lc_2,n,T_n^{f/r},dn,t} \right\} \\
&\text{subject to} \\
&CAPEX \leq \epsilon_{\text{CAPEX}} \\
&\text{Eq. 2.1 - Eq. 2.32, Eq. 2.42 - Eq. 2.46 and Eq. B.6 - Eq. B.9} \\
&y_n = \mathrm{y}_n \ \text{ and } \ y_{n,T_n^{f/r}} = \mathrm{y}_{n,T_n^{f/r}}
\end{aligned}
\tag{2.48}
$$

The last row of constraints in Eq. 2.48 represents the iterative screening of the networks activation and temperature couple selection, used to build the Pareto frontiers associated to the different network configurations. To evenly screen the solution space between the two extreme points of each Pareto frontier, the problem reported in Eq. 2.48 is solved also to minimize the CAPEX, while enforcing the ε-constraint on the OPEX. This specific formulation is used for solving the problem presented in this chapter. The modelling framework is implemented in AMPL [79] and the computations reported in this chapter are performed with the commercial solver CPLEX [80] on a machine with following processor details: Intel(R) Core(TM) i7-9700K CPU @ 3.60GHz and 16,0 GB of RAM. The maximum tolerated relative optimality gap (MIP gap) is set to 1%.

2.4 Application

To demonstrate the developed modelling and optimization framework, the latter is applied to a fictitious urban district. The site includes buildings of different construction years and usage profiles. Heating and cooling needs are estimated through the signature approach presented by Girardin [33], while required temperatures are assigned based on the year of construction and eventually renovation of the buildings. Electricity and DHW demand profiles are estimated based on the standards recommended in [52, 81] . Figure 2.9 shows the schematic of the case study, while Table 2.2 lists the characteristics of the buildings considered: usage, period of construction, renovation status, position, heating signature parameters (k_1^{hs}, k_2^{hs}), heating threshold temperature (T_{tr}^{hs}), heating supply and return temperature at design conditions ($T^{hs,f}$ / $T^{hs,r}$), cooling signature parameters (k_1^{hs}, k_2^{hs}), cooling threshold temperature (T_{tr}^{cs}), cooling supply and return temperature at design conditions ($T^{cs,f}$ / $T^{cs,r}$), ambient temperature at design conditions for heating and cooling ($T^{0,H}$ / $T^{0,C}$), building surface (A), available

[2] In Eq. 2.48 the slack variables included to guarantee the solutions' efficiency, as suggested by [78], are omitted for clarity purposes.

roof surface ($A^{PV,max}$), required temperature for DHW (T^{dhw}), annual electricity demand (E^{el}), annual demand of DHW (Q^{dhw}), and annual demand for process cooling (Q^{frg}) and corresponding required feeding and returning temperature ($T^{frg,f}$ / $T^{frg,r}$).

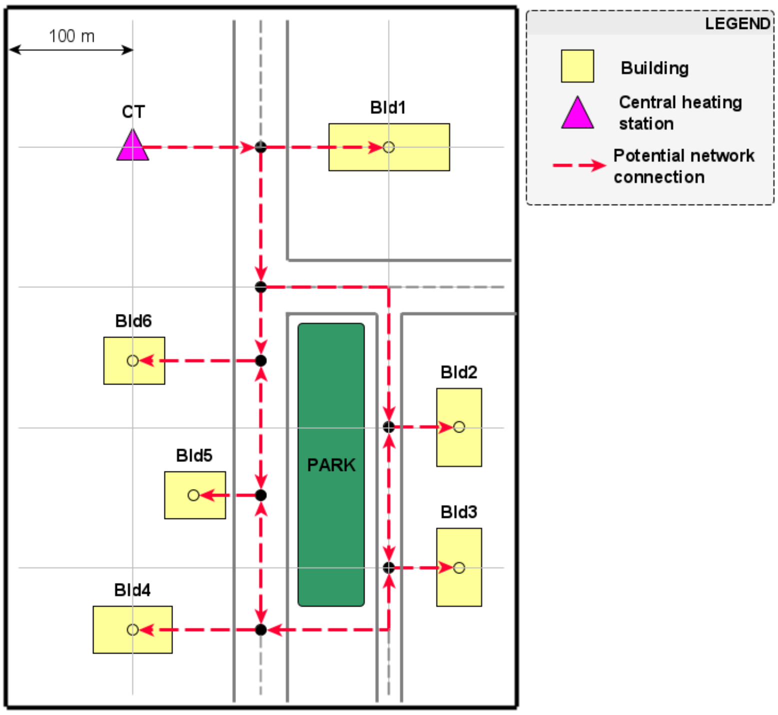

Figure 2.9: Schematic of the case study.

Figure 2.10 shows the heating and cooling signature associated to the building with "administrative" usage, constructed in the period 1980-2005 and renovated . The graph shows the values of the specific heating and cooling demand as well as the supply and return temperatures, all linearly dependent on the ambient temperature. For the other types of buildings included in the case study the same type of graphs are reported in Section B.4.

Electricity profiles are estimated based on the standard profiles of occupancy and usage of electric appliances published in [52][3] and the annual energy consumption for building type and year of construction in [33]. Days of limited usage (like weekends for the schools) and monthly variations are neglected. For DHW, a similar approach is followed, with the only difference that for the residential and the hotel buildings, to avoid an unreasonable consumption of DHW during the night, arising from the use of the occupancy profiles suggested by [52], the trends reported in [81] are employed. Figure 2.11 shows the specific hourly consumption profiles for all types of buildings included in the case study. These profiles are assigned to all typical operating periods.

[3]For all types of usage except "hotel" the standards provide a mix of typical building uses (Table 15 at page 144 in [52]) and the resulting profile is given by a weighted average of the reference ones. For the hotel an assumption

Table 2.2: List of buildings included in the case study and their details.

		Bld1	Bld2	Bld3	Bld4	Bld5	Bld6
Usage[a]		C	R	R	A	E	H
Period[b]		1980-2005	2005-2020	2005-2020	1980-2005	1980-2005	1980-2005
Renovated		✗	✗	✗	✓	✗	✓
Location (x,y)	$[(m, m)]$	(400,400)	(450,200)	(450,100)	(200,50)	(250,150)	(200,250)
$k_1^{hs\dagger}$	$[W/°C/m^2]$	-0.84	-0.83	-0.83	-1.15	-2.03	-0.83
$k_2^{hs\dagger}$	$[W]$	13.77	12.86	12.86	16.33	28.83	13.61
$T_{tr}^{hs\dagger}$	[°C]	16.4	15.5	15.5	14.2	14.2	16.4
$T^{hs,f}/T^{hs,r\diamond}$	[°C/°C]	70/55	40/30	40/30	60/45	70/55	65/50
$k_1^{cs\dagger}$	$[W/°C/m^2]$	5.35	0	0	3.09	0.37	1.31
$k_2^{cs\dagger}$	$[W]$	-96.3	0	0	-55.62	-6.66	-23.58
$T_{tr}^{cs\dagger}$	[°C]	18	18	18	18	18	18
$T^{cs,f}/T^{cs,r\dagger}$	[°C/°C]	12/17	12/17	12/17	12/17	12/17	12/17
$T^{0,H}/T^{0,C\dagger}$	[°C/°C]	-6/35	-6/35	-6/35	-6/35	-6/35	-6/35
$A^{\dagger}$	$[m^2]$	5000	2000	2000	3000	1000	1000
$A^{PV,max\ddagger}$	$[m^2]$	875	280	280	525	140	0
T^{dhw}	[°C]	55	55	55	55	55	55
$E^{el\ \dagger}$	$[kWh/y/m^2]$	33.33	27.78	27.78	22.22	11.11	33.33
$Q^{dhw\ \dagger}$	$[kWh/y/m^2]$	22.85	34.28	34.28	11.43	22.85	45.71
$Q^{frg\ \S}$	$[kWh/y/m^2]$	30	-	-	-	-	-
$T^{frg,f}/T^{frg,r\ \S}$	[°C/°C]	3.5/6	-	-	-	-	-

[a] Usage: C: commercial, R: residential, A: administrative, E: education, H: hotel
[b] Period of construction
‡ The available surface for PV installation is calculated based on the assumption of the number of floors for each building (5 floors for commercial, residential and educational and 4 floors for administrative) and a factor 0.7 to estimate the available roof area [82]
† From [33]
⋄ Adjusted from [33]
§ The need of process cooling is considered only for commercial buildings. The demand is estimated as 30 kWh/y/m^2 and constant at every hour [22] at a temperature of 3.5/6°C.

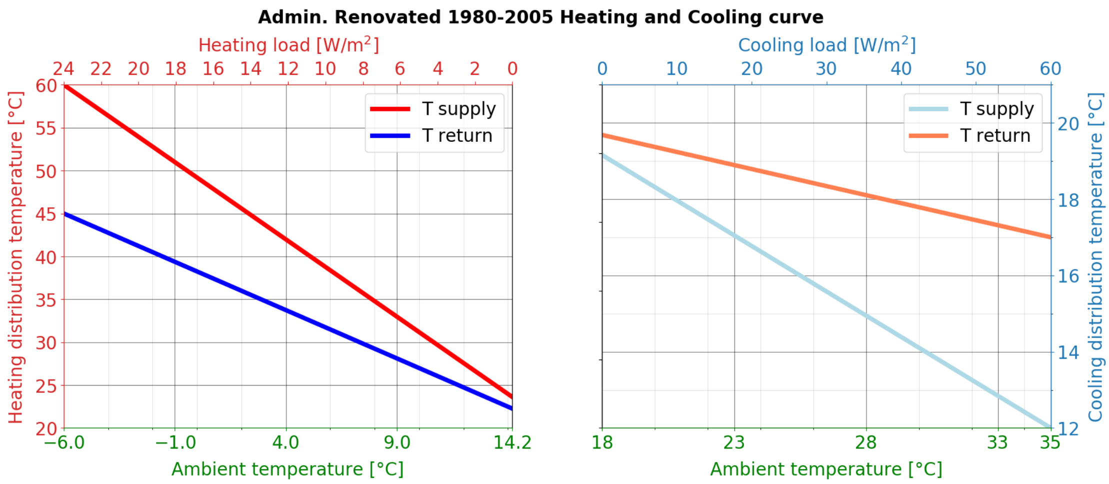

Figure 2.10: Heating and cooling signature for a building of type administrative, constructed in the period 1980-2005 and renovated.

The position of the central heating station is fixed and not subjected to the optimization. In

is made as the mix is not available.

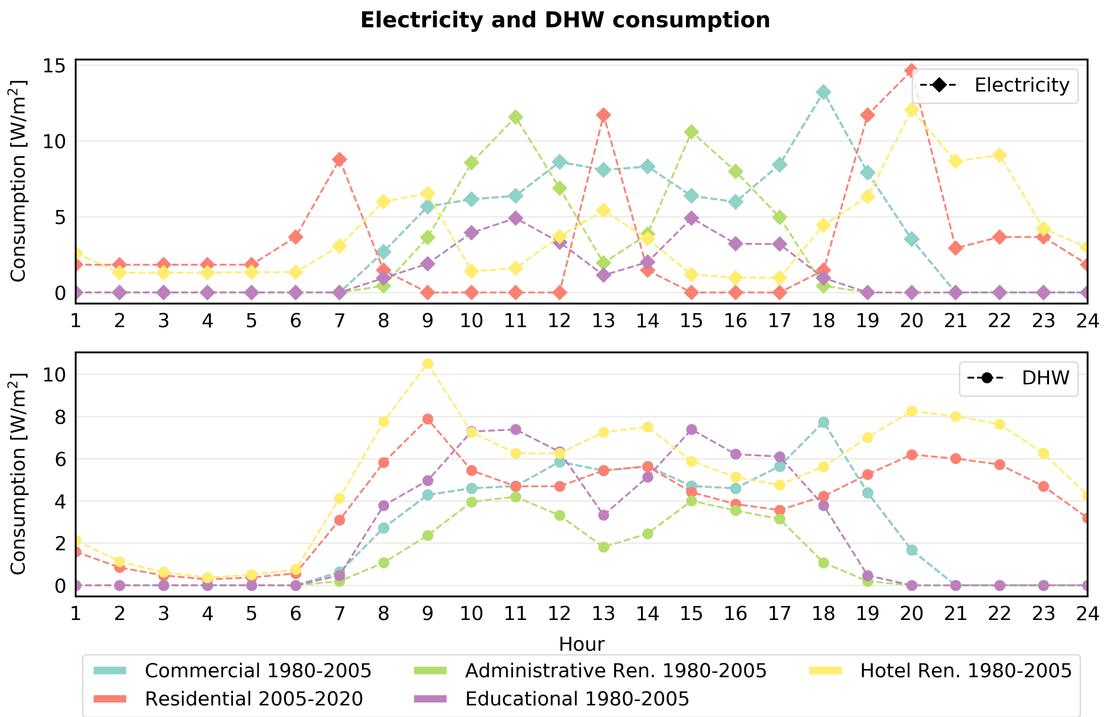

Figure 2.11: Electricity and domestic hot water consumption profiles for all building types. Source: adjusted from [52] and [33].

this location the LTH is available and a central HP can be eventually installed to distribute the heat to the buildings at higher temperature. A set of networks nodes and directional potential connections is identified, to connect each of the building to the central plant. The same potential layouts are employed for all types of distribution networks: heating, cooling and anergy. At the building locations, the heat demand can be supplied by standalone conversion technologies, such as the BOI, ELH, and air/water HP or by connecting to the heating or anergy network eventually in combination with a decentralized water/water HP to raise the network temperature to the required needs. The cooling demand can be supplied by decentralized CHI or by direct cooling with the LTH, through the cooling or anergy network. Refrigeration needs, due to their lower temperature requirement, can be satisfied only by the use of a decentralized CHI. In all the buildings PV panels can be also potentially installed, according to the maximum roof surface available. To define the excess electricity production a lumped systematic perspective is assumed: the electricity produced by one building can be used by its neighbors and only the excess resulting from the overall balance at the district level is sold to the grid.

Typical and extreme periods of operation

As explained in the previous chapter (Section 1.4.1), the problem size is reduced using a series of typical and extreme operating periods, reproducing the conditions the system will face during the project life time in a limited number of time steps. For this purpose the k-medoids clustering approach presented by Stadler et al. [72] is employed, choosing as attributes the ambient temperature and solar irradiation. Six typical operating periods are thus defined. For the extreme conditions, the extreme ambient temperatures reported in Table 2.2 and used to define the buildings signatures are taken. To these time steps the maximum values of heating and cooling demand and corresponding required temperatures are associated.

2.4.1 Results

Given the limited diversity of the users' temperature requirements, the selected solving strategy relies on an iterative screening of potential network temperatures. For each configuration several optimal solutions with respect to the conflicting OPEX and CAPEX objectives are generated through an ε-constraint. The choice of the iterative network temperatures screening is justified by the limited number of users and the fact that operating the network at a temperature that none of the users requires would result in the need for decentralized units for the users demanding a higher temperature and in a waste of exergy otherwise. Therefore, only temperatures from the lowest to the highest requirement with a 5°C interval are investigated. For the sake of simplicity and clarity of the representation, the network profiles included in this first screening are designed to follow a heat curve, therefore not allowing the supply of DHW directly by the network. It is assumed that at design conditions, the temperature is the highest, decreasing linearly until reaching the highest cut-off temperature among all buildings, while ensuring that the minimum ΔT in the network is preserved. Figure 2.12 shows examples of temperature profiles following this approach.

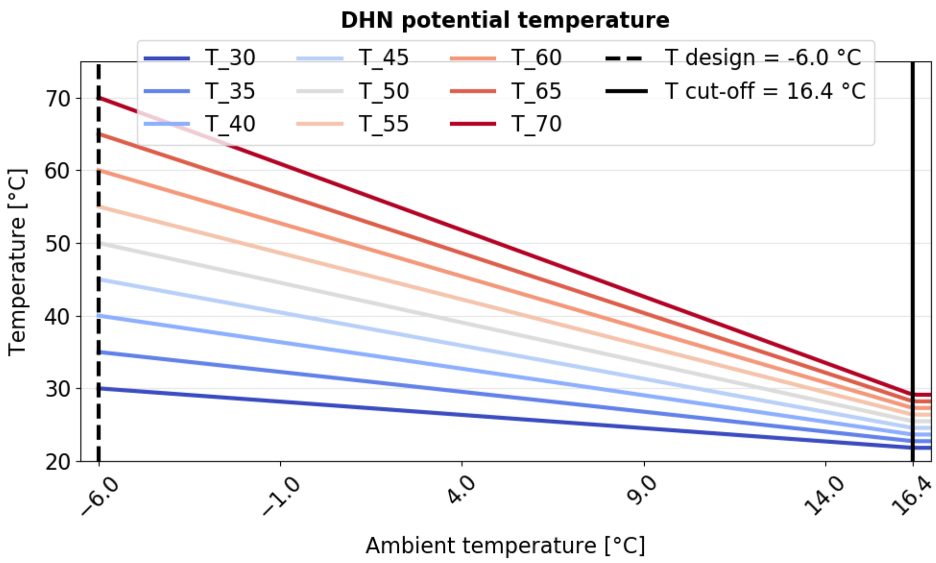

Figure 2.12: Potential supply and return temperature profiles for the HN.

Figure 2.13 shows the Pareto frontiers correlated to different HN temperatures and the activation of the AN as reported in the legend. The solutions showed with a cross in Fig. 2.13

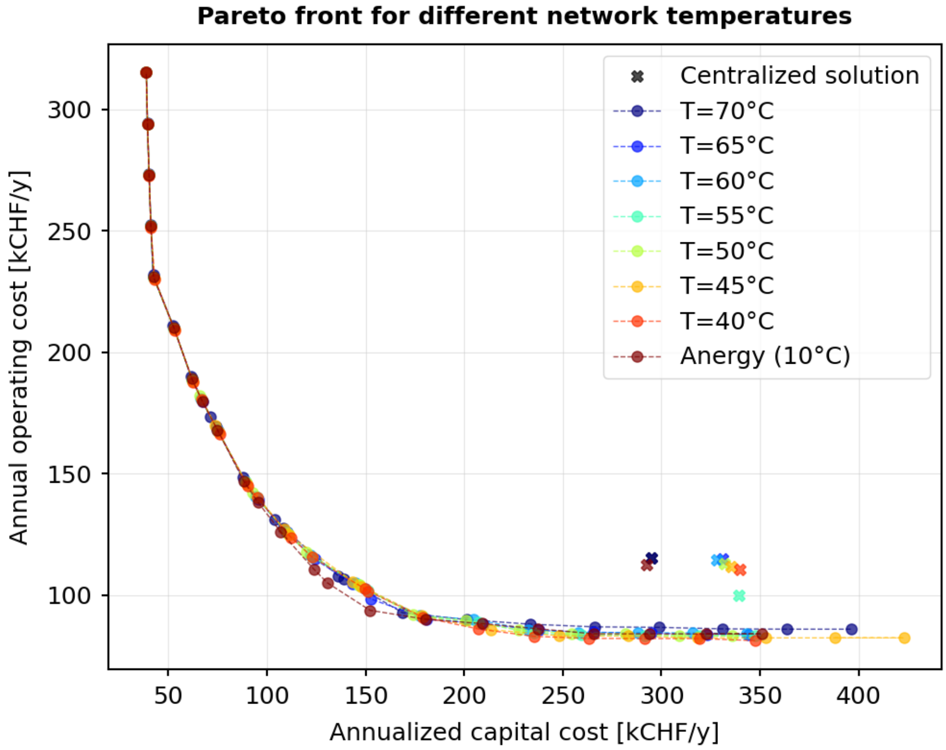

Figure 2.13: Pareto optimal solutions for different HN temperatures and the AN. Centralized solutions represent designs excluding standalone units.

represent fully centralized solutions at a degree depending on the network temperatures. Those configurations are achieved by minimizing the system TOTEX and forbidding the use of standalone units such as BOIs, air-water HPs and ELHs. Decentralized CHIs can potentially be activated, but only for the supply of refrigeration demand and not space cooling. Figure 2.13 demonstrates that all the configurations show very similar Pareto frontiers for the objective of minimum annualized CAPEX and OPEX. This result is not surprising in the region of low CAPEX, since the configurations reducing the CAPEX are those relying on decentralized units and therefore not dependent on the network type or temperature. In the region of higher capital investment, these results highlight the cost-equivalence of the different network configurations.

To investigate the solutions from a different perspective, a new indicator is introduced, defined as the heat rejected to the environment normalized with respect to the total demand, as reported in Eq. 2.49:

$$KPI^{env} = \frac{Q^{env,+} - Q^{env,-}}{Q^{H} + Q^{dhw} + Q^{C} + E^{el}} \tag{2.49}$$

where $Q^{env,+}$ is the annual heat released into the environment, $Q^{env,-}$ is the annual energy taken from the environment and the denominator sums up the annual demand for respectively space heating (Q^H), DHW (Q^{dhw}), space cooling and refrigeration (Q^C), and electricity (E^{el}). The heat released into the environment is expressed by Eq. 2.50.

$$Q^{env,+} = Q^H + Q^{dhw} + Q^{ng} \cdot (1/\eta_{BOI} - 1) + Q_{CH}^{cond,air} + Q_{lth}^{+} + Q_{grid} \tag{2.50}$$

The heat is released to the environment through the building thermal losses (Q^H), the use of hot water[4] (Q^{dhw}), the flue gases released by the boilers ($Q^{ng} \cdot (1/\eta_{BOI} - 1)$), the condenser of CHIs when cooled down by ambient air $Q_{CH}^{cond,air}$, the heat rejected into the low temperature source Q_{lth}^{+} and the heat released by the power plants producing the electricity bought from the grid Q_{grid}^{-}. This last term must take into account also the production of the PV panels and the injection of electricity into the grid eventually bought with a time delay, as reported by Eq. 2.51:

$$Q_{grid} = (E_{grid}^{-} - E_{grid}^{+} \cdot \eta_{BAT}) \cdot (1/\eta_{grid} - 1) + E_{grid}^{+} \cdot (1 - \eta_{BAT}) \tag{2.51}$$

where E_{grid}^{-} is the electricity bought from the grid, while E_{grid}^{+} is the one injected into the grid for which a round-trip efficiency of 0.85 is assumed (η_{BAT}). The average efficiency of thermal power plants powering the grid (η_{grid}) is assumed equal to 0.6 referring to combined cycle power plants. The grid round-trip inefficiency ($1 - \eta_{BAT}$) also contributes to the heat directly injected into the environment.

Figure 2.14 reports in the new domain the Pareto frontiers of the configurations previously investigated. Also the analyses of the Pareto frontiers on the new domain does not allow a diversification of the different configurations. Meaning that also with respect to the newly introduced environmental KPI all the network temperatures show the same performance.

For this reason a second KPI is investigated. The latter aims at assessing the exergy losses as expressed by Eq. 2.52.

$$Ex_{loss} = 1 - \frac{Ex_{used}}{Ex_{input}} \tag{2.52}$$

Where the exergy input to the system Ex_{input} is given by the contribution of the natural gas, the net import of electricity and the one generated by the PV, as reported in Eq. 2.53.

$$Ex_{input} = Q^{ng} + E_{grid}^{-} - E_{grid}^{+} \cdot \eta_{BAT} + E^{PV} \tag{2.53}$$

Whereas the exergy used in the system is calculated as the contribution of the electricity, heating and cooling demand. The reference temperature assumed for the estimation of the exergy content of thermal streams is the one of the LTH. Exergy content of the ambient air is neglected.

$$Ex_{used} = E^{el} + Ex^{Q,H} + Ex^{Q,dhw} + Ex^{Q,C} \tag{2.54}$$

[4] It is assumed that no heat recovery between the used hot water and the cold fresh one is allowed

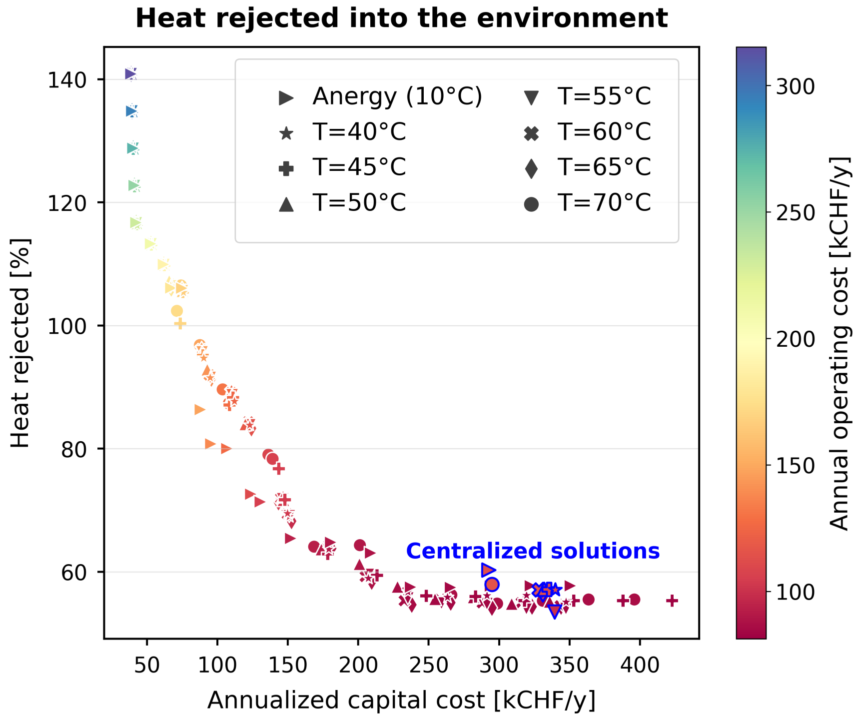

Figure 2.14: Pareto optimal solutions for different HN temperatures and the AN plotted in the CAPEX-KPI^{env} domain. Centralized solutions represent designs excluding standalone units.

Figure 2.15 shows the Pareto frontiers in the CAPEX-exergy loss domain.

The analysis of the exergy loss highlights that configurations relying heavily on TENs are best at exploiting the exergy input to the system. Among these, the effect of the network temperature on the exergy efficiency is only marginal. Referring to the Pareto frontiers once again the variation among the different network temperatures is very limited, highlighting the equivalence of the different configurations with respect to exergy losses.

To further investigate how investment decisions evolve at increasing capital allowance, the Pareto frontier related to one single temperature profile is selected and further investigated. The temperature selected is the one of the HN at 40°C at design conditions, therefore potentially able to supply only the space heating demand of the residential buildings without the use of decentralized units.

Figure 2.16 shows the installed capacity and the equivalent operating hours for each unit in each solution, defined as the unit annual energy over the installed capacity.

It is visible from Fig. 2.16 that in the lower investment region, the units installed to supply the heat demand are decentralized natural gas BOIs and ELHs, while cooling is supplied by CHIs and that the low investment does not allow the purchase of PV panels. Higher capital allowance shows emergence of air-water HPs, as well as investment in PV. In the region of highest CAPEX

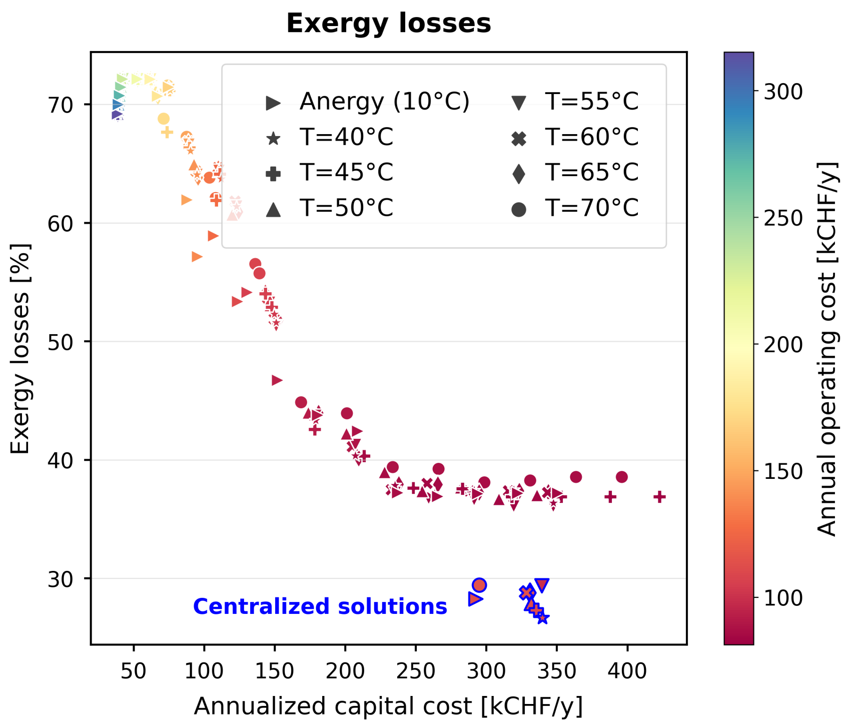

Figure 2.15: Pareto optimal solutions for different HN temperatures and the AN plotted in the CAPEX-Ex_{loss} domain. Centralized solutions represent designs excluding standalone units.

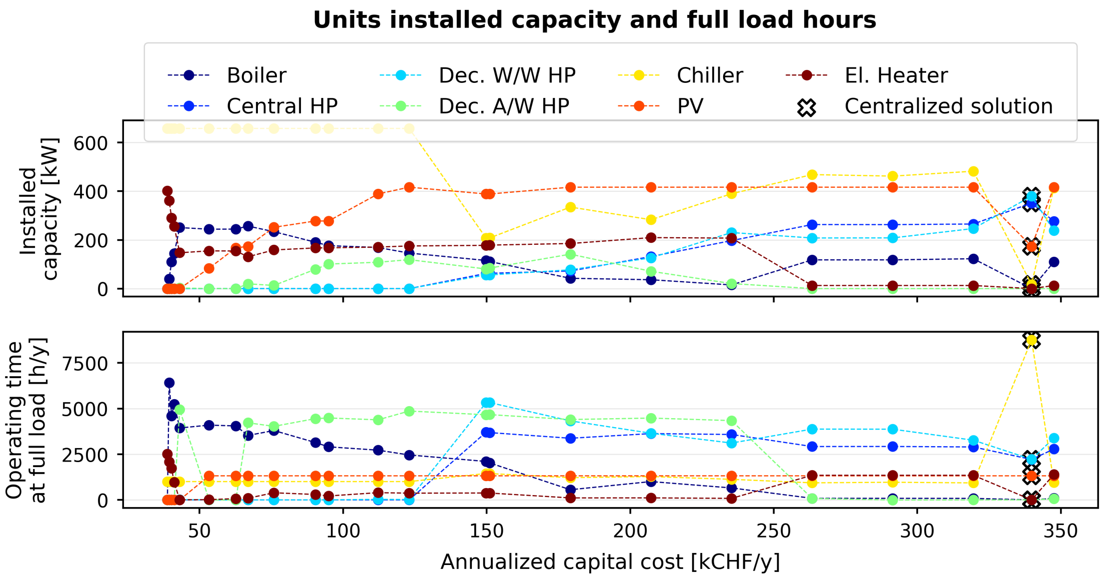

Figure 2.16: Units installed capacity and equivalent full load operating hours for the Pareto-optimal configurations (and fully centralized one) related to the HN at 40°C. Capacity expressed as KW_{el} for PV and ELH, as kW_{th} at the condenser for the HP, as kW_{th} at the evaporator for the CHI and as kW_{th} of heat delivered for the BOI.

(and low OPEX) most of the heating demand is supplied either by the thermal network or with the use of decentralized water-water HPs for buildings requiring higher temperatures. The minimal share of decentralized units installed can be justified by the coverage of DHW demand. Regarding the supply of cooling, part of it remains supplied by the CHIs even in the region of higher capital investment. This result is justified partially by the need of using the chillers to supply the refrigeration demand and partially by this operation being more economical in combination with the PV, with respect to the direct cooling.

Figure 2.17 shows the investment cost breakdown at increasing CAPEX for the same system configurations.

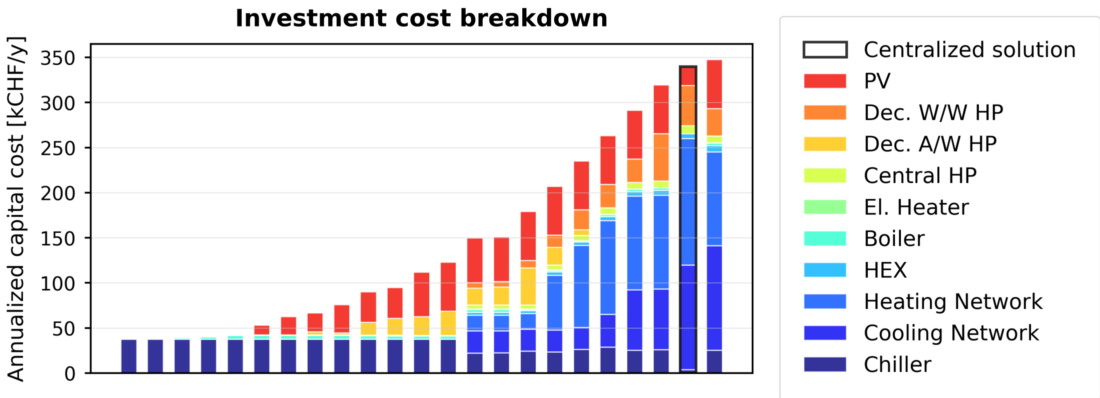

Figure 2.17: CAPEX breakdown for configurations with the HN at 40°C.

Figure 2.17 highlights that the investment of the heating and cooling networks appears only in the region of higher CAPEX. The trend of the shares of the different technologies follows that of installed capacity investigated in Fig. 2.16. The relevance of the cost devoted to the network investment compared to that of the equipment is also evident at higher CAPEX.

Figure 2.18 shows how heating and cooling demands are satisfied for each Pareto-optimal solution and for the fully centralized solution. As also concluded from the previous results,

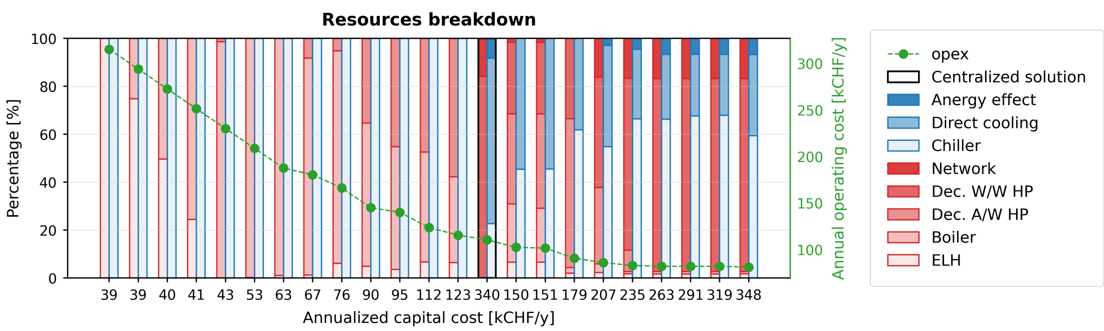

Figure 2.18: Heating and cooling breakdown for configurations with the HN at 40°C.

this further investigation proves that moving towards more capital-intensive configurations the heating demand is supplied first by ELHs, then by BOIs, followed by air-water HPs and finally by the HN with a portion upgraded by water-water HPs. As discussed previously, the minor portion related to DHW demand remains covered by the ELHs. The reason being that one unique supply temperature can be chosen for the HPs, meaning that the coverage of the DHW would result in an amount of heat at an unnecessarily high temperature during warmer days. In terms of cooling, the decentralized CHIs are extensively used in the whole first part of the Pareto frontier, before the direct cooling and the anergy effect are exploited. The latter aspect refers to the possibility of balancing the co-existing heating and cooling requirements in the central station, therefore recovering the heat rejected into the network by consumers needing cooling to feed the evaporator of the central plant. This solution enables a decrease in the use of external LTH.

Figures 2.19 and 2.20 show respectively how the heating and cooling networks expand at increasing capital allowance.

Both networks logically expand from the central station outward, connecting first to the closest location (Bld1). Even though the next closest building is Bld6, the next connections for the HN are made to the two residential buildings (Bld2 and 3), as these are the only ones whose space heating demand can be supplied directly by the network without the need of a decentralized HPs. At higher capital investment allowance, the HN expands so as to connect all buildings. The cooling network also starts with the closest buildings and finally connects all those needing cooling (Bld2 and Bld3 do not have any cooling requirement). In terms of pipe diameter, the best solutions for the HN require pipes DN100 for all configurations except the fully centralized one (CAPEX = 340), for which a larger diameter is chosen. This latter result is explained by the fact that the use of standalone units is forbidden in these configurations, including the supply of DHW; therefore this must be covered by decentralized water-water HPs, whose evaporators are connected to the network. Furthermore, the HN must provide a larger amount of heat resulting in larger mass flow rates, as the ΔT is fixed. The cooling network (CN) diameter is larger, ranging from DN200 to DN300.

Figure 2.21 summarizes the breakdown of the total cost, for each of the configurations on the Pareto frontier and the fully centralized one. Solutions are ordered by increasing TOTEX.

At increasing TOTEX, the relevance of the OPEX for solutions with low investment allowance and of the CAPEX towards those with higher investment allowance can be noticed. The latter is mostly due to the network installation.

2.4.2 Sensitivity analysis

To assess the robustness of the different system configurations against cot uncertainties, OPEX and CAPEX are recalculated after changing the investment rate and cost parameters of resources, units and network investment costs. Each parameter is assigned an upper and lower

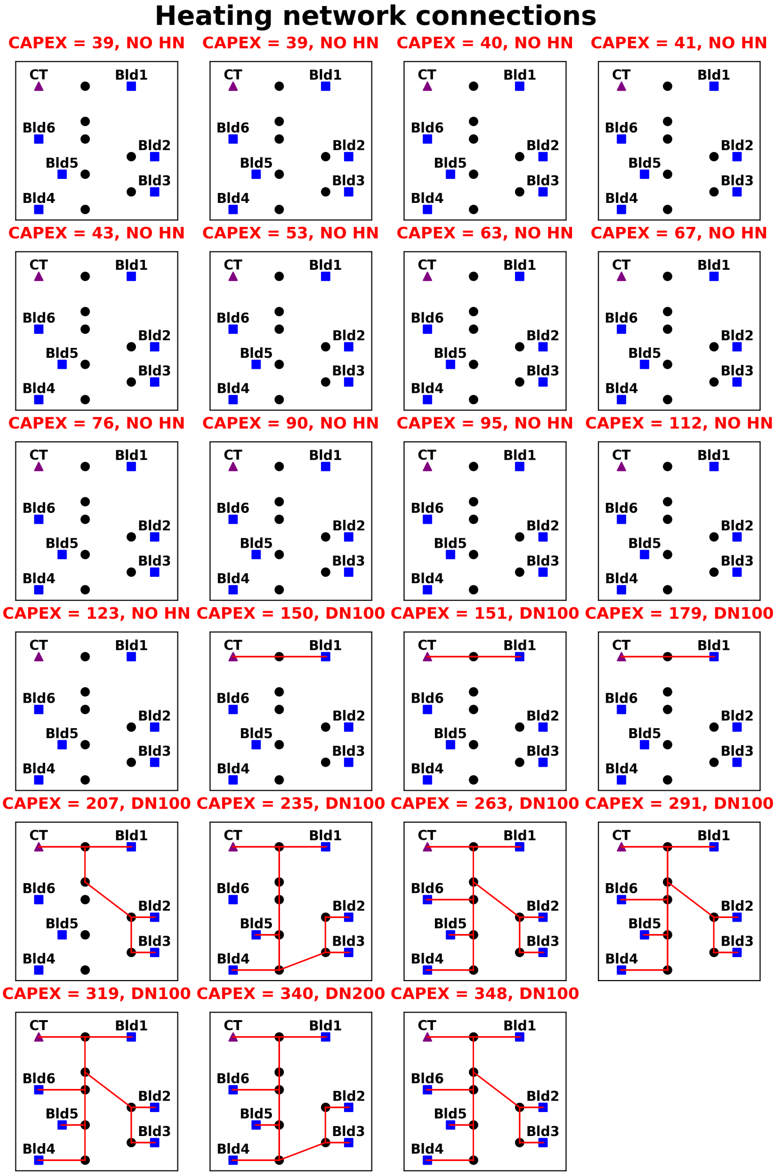

Figure 2.19: Layout of the HN for configurations with the HN at 40°C. Capital cost expressed in kCHF/y.

bound, equal to the current value ±20%. Multiple scenarios are considered by varying the value of each parameter within its range, following a Sobol sequence to define 1000 different combinations, representing at best the different potential options. Results are first presented as a single Pareto frontier (the one related to the HN at 40°C at design conditions) and then applied to all temperature profiles. Statistics on results involving sensitivity on only one of the two axes (i.e., either on the operating or on the investment cost) are represented using box plots: the box extends from the lower to the upper quartile values of the data with a line at the median. The whiskers show the 5th and 95th percentile of the distribution, while the

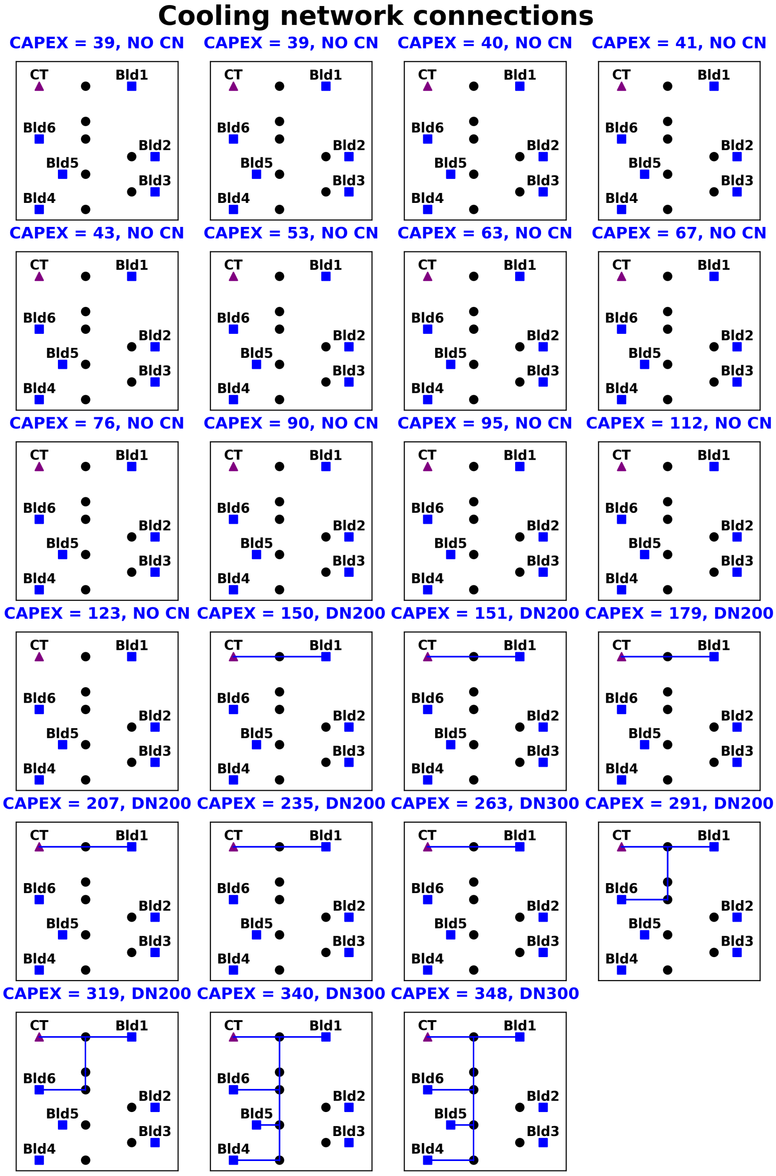

Figure 2.20: Layout of the CN for configurations with the HN at 40°C. Capital cost expressed in kCHF/y.

remaining data are represented as outliers. When both the axes are involved, statistics are represented in the form of ellipses around the median values: the lower and upper quartile are shown, as well as the standard deviation and the 5$^{\text{th}}$ and 95$^{\text{th}}$ percentile.

Cost of the resources The resources taken into account in the sensitivity analysis are the electricity bought from the grid, LTH and natural gas, for which the cost per unit of energy C^{op} is systematically varied. Figure 2.22 shows the statistics on the recomputed system costs.

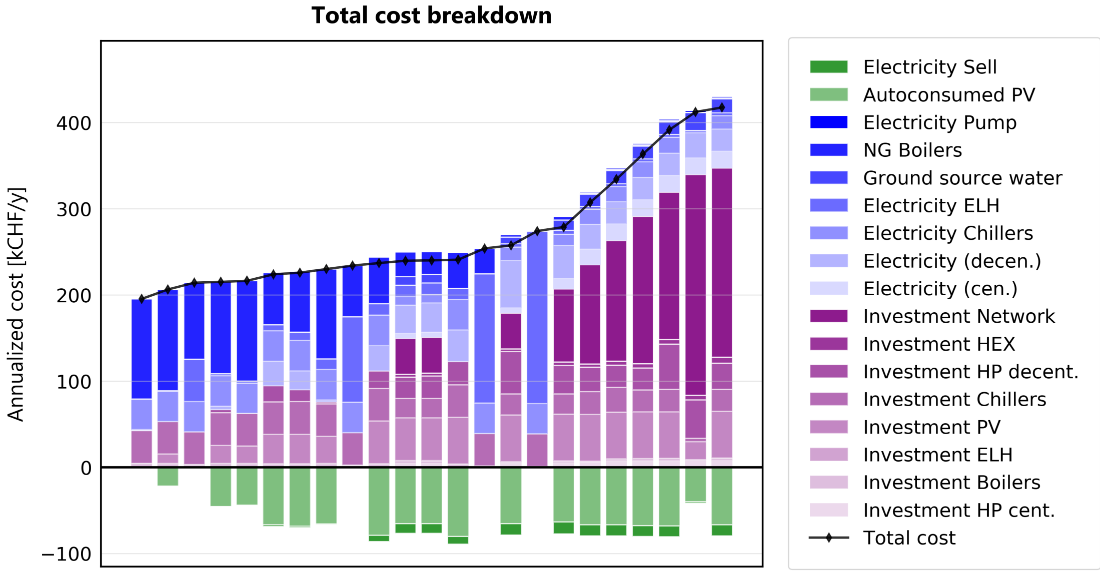

Figure 2.21: TOTEX breakdown for the Pareto-optimal configurations (and the fully centralized one) related to the HN at 40°C.

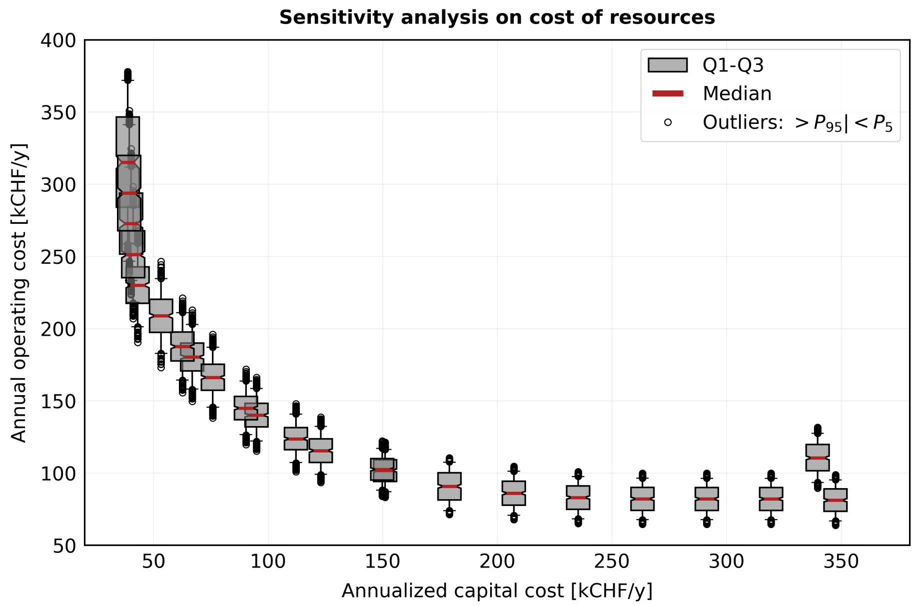

Figure 2.22: Sensitivity analysis on cost of resources for configurations relative to the HN at 40°C.

Figure 2.22 highlights how solutions at lower CAPEX, with the highest exploitation of standalone units, are the most sensitive to changes in resources cost. This result is expected since, as previously shown, the OPEX constitute the major contribution to the overall cost in these configurations. This analysis also reveals that solutions constituted by higher CAPEX fall within the range of uncertainty of each other. This overlap could lead to the choice toward the least capital intensive configurations, if the cost of resources is the only source of uncertainty.

The sensitivity to the resources cost is mostly driven by the uncertainty on the electricity tariff, as shown by Fig. 2.23, which reports the results relative to the only variation of this tariff. The reason is that, even if the consumption of LTH might be greater than the one of electricity for the solutions relying the most on the distribution network, the higher tariff defined for the purchase of electricity is the predominant aspect.

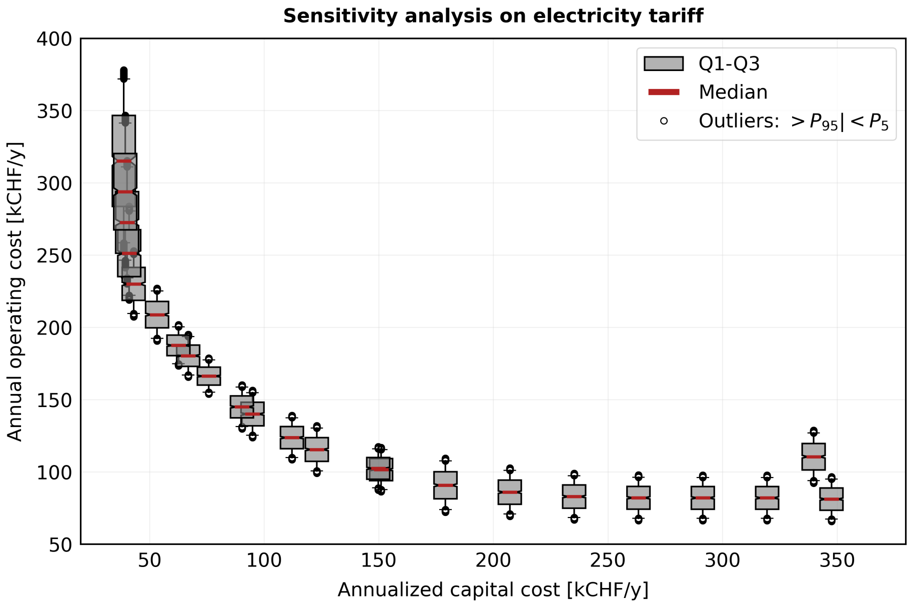

Figure 2.23: Sensitivity analysis on electricity tariff for configurations relative to the HN at 40°C.

Units investment cost The technologies taken into account for the sensitivity analysis are the BOIs, HPs, CHIs and ELHs. For each technology, the variable ($C^{inv,1}$) and fixed ($C^{inv,2}$) investment cost parameters are varied and the new investment cost of each installed unit is recalculated. Figure 2.24 shows the statistics on the recomputed system annual costs.

Figure 2.24 highlights that all the configurations are not very sensitive to the uncertainty on the investment cost of technologies. In particular, the solutions with low investment allowance are mostly affected by the uncertainty on CHI cost, while the others on that of HPs, since these have a larger share of the investment devoted to equipment purchase. The configurations showing the most sensitivity are those characterized by a larger capacity of air-water and water-water HPs installed (configurations with CAPEX around 320 kCHF/y and 180 kCHF/y, as visible through the comparison of Figs. 2.17 and 2.24).

Network investment cost Figure 2.25 shows the statistics on the recomputed system costs after changing the network costing parameter ($C_{dn}^{inv,2}$) within ±20% of its original value.

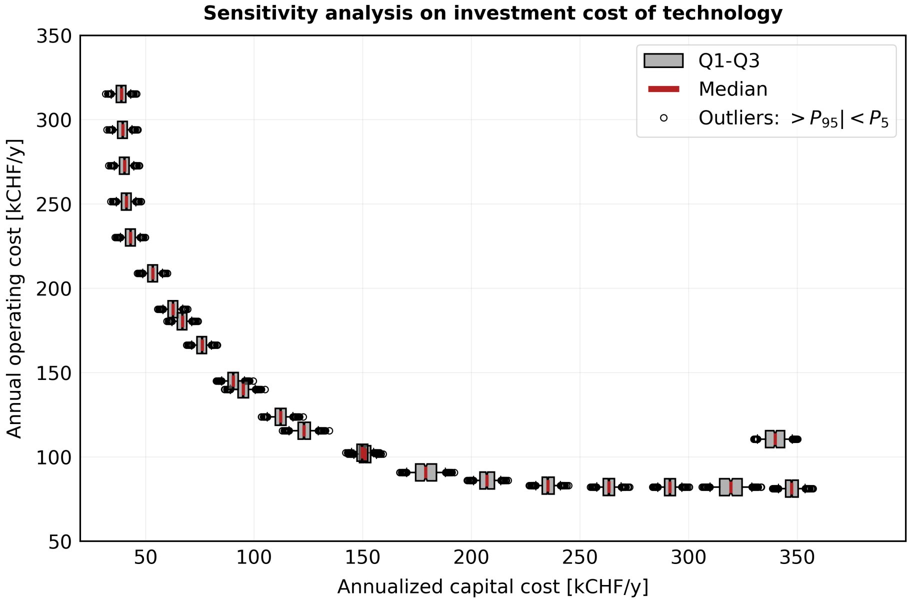

Figure 2.24: Sensitivity analysis on investment cost parameters of technologies for configurations relative to the HN at 40°C.

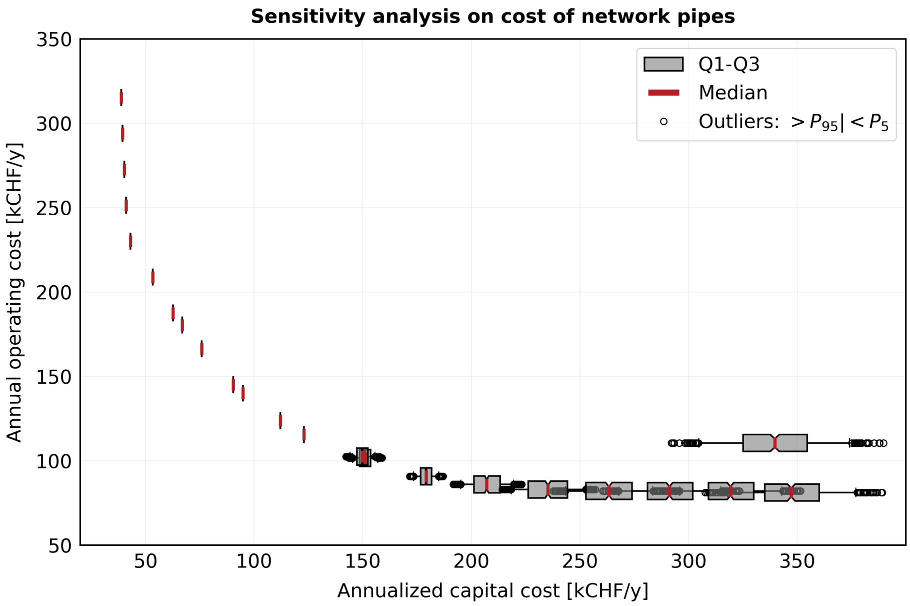

Figure 2.25: Sensitivity analysis on investment cost parameters of network for configurations relative to the HN at 40°C.

As expected, Fig. 2.25 highlights that the configurations sensitive to changes of the pipes investment cost parameters are those in which networks are installed, with an increased sensitivity for solution characterized by larger networks. However, even if characterized by large variation, most solutions do not overlap within the first quartile, meaning that they are likely to be differentiable from their neighbors.

Interest rate Figure 2.26 shows the statistics on the recomputed system costs after changing the interest rate (i), employed for the annualization of the capital cost.

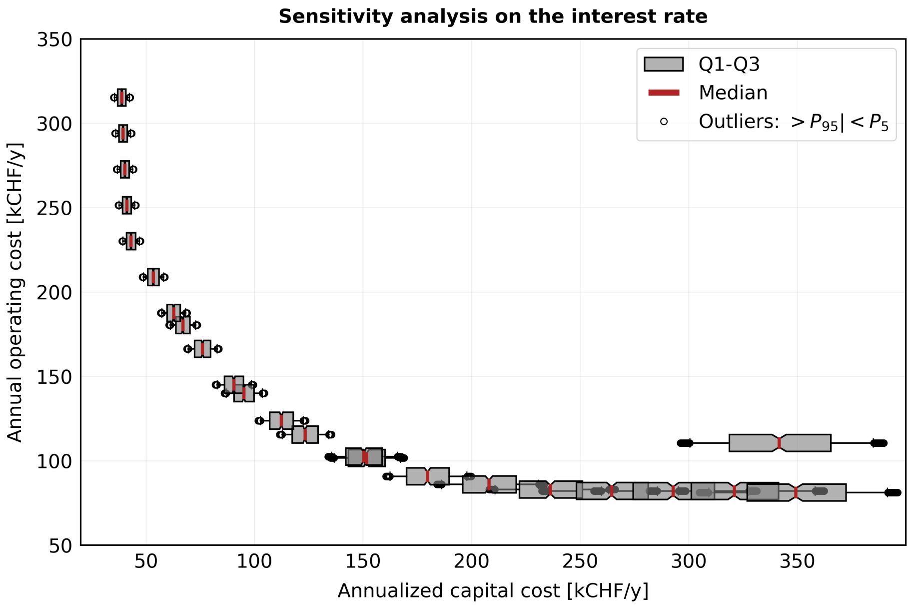

Figure 2.26: Sensitivity analysis on the interest rate for configurations relative to the HN at 40°C.

Figure 2.26 highlights that even though all configurations show sensitivity to changes of the interest rate, those more affected are the ones characterized by a higher contribution of the CAPEX to the total cost, with configurations largely overlapping towards the extreme of the Pareto frontier.

All uncertain parameters combined Figure 2.27 shows the statistics on the recomputed system costs after changing all parameters mentioned in a systematic manner.

Results suggest that solutions at the extremes of the Pareto frontier are more sensitive in the direction of the predominant cost contribution, whereas configurations in the middle of the Pareto frontier, characterized by moderate investment and operating costs are the most robust.

Sensitivity analysis on all Pareto frontiers Figure 2.28 gathers the statistics arising from the sensitivity analysis on all mentioned parameters performed on all the Pareto frontiers. The ellipse around each point represents the area defined by a distance equal to the standard deviation in each direction. The area of uncertainty is calculated as the area of these ellipses.

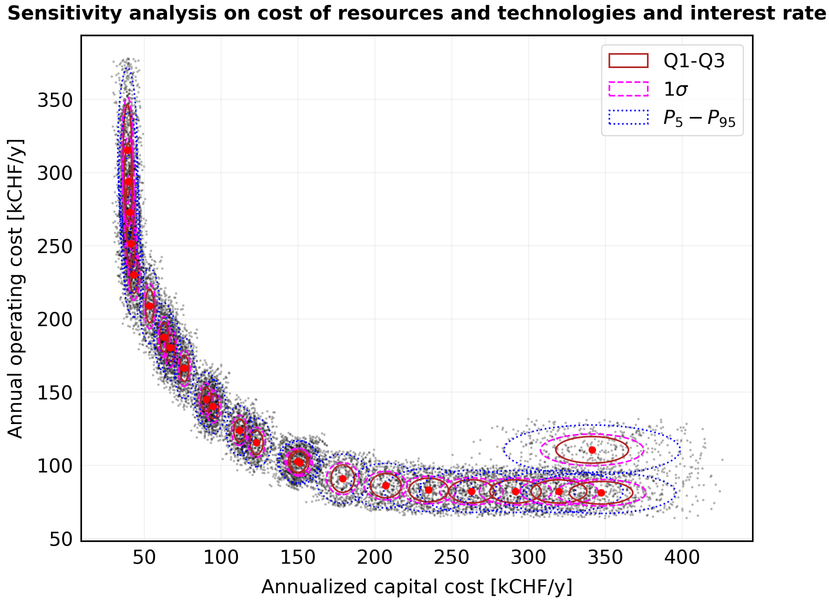

Figure 2.27: Sensitivity analysis on resource tariffs, technology costs, and interest rate for configurations relative to the HN at 40°C.

Results show that all configurations at different network temperatures are similarly affected by

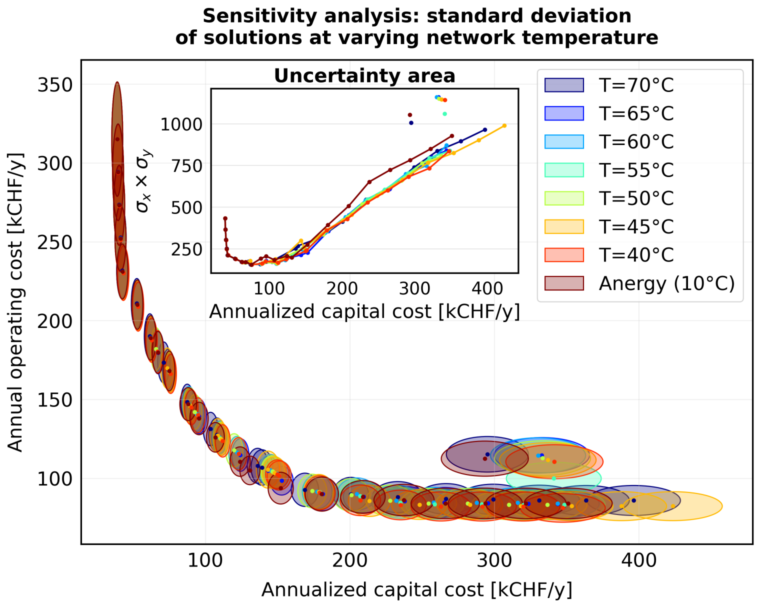

Figure 2.28: Sensitivity analysis on cost parameters for all the Pareto frontiers at different network temperatures.

the changes of the investigated parameters across multiple Pareto frontiers.

Figure 2.29 shows the frequency of being the design characterized by the lowest TOTEX for each network configuration. Figure 2.29 highlights that the configuration most likely to show

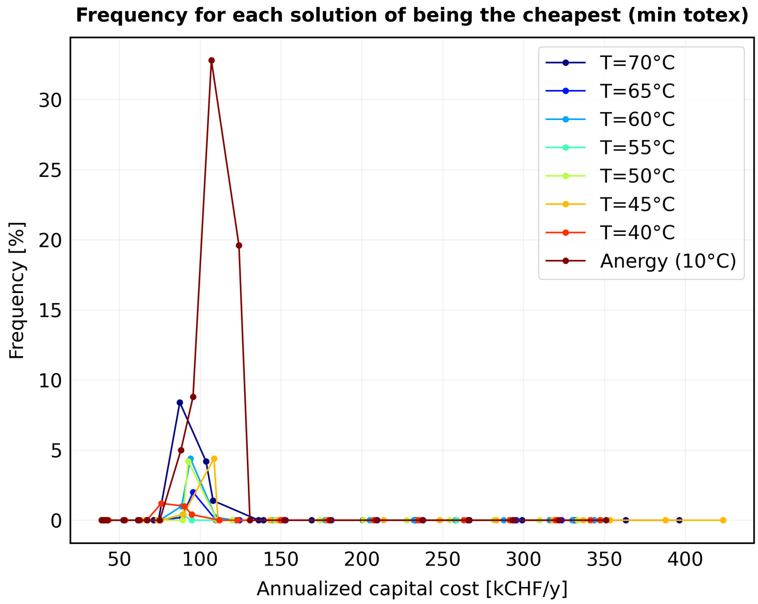

Figure 2.29: Probability of each solution of having the lowest TOTEX.

the lowest total annualized cost under the uncertainties investigated is the one equipped with the AN. In particular, the solutions in question are those characterized by a CAPEX around 100 kCHF/year, which represent hybrid solutions constituted by demand partially covered by the network (with the use of decentralized water-water HPs) and partially by standalone units (results relative to configurations equipped by the AN are reported in Section B.4.2). However, the exploitation of the AN is still very limited, since only the building closest to the central station (Bld1) is connected to the network. By comparing the CAPEX breakdown of the configuration equipped with the HN at 40°C (Fig. 2.17) and the one relative to the AN (Fig. B.18), it can be observed that despite the capital investment devoted to the network installation are much lower in the case of the AN (only one pair of pipes is installed), the difference is compensated by the higher cost of decentralized water-water HPs. For this reason, the results of the configuration with the AN are also more sensitive to uncertainty on the investment cost of technology, as highlighted by the comparison of Figs. 2.24 and 2.30.

Further investigation shows the high CAPEX of the water-water HP allocated to the commercial building (Bld1) as being highly influential. The cost functions used for HPs are expressed in terms of compressor nominal capacity and to better distinguish between central and decentralized units, two different function linearizations are employed as suggested in [83], with validity in different size intervals. However, in the case of the AN, the decentralized units show a much lower COP with respect to configurations equipped with a HN, resulting in higher compressor capacity. Particularly, in the case of this specific building which represents the largest user requiring the highest temperature, the size of the unit installed exceeded the range of validity of the cost function linearization resulting in an overestimation of the investment

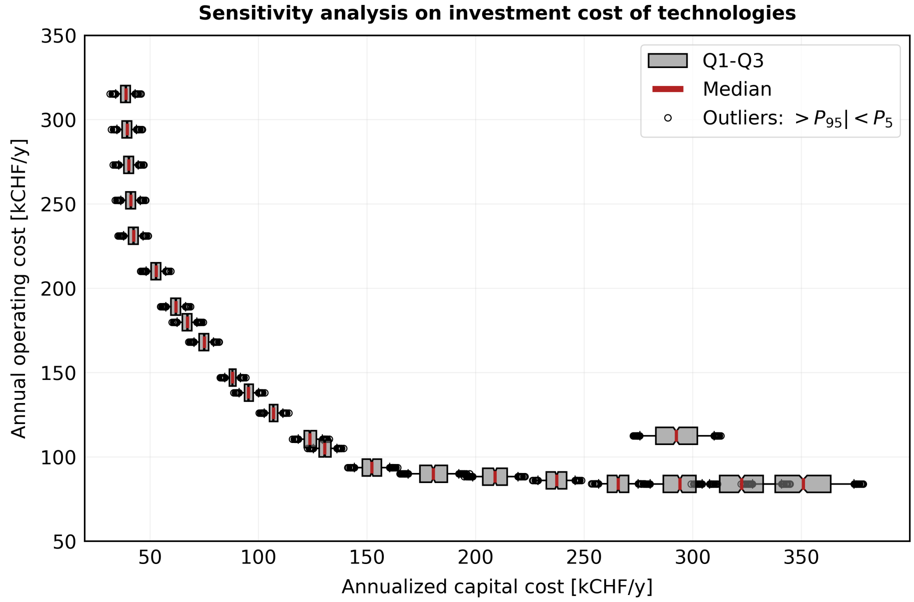

Figure 2.30: Sensitivity analysis on investment cost parameters of technologies for configurations relative to the AN.

cost up to 60 kCHF/y[5]. Therefore, all solutions are post-processed to recalculate the cost of the HPs with the correct linearization.

Figures 2.31 to 2.33 show respectively all the recomputed Pareto-frontiers (and fully centralized solutions) for the different network temperature configurations respectively in the CAPEX-OPEX, CAPEX-KPI^{env} and CAPEX-Ex_{loss} domain.

[5]With respect to the use of the cost function employed in this work for the corresponding size range.

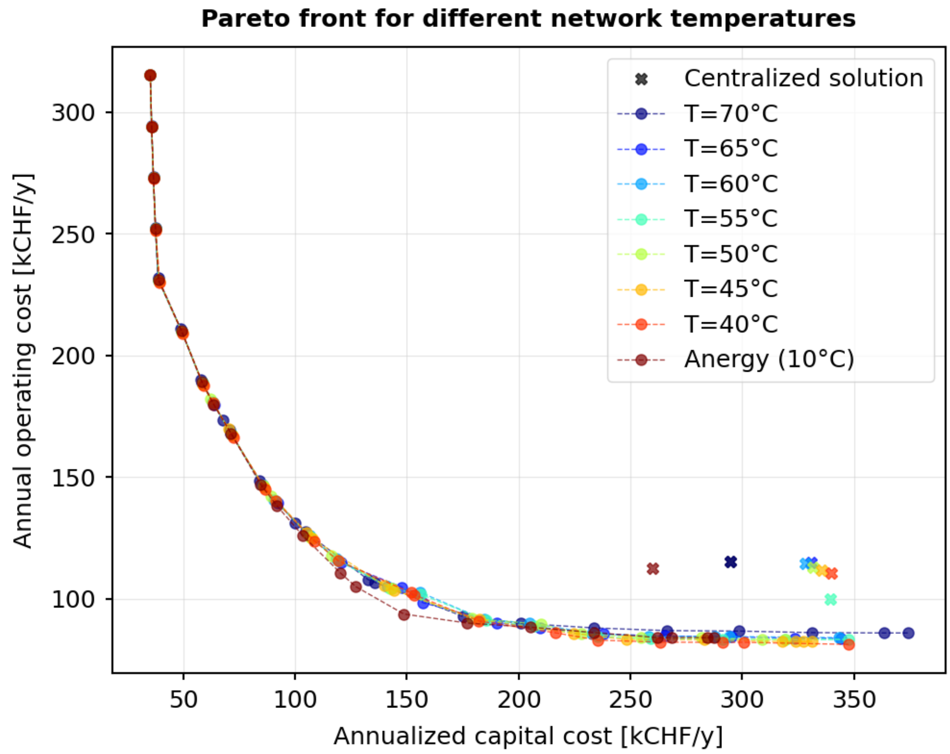

Figure 2.31: Recomputed Pareto optimal solutions for different HN temperatures and the AN. Centralized solutions represent designs excluding standalone units.

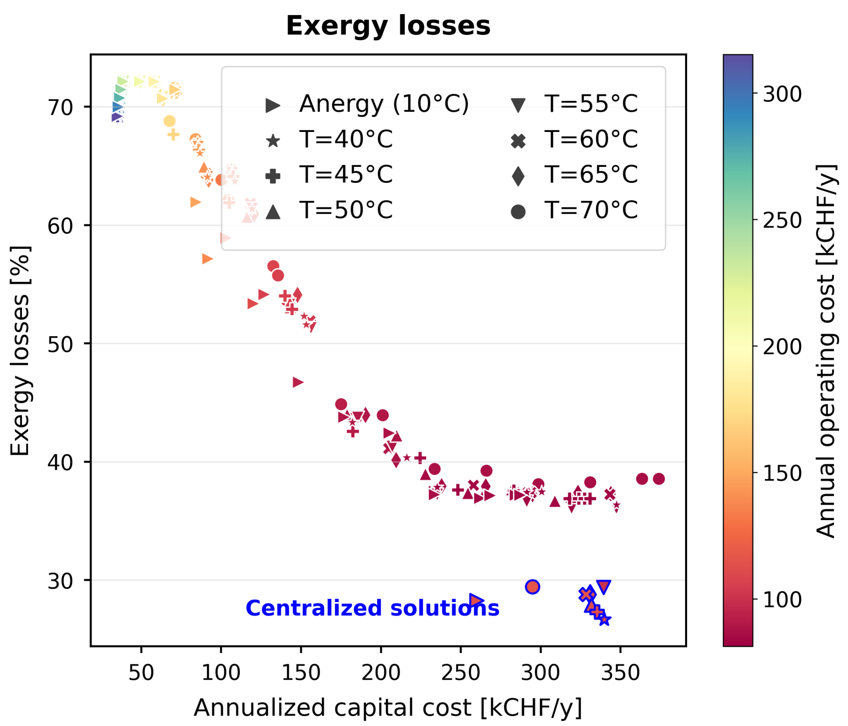

Figure 2.33: Recomputed Pareto-optimal solutions (and fully centralized configurations) for different HN temperatures and the AN plotted in the CAPEX-Ex_{loss} domain.

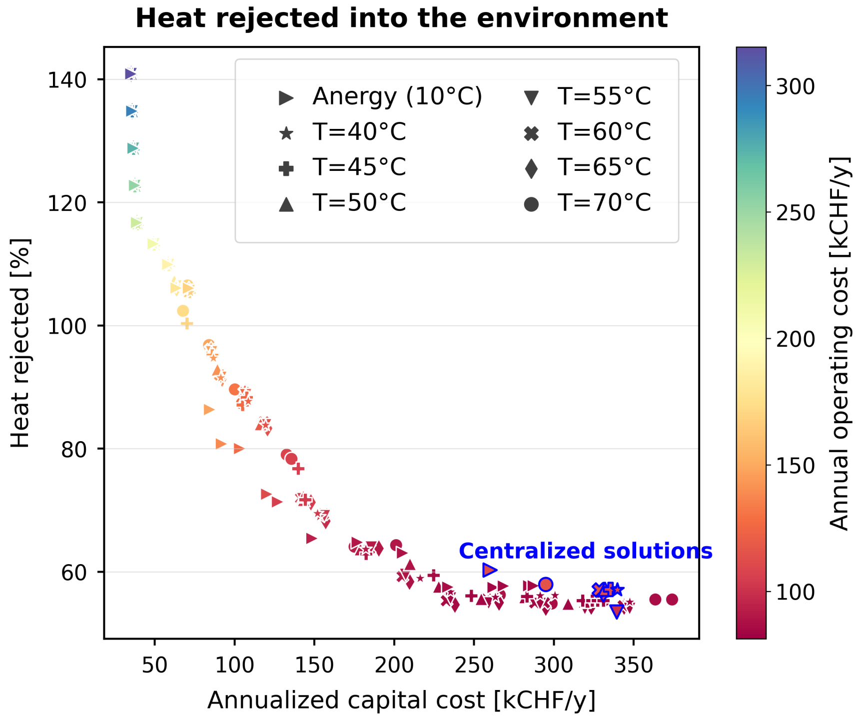

Figure 2.32: Recomputed Pareto-optimal solutions (and fully centralized configurations) for different HN temperatures and the AN plotted in the CAPEX-KPI^{env} domain.

The comparison of these results with the original ones shown in Figs. 2.13 to 2.15 highlights that all Pareto-frontiers show reduced x-axis range, resulting in lower CAPEX for solutions the most capital-intensive, but not by the same magnitude for each network configuration. Solutions including the AN are the most affected by the cost function linearization, with the result that such configuration achieves similar performance in terms of all indicators, but with lower investment. Also among the fully centralized solutions, relying the most on the TENs, the one equipped with the AN appears the least capital-intensive.

2.5 Conclusion

The foundational MILP superstructure and optimization framework for preliminary optimal sizing and operation of DES equipped with TENs was introduced in this chapter. The formulation relies on the combination of the heat cascade to ensure the feasibility of heat exchanges with mass and energy balances performed at each location. The underlying network models account for thermal and pressure losses as well as maximum flow constraints while optimizing the network layout and diameter. The strength of this formulation is the possibility of systematically investigating trade-offs between centralized and decentralized heat and cold provision with multiple types of TEN, which fills several gaps in the domain of DES optimization.

The proposed optimization framework was applied to a fictitious case study, representing a neighborhood of six buildings characterized by different years of construction and usage. Cost-optimal system configurations were generated for different network temperatures of the HN and considering an AN. The resulting solutions were analyzed with respect to different KPIs. One network temperature was selected to explore different solutions associated with increasing capital investment allowance. Concurrently, the ways of supplying heating and cooling demand and the expansion of the TENs along the Pareto frontier were shown. Last, sensitivity of the results to the cost of resources (electricity, LTH and natural gas) as well as the investment cost function parameters of technologies, network and the interest rate was systematically investigated, to assess the robustness of the different configurations.

Under the assumptions made, the following conclusions were drawn:

- To simultaneously investigate different thermal network temperatures by relying on an ε-constraint to identify the Pareto frontiers is an effective strategy to generate a set of optimal solutions for DES, characterized by distinct investment decisions and exploitation of resources. The definition of different KPIs allows to compare solutions under multiple aspects.
- The comparison of the Pareto frontiers in the CAPEX-OPEX domain shows that many configurations are equivalent in terms of operating expenses. However, the use of an AN enables to achieve the same performance with lower investment, both for the configuration relying the most on the TEN (i.e., for which the use of standalone units is allowed only for the supply of refrigeration needs) and for the hybrid ones. This results from the significant contribution of the network investment cost to the total expenses and potential savings arising from the use of a single network for the coverage of both the cooling and heating needs (in combination with decentralized units).
- Different indicators expressing environmental and exergy efficiency highlighted that solutions at higher capital cost make a better use of the exergy input to the system, resulting in a lower amount of heat released to the environment. Many configurations also perform similarly in terms of these indicators, but the AN again achieves similar performance with lower investment.
- Configurations relying heavily on TENs (i.e., those in which the only allowed standalone machines are CHIs to provide refrigeration) are less economically favorable, often being dominated by partially decentralized solutions. However, fully connected configurations appear the most efficient to exploit exergy input to the system.
- The analysis of a single Pareto frontier highlighted that by allowing more capital investment, solutions switch from decentralized configurations, relying on standalone units, to those exploiting the thermal network. To supply the heating demand, technologies tend to be installed in order, starting from ELHs, natural gas BOIs, air-water HPs and finally combinations of a central HP with decentralized water-water HPs connected to the TEN. For supplying cooling demand, CHIs appear as the least capital intensive solution,

while more efficient configurations favor installation of cooling network. However, even at the extreme end of the Pareto frontiers, the decentralized CHIs still appear to partially cover the demand. This result is attributed to the higher operating cost of using direct cooling with respect to the combination of decentralized machines and PV panels.

- Sensitivity analysis highlighted that the most robust configurations are those in the middle of each Pareto, where solutions are characterized by medium CAPEX and OPEX. Configurations at the extreme ends show higher sensitivity on the direction of the predominant annualized cost contribution. Sensitivity to the investment cost of technologies is minor when compared to that of the network cost and interest rate. The latter is the most influencing parameter on the CAPEX.

- The results of the sensitivity analysis suggest that the AN is the most likely to have the lowest TOTEX. However, the solutions generated show a tendency to exploit the TEN less then its potential. This result is linked to probable overestimation of the cost of the decentralized water-water HP for the larger building which limits the use of capital for network expansion.

The scope of the current work has been to develop a MILP superstructure and optimization method for the optimal design of DES equipped with different TENs and propose indicators and reasoning to distinguish the different configurations. Although many solutions show similar performance for the case study included in this chapter, the method proved to be powerful and capable of providing significant insights into the complex problem of decision-making in the DES domain.

Limitations and perspectives The main limitation of the developed superstructure arises from one of its strengths, that is the flexibility of the MILP formulation, enabling exploration of a large set of technologies and network options. However, such an approach leads to a significant burden in computational complexity. This is expressed by the number of variables, especially binaries, linked to the number of locations and the potential network layout configurations and operation (network types, allowed connections, diameters, temperature options). Moreover, depending on the problem and the choice of objective function, different configurations might provide equivalent or similar performance. This was demonstrated in the case study to be true for different network temperatures with respect to economic objectives. In this situation, the solver needs longer computational time to distinguish among the different configurations, making the solving strategy relying on the integer-cut constraint less effective. An option to overcome this problem is to add additional constraints, for example the iterative investigation of different network types and temperatures, as shown in this chapter, enables to greatly reduce the problem size. Adopting this latter strategy requires that the network temperature profiles to be investigated must be defined prior to optimization. Therefore, the potential options must be predefined and investigated separately. For example, beyond the buildings' cut-off temperatures (i.e., in the absence of space heating demand), in this study, the network temperature was defined constant and greater than that of the LTH. In this situation, to cover DHW needs, decentralized water-water HPs must always be operated in combination of the central plant. Otherwise, standalone units, such as ELHs, BOIs or air-water HPs can be used. Another option that was not investigated would be to run the network at the temperature of the LTH, allowing the use of water-water HPs in standalone operation (i.e., without the need of running the central HP).

An additional area for improvement is that in the current formulation the return temperature from the hydronic systems within the buildings must be set as an input and it is not subject to optimization. Therefore, to supply the heating demand directly with the network, the return temperature of the latter must be greater than the highest among all buildings which might be supplied directly, that is without the need of a decentralized HP. In reality, the control is made on the mass flow rate which can be varied to satisfy all buildings. However, the mass flow rate in the model is estimated as a consequence of the network temperature difference and not the opposite. An effort has been made to distinguish between buildings fed by the network directly through HEXs and those having a water-water HP in between. In the latter case, the ΔT remained fixed so as to not reduce the HP performance as a consequence of the network return temperature. However, the real returning temperature at the central station (which would be determined by non-isothermal and thus non-linear mixing) is unknown and was not considered in the estimation of the performance of the central plant, making the assumption that the two systems are hydraulically decoupled.

Analyses that have not been carried out during this study include the investigation of different temperatures for the LTH, the influence of the location of the central station on the results and finally sensitivity analysis on demand variation. The latter, given the long lifetime of DES projects, would represent a powerful tool to assess the robustness of the different system configurations in the long term. Heating demand might vary in the future both in terms of power and temperature as a consequence of retrofit actions, while cooling demand is expected to increase mostly due to warmer weather caused by climate change. The buildings renovation would result in a lower and more homogeneous required temperature distribution of the heat demand, potentially driving the choice towards a specific network temperature. On the other hand the better COP would require larger consumption of the LTH. Moreover, in the current work all results have been computed from a systematic perspective, meaning that the district has been considered as a community sharing all investment and operating cost. In reality, the cost of infrastructure and energy distribution would be allocated to the utility provider, while the cost of decentralized units, buying the resources, and potentially selling the extra PV electricity production would be associated with the single users. The price of the distributed heat and cold would be set by the distribution company to pay back the investment cost of the infrastructure. Therefore, it would be interesting to investigate the different network temperatures from the position of different stakeholders and estimate the cost of energy (distributed heat and direct cooling) that the company should define for each network configuration such that to recover its investment.

Further work could also include the scaling up of the method to the district level. One potential approach would be to rely on iterative screening of the possible network layouts and operating temperatures to simplify the MILP superstructure and geographical building clustering to reduce the number of locations. The optimization could be decoupled to an upper- and a lower-level stage. The former would deal with the design of the primary network and position of the central plant, with the buildings within each cluster aggregated in a unique location, whereas the latter would solve the system design within each cluster in parallel. A preliminary study including the first stage of such a potential method (i.e., the geographical clustering of the districts and the optimization of the primary network) has been published in [60].

Finally, the sensitivity analysis on the cost parameters highlighted how the use of a imprecise linearization for the investment cost function of machines might influence the results. In particular, the technology whose cost must be estimated with care is the HP and especially the water-water configuration. Whereas all the other technologies impact all the network configurations in a similar way, this latter element plays a significant role in the choice of the degree of decentralization. Especially in the current study, in which cost functions of HPs are expressed in terms of compressor capacity, the network temperature affects the estimation of the machine cost (lower network temperatures result in lower COP and therefore larger compressor capacity for the same heat delivered).

Moreover, the author would like to emphasize the potential benefits of supplying heating and cooling with a single network (in combination with decentralized units). The AN, depending on the temperature of the source, is able to cover the space cooling demand through direct cooling and act as a source for decentralized HPs (and CHIs in case of refrigeration needs). Considering that the investment in the network represents the most relevant cost contribution for all network temperatures, the configuration with the AN appears as a solution to sell more services with the same investment cost. Moreover, the coexistence of cooling and heating requirements enables recovering the heat injected into the network by the consumers of cooling as a source for decentralized HPs. This anergy effect reduces the network's consumption of heat and cold from its source (i.e., the LTH), thereby reducing its operational costs and giving it an additional economic advantage over a conventional DHN.

Lastly, the investigation of different working fluids for the AN was not included in this work. Pioneering study in this direction was presented by Henchoz et al. [83], whereas more recently Suciu [23] integrated the refrigerant-based network into the analysis of zero- or negative-emission, autonomous DES. The main advantages with respect to a water-based network are the use of pressurized pipelines leading to smaller diameters, the lower dependence on the temperature of the source [6], and the greater heat transfer capacity of the fluid in phase change, leading to lower HEX surfaces. Due to the fact that the technology is not yet commercially available in the field of urban districts and intrinsic limitations of the developed model which

[6] The presence of condensing and evaporating fluid enables efficient temperature changes by simply varying the pressure by means of a compressor or an expansion valve, without the need of an additional thermodynamic cycle and HEXs as in the case of water.

would not enable the inlcusion of some advantages of using a refrigerant (i.e., HEXs are costed in terms of exchanged power and not surface and the effect of the temperature of the source was not investigated) this analysis was left to future studies.

Given that most of the existing DES are still supplied by fossil fuels (90% in the World and 70% in Europe [63]), the following chapter tackles the optimal retrofit of existing systems, to both increase the penetration of DHC and integrate RES in urban areas.

3 Retrofit of district energy systems to integrate renewable energy

Chapter overview

- Deep energy retrofit of complex energy systems equipped with thermal networks
- Preliminary optimal design and operation of energy systems including multi-level temperature networks
- Decision support tool to assist large energy users during the transition to low temperature networks

This chapter is the result of a study carried out to assist an international airport during their transition from a fossil-based energy system to the connection to a low temperature network.

3.1 Introduction

Given the proven advantages of TENs during the ongoing energy transition, small-scale district networks are increasingly being deployed to service larger buildings or groups of buildings such as university campuses, hospitals or airports [4]. With respect to the challenges already mentioned in Chapter 2, further complications in these cases include the heterogeneous mix of services provided (heating, cooling, electricity, humidification), the strict standards of comfort and safety to fulfill, and the substantial financial loss linked to the interruption of operation. Nevertheless, non-residential buildings are on average 40% more energy intensive than residential ones [84], representing a big potential for energy and emission reduction.

Whereas new systems are nowadays designed for low-energy buildings, well insulated and equipped with suitable space conditioning technologies such as floor heating or low temperature radiators, the current challenge appears to be the transition from old systems to the newer generations, calling for refurbishment and retrofit actions [20]. It has been estimated that about 70% of the building stock in 2050 will still be constituted by currently existing buildings, and no more than one deep refurbishment cycle is possible during this time frame

[85]. Beyond refurbishing the building stocks, also the existing DES might need retrofit and expansion actions to supply the increasing demand and replace old fashioned technologies. Most of the current district systems are still based on fossil fuels (90% in the World and 70% in Europe [63]), whereas the ongoing energy transition calls for efforts not only to increase the penetration of DHC systems, but also the share of RES in the sector. Therefore, the evident need appears to be the retrofit and expansion of existing and obsolete systems. From one side the expansion of the TENs promotes the exploitation of DHC and on the other replacing fossil-fuel technologies with more sustainable options improves the share of RES in the urban sector.

One option to improve the performance of existing DES is to decrease the operating temperature, crucial aspect to promote the sector electrification towards more sustainable heating systems. despite the well recognized benefits of low-temperature district heating [12, 18–21], existing systems are still behind the state of the art. About 350 districts among Sweden and Denmark are still operated as 3rd generation systems (supply and return temperatures around 80°C and 40°C, respectively), while other European examples such as that in Brescia and Geneva, with their supply temperature around 100°C, can be categorized as part of the 2nd generation [86]. Therefore, whereas new systems are intentionally designed to sustain the LTNs (e.g., significant building insulation), traditional systems need alternative approaches. The transition to lower-temperature networks is a challenging issue and should be carefully conducted. The different steps that have to be included are [86]: 1) eliminating system errors and improving system control, 2) enhancing heat transfer performance of HEXs and improving system design, 3) eventually renovating the buildings, 3) integrating various heat sources and TES systems, 4) taking into account all technical issues such as ways of heat feed-in, distribution heat losses, operation strategies, etc. Neirotti et al. [87] included among the different simulated scenarios aiming at lowering the network operating temperature, also the possibility of installing decentralized HPs. The latter was pointed out as a valid alternative in buildings that cannot be easily renovated, such as historical buildings in cities. Another example is the one of large public sites, such as hospitals or airports in which the need of ensuring the continuity of services might not allow a deep renovation of all the buildings at once.

Large energy users, such as commercial sites, university campuses, hospitals or airports are rarely the object of research studies in the field of optimal energy systems design with the integration of TENs. However, their characteristic of representing an heterogeneous building stock, with different services to be provided in a limited geographical area, makes them the perfect starting point for the modernization of the whole district. Airports in particular represent large energy consumers that due to their particular features may resemble small cities [88]. Therefore, methods developed in the field of urban energy systems can be applied, with the due modifications, to airports as well.

3.2 State of the art and contributions

As reported in Chapter 2, a significant amount of studies in the literature focus on the green field design optimization of DES, implying that the energy system is newly designed, without any constraint regarding existing infrastructure. On the contrary, studies in the literature dealing with network expansion remain scarce: only a very small number of articles detail the used approach or the associated modelling aspects. Moreover, these few reports are often own by the commissioner, mostly private companies, limiting their dissimination [89]. In this section an attempt is made to gather recent studies in the field of DES retrofit and expansion and to highlight the main characteristics.

Popovski et al. [90] analyzed the cost-effectiveness of decarbonizing and expanding the existing DHN of a city in Germany. The authors compared different scenarios including the replacement of the existing coal-fired CHP with large-scale HPs. The study highlighted that the city's emission reduction targets could not be reached without changing the heat supply system. In particular, only the scenario relying on a HP to cover up to 60% of the demand was able to reach the climate targets. The authors pointed out that, with the current tariffs, the usage of HPs was economically not competitive with systems based on fossil fuel. Hence, different strategies were suggested to reduce the heat supply costs such as the reduction of the supply temperature, by zoning sub-neighborhoods of renovated buildings. The latter was recommended as a solution to improve the HPs performance and therefore reduce its operating cost.

Guelpa et al. [91] optimized the connection of new buildings to an existing DHN without modifying the existing pipelines. The authors proposed a method to optimally select the buildings that must be connected, taking into account the maximum flow rates constraints. The method was applied to the city of Turin, equipped with the largest DHN in Italy. The study focused on the network layout, excluding the heat production system. However, in case of retrofit of the distribution network and in particular when switching from a fossil-fuel fired technology to HPs, both supply and return temperatures should be considered to optimize the new operation, while respecting the maximum flow constraints.

Rämä and Wahlroos [92] investigated the effect of including HPs and solar collector in the existing DH system of Helsinki. The authors concluded that relying on new HPs clearly resulted as the best option both in economic and environmental terms, and lowering the distribution temperature improved the performance of all the investigated systems.

Delangle et al. [89] developed a MILP based method to assess the optimal DHN expansion strategy and the mix of technologies to be installed, together with their operating mode, to minimize cost or environmental impact. The authors included an investment planning strategy to optimize the time when to invest into a technology within the project lifetime. However, the study neither took into account the temperature requirements nor the one of the distribution network. Moreover, the cooling needs were not included into the analysis, missing the potential of synergies between the heating and cooling sectors. Nevertheless, the authors concluded that results on the optimal mix of technologies significantly vary according to the modelling hypotheses made and the objective function used. As an example, whereas the cost-based optimization mainly relied on the existing technologies, the emissions-driven objective suggested to replace the existing fossil fuel BOIs with biomass options in combination with HPs, TES systems and eventually CHP units to cover the peak demand. Moreover, the authors emphasized the need of using optimization to study DH systems expansion.

Dominković et al. [93] proposed a MILP based method to optimally define the potential interconnection between four existing DHNs in the city of Zagreb (Croatia) and neighboring towns, whose demand is aggregated in four single locations. The authors also investigated the increase of the share of RES within the four districts in future configurations, including TES, ELHs and HPs. Results showed that if interconnections were not allowed, the optimal mix of installed technologies included HPs coupled with electric back-up BOIs to cover the peak demand in all the four regions. On the contrary, when interconnections between the zones was allowed, the use of the existing CHP unit resulted the most profitable option. Moreover, interconnecting the neighboring towns to the main city, even if located 19 km apart, appeared always the best solution under socio-economical aspects.

Qaeini et al. [94] developed a three-stage iterative heuristic optimization framework to define the expansion planning of electrical and heating networks and corresponding distributed energy resources. The authors took into account the impacts of electricity transactions among industrial micro grids under the uncertainty of different planning and operational parameters. The three resolution phases aimed at 1) determining the energy system facilities, 2) defining optimal electric transactions and energy resource scheduling in typical operation, 3) choosing alternatives such as demand response for contingent situations. The objectives were defined as the minimization of investment, operating and emissions costs, while maximizing the energy reliability. The authors verified their methods on different case studies of increasing size.

Bordin et al. [69] focused on the optimization of large scale networks layout within the context of DHN expansion. The authors developed a MILP framework taking into account existing and potential new connections as well as essential hydraulic characteristics by means of pressure drop and maximum flow constraints. The method was tested on both a real case study and a fictitious one incorporating up to 1000 potential new and 500 existing users. The objective function maximized the difference between revenues and cost associated with the connection of new users, over a five- and ten-year time horizons.

Hou et al. [95] proposed a systematic approach for the expansion of current DES to increase the energy supply capacity and to improve the operational efficiency. The presented framework included four phases: 1) evaluation of the existing DES limitations, 2) demand analysis, 3) available energy resource assessment and 4) DES expansion. The choice of the optimal expansion scheme relied on the comparison of three different predefined scenarios. The method was demonstrated on the Ningbo Hi-Tech district in China, showing that input energy, input exergy and CO_2 emissions could be reduced respectively by 22.7–24.1%, 14.5–14.9% and 5.9–6.6% with respect to current values.

The studies presented above are listed in Table 3.1, which highlights their main characteristics relevant in the current field: 1) the use of an optimization approach, 3) the application chosen to validate the methods, 3) if the retrofit of the network infrastructure was included in the analyses, 3) if the authors addressed the retrofit of the current technology mix, 4) if the network operating temperature was investigated (either by optimization or scenarios definition), 5) which kind of TEN was included, 6) which technologies were considered. The studies are also compared to the work presented in this chapter.

Table 3.1: Review of studies on optimal retrofit of district energy systems.

Study	Optimization	Application[a]	Network retrofit	Technology retrofit	Temperature selection	Type of network[b]	Technologies[c]
Popovski et al. [90]	✗	C	✓	✓	✗	DHN	BOI, CHP, HP, ST
Guelpa et al. [91]	✗	C	✓	✗	✗	DHN	-
Rämä and Wahlroos [92]	✗	C	✗	✓	✓	DHN	BOI, CHP, HP, ST, TES
Delangle et al. [89]	✓	D	✓	✓	✗	DHN	BOI, CHP, HP, TES
Dominković et al. [93]	✓	AD	✓	✓	✗	DHN	BOI, CHP, HP, TES
Qaeini et al. [94]	✓	D	✓	✓	✗	DHN	BOI, CHP, PV, WT, BAT, TES
Bordin et al. [69]	✓	D	✓	✗	✗	DHN	-
Hou et al. [95]	✓	AD	✗	✓	✗	-	BOI, CHP, PV, CHI
This work	✓	D	✓	✓	✓	DHN, DCN, DHCN	BOI, HP, ELH, CHI, TES

[a] AD: aggregated district, D: district, C: city
[c] DHN: district heating network, DCN: district cooling network, DHCN: district heating and cooling network
[c] BOI: boiler (fossil or biomass), HP: heat pump, CHI: chiller, ELH: electrical heater, TES: thermal energy storage, ST: solar thermal, CHP: combined heat and power, WT: wind turbine, PV: photovoltaic panel, BAT: stationary battery

The presented literature review highlighted a scarcity of studies employing optimization approaches for the simultaneous retrofit of network infrastructure and technology mix. In addition, most of the authors do not make any consideration about operating temperatures, which is proven to highly effect the performance of DHNs, from the energy conversion to the distribution process. Moreover, despite DHC systems have already proven their effectiveness in North European countries, most of the studies still focus only on DH. However, the retrofit of existing infrastructure gives a precious opportunity to promote synergies between the heating and cooling requirements. Therefore, based on the gaps highlighted in the current literature, this chapter attempts to contribute the optimization of deep energy retrofit of complex energy systems equipped with TENs, by answering the following research question:

How can existing district energy systems be retrofitted to optimally integrate renewable energy sources and exploit synergies between heating and cooling requirements?

The proposed approach, aiming at answering the latter question, consists in combining the following elements:

- the methods shown in Chapter 1 for the estimation of the thermal energy requirements in existing complex buildings;
- the methods presented in Chapter 2 for the optimal design of complex energy systems equipped with TENs;
- the further expansion of the MILP superstructure to take into account the existing infrastructure and technologies including their technical constraints;
- the collection of all the results in an online visualization platform for decision support.

Combining the use of LTH and HP integration, this chapter proposes solutions to promote the electrification of DHC systems towards fossil-free configurations. Moreover, the application to a block of complex non-residential buildings, characterized by different usage and demand profiles, allows to investigate potential synergies of heating and cooling requirements. One of the options in this regard consist on recovering the heat rejected by consumers needing cooling for heating purposes, for example by feeding the evaporators of the HPs. This outcome, enabled by the use of a LTN, is defined as anergy effect.

The work presented in this chapter has been developed in close collaboration with an international airport. With the final aim of assisting their transition to a LTN, part of the study consisted in the development of a decision support tool. The aim of the collaboration has been to provide suggestions and guidelines towards an optimal fossil-free energy system configuration supported by a set of different system designs and relative KPIs. The final considerations were not supposed to represent precise system configurations, but rather a well-grounded starting point for further discussion and investigations.

3.3 Application

To validate the methods proposed in this chapter the same international airport introduced in Chapter 1 is chosen as case study. The airport has recently committed to decrease its CO_2 emissions allocated to the buildings operation by 5,000 tonnes by 2030 as compared to 2012. Whereas the electricity is already supplied by RES, the current goal is to eliminate the use of fossil fuels for heating and cooling by the year 2025. The refurbishment project aims at substituting, by the year 2022, the existing BOIs with HPs, exploiting the lake nearby as a source of LTH for heating and cooling purposes. In short, the lake water is sucked in at 60 meters below the surface to ensure temperature stability and is delivered to the airport site thorough a LTN. HPs are employed to rise the temperature of the source and satisfy the buildings' heating demands. At the same time the LTH can be directly used for cooling purposes, eventually coupled with CHIs. Given that the electricity bought on the site is already produced by RES, the final energy system based on HPs and CHIs would result 100% renewable.

The correct sizing of machines and infrastructure for the new system is a challenging task, due to the wide range of potential configurations, ranging from a fully centralized heat production to a completely decentralized one. The former implies the exploitation of the existing infrastructure, eventually combined with the installation of new pipelines, to supply all the users with high temperature heat, produced by the central HP. This scenario would result in significant thermal losses for the heat distribution, exergy losses due to the unnecessarily high temperature for most of the users and a poor performance of the central station. However, a small number of new conversion technologies is required. The fully decentralized configuration is based on the distribution of the LTH to all the substations and the installation of decentralized HPs to satisfy the temperature requirements of all the users. The latter allows better system performance but results in a greater number of installed machines. Hybrid solutions with multi-temperature networks have the advantages of combining the benefits of the two extreme configurations. Simultaneously, the cooling demand can be supplied by the distribution of the LTH and the exploitation of free-cooling, by the usage of decentralized CHIs or by a combination of the two. Finally, the connection to a LTN allows to exploit the anergy effect, that is to recover the heat injected into the network by consumers needing cooling for heating purposes, for example by feeding the evaporators of HPs. This operation, based on synergies between heating and cooling services results in savings of the LTH.

3.3.1 Estimating the thermal energy requirements

The TER at the site is estimated for each substation following the procedure reported in Chapter 1. The proposed method is hereby quickly summarized. Heating power measurements, recorded at the substation level, are employed to calibrate a linear grey-box model and tailored parameter values are used to assess the heat delivered by static appliances and ventilation units. In each substation for each type of space conditioning technology, two different generations of users are supposed to be installed. Finally, for each user the installed capacity is assigned, based on available data or assumptions. By minimizing the exergy losses and exploiting the available heat exchanger capacity while respecting the design mass flow constraint, the new operating temperatures are estimated. For further information the reader is readdressed to Section 1.4 for thermal models definition and calibration, to Section 1.4.4 for the definition of the optimized operating temperatures and to Section A.5 for assumptions on HEXs capacity and values of users' temperature requirements. The DHW demand is estimated based on the current measurements of allocated heat load and mass flow rate to derive a daily average profile, considered constant throughout the year (see Section 1.5.1).

The cooling demand is evaluated by the combination of current electricity consumption of the CHIs and the estimation of the COP for each machine. The latter is derived based on measurements and information reported on technical sheets. Two types of users are distinguished: radiative panels and ventilation units, whose operating temperatures are assigned based on suggestions from experts in the field. Further information on the thermal model are reported in Section 1.5.2, while the values assumed for the users' temperature requirements can be found in Section A.6.3 .

The annual operation is approximated with the use of typical and extreme periods, identified following the k-medoid clustering approach reported in [72]. Specifically seven typical days constituted by 24 hours of operation and two extreme periods with a single time step (extreme heating and cooling demand) are used to model the current and future operation during the project lifetime. The reader is readdressed to Section A.4 for more insight about the choice of typical and extreme operating periods. Figure 3.1 shows the distribution of the typical operating periods over the reference year together with the trend of the ambient temperature.

The LTH is considered available at the site excluding eventual investment and operating cost for the connection to the nearby lake. The temperature of the source is considered constant during the day and depending on the season (summer, winter and mid seasons). The values are reported in Section C.1.1.

3.4 Modelling framework

This section describes the modifications made to the original MILP superstructure and corresponding models presented in Section 2.3 to include the existing infrastructure, technologies and their respective technical constraints.

3.4.1 Existing pipelines

The energy system is equipped with an existing TEN operated at high temperature. The existing pipes are modelled by adding an additional network element to the set gathering all the network types **N**. For this network the binaries related to the network activation y_n, choice of the diameter $y_{n,dn}$ and the activation of connections $y_{n,lc1,lc2}$ are fixed to reflect the current

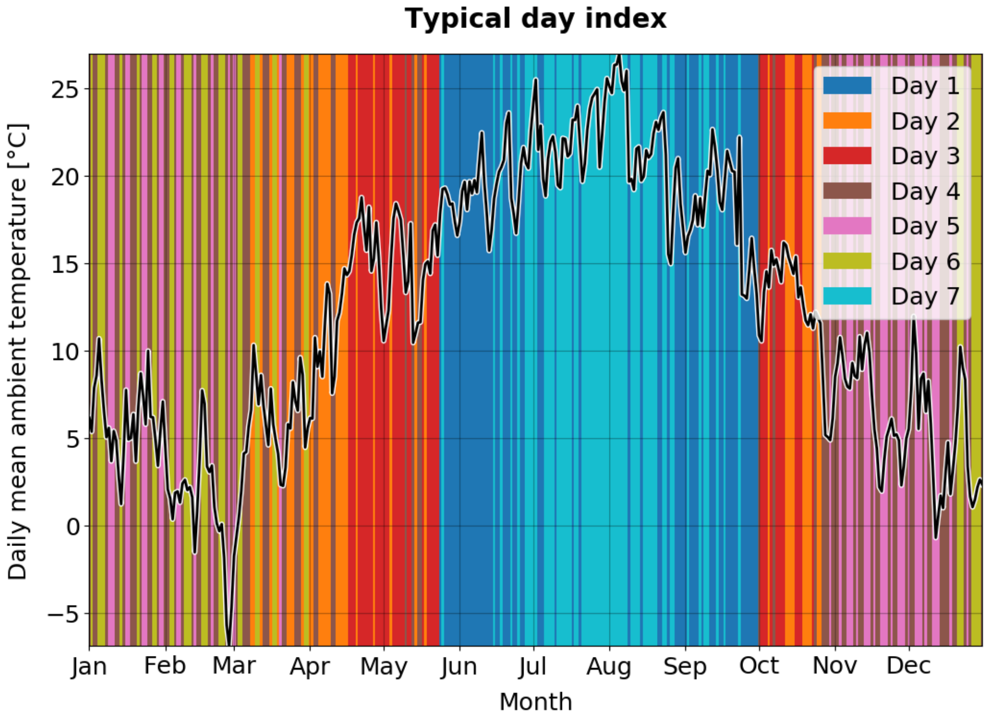

Figure 3.1: Distribution of the typical operating periods over the reference year and trend of the ambient temperature.

situation, respectively by Eqs. 3.1a to 3.1c.

$$y_n = 1 \qquad \forall\ n \in \mathbf{N} : n = \text{HN1} \quad (3.1a)$$

$$y_{n,dn=\text{dn}_{HN1}} = 1 \qquad \forall\ n \in \mathbf{N} : n = \text{HN1} \quad (3.1b)$$

$$y_{lc_1,lc_2,n} = \text{y}_{lc_1,lc_2,n} \qquad \forall\ n \in \mathbf{N} : n = \text{HN1},\ \forall (lc_1, lc_2) \in \mathbf{LC^N} \quad (3.1c)$$

HN1 represents the existing network and dn_{HN1} its diameter, which similarly to HN1 in $\mathbf{N}$ is included within the set of potential diameters $\mathbf{DN}$.

Beyond the existing network whose operating temperature is still optimized through the variable $y_{n,T_n^{f/r}}$, other two networks can be potentially installed: an additional heating network (HN2) and an anergy network (AN). The extensive formulation of the networks' models is reported in Section 2.3.2. The pipes' potential diameters and corresponding technical characteristics (i.e., insulation thickness, maximum flow velocity, thermal conductivity) are chosen among the ones reported in Section B.3.

3.4.2 The central plant

Due to the possibility of operating the two HNs (i.e., the existing and the eventually newly installed one), at two different temperatures, the model of the central plant is slightly modified to represent a simplified model of a two stage machine working at the two temperature levels. The core of the unit model remains identical to the original version presented in Section 2.3.3, whereas the modifications mainly affect the definition of the evaporator/condenser couples $c_{e/c}$ belonging to the unit. In the central location two machines are defined:

1. HP 1: represents a double-stage machine, connected to the LTH and equipped with an additional condenser at an intermediate temperature level to eventually supply the high and the medium temperature HNs;
2. HP 2: represents one single stage machine upgrading the heat received by the previous machine or the HN, from the intermediate to the upper level temperature.

For the first machine (HP 1 in Fig. 3.2) two couples of condenser/evaporator streams are defined for each potential combination of temperature levels included for the two HNs. For example, if for each network (the existing one, HN1, and the potentially newly installed one, HN2) only one potential operating temperature couple is defined (respectively $T^{f/r}_{HN1}$ and $T^{f/r}_{HN2}$ with $T^{f}_{HN1} > T^{f}_{HN2} + \Delta\mathrm{T}_{HN1/HN2}$) then two couples of thermal streams are assigned to the first machine: the first couple including an evaporating stream connected to the LTH and a condensing one at the intermediate temperature T^{f}_{HN2}, and the second consisting of an evaporating stream still supplied by the LTH and a condensing stream at the upper temperature level T^{f}_{HN1}. A minimum difference among the two networks' temperature levels ($\Delta\mathrm{T}_{HN1/HN2}$) is set to avoid such a configuration when the two networks present very close operating temperatures. A minimum temperature difference at the evaporators side is also included, while the condensing temperature refers to the feeding temperature of the network they are connected to.

The second machine (HP 2 in Fig. 3.2) includes one evaporator connected to the intermediate temperature level T^{r}_{HN2} and one condenser to the upper temperature level T^{f}_{HN1}. In this case the minimum temperature difference at the evaporator side is calculated from the network return temperature. This second machine is included to eventually upgrade the heat recovered at the condenser of the CHIs and rejected into the intermediate HN to supply consumers requiring higher temperature. Figure 3.2 represents a schematics of the evaporator/condenser couples assigned to the two machines in case only one couple of temperatures $T^{f/r}$ is defined for each HN.

3.4.3 Chillers

As the HPs, CHIs are modelled to work between different levels of temperature of the heat source and sink as presented in Section 2.3.3. However, further to the usual operation previously explained, additional evaporator/condenser couples are included to eventually recover the heat at the condenser at a medium temperature level. All the potential modes of operation are reported in Section C.1.2.

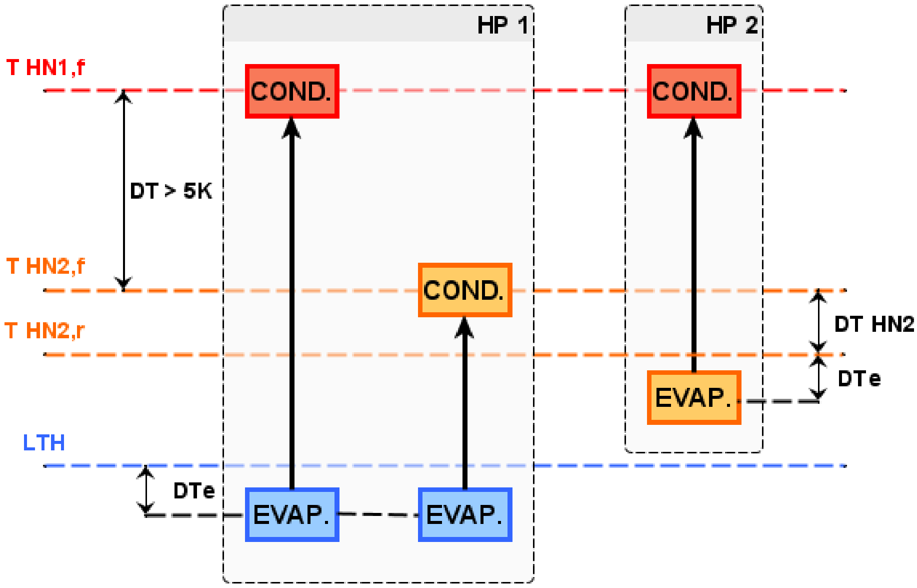

Figure 3.2: Scheme of the temperature levels assigned to the two central HPs in the case only one temperature couple is defined for each of the two HNs.

Moreover, in the substations where cooling installations are already present, CHIs are considered to be installed and available (without any cost). The available electrical capacity is estimated though the given cooling capacity and the COP of each machine at design condition, evaluated with the information on the technical sheets. For such machines the unit binary variable y_u is fixed to 1 as well as the lower and upper bounds of the unit multiplication factor ($F_u^{min} = F_u^{max} = 1$). The existing machines are redistributed among the different locations, by taking into account their cooling requirements. In this way, the potential surplus of installed capacity in some substations can be exploited in others.

Beyond the existing machines, it is possible to install new CHIs to eventually cope with the increased cooling demand (e.g., in newly constructed buildings). The new machines are modelled as the existing ones but including an increased Carnot efficiency to represent the technological progress.

3.4.4 Thermal storage

A simplified model of TES is included to the superstructure in order to take into account the thermal capacity of the AN. Indeed, due to the large mass of water circulating in the pipelines, the network can act as a buffer to the variation of heating and cooling needs. Exploiting the synergies between the two requirements results in savings of the LTH. Due to the lack of the dynamic component in the models, all defined as steady-state, the thermal capacity of the network cannot be directly included. Therefore, not to miss potential synergies between heating and cooling requirements, in the current case study, it is assumed that a TES in the central location is available at no cost. The implementation of such a unit is also intended to overcome the uncertainty on the estimation of the demand profiles. The latter is particularly important in the current application, in which due to the current use of the iced water storage during the night, the hourly profile of the cooling demand could not be accessed.

A similar model to the one presented in [54] is adopted. Aiming at the integration of a daily storage, cyclicity constraints are needed to ensure that the storage's state of charge at the beginning of one day is the same then that at the end of the previous day. One option to enforce it without taking into account the sequence of the typical periods over the year is to impose that this constraint is valid for all days. To do so, the time steps are grouped into the original typical periods ($p \in \mathbf{P}$), each one constituted by 24 time steps ($h = 1..N_h \in P_h,\ N_h = 24$), representing the typical days. Whereas during the extreme periods of operation it is assumed that the storage cannot be used, Eq. 3.2 defines in each hour of each typical day its state of charge:

$$V_{p,h} = \begin{cases} (1-\sigma_s)\cdot V_{p,N_h} + \mathrm{V}^{max}\cdot\left[\left(\eta_s^+\cdot f_{u,t}^+ - \frac{1}{\eta_s^-}\cdot f_{u,t}^-\right)\cdot \mathrm{d}_t\right]_{t=p\times N_h} & \text{if } h=1 \\ (1-\sigma_s)\cdot V_{p,h-1} + \mathrm{V}^{max}\cdot\left[\left(\eta_s^+\cdot f_{u,t}^+ - \frac{1}{\eta_s^-}\cdot f_{u,t}^-\right)\cdot \mathrm{d}_t\right]_{t=(p-1)\times N_h+h-1} & \text{otherwise} \end{cases}$$
$$\forall\ p \in \mathbf{P}, \forall\ h = 1..N_h, \forall\ u \in \mathbf{TS} \quad (3.2)$$

where:

- $V_{p,h}$, expressed in [m^3], represents the state of charge of the storage during the hour h of the typical period p;
- V^{max} is the storage volume in [m^3];
- **TS** groups the thermal storage utilities (one for charging and one for discharging);
- σ_s is the self discharge rate;
- $\eta_s^{+/-}$ are the charging and discharging efficiencies;
- $f_{u,t}^{+/-}$ stand for the charging and discharging rates, expressed as a percentage of the maximum volume.

In each hour the state of charge of the storage cannot exceed its volume, as expressed by Eq. 3.3.

$$V_{p,h} \leq \mathrm{V}^{max} \qquad \forall\ p \in \mathbf{P}, \forall\ h = 1..N_h \quad (3.3)$$

Values of parameters can be found in Section C.1.3. Since the storage is included with the aim of taking into account the thermal capacity of the network and coping with the uncertainty in the definition of cooling and heating profiles, only the operation of the storage is subject to optimization. Therefore, the unit binary activation y_u, as well as upper and lower bound of the multiplication factor ($\mathrm{F}^{\mathrm{max}}$ and $\mathrm{F}^{\mathrm{min}}$) are all set to 1.

3.4.5 Model superstructure

To better visualize the complex model superstructure, a generic location and that devoted to the installation of the central heating station are represented in 3.3.

Each light grey box represents a unit, with the corresponding streams, depicted in dark grey boxes: thermal cold streams, thermal hot streams and electricity streams are represented with a blue, red and black contour, respectively. Each white parallelogram represents a layer: colorful contours indicate heat cascade layers, while black contour the electricity layer. The grey rhombuses in the bottom represent different networks, the two HNs (the existing and the new potential one) and the AN. Potential exchanges of mass or energy are represented by arrows: the direction of the arrow indicates the direction of the exchange. Solid colored arrows indicate heat streams and their associated layer. A solid arrow incoming to a stream (grey boxes) means that the stream receives heat, while an outgoing one means that the stream supply heat. It can be noticed that cold streams receive heat while hot ones supply it. Heat balances are closed in each layer at the location level, through the heat cascade equation reported in Eq. 2.5 which ensure the feasibility of the heat exchanges. In each heat cascade layer the heat balances are solved such as to respect the second law of thermodynamics, therefore streams can exchange heat only if their temperature levels allow the exchange. Dashed lines correspond to resource flows. Opposite to the heat balances, resource balances are closed at the system level. This choice is due to the fact that the electricity grid is considered already existing and its layout is not optimized. Last, dotted lines correspond to mass flows, with the arrow indicating the direction of the flow in the feeding line. As previously mentioned and reported in Eqs. 2.19 and 2.20 two parallel mass balances are solved: one for the flow assumed at the network supply and return temperatures, and another for the flow feeding the evaporators of decentralized HPs and CHIs, for which a fixed ΔT independent from that of the network is assumed. As visible from the scheme in Fig. 3.3, network hot utilities are responsible for "converting" the mass flow into available heat at the location level, while network cold utilities do the opposite.

In the following, an exemplary interpretation of Fig. 3.3 is provided. Considering the CHIs in the generic location, the compressor of the CHI is linked to the electricity layer, while the evaporator to two heat cascades: *Evap HC* and *Cold HC*. The former is used to supply the evaporator through the hot utility of the AN, while the latter to satisfy the building's cooling requirements. Since the hot utilities of HNs are connected to the same heat cascade *Evap HC*, they could eventually be used to supply the evaporators of the CHIs. However, in this case the heat cascade constraint forbids the exchange due to the respective operating temperatures, non compliant with the second law of thermodynamics. The condenser of the CHI may be cooled down by the ambient air (layer *Chiller HC*) or reject the heat into the HNs (layer *Network HC*) to make it available in another locations or at the central location to supply the evaporator of the single stage HP.

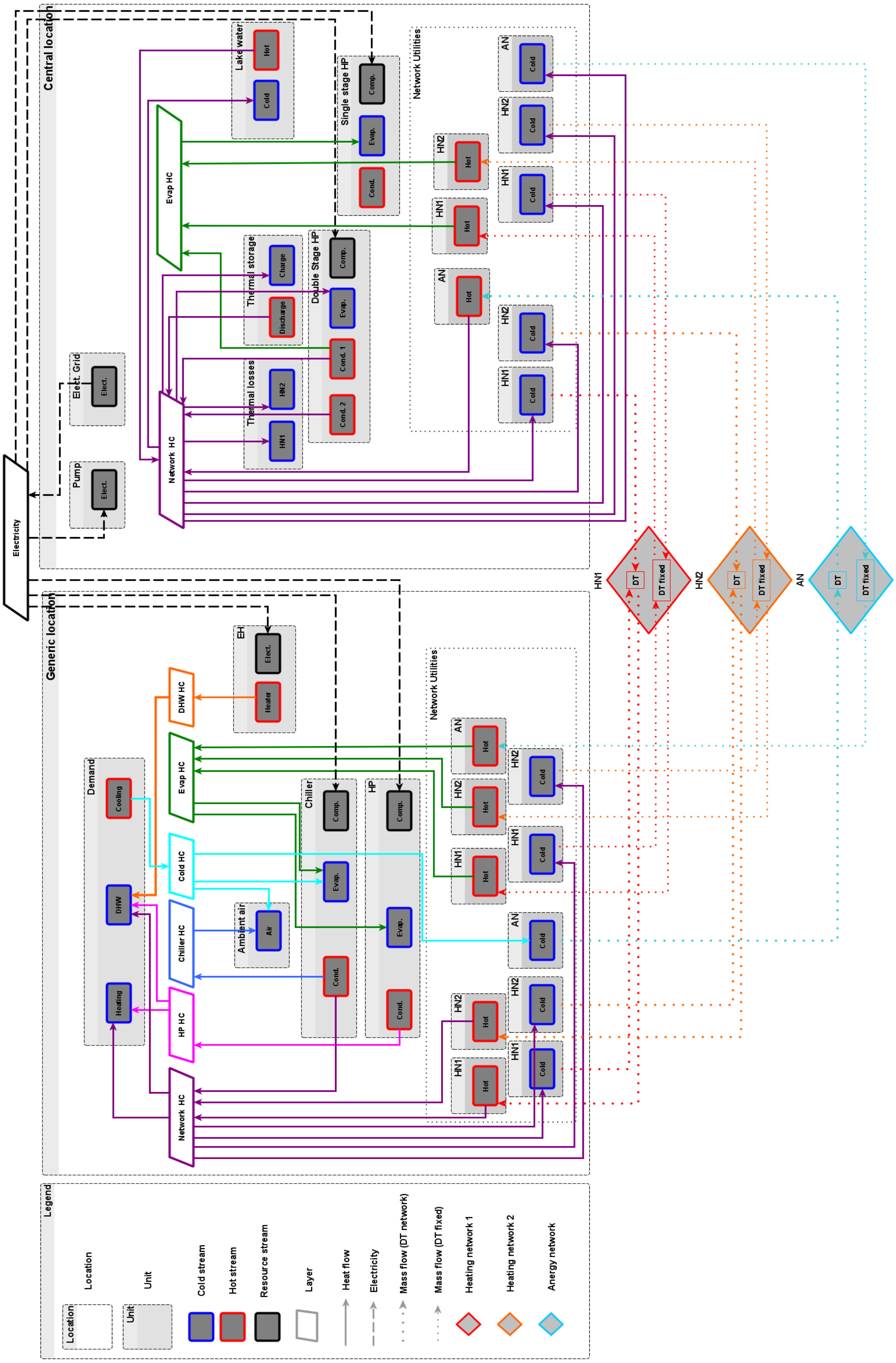

Figure 3.3: Model schematic representation

3.5 Problem solving strategy

To reduce the problem size and therefore the computational time, the solving strategy relies into a decomposition in two levels. At the upper level, also defined master, an heuristic optimization, performed by the multi-objective genetic algorithm of the software Dakota [96] defines the existence, operating temperatures and diameter of each network. At each iteration this information becomes an input to the lower (or slave) level optimization, performed by the solver CPLEX [80], which defines the best utility integration. The scope of the optimization framework is to generate a set of system designs, among which interesting options can be further analyzed and compared. The variables optimized by the genetic algorithm are reported in Table 3.2 together with the corresponding lower and upper bounds, whereas Table 3.3 lists the variables optimized at the slave level and their associated type.

Table 3.2: Variables of the master level optimization.

Var	L_b	U_b	Unit	Description
$\mathbf{T^f_{HN1}}$	40	80	°C	Design temperature of the existing HN
$\mathbf{DT_{HN1}}$	4	10	°C	ΔT of the existing HN (at design)
$\mathbf{DT^f_{HN1/HN2}}$	-5	4	-	The design temperature of the new HN is calculated as $T^f_{HN2} = T^f_{HN1} + 10 \cdot \Delta T^f_{HN1/HN2}$
$\mathbf{DT_{HN2}}$	4	10	°C	ΔT of the new HN (at design)
$\mathbf{DN_{HN2}}$	1	3	-	Integer to choose the diameter of the new HN within the set [DN300, DN500, DN600]
$\mathbf{DN_{AN}}$	0	4	-	Integer to choose the diameter of the AN (if installed $DN_{HN2} \geq 1$) within the set [DN250, DN300, DN500, DN600]

Every iteration of the heuristic optimization, with the definition of an individual, determines the variables listed in Table 3.2. Consequently, the networks choice, operating temperature and diameter serve as inputs to the slave optimization. Hence, the corresponding binaries (y_n, $y_{n,T_n^{f/r}}$, and $y_{n,dn}$) become parameters, drastically reducing the MILP superstructure and problem size.

The objective function is the simultaneous minimization of CAPEX (see Eq. 2.44) and OPEX. To the previous definition of OPEX, an additional term, taking into account the maintenance cost of equipment, is added, as reported in Eq. 3.4.

$$OPEX = \sum_t \left[\sum_u \mathrm{C}_u^{op} \cdot f_{u,t} \cdot \mathrm{f}_t \cdot \mathrm{d}_t \right] + \sum_u \mathrm{C}_u^m \cdot y_u \tag{3.4}$$

The cost parameter C_u^m defines for each unit a fixed cost per year devoted to the maintenance of the equipment. It is assumed that once a machine is installed it is also operated. This component is useful when no information about the maintenance cost correlated to the level of usage of the machine is available. Parameters used are a result of discussions with experts

Table 3.3: Variables of the slave level optimization.

Var	Type	Unit	Description
$\mathbf{y_{lc_1,lc_2,n}}$	binary	-	Choice of installing network n between locations lc_1 and lc_2
$\mathbf{y_u}$	binary	-	Utilities investment decision
$\mathbf{f_u}$	continuous	-	Utilities installed capacity
$\mathbf{f_{u,t}}$	continuous	-	Utilities operating load for each time step t
$\mathbf{f_{s,ly,t}}$	continuous	-	Streams multiplication factor for the layer ly and time step t
$\mathbf{y_{c^{c/e}}}$	binary	-	couple activation for HPs and CHIs
$\mathbf{\dot{R}_{ly,k,lc,t}}$	continuous	kW	Heat cascaded in the location lc and layer ly from the interval k to the lower temperature ones during the time step t
$\mathbf{\dot{M}^{+/-}_{u,ly,t}}$	continuous	kW	Input/output contribution of unit u to the layer ly during the time step t
$\mathbf{\dot{m}_{lc_1,lc_2,n,T_n^{f/r},dn,t}}$	continuous	kg/s	Mass flow rate flowing between the locations lc_1 and lc_2 in the network pipe of type n and diameter dn, at the supply/return temperatures defined by the couple $T_n^{f/r}$, during the time step t
$\mathbf{\dot{m}^{c}_{lc_1,lc_2,n,T_n^{f/r},dn,t}}$	continuous	kg/s	Mass flow rate for cooling purposes with dependencies as the previous
$\mathbf{\dot{m}^{hp}_{lc_1,lc_2,n,T_n^{f/r},dn,t}}$	continuous	kg/s	Mass flow rate to feed evaporators of HPs and CHIs, with dependencies as the previous except that the return temperature is fixed
$\mathbf{V_t}$	continuous	m^3	State of charge of the storage during the time step t

in the field, here omitted for confidentiality clauses. The two objectives are simultaneously minimized by the multi-objective master level and combined into the overall system TOTEX for the single-objective slave optimization.

In order to reduce the computational effort, the networks investment cost is not considered in the objective function of the slave optimization, with the consequence that the network layout is not optimized. Therefore, the feedback given to the heuristic optimization in this regard represents only an upper bound of the investment cost of the optimized layout. However, to assess the potential benefit of the network layout optimization and its effect on the objective function, the most interesting solutions have been re-optimized considering the network cost (results of this analysis are shown in Section 3.6.2). Consequently an alternative solving strategy, based on an improved feedback to the master optimization, is proposed (details in Section 3.6.5).

3.6 Results

3.6.1 Definition of a reference case

To ease the comparison among different solutions and to normalize results for the sake of confidentiality, a reference case is first introduced. The latter represents the expansion of the current situation to satisfy the demand estimated for the year 2030, implying the connection of new buildings. It is assumed that the current oil BOIs, at the end of their life time, are replaced with those fed by natural gas. The resulting system design of the reference case relies on a high temperature HN, using fossil-fired BOIs and CHIs to cover the cooling demand. Due to maximum flow constraints, the current pipe diameter would not be large enough to supply the increased demand. However, with the aim of only estimating a reference scenario, this aspect is neglected. The resulting annualized cost is dominated by the operating expenses due to the consumption of natural gas and electricity. All the economic results presented in this chapter are shown normalized to the TOTEX of this reference system configuration.

3.6.2 Identification of the Pareto frontier

A multi-objective optimization never suggests one optimal solution but rather a set of options, all optimal with respect to the two objectives (i.e., CAPEX and OPEX). These non-dominated solutions constitute the Pareto frontier. Moving away from a solution on the Pareto frontier, any other solution which itself does not lie on the frontier, would deteriorate at least one of the two objectives without improving the other. Figure 3.4 shows all the solutions and highlights those laying on the Pareto frontier.

Table 3.4 lists for all the solutions on the Pareto frontier and for the fully decentralized configuration (which is not on the frontier, but still considered as an interesting option) the network temperatures, pipes diameters, TOTEX and investment decisions. The fully decentralized solution reflects the configuration with the solely AN installed in combination with decentralized HPs, generated by simply imposing the activation of the AN and forbidding the use of the HNs ($y_{AN} = 1,\ y_{HN1} = 0,\ y_{HN2} = 0$).

All the solutions belonging to the Pareto frontier either present the two HN at high temperature (70°C) or the existing HN at high temperature and the new at a medium level (50°C). The best solutions show normalized TOTEX lower than 1 meaning that all configurations result less expensive with respect to the reference case. Moreover, it can be noticed how the variation of the OPEX is marginal with respect to that of the CAPEX.

3.6.3 Network layout optimization

The solutions on the Pareto frontier and the fully decentralized configuration are further analyzed to assess the effect of the network layout optimization, neglected in a first step. All configurations are re-optimized by keeping the variables defined at the master level fixed

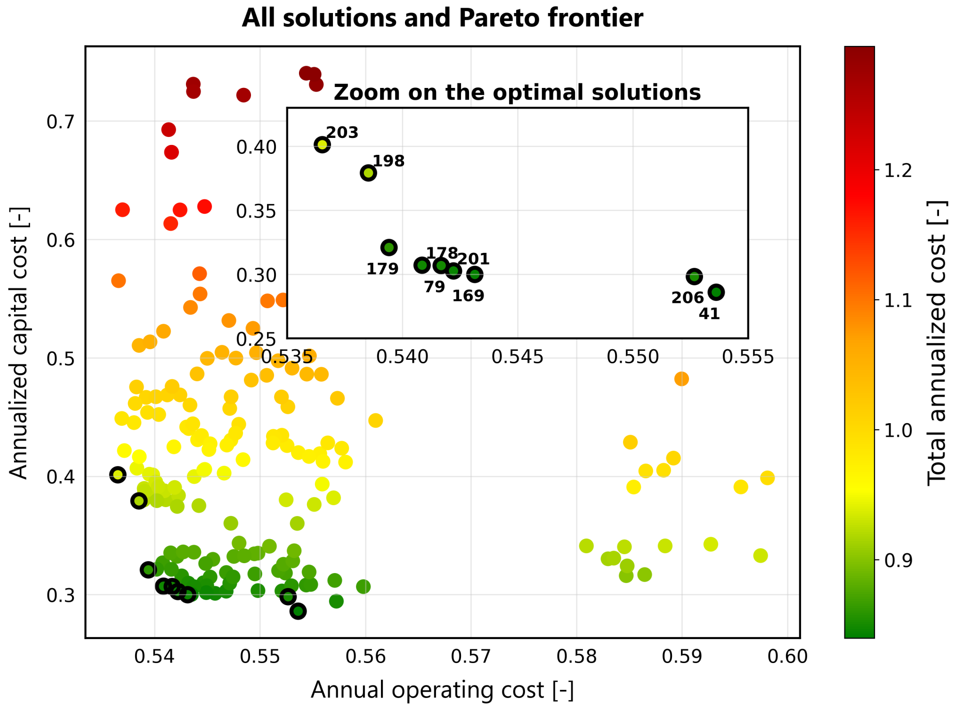

Figure 3.4: All solutions in the OPEX-CAPEX domain and highlighted Pareto frontier. TOTEX in colormap. Values normalized with respect to the TOTEX of the reference case.

Table 3.4: Solutions on the Pareto frontier and fully decentralized configuration. TOTEX normalized with respect to the one of reference case and installed capacity (all expressed as heat rejected at the condenser) with respect to peak heating demand.

Nr.†	Id.†	TF1⋆	TF2⋆	DN HN⋆	DN AN⋆	TOTEX⋆	HP CT⋆	HPs Dec.⋆	CHIs⋆
[#]	[#]	[°C]	[°C]	[mm]	[mm]	[-]	[MWth]	[MWth]	[MWth]
41	1	70	70	500	250	0.840	0.769	0.256	0.250
79	2	69	49	300	300	0.849	0.468	0.372	0.199
169	3	69	49	300	250	0.843	0.526	0.372	0.250
178	4	70	50	300	300	0.848	0.481	0.321	0.199
179	5	70	50	300	600	0.860	0.333	0.321	0
198	6	69	49	500	250	0.918	0.526	0.327	0.250
201	7	70	50	300	250	0.845	0.538	0.308	0.269
203	8	70	50	300	600	0.863	0.558	0.327	0.122
206	9	70	70	500	300	0.851	0.769	0.256	0.199
-	10	-	-	-	500	0.991	0	0.769	0

† Column “Nr.” refers to the numbers in Fig. 3.4, while column “Id.” will be used later as solution identification.
⋆ TF1: network HN1 feeding temperature (at design conditions), TF2: network HN2 feeding temperature (at design conditions), DN HN: diameter of network HN2, DN AN: diameter of AN, TOTEX: total annualized cost, HP CT: central heat pump, HPs Dec.: decentralized heat pumps (summed), CHIs: chillers.

and performing the slave level optimization including the networks investment cost in the objective function. Figure 3.5 shows how the solutions move in the OPEX-CAPEX domain once the network layout is optimized.

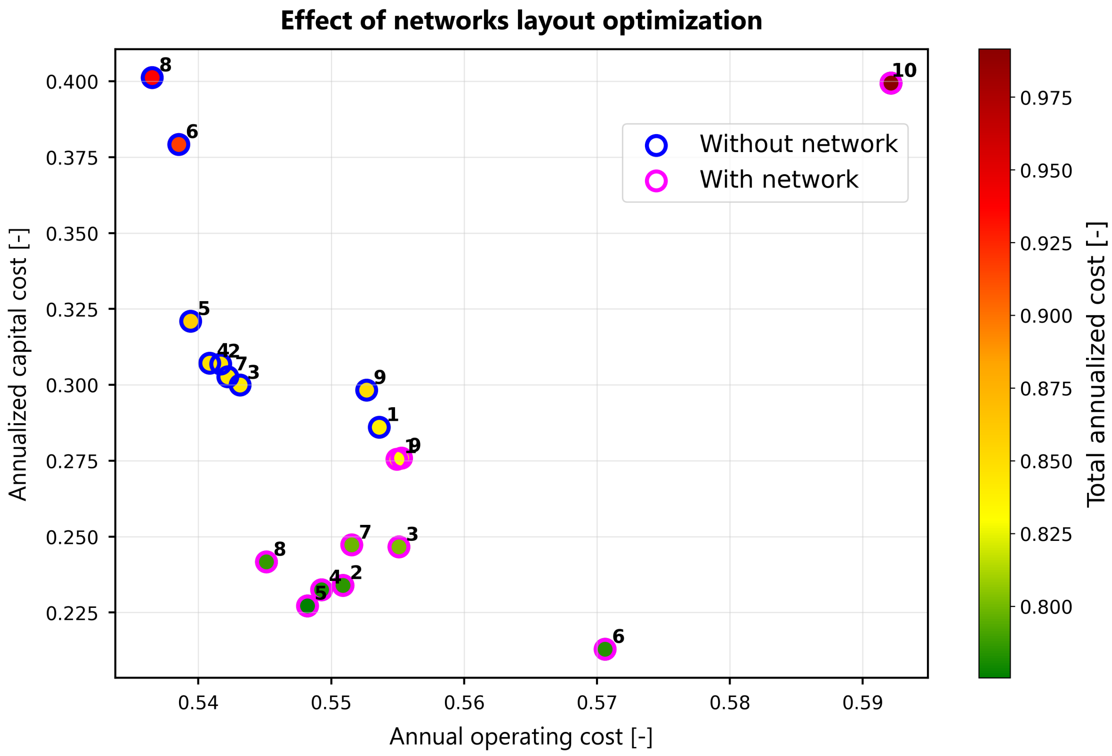

Figure 3.5: Effect of the networks layout optimization on the Pareto optimal solutions in the OPEX-CAPEX domain. "Without network": network cost not included in the objective function (values tend to the upper bound), "With network": network cost included in the objective function. Values normalized with respect to the TOTEX of the reference solution.

Figure 3.5 highlights that the TOTEX of all of the solutions decreases, as expected, after optimizing the network layout. The fully decentralized solution, equipped with the AN is not affected by the layout optimization, since the network needs to connect all the locations due to the fact that standalone options are not allowed. Moreover, among the solutions on the Pareto frontiers only three of them remain non-dominated (solution 5, 6 and 8, where identifiers refer to the column “Id.” of Table 3.4). Therefore, a deeper investigation on the investment decisions is performed to analyse if including the networks investment cost in the objective function would drive the optimizer to choose different investment decisions. Figure 3.6 shows the installed capacity of the conversion units without and with network layout optimization.

In a nutshell, the optimization of the network layout results in the decision of shortening the networks, which implies larger investment in conversion technologies. The savings related to the optimization of the AN layout are for most of the solutions around 70% (except for solution 3 and 7 showing 60 and 40% reductions, respectively). Regarding the HN, savings depend on the operating temperatures of the two networks: no savings are registered in case the two

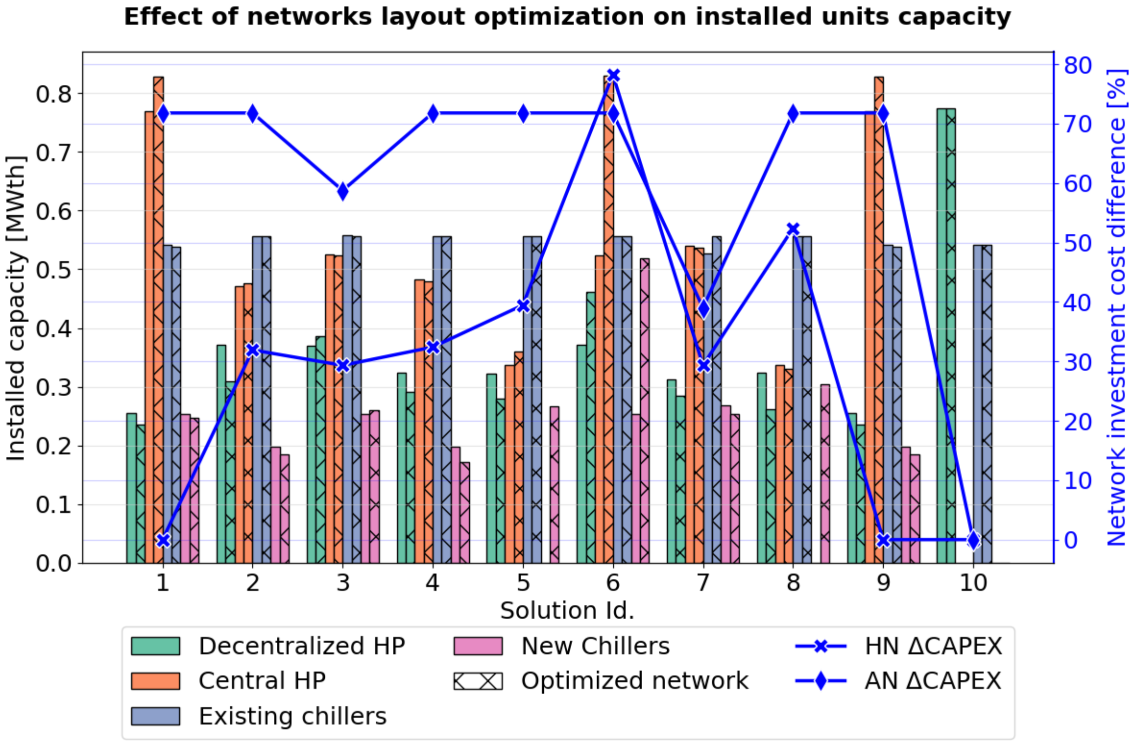

Figure 3.6: Effect of the networks layout optimization on technologies investment decisions for the Pareto-optimal solutions in the OPEX-CAPEX domain. Network Δ CAPEX calculated as relative savings with respect to the not optimized layout. Values normalized with respect to the heating peak demand. Capacity referred to the heat rejected at the condenser.

networks are operated at high temperature, while from 30 to 80% of the original cost can be saved if the two networks deliver water at high and medium temperatures. As previously mentioned, for the fully decentralized configuration (solution 10 in Fig. 3.6), the optimization of the network layout does not effect the investment decision, the reason being that in this option the network is already present everywhere and could not be further shortened.

3.6.4 Definition of the most interesting solutions

After the optimization of the network layout only three of the original non-dominated solutions still belong to the Pareto frontier: solutions 5, 6 and 8. Solution 5 and 8 appears very similar, since they show the same networks temperatures, similar installed capacity and were proven to have similar energy and cost breakdown. Therefore, in the following sections, only solution 5 is shown as representative of the two. In combination with solutions 5 and 6, the option characterized by the two networks at high temperature (solution 1) and the fully decentralized configuration (solution 10), considered interesting even if dominated, are also investigated in more details.

Annual cost breakdown

Figure 3.7 shows the breakdown of the total cost for the most interesting solutions identified in the previous section. All the figures show the results generated including the networks investment cost in the objective function and are normalized with respect to the TOTEX of the reference solution.

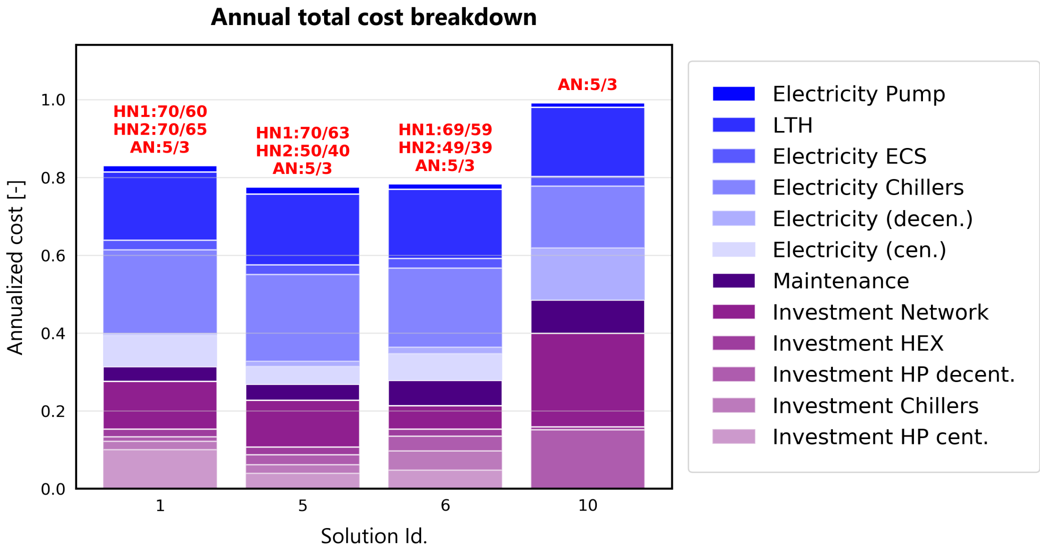

Figure 3.7: TOTEX breakdown of the solutions identified as interesting including the optimization of the networks layout. Values normalized with respect to the TOTEX of the reference configuration. Networks supply and return temperatures at design conditions also detailed on top of each bar.

Table 3.5 lists for each of the solutions shown in Fig. 3.7 the percentages of the TOTEX devoted to CAPEX and OPEX and for each of the two components the breakdown in the main contributions.

Table 3.5: Cost breakdown for solutions identified as interesting.

Solution		**1**	**5**	**6**	**10**
CAPEX	Network*	44	53	28	60
	Equipment*	56	47	72	40
	Total†	33	29	27	40
OPEX	Electricity§	61	59	58	56
	LTH§	32	33	31	30
	Maintenance§	7	8	11	14
	Total†	67	71	73	60

* Percentage of CAPEX
§ Percentage of OPEX
† Percentage of TOTEX

In all the solutions the main contributor to the TOTEX is the OPEX, covering from 60 to 73%. The allocation of the OPEX highlights a significant electricity consumption, responsible for around 60% of the operating expenses and mainly devoted to the use of the central plant, the decentralized HPs and CHIs, whereas minor shares are covered by back-up ELHs for the coverage of DHW and the circulating pump. The purchase of LTH contributes to around 30% of the OPEX, with minor variation among the different solutions. Cost due to equipment maintenance ranges from 7 to 14%, increasing with the degree of decentralization. This trend is due to the linear dependence of this cost component on the number of units installed.

In terms of CAPEX, solutions show a different distribution between the shares devoted to the installation of conversion technologies and to the networks. At first glance, solution 5 and 6 seem similar, both characterized by the two HNs operated at high and medium temperatures and a similar share of CAPEX and OPEX over the total. However, solution 6 with respect to solution 5, shows a significantly higher share of investment devoted to the equipment installation rather than to the networks. On the other hand, the greatest share for the networks investment is registered by the fully decentralized configuration (solution 10).

Resources breakdown

Figure 3.8 shows the breakdown of the resources used to supply respectively the heating (on the left) and the cooling (on the right) demand.

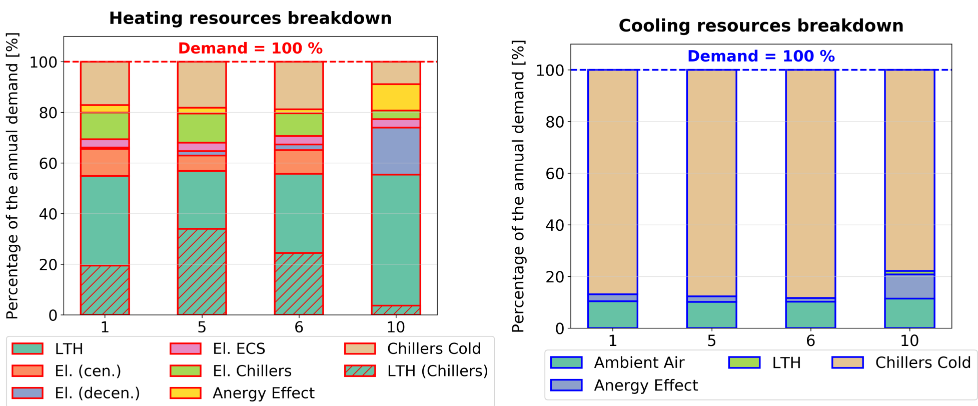

Figure 3.8: Energy breakdowns of resources employed to supply the heating (on the left) and the cooling (on the right) demand.

In heating mode the most exploited resource is the LTH, with a total annual consumption corresponding to 55% of the total demand. The LTH is partially used to supply the evaporator of HPs (the central HP in solution 1, 5 and 6 and decentralized ones in solution 10), whereas the rest provides heat to the evaporators of the CHIs (this portion is highlighted in Fig. 3.8 as *LTH (Chillers)*). The CHIs contribute to the heat demand either by working as HPs (i.e., with the evaporator supplied by the AN), or by simultaneously supplying the cooling requirements

(*Chillers Cold*) and recovering the heat at the condenser. Overall, these machines supply 47%, 64%, 52% and 16% of the total demand for solutions 1, 5, 6 and 10, respectively. These values are given by the sum of the energy at the evaporator (*LTH (Chillers)* and *Chillers Cold*) and the electricity required during this operation (*El. Chillers*). The heat recovered at the condensers of the CHIs while simultaneously supplying cooling demand can contribute up to the 25% of the total needs. The anergy effect allows to save in terms of LTH from 1.5 to 10% of the total heat demand (the total savings are doubled since the same amount should be purchased to supply the cooling requirements). ELHs, employed as back-up units for DHW, contribute to 3% of the total demand. The remaining portion (from 33 to 80%) is covered by the HPs, mainly the central plant in solution 1, the decentralized machines in solution 10 and a combination of the two in the other configurations.

Cooling requirements are almost entirely covered by CHIs, which supply from 78 to 88% of the total demand. Only a small percentage is supplied by the free-cooling with ambient air (around 10%) and by exploiting the anergy effect (from 1.5 to 10%). The use of direct cooling with LTH is not exploited (only 1.4% of the demand is covered by this operation in solution 10). The reason of this result is that under the assumed energy tariffs, the CHIs appear more economical than the direct cooling. Further considerations about the minor exploitation of direct cooling and its potential are reported in the following paragraph "The supply of cooling requirements".

Distribution networks

In all solutions, the existing infrastructure characterized by pipes DN250, can be exploited to distribute the heat from the central heating station. In addition, a new HN can be installed, as well as an AN to distribute the LTH. From the previous analyses, the best option in terms of TOTEX appears to operate the existing network at high temperature (around 70°C) and to install a new one to deliver the heat at a temperature around 20°C lower. In this way, the heat rejected by the CHIs can be valorized. Figures 3.9 and 3.10 show respectively the networks configurations for solution 5 and 6, both characterized by the two HNs operated at high and medium temperature respectively, but defined by different investment decisions.

The newly installed HN, HN2, is always exploited to connect the new buildings. An example is the connection between the substations 1 and 2 not existing nowadays. The optimal extension of this networks depends on its diameter. Smaller tubes as in the case of solution 5 enables a deeper expansion, since, given the reduced piping cost, a longer distance can be covered with the same investment. The discontinuity of the medium temperature network can also be noticed in Fig. 3.10, suggesting that the portion disconnected by the central station are fed by the heat recovery from the CHIs. The AN is installed only in the proximity of the central station to connect the first substation which is characterized by a relevant cooling demand. The short distance covered by the AN explains the minor exploitation of the direct cooling previously highlighted. The reason is the economic advantage of using the CHIs with respect to the LTH. Further studies on the topic are reported in the following paragraph.

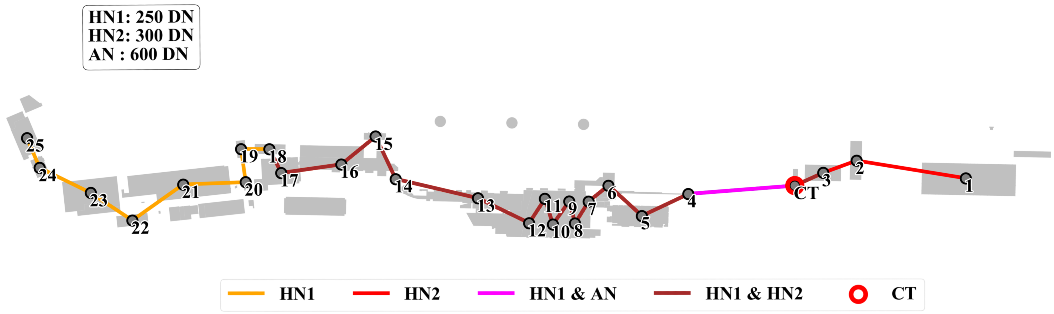

Figure 3.9: Networks topology of solution 5.

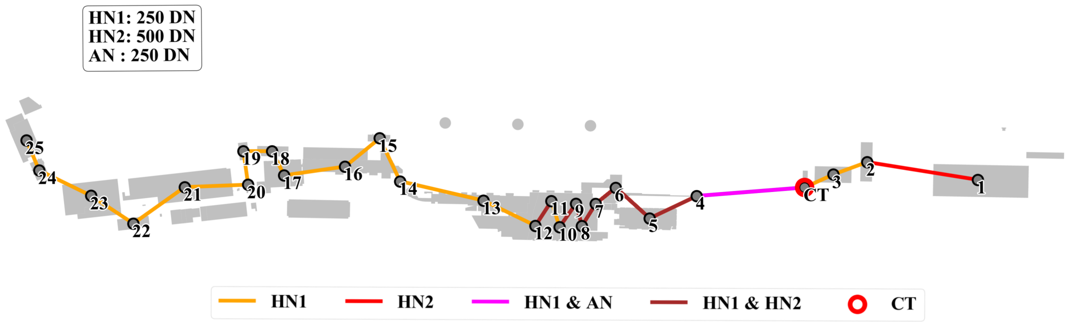

Figure 3.10: Networks topology of solution 6.

The supply of cooling requirements

As visible in Fig. 3.8 the cooling demand is almost entirely covered by the CHIs (around 80%). About 10% of the demand is covered by free-cooling with ambient air and only a minor portion (from 0 to 1.4%) by direct cooling through the AN. The remaining is supplied by exploiting the anergy effect. To better understand the reasons behind these results, the options to satisfy the cooling demand are here listed and compared.

In winter and mid-seasons, to exploit synergies between heating and cooling requirements one possibility is to recover the heat rejected at the condensers of the CHIs. The heat recovered can then be used directly to satisfy the demand of the substation or, if the network temperature level allows it, delivered to other locations by the network. Another option is to exploit the anergy effect: the heat rejected into the AN by the consumers of direct cooling can be valorized and used at the central station to supply the evaporator of the HP. This second operation would be economical with respect to the previous one if $COP_{CHI} < COP_{HP} + 1$ (excluding the network losses).

In summer, the cooling demand can be covered by direct cooling or by the CHIs, whose condenser, in absence of heating demand would reject the heat into the environment. In this case the most economical option depends on the LTH tariff and the cost of the electricity. Under the assumptions made, the CHIs are more economical whenever their COP is greater than 2.3. The latter condition is satisfied if the ambient temperature is lower than 36°C. Naturally, this is only valid for the assumptions made on the machines Carnot factor and the required temperature level of the cooling demand.

Even if the use of direct cooling is not economically viable under the assumptions made, it is still the recommended option, in case the heat rejected to the environment is to be reduced or if the cooling tower must be dismantled. If direct cooling is used to supply the total cooling demand, the following aspects should be taken into account:

- The temperature of the AN should be low enough to be able to supply the cooling demand. If the LTH is too warm in summer, one option is to renovate the space cooling technologies, by increasing the heat exchange surfaces. Another possibility is to reduce the temperature of the source to the required needs by connecting the condenser of the CHIs to the network.
- The diameter of the network and its ΔT have to be large enough to ensure the supply of the peak power while respecting the maximum flow constraint.

To better study the opportunity of supplying the cooling demand via direct cooling, the four solutions previously identified (solutions 1, 5, 6 and 10 with identifiers referring to the column "Id." in Table 3.4) are post-processed. The new operation implies the replacement of the CHIs, when rejecting the heat into the environment, with direct cooling. The operation of the CHIs while recovering the heat at the condenser is considered unchanged.

The cooling demand for this analysis is supposed to be at the temperature required by the ventilation units (i.e., the lowest temperature, since the radiant panels are supposed operated at a temperature 3°C higher). Two different scenarios are studied:

1. "Direct cooling + Chillers": the temperature of the AN corresponds to the values assumed and it is therefore not able to cover the whole cooling demand.
2. "Direct cooling": the temperature of the AN is supposed to be low enough to cover the total cooling demand[1].

In both the scenarios, in winter and mid-seasons, the AN temperature is cold enough to entirely satisfy the cooling demand, whereas in the first scenario the CHIs must be used to cool down the AN until the required needs during the summer.

[1]This second scenario is investigated because the temperature assigned to the LTH during summer represent an extreme value and it is likely to be encountered in very limited situations.

For each of the four solutions, the new operation is compared to the original results of the optimization. Focus is thereby given to annual cost for investment and the purchase of electricity and LTH. Potential changes in optimum installed capacity of the CHIs and consequent variation of their investment cost are neglected. Results are presented in Fig. 3.11.

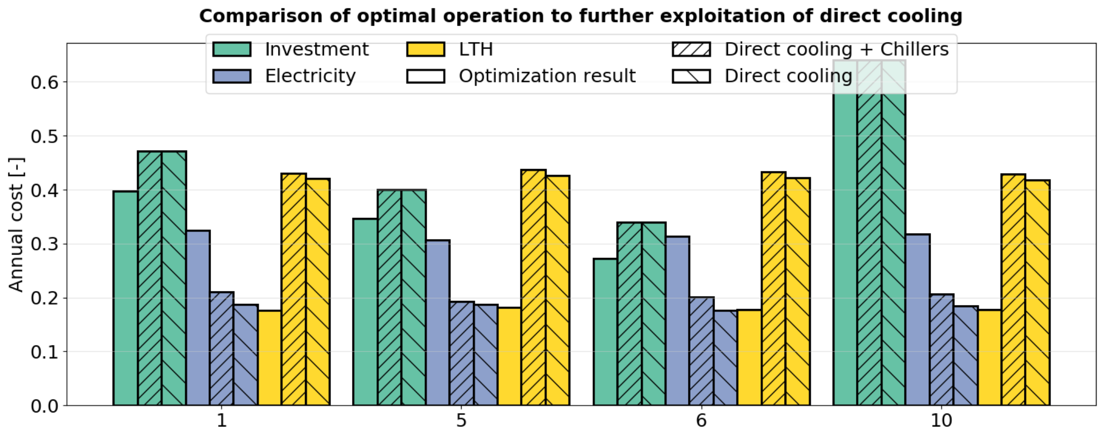

Figure 3.11: Comparison of economic performance indicators for three different operations in cooling mode: original results from the optimization process, the combination of direct cooling and chillers, and only direct cooling.

The new investment is due to the purchase of the pipelines to expand the AN until the substation needing cooling requirements and located the furthest from the central plant. The amount of electricity is reduced due to the replacement of the CHIs with direct cooling, whereas the purchase of the LTH is increased for the same reason. If the temperature of the source is not cold enough to supply the demand, a greater amount of LTH is used with respect to the operation fully relying on direct cooling. The reason is that to decreased the temperature of the source to the required needs, the LTH cannot be used directly, but it is employed at the condenser of the CHIs, whose evaporator supplies the demand. Therefore, the difference is the amount of electricity used by the CHIs during this operation. The cost of the LTH that would make the use of direct cooling economically equivalent to the cheapest solution (solution 5 under the original operation) is estimated to be around 40% lower than the current tariff. In this situation, the configuration of solution 6 operated in direct cooling mode would achieve the same total cost of solution 5 relying on the CHIs connected to ambient air to cover the cooling requirements.

In conclusion, the direct cooling is not exploited because the cost of the LTH assumed is too high. Moreover, due to high investment cost of the network pipes, only a negative cost of such a resource would make the fully decentralized solution (solution 10) economical. Therefore, such configuration would need incentives to appear cost-competitive. However, this option corresponds to the lowest electricity consumption. The cost of the pipelines could be drastically reduced with the use of a pressurized refrigerant at the place of the water. Refrigerant based network have been largely investigated by Henchoz [22] and Suciu [23].

3.6.5 Improved problem decomposition

To reduce the computational time, the original set of solutions (showed in Fig. 3.4) is achieved by neglecting the network layout optimization during the slave level optimization. As a result the solver of the MILP sets the variables related to the network connections to their upper bound. Therefore, the feedback given to the upper level optimization about the networks investment cost represents an overestimation with respect to the one of an optimized layout. To investigate the effect of networks layout optimization the solutions on the Pareto are re-optimized including the network cost in the objective function. The results (discussed in Section 3.6.3) showed that including the network layout optimization shifts the investment decisions towards the units installations, since optimized configurations tend to shorten the connections and invest more in decentralized units. Most of the solutions previously belonging to the Pareto frontier now appear dominated pushing the best network design to clearly one layout at high temperature (around 70°C) and the another at around 50°C.

To make sure that the solution space is fairly investigated during the first optimization and that interesting solutions are not missed due to poor feedback about the networks investment cost, an advanced solving strategy is implemented. In this scheme, a new variable is optimized by the heuristic optimization, representing an upper bound for the networks investment cost (ϵ_n) during the resolution of the MILP, as reported in Eq. 3.5. The objective functions are not modified.

$$\sum_{n \in \mathbf{N}} C_n \leq \epsilon_n \tag{3.5}$$

C_n represents the networks investment cost, calculated according to Eq. 2.46. Moreover, a longer computational time is allowed resulting in an higher number of iteration of the heuristic optimization. Figure 3.12 shows the solutions achieved with the new resolution strategy in the OPEX-CAPEX domain and highlights the configurations belonging to the Pareto frontier.

The comparison of Figs. 3.4 and 3.12 reveals that the non-dominated solutions, resulting from the two solving strategies, fall in the same range of operating and capital expenses. Table 3.6 lists all the solutions belonging to the new Pareto frontier, together with information on the networks temperatures, TOTEX and installed units capacity.

All the non-dominated solutions are characterized by one HN operated at high temperature (around 70°C) and a second one at medium temperature (i.e., around 20°C lower). This result agrees with the conclusion drawn from the solution of the previous solving strategy and their consequent analyses. Also the investigation of the cost and energy breakdowns is consistent with the previous one. The related figures are therefore here omitted and reported in Section C.2. In terms of computational time, the new solving strategy performs worse than the previous one, as visible from the comparison shown in Fig. 3.13.

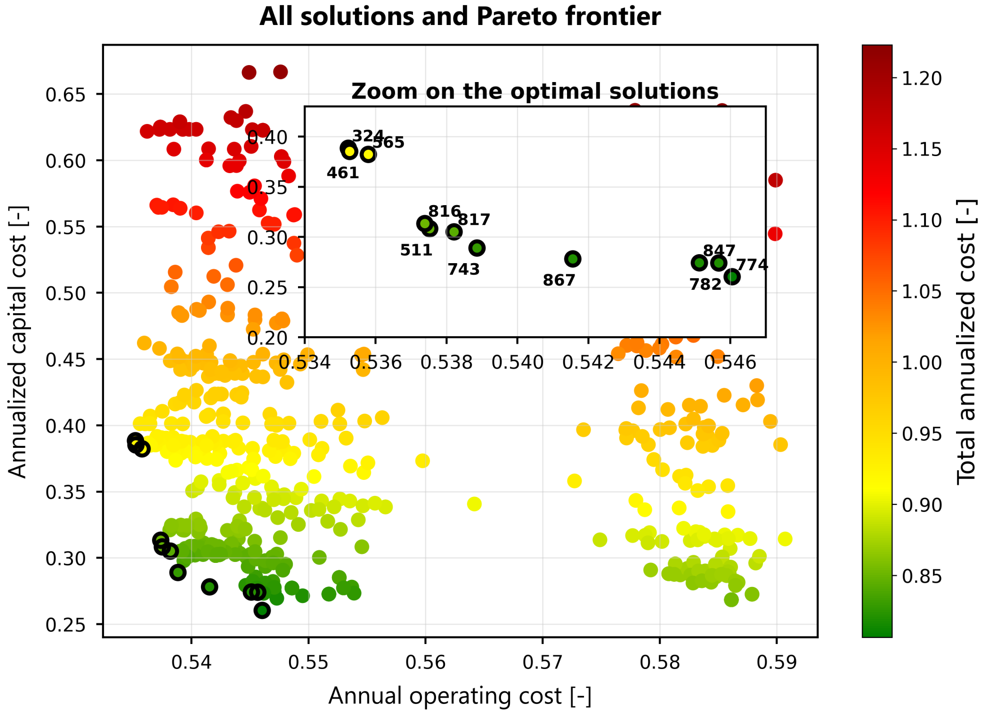

Figure 3.12: All solutions in the OPEX-CAPEX domain and highlighted Pareto frontier achieved with advanced solving strategy. TOTEX in colormap. Values normalized with respect to the TOTEX of the reference case.

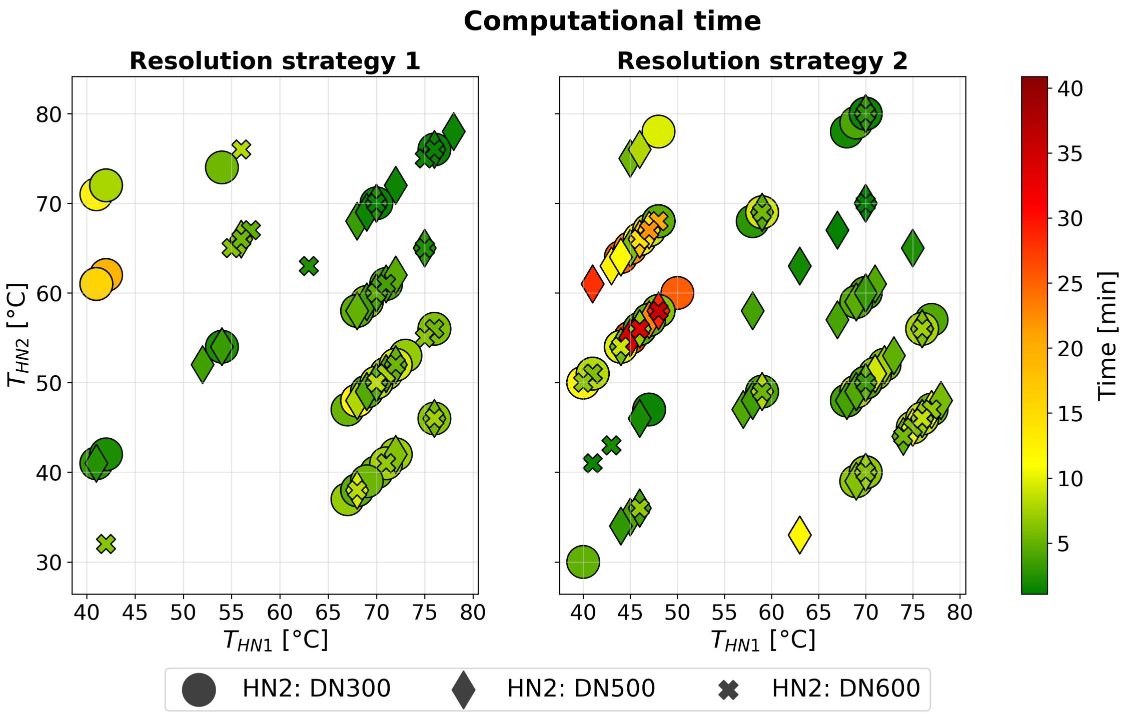

Figure 3.13: Comparison of the two solving strategies in terms of computational time. On the left results achieved without optimizing the networks investment cost upper bound, whereas results on the right include the latter as a variable at the master level.

Table 3.6: Solutions of the Pareto frontier achieved with advanced solving strategy. TOTEX normalized with respect to the one of the reference solution. Installed capacity, expressed as heat rejected at the condenser, normalized with respect to peak heating demand.

Nr.†	Id.†	TF1⋆	TF2⋆	DN HN⋆	DN AN⋆	TOTEX⋆	HP CT ⋆	HP Dec.⋆	CHIs⋆
[#]	[#]	[°C]	[°C]	[mm]	[mm]	[-]	[MWth]	[MWth]	[MWth]
324	11	70	50	500	500	0.924	0.329	0.323	0.037
461	12	70	50	500	500	0.920	0.337	0.321	0
511	13	70	50	300	500	0.846	0.330	0.318	0.050
565	14	70	50	300	300	0.850	0.491	0.233	0.205
743	15	70	50	300	500	0.828	0.289	0.311	0.095
774	16	46	66	300	500	0.806	0.289	0.399	0
782	17	47	67	300	500	0.820	0.320	0.316	0
816	18	70	50	300	300	0.851	0.493	0.231	0.233
817	19	70	50	300	500	0.843	0.338	0.336	0
847	20	46	66	300	500	0.819	0.313	0.308	0
867	21	48	68	300	2300	0.883	0.494	0.288	0.197

† Column "Nr." refers to the numbers in Fig. 3.12, while column "Id." is used in Figs. C.1b and C.2 as solution identification.
⋆ TF1: network HN1 feeding temperature (at design conditions), TF2: network HN2 feeding temperature (at design conditions), DN HN: diameter of network HN2, DN AN: diameter of AN, TOTEX: total annualized cost, HP CT: central heat pump, HPs Dec.: decentralized heat pumps (summed), CHIs: chillers.

Figure 3.13 shows also that in both cases, there is no link between the variables set by the heuristic and the computational time. The new resolution strategy demands the longest computational time for solutions which appear missing in the previous case, probably due to the lower number of computed individuals and the less effective feedback between the slave and the master optimization.

3.6.6 Definition of alternative scenarios

Three new scenarios are investigated to assess the robustness of the solutions proposed towards potential changes of the users' temperature requirements and of the LTH tariff. All the scenarios are listed in Table 3.7. Scenario 0 and 1 both represent the base case, the former relying on the original solving strategy and the latter referring to the advanced one, presented in the previous section. Scenario 2 and 3 implies the reduction of the most critical users' operating temperatures. As largely investigated in Section 1.4.4, the potentially oversized heat exchanges surfaces can be exploited to reduce the required supply temperatures. Such a result can be also obtained by the retrofit of the space conditioning technologies with consequent expansion of their surface. Later in this section the load curve of the users' operating temperatures after optimization of the heat curves are compared to the original one. Last, scenario 4 includes and increased LTH tariff.

Table 3.7: Scenarios.

Sol [id.]	Characteristics
0 - 0.5[a]	Base case resolution strategy 1
1 - 1.5[a]	Base case resolution strategy 2
2	First stage of buildings renovation [b]
3	Second stage of buildings renovation[c]
4	Increased tariff of the LTH of around the 60% of its original value

[a] Scenarios 0 and 1 both refer to the base case, including results obtained with the two resolution strategies mentioned in the above sections. 0.5 and 1.5 includes only the solutions belonging to the Pareto frontiers for the respective scenario.
[b] Reduction of the most critical users temperature: see Fig. 3.15a.
[c] Reduction of the temperature for the second most critical users (if present): see Fig. 3.15b.

To be able to visualize all the design configurations under different KPIs, all the solutions are reported on an online visualization tool. Section 3.6.7 gives more insight on this topic.

Users' operating temperature reduction

The two scenarios imply the reduction of the most critical users' operating temperatures. Values are the result of discussions with experts in the field. This effect can be obtained by exploiting the potential overcapacity of heat exchange surfaces or by retrofitting the space conditioning technologies. The original distribution of the users' temperature requirement is shown in Fig. 3.14. A generic (X,Y) point on the graph indicates that heat at a temperature of X°C can supply up to Y% of the annual energy heating demand.

Figure 3.15 shows the distribution of the user's temperature requirements after respectively the first (Figure 3.15a) and the second (Figure 3.15b) stage of users' temperature reduction. In each substation, only one user at the time can be tackled and priority is given to those requiring the highest temperature level.

3.6.7 Decision support tool

To visualize simultaneously all the solutions arising from the system optimization under the different scenarios, an online platform is developed based on parallel coordinates. The latter represent an effective method to explore a wide range of criteria and alternatives, while offering an intuitive and natural interactive way of specifying preferences [97]. Thanks to their flexibility they are employed in different fields of applications: for example, Schüler [98] relies on parallel coordinates as support for online optimization of planning strategy in urban districts, Wallerand [99] includes them in an online decision support tool for the optimal

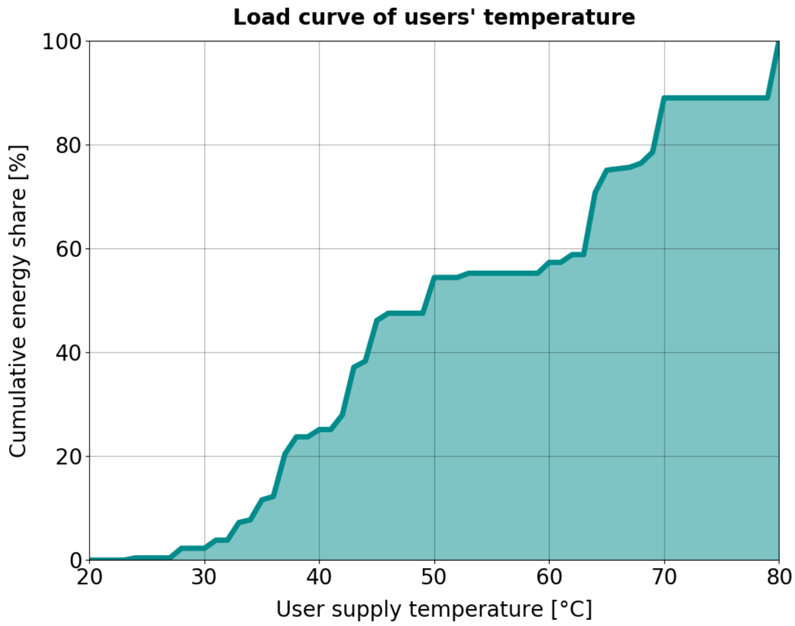

Figure 3.14: Load duration curve of users' temperature requirements.

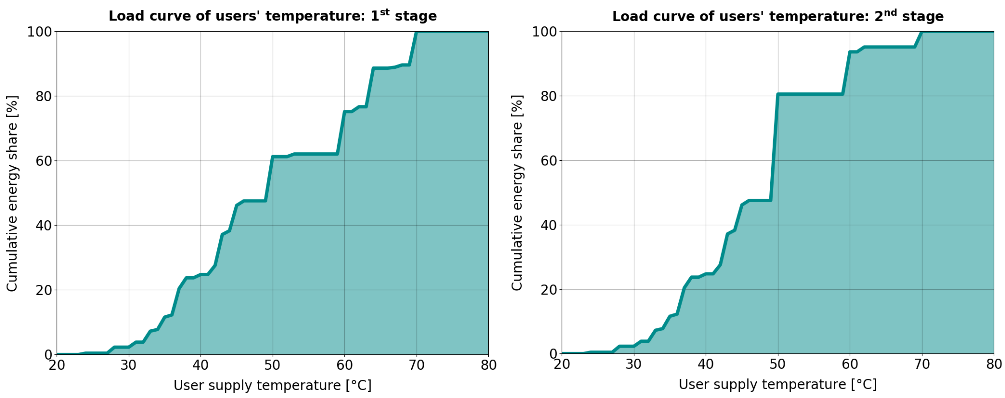

(a) 1st reduction stage (scenario 2)

(b) 2nd reduction stage (scenario 3)

Figure 3.15: Load duration curve of users' temperature requirements after the two temperatures reduction stages.

choice of refrigerant in industrial HPs and Stadler [54] employs them to visualize optimal solutions for the Swiss national building energy system design.

In this work parallel coordinates are used to visualize on a webpage both optimal and sub-optimal system design solutions relative to the different scenarios (listed in Table 3.7). The developed online platform allows the user to investigate different configurations over a wide range of KPIs. The user can easily specify ranges for these indicators, select/deselect the ones to visualize and assess a table where all the results are printed for each configuration. The tool is meant to assist the decisions making, offering the opportunity of investigating the full spectrum of solutions. Interesting configurations might be pointed out by the user, according to their preferences, and could be investigated further as done in the sections above for the ones belonging to the Pareto frontier of the base case scenario.

The following KPIs are chosen for the axes of the parallel coordinates. Due to the their large numbers, the indicators are grouped into different categories as reported in the list below:

- Summary:
  - **id.**: scenario identifier referring to Table 3.7
  - **TF1 [°C]**: supply design temperature of the existing HN
  - **TF2 [°C]**: supply design temperature of the new HN
  - **DN HN [mm]**: diameter of the new HN
  - **DN AN [mm]**: diameter of the AN
  - **totex [kCHF/y]**: total annual cost
  - **opex [kCHF/y]**: annual operating expenses
  - **capex [kCHF/y]**: annualized investment cost
  - **COP [-]**: global system COP, calculated, according to Eq. 3.6, as the ratio between the heat rejected to the environment (sum of the heating requirements, DHW demand and the heat rejected to the environment to cover the cooling needs, either by direct cooling with ambient air or through the CHIs) and the electricity consumption
- Conversion technology installation:
  - **HP CT [MW_{el}]**: total installed capacity of the central HP
  - **HP [MW_{el}]**: total installed capacity of the decentralized HPs
  - **CH new [MW_{el}]**: total installed capacity of the new CHIs
  - **HP CT [MW_{th}]**: total installed thermal capacity of the central HP
  - **HP [MW_{th}]**: total installed thermal capacity of the decentralized HPs
  - **CH new [MW_{th}]**: total installed thermal capacity of the new CHIs (condenser side)
  - **CH exis. [MW_{th}]**: total installed thermal capacity of the existing CHIs used (condenser side)
  - **HP CT2 [-]**: existence of a second central HP equipped with a single stage to upgrade the heat from the medium to the high temperature network
- Investment cost:
  - **Inv. Units [kCHF/y]**: annualized investment cost of conversion technologies (HPs, HEXs, CHIs)

  - **Inv. Networks [kCHF/y]**: annualized investment cost of the network[2]
  - **Inv. HP CT [kCHF/y]**: annualized investment cost of the central HP
  - **Inv. HP [kCHF/y]**: annualized investment cost of the decentralized HPs
  - **Inv. HEX [kCHF/y]**: annualized investment cost of the HEXs
  - **Inv. CH [kCHF/y]**: annualized investment cost of the new CHIs

- Operating cost:
  - **O&M [kCHF/y]**: annual operating cost due to equipment maintenance
  - **Op. LT source [kCHF/y]**: annual operating cost due to the purchase of the LTH
  - **Op. El. [kCHF/y]**: annual operating cost due to the purchase of the electricity
  - **Op. LT source saved [kCHF/y]**: annual savings in the purchase of the LTH granted by the exploitation of the anergy effect

- Energy consumption:
  - **Electricity [GWh]**: annual electricity consumption
  - **LT source energy [GWh]**: annual consumption of the LTH
  - **Air energy [GWh]**: annual usage of ambient air for free-cooling or to cool down the condensers of the CHIs
  - **Cold by LT source [%]**: share of the annual cooling demand covered by direct cooling with the LTH (anergy effect excluded)
  - **Cold by CHI [%]**: share of the annual cooling demand covered by the CHIs
  - **Cold by Air [%]**: share of the annual cooling demand covered by free-cooling with ambient air
  - **Dec. HP [%]**: heat supplied by the decentralized HPs as percentage of the total annual heating demand
  - **Dec. CHI [%]**: heat recovered from the CHIs and used for heating purposes as percentage of the total annual heating demand

$$\overline{COP} = \frac{Q^{env,+}}{E^{el}} = \frac{Q^{H} + Q^{dhw} + Q^{cond,air}_{CHI} + Q^{air}}{E^{el}} \tag{3.6}$$

Figure 3.16 reports a screenshot of the online results visualization platform. Due to the large numbers of KPIs, the latter are shown in three different plots. All the data are reported normalized because of the confidentiality of the results. The check boxes menu on the left

[2] This information represents for some scenarios an upper bound of the optimized cost as discussed in Section 3.6.2.

side allows to select/deselect groups or single KPI from the plots. The table below the figures reports the numerical values of all the axes shown. Each line in the figure (corresponding to a row in the table) represent a complete system design configuration. By brushing the axes the user can select ranges for the corresponding KPI so that only the configuration falling in those ranges are shown in the plots. The table underneath is updated accordingly.

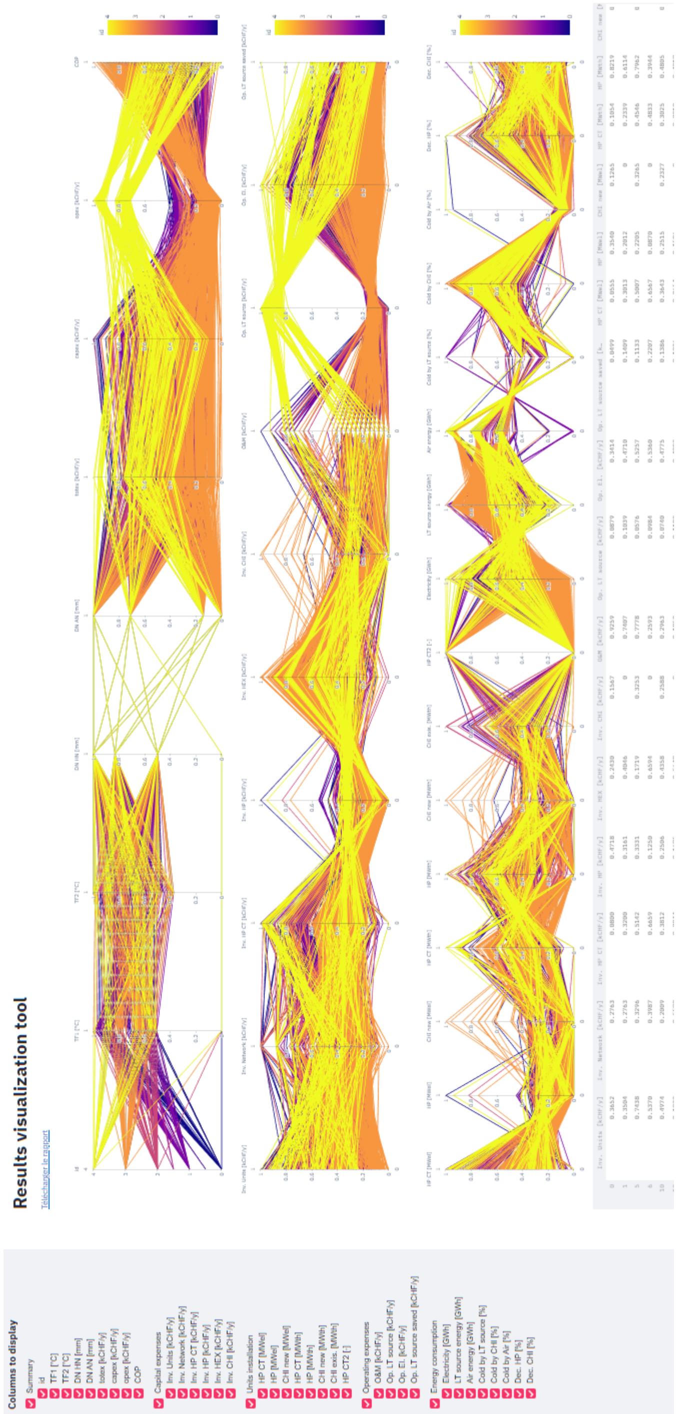

Figure 3.16: Screenshot of the results visualization platform.

3.7 Conclusion

This chapter focused on the optimal energy retrofit of complex DES, including heat and cold supply systems as well as the distribution networks. The model developed aimed at defining the optimal size, location and operation strategy of the newly installed conversion technologies together with the type, existence, diameter and operating temperatures of new TENs. Moreover, the decision weather to use the existing infrastructure, such as pipelines or equipment, was also included in the problem. The proposed framework integrated the work presented in Chapter 1 to estimate the thermal demand of existing, non-residential buildings and that reported in Chapter 2 to optimally define the size and operation of complex DES equipped with TENs. The MILP superstructure was further developed to take into account the existing infrastructure and equipment with the corresponding technical constraints. The latter included limitation on capacity and operating temperatures for the CHIs as well as position and maximum flow constraints for the existing pipelines. In particular, the flexible MILP formulation allowed to easily include the possibility of recovering the heat at the condensers of the CHIs, effectively transforming some of the buildings in “prosumers”. The latter are defined as users connected to the DH with the possibility of delivering excess heat to the network, offering great opportunities to integrate distributed RES and support the transition to smart thermal grids [21].

The proposed method was applied to a case study of an international airport located in Central Europe and that recently committed to become fossil-free in supplying heating and cooling demand to the buildings. The work was carried out in close collaboration with the latter transportation hub, to assist their energy transition. The strategy defined to achieve the challenging target included the connection to a future LTN and consequently, the replacement of the existing fossil-fired BOIs with more efficient HPs. Another objective was to exploit the synergies between the heating and cooling requirements via the anergy effect, allowing savings in terms of the LTH. The purchase of electricity on the site from renewable origin would make the final energy system fossil-free. The aim was to provide general guidelines and suggestions supported by a set of different system designs and relative KPIs. The recommendation offered were not supposed to represent precise system configurations, but a starting point for further discussion and investigations.

Due to the problem complexity the proposed solving strategy relied on the decomposition into 1) an upper level optimization, performed by an heuristic algorithm and aimed at defining the networks existence, operating temperatures and diameters and 2) a slave level optimization devoted to the resolution of the MILP. To limit the computational time, the network layout was excluded from the optimization. Nevertheless, its impact was assessed both by re-optimizing the solutions belonging to the Pareto-frontier and finally, through the definition of a second solving strategy. The latter included a new variable at the upper level, which represented an upper bound for the networks investment during the MILP. Additional scenarios, including potential reductions of the users’ temperature requirements and an increased LTH tariff were also investigated.

Finally a wide range of KPIs were defined to characterized the different system configurations, including information on installation and operating strategy of both networks and equipment, OPEX and CAPEX, system performance, and breakdowns of the heating and cooling supplied. All the results were deployed into an online visualization tool based on parallel coordinates, in which the user can easily interact with the solutions displayed by selecting/deselecting the KPIs as well as brushing the axes to highlight specific ranges of configurations.

Under the assumptions made, the analyses of the results led to the following conclusions:

- The best option for the case study investigated and for all scenarios seems to run the existing HN at high temperature (around 70°C) and to install a new one to be operated at medium temperature (around 50°C). The optimum layout of the latter is linked to the choice of the diameter. Solutions characterized by different extensions of the medium temperature HN equally appear to be cost-optimal, the difference being the distribution between the CAPEX devoted to the purchase of technologies and that to the installation of the pipelines. Nevertheless, the new connections are always exploited to reach new buildings, nowadays not supplied by the existing infrastructure. The presence of the medium temperature network allows to recover the heat rejected by the CHIs and exploit it for heating purposes not only within the same building, but also in different locations. This contribution allows to cover around 25% of the total heat demand.
- In the solutions identified as the most interesting the OPEX (including the equipment maintenance) covers from 60 to 73% of the TOTEX. The rest is devoted to the installation of equipment and TENs. The OPEX are mainly due to the purchase of electricity and LTH, covering respectively 60 and 30% of the total operating expenses. The former is distributed among the operation of the central HP, decentralized HPs, CHIs and back-up ELHs for DHW. All solutions appear more economical with respect to a fossil-based configuration, defined as the replacement of the oil-fired BOIs with natural gas ones and the expansion of the current system to accommodate the needs estimated for the project lifetime.
- The LTH appears the most exploited resource in heating mode, with an annual consumption corresponding to 55% of the total heat demand. The LTH is exploited to supply the evaporators of the HPs and of the CHIs. The latter contribute up to 64% of the heating demand, either by working as HPs, connected to the AN, or by recovering the heat at the condenser while supplying the cooling requirements. With the latter operation these machines supply around 25% of the heating needs. The remaining is partially covered by the central HP, through the high temperature network, and partially supplied by decentralized HPs, whose installation is preferred in locations including high temperature users and less likely to be renovated in the future.
- The cooling demand is almost entirely covered by the CHIs, contributing from 78 to 88% of the requirements for the four configurations, identified as the most interesting. The remaining needs are partially covered by the free-cooling with ambient air (around 10%)

and the anergy effect (from 1.5 to 10 %). The purchase of LTH to supply the demand in direct cooling mode is not exploited. Further analyses on the economical feasibility of direct cooling highlighted that under the assumptions made, only a reduction of 40% of the LTH tariff would make this option economically equivalent to the use of the CHIs. On the other hand, the decentralized solution, fully relying on the AN, would be competitive only with economic incentives. Moreover, in this latter configuration additional technical aspects, such as the temperature of the source and the pipes' diameters, should also be addressed.

- The advanced solving strategy, based on a more precise feedback between the slave and master level optimizations in terms of networks investment cost, steer towards similar conclusions as the simplified approach. The optimizer is able to refine the Pareto-frontier mainly acting on the networks temperature difference without affecting the general guidelines on the networks' supply temperatures and cost and energy breakdowns. Hence, it can be concluded that excluding the network layout in a first step does not penalize the optimal decision strategy. However, to avoid re-processing solutions, the solving strategy including an optimized upper bound for the networks investment cost appear overall more effective.

- The use of an online visualization platform based on parallel coordinates allows to gather all the system configurations and highlight trends in investment decisions. This aspect is consistent with the final aim of offering decision making support, rather than suggesting a precise configuration.

- The investigation of potential reductions of the users' temperature requirements highlight that only marginal savings in terms of total cost can be achieved by acting on the most critical users in each substations. However, with a second step of users' operating temperature reduction, the impact is increased up to 7% of the TOTEX of the reference configuration. The reason being that if within a given substation two users need a high supply temperature, after the first stage only one of them is reduced. Therefore, if the network temperature is not high enough to supply all the users in the location, one decentralized HP should still be installed. On the contrary, after the second stage of temperature reduction, also this last critical user is reduced, increasing the possibility of relying on the network to satisfy the demand, without the need of decentralized units. The cheapest solutions still present the two networks operated at respectively high and medium temperature. The electricity consumption is lowered because of the better overall COP of the system (linked to the lower temperature requirements). The amount of heat provided by the decentralized HPs drops to 10% of the total demand, whereas the share covered by recovering the heat from the CHIs is still relevant.

- An higher tariff of the LTH results, as expected, in increased TOTEX. The cheapest solutions are still represented by configurations showing HNs at respectively high and medium temperature levels. The fully decentralized solution remains not economical but the difference in terms of TOTEX with respect to the cheapest solution is lower than that in the base case scenario. Exploiting the anergy effect becomes more profitable, with savings reaching 20% of the OPEX, due to the higher cost of the LTH.

Results and conclusions presented in this chapter, even if influenced by the case study and the assumptions made, highlighted the potential of the underlying modelling and optimization framework. Opposite to the outcome from Chapter 2, in which system configurations based on different network operating temperatures appeared equivalent, the retrofit application showed a clear benefit in running the two heating networks at respectively high and medium temperatures. This result is mainly justified by the possibility of recovering heat from the condenser of the CHIs. Therefore, this study pointed out the advantage of investigating the network operating temperatures during the optimal design and retrofit of DES. Another major difference with the conclusions drawn from the previous green field application is that the AN, which in the work presented in Chapter 2 appeared as a solution to decrease investment cost while ensuring the same system performance, is not economically competitive in the current application. What influenced the two different outcomes is the LTH tariff, that in the work presented in this chapter was considered three times higher with respect to the previous one, due to the additional cost of the infrastructure to bring the water from the lake to the airport site. These differences suggest that the results here proposed cannot simply be extrapolated to different transportation hubs, whereas the methods presented remain valid.

Limitations and perspectives The main limitation of the proposed methodology arises from the underlying complex MILP superstructure. Since the core of the formulation is not changed with respect to that presented in Chapter 2, the weaknesses previously mentioned related to modelling assumptions and simplifications are inherited. Moreover, applying the method to such a complex case study required tailored constraints to take into account the technical limitations of this specific application. On the other hand, modelling techniques always require assumptions and simplifications, what is most important is the right trade-off between model details and level of accuracy required by the application. For example, the flexible operation of the CHIs implies that the evaporator can recover the heat from the users needing cooling and at the same time be connected to the AN to effectively work as HPs. Meanwhile, the condenser can be cooled down by both ambient air and the HN. Such a configuration would require further technical solutions which are not taken into account in the cost functions assumed during this study. Similarly, in each substation, the heat demand of all the associated users is aggregated and it is supposed that it can be partially covered by the network and partially by the decentralized HP. Also this configuration might require changes in the substation, due to the presence of the collectors, whose cost was not taken into account during this study. Estimating the additional cost of these technical modifications is very case-specific and difficult to generalize. This is one of the reasons why the aim of the method developed is not to define a single optimal configuration, but rather a set of options. The final decision is left to experts in the field and of the particular application that could judge each solution including technical feasibility and potential additional costs.

Moreover, to cope with the problem complexity, the latter was decoupled into two levels and the network layout could not be optimized. As a result, numerous iterations of the heuristic optimization needed to be performed together with additional analyses to assess the effects of including the network layout optimization. A further restriction of the proposed approach is the limitation of network diameters and operating temperatures, by imposing a predefined set of possible choices.

For the reasons above and as previously mentioned in this chapter, the developed tool is intended to offer general guidelines to define a solid starting point for further discussions and analyses. As a consequence, the results of the optimization should be refined via simulation to better take into account the technical constraints arising from the complex application.

Further work should include the implementation of a staged investment strategy to take into account the possibility of installing equipment at different times during the project. This approach, implemented in a previous study presented in [46], appeared to be an effective solution to take into account the long lifetime of projects in the field of DES design. The use of additional binary variables for the purchase of equipment allows to stage the investment decisions, taking into account the possibility of replacing old equipment or reselling them. Furthermore, the decision of renovating buildings should be included among the decision variables during the optimization process. Reducing the building's requirements in terms of heat would result in smaller capacities of the equipment installed. Concurrently, reducing their temperatures implies a better performance of the energy system (with improved COP of the HPs), but also a larger exploitation of the LTH for the same reason. An attempt to investigate this aspect was conducted during this study, by reducing the users' temperature requirements, but a more systematic approach would be needed.

Conclusion

Chapter overview

- Summary of proposed methods and results
- Key messages and contributions
- Limitations and perspectives

In light of the urgent need of speeding-up the ongoing energy transition, of the key role played by the building sector and of the recognized potential to district heating and cooling (DHC) systems, this thesis focused on the optimal design of district energy systems (DES) with the aim of integrating renewable energy sources (RES) in urban areas. Particularly, given the gaps highlighted in the literature, three main research questions have been formulated and tackled in the corresponding chapters. The following sections report a concise summary of the methods developed, the main conclusions drawn from the associated results and the major contributions generated in the correlated fields of research. A more extensive explanation is given in the concluding sections of each chapter. The final section recalls the main limitations of the developed methods and of the proposed future perspectives.

Chapter 1 *"How can the thermal energy requirements of existing, non-residential buildings be modelled for the integrated system design?"*
Authors commonly overcome the challenges of modelling the thermal energy requirements (TER) in complex, non-residential buildings either by adopting sophisticated building simulation software or by relying on data-driven approaches. However, the need of precise information on the buildings' structures and usage in the first case and of an extensive amount of measured data in the second, render these methods often not suitable in the field of energy system design. In this situation, particularly when referring to existing buildings, most of the studies rely on highly simplified methods, as the one based on heating and cooling signatures, and rarely disclose information on the modelling and calibration processes. Hence, the first chapter proposed to fill the gaps in the literature by defining different grey-box models with level of details adjusted to the time resolution of the available data. The models performance in reproducing the original profiles was assessed taking into account also the errors arising from the subsequent clustering process. Defining typical operating periods is required to

reduce the size of the following optimization problem, which aims at designing the integrated energy system. In view of the crucial role of the supply temperature in systems based on heat pumps (HP), a novel method to define new operating temperatures by exploiting the heat exchange surfaces was presented. Suggestions on how to estimate domestic hot water (DHW) and space cooling demand, based on the available measurements, were also provided.

The application of the proposed methods to the case study of an international airport highlighted that, for the given application, all thermal models performed similarly, with a weighted mean absolute percentage error (MAPE) of around 20%. A marginal improvement of 2% was registered by including the contribution of the current control strategy and buildings' inertia, whereas the standard occupancy profiles failed at representing the internal gains. The resulting thermal model comprised: 1) thermal losses through the building's envelope and the ventilation system, 2) solar gains, 3) internal gains due to people's presence, 4) ramp-up (-down) of switching from the night to daily operation (and viceversa). After the comparison of different number of typical operating periods, seven were found to be the optimal compromise between model accuracy and complexity. The clustering process highly deteriorated the MAPE, doubling the average value for all the thermal models. However, relying on clustered profiles improved the estimation of the yearly demand, balancing out the modelling errors at the annual level. The analysis on the time resolution of available measurements highlighted that the model calibrated on hourly data showed overall better performance in terms of representing the original hourly profiles, with respect to the heating signature approaches.

The proposed methods, to the best of the author's knowledge, compared for the first time different thermal models to estimate the TER of existing, non-residential buildings in the wider field of integrated energy system design. Given the broader application, the estimation of the energy requirements did not end at the power profiles, but included the required operating temperatures for a future energy system.

Chapter 2 *"How can optimal design solutions for district energy systems equipped with thermal networks be defined, and how can the best configuration be selected?"*
The second chapter proposed a flexible mixed-integer linear programming (MILP) superstructure and optimization framework to tackle the optimal design and operation strategy of DES, focusing on integrating RES in urban areas. Decision variables included location, size and operation of conversion technologies, as well as type, layout, diameter and operating temperatures of the thermal energy networks (TEN). The proposed solving strategy aimed at defining configurations characterized by different degrees of centralization, and respectively decentralization, of the heat and cold production. Solutions were compared on the basis of economic, environmental and exergy related key performance indicators (KPI). The sensitivity of the results to the cost of resources (electricity, low-temperature heat (LTH) and natural gas) as well as the investment cost function parameters of technologies, network and the interest rate was systematically investigated, in order to assess the robustness of the different configurations. A fictitious case study of a neighborhood composed by six buildings of different usage

and construction years was used to validate the proposed methods.

Results highlighted that in all the network configurations, higher capital allowance enables more efficient and sustainable solutions. In terms of installed technologies, standalone options such as boilers (BOI), electrical Heaters (ELH), chillers (CHI) and air-water HPs are gradually replaced by water-water HPs, connected to the network, in combination with back-up units. The comparison of the different network configurations showed the equivalence in terms of operating cost, environmental and exergy related KPIs of the investigated options. However, the configuration equipped with an anergy network achieves the same performance with a lower investment cost. The most robust solutions against uncertainties appeared to be those lying in the middle of the Pareto frontier, characterized by a moderate degree of decentralization. Solutions at the extreme ends of the Pareto, showed the greater sensitivity in the direction of the predominant cost contribution (operating expenses (annual) (OPEX) or capital expenses (annualized) (CAPEX)). Finally, the interest rate appeared to be the parameter affecting the most the variation of the CAPEX.

The strength of the developed MILP arises from the combination of different elements: 1) energy and mass balances, 2) heat cascade constraints to ensure the feasibility of the heat exchanges, 3) network model, including thermal and pressure losses, as well as maximum flow constraints, 4) geographical locations to account for spacial constraints. As a result, to the best of the author's knowledge, this approach enables the first systematic definition of DHC systems configurations, including optimal sizing and operation of equipment and distribution networks and consequently the investigation and comparison of the different solutions under economic, environmental and exergy related considerations.

Chapter 3 *"How can existing district energy systems be retrofitted to optimally integrate renewable energy sources and exploit synergies between heating and cooling requirements?"*
Given the combined need of increasing the penetration of DHC systems and the share of RES in urban areas, and considering that the current systems are still mostly based on fossil fuels, the third chapter focused on the optimal retrofit of DES. Studies in this field rarely combine technology retrofit to network expansion. Moreover, the focus is still on district heating (DH), despite DHC systems having already demonstrated their advantages, offering an opportunity to combine heating and cooling requirements. Finally, the network temperature is usually not investigated in the current studies. To fill the gaps in the literature, the proposed approach consisted in first combining the methods presented in the first chapter to estimate the thermal needs of existing, non-residential buildings with the approach proposed in the second chapter to optimally design DES. Secondly, the proposed MILP superstructure was further developed to take into account existing equipment and infrastructure and optimize their operating strategy. The resulting model enabled the definition of multi-level temperature networks and the possibility for users to act as "prosumers", promoting the recovery of heat otherwise wasted. Moreover the implemented solving strategy, based on a problem decomposition, allowed to cope with the resulting problem complexity. Finally, the developed online visualization

platform, using parallel coordinates, served as a decision support tool. The methods were applied to the case study of an international airport, located in Central Europe, with the goal of assisting their transition from a fossil-based energy system to the connection to a low-temperature network (LTN).

The results clearly highlighted the benefit of running the existing network at high temperature (around 70°C) and installing a new one to be operated at a medium temperature (around 50°C). The latter is justified by the possibility of recovering the heat from the condensers of CHIs, contributing to around 25% of the heating demand. For the solutions identified as the most interesting, the OPEX dominated the total cost, with an allocated share between 60% to 73%. Most of the operating expenses were mainly devoted to the purchase of electricity and LTH (around 60% and 30%, respectively). The layout of the new network is mainly defined by the choice of its diameter and the decision of devoting the major share of the investment either to the conversion technologies or to the distribution networks. However, the new pipelines always allowed to connect new buildings, expanding the existing network. Further analysis on the supply of cooling requirements highlighted that the assumed value of the LTH tariff rendered the CHIs always more economical then direct cooling, which as a result covered only a marginal share of the requirements (from 1.5 to 10% including the anergy effect). The parallel coordinates appeared to be an effective tool to show multiple KPIs of different design configurations and investigate the major trends of investment decisions.

Limitations and perspectives

Although limitations and perspectives have already been highlighted in the concluding section of each chapter, the following paragraphs summarize the main considerations and recall the suggested future developments.

Thermal energy requirements assessment The challenges of estimating the TER of non-residential buildings become even more relevant if the structures are not standalone but part of a larger building complex, such as the case of educational campuses, hospitals or airports. On the other hand, the final aim of designing the integrated energy system includes constraints on the required level of details. As an example, in case that the potentially installed equipment would supply only a portion of the building (e.g., through a substation), the thermal demand must be estimated for that zone. At the same time, taking into account the effect of neighboring zones in a steady-state model and given the measurements commonly available is very difficult, if not impossible. Therefore, models developed based on building physics were applied to single building zones, restraining the comparison of the calibrated parameters with the ones recommended by the standards. Similarly, due to the lack of available measurements, some of the assumptions and results could not be validated, such as the share of demand supplied by static appliances and that covered by ventilation units.

Future studies should include the investigation of the effects of the assumptions, made in the phase of the demand estimation, on the final investment decisions. Among them the number and choice of the typical operating periods should also be evaluated not only in terms of the model performance in representing the original profile, but also in potential deviation on investment decisions. Moreover, a systematic approach to include in the clustering approach the original measurements, which incorporate precious information on the system requirements, should also be included.

Optimal sizing and operation of district energy systems Due to the intrinsic complexity of the simultaneous optimization of the utility integration and distribution networks, the problem size inevitably rapidly increases with the number of time steps, locations, potential network temperatures, configurations and diameters. Moreover, if multiple solutions appear equivalent in terms of the objective function defined, the computational time increases even further. Additional limitations arise from the need of model simplifications, such as the definition apriori of potential return temperatures without taking into account the possibility of acting on the mass flow rate as a control strategy and the disregard of the return temperature in estimating the central HP performance. Further analyses should include the investigation of different temperatures for the LTH, the influence of the central station's location on the results, the potential building renovation and the robustness of the solutions against uncertainty on the demand. Moreover, beyond the holistic approach as the one presented in this thesis, solutions should be evaluated under different perspectives, such as the one of the distribution company or the single users.

Optimal retrofit of district energy systems In the optimal retrofit of DES, to limit the problem complexity, simplifications were introduced without taking into account the potential technical constraints. As an example, at the substatation level it was assumed that the demand could be partially covered by a decentralized HP and directly supplied by the network through an heat exchnager (HEX). However, the potential additional costs to adapt the substation to such an operation were neglected. Similarly a very flexible operation of the CHIs, including source and sink at different temperatures, was included, without considering potential technical limitations or additional costs with respect to a standard operation. Due to these limitations, as all the other modelling simplifications, the final solutions should be validated by simulation. Further work should include the implementation of investment staging and the possibility of buildings' renovation among the decision variables.

Appendices

A Chapter 1: Thermal building models additional information

A.1 Application

Figure A.1 offers a schematic view of the largest buildings belonging to the system investigated, including the thermal network, all the HEXs, substations and final end-users.

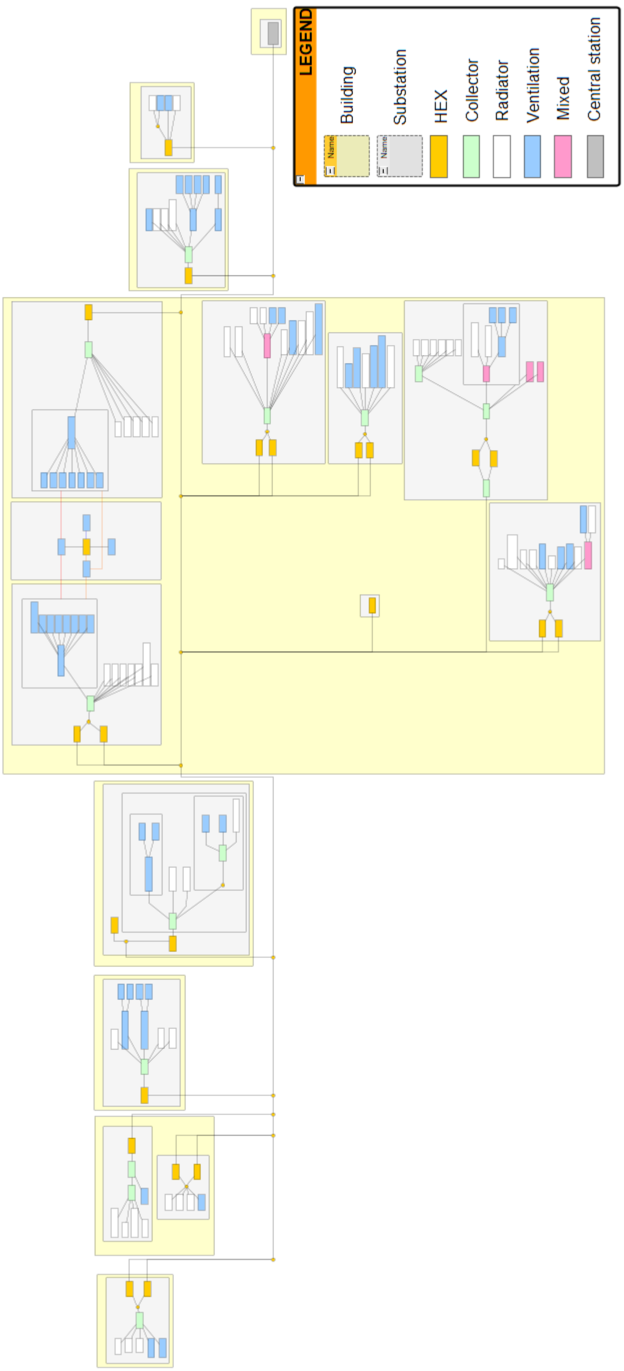

Figure A.1: Schematic of the case study. Buildings in light yellow, substations in light grey, heat exchangers in dark yellow, static appliances in white, ventilation units in light blue, mixed users in pink and the central plant in dark grey.

Figure A.1 shows that the different buildings (light yellow boxes) include one or more subsations (light grey boxes). The thermal network (black line) connects the central plant (dark grey box) to the different substations by means of one or two heat exchangers (dark yellow boxes). The latter transfer the heat to the final users (radiators, ventilation units or mixed respectively depicted in white, light blue and pink) eventually through the use of collectors (light green boxes). The measurements of the power delivered at the substation level are recorded at the secondary side, on the collector, after the heat exchangers connecting each substation to the primary network.

A.2 Defining potential exergy savings by optimal operation

The potential exergy savings showed for diferent substation in Fig. 1.4 are defined as the potential saving achievable by optimizing the operation normalized with respect to the current value, as reported in Eq. A.1.

$$\Delta Ex_s = \frac{Ex_s - Ex_s^{opt}}{Ex_s} \cdot 100 \qquad \forall s \in \mathbf{SS} \quad (A.1)$$

As optimal operation is intended the one exploiting at most the available heat exchange surface and mass flow limitations to be able to lower the supply and return temperatures. The exergy content associated to the current operation Ex_s is estimated based on the measurements of power delivered, mass flow rate and operating temperatures, as shown in Eq. A.2:

$$Ex_s = \sum_{t \in \mathbf{T}} \dot{Ex}_s = \sum_{t \in \mathbf{T}} \widetilde{\dot{Q}}^H_{s,t} \cdot \left(1 - \frac{T_t^{amb} + 273}{\widetilde{T}^{f/r}_{LM,t,s}}\right) \cdot \mathrm{d}_t \qquad \forall s \in \mathbf{SS} \quad (A.2)$$

where d_t is the duration of the time interval and $\widetilde{T}^{f/r}_{LM,t,s}$ is the logarithmic mean temperature between the supply and return, calculated as reported in Eq. A.3.

$$\widetilde{T}^{f/r}_{LM,t,s} = \frac{(\widetilde{T}^f_{s,t} - \widetilde{T}^r_{s,t})}{\log \frac{\widetilde{T}^f_{s,t} + 273.15}{\widetilde{T}^r_{s,t} + 273.15}} \qquad \forall s \in \mathbf{SS},\ \forall t \in \mathbf{T} \quad (A.3)$$

When not available, the return temperature $\widetilde{T}^r_{s,t}$ is calculated based on the other measurements as follows:

$$\widetilde{T}^r_{s,t} = \widetilde{T}^f_{s,t} - \frac{\widetilde{\dot{Q}}^H_{s,t}}{\widetilde{\dot{m}}_{s,t} \cdot c_p} \qquad \forall s \in \mathbf{SS},\ \forall t \in \mathbf{T} \quad (A.4)$$

The substation is simplified as an aggregated heat exchangers in which the mass of water $\widetilde{\dot{m}}_{s,t}$ arriving at $\widetilde{T}^f_{s,t}$ and leaving at $\widetilde{T}^r_{s,t}$ delivers heat to the room supposed at a constant comfort temperature of 21°C (T^c). The (UA) of the this heat exchanger is estimated as being the 95$^{\text{th}}$ of the values calculated in each time step according to Eq. A.5:

$$(UA)_s = \mathrm{P}_{95}((UA)_{s,t}) = \mathrm{P}_{95}\left(\frac{\widetilde{\dot{Q}}^H_{s,t}}{\mathrm{LMTD}_{s,t}}\right) \qquad \forall s \in \mathbf{SS} \quad \text{(A.5)}$$

with the mean logarithmic temperature difference $\mathrm{LMTD}_{s,t}$ calculated as:

$$\mathrm{LMTD}_{s,t} = \frac{\widetilde{T}^f_{s,t} - \widetilde{T}^r_{s,t}}{\log \frac{\widetilde{T}^f_{s,t} - T^c}{\widetilde{T}^r_{s,t} - T^c}} \qquad \forall s \in \mathbf{SS},\ \forall t \in \mathbf{T} \quad \text{(A.6)}$$

Supposing that the heat transfer coefficient does not vary during the operation by exploiting the two equations governing the heat exchange, respectively Eqs. A.7a and A.7b, the optimal return and supply temperatures can be estimated as shown in Eqs. A.7c and A.7d.

$$\widetilde{\dot{Q}}^H_{s,t} = \widetilde{\dot{m}}_{s,t} \cdot c_p \cdot (\widetilde{T}^f_{s,t} - \widetilde{T}^r_{s,t}) \qquad \forall s \in \mathbf{SS},\ \forall t \in \mathbf{T} \quad \text{(A.7a)}$$

$$\widetilde{\dot{Q}}^H_{s,t} = (UA)_s \widetilde{\mathrm{LMTD}}_{s,t} \qquad \forall s \in \mathbf{SS},\ \forall t \in \mathbf{T} \quad \text{(A.7b)}$$

$$T^{r,opt}_{s,t} = T^c + \frac{\widetilde{\dot{Q}}^H_{st} / \mathrm{P}_{95}(\widetilde{\dot{m}}_{st}) / c_p}{e^{\alpha} - 1} \qquad \forall s \in \mathbf{SS},\ \forall t \in \mathbf{T} \quad \text{(A.7c)}$$

$$T^{f,opt}_{s,t} = T^{r,opt}_{s,t} + \frac{\widetilde{\dot{Q}}^H_{s,t}}{\mathrm{P}_{95}(\widetilde{\dot{m}}_{st}) \cdot c_p} \qquad \forall s \in \mathbf{SS},\ \forall t \in \mathbf{T} \quad \text{(A.7d)}$$

In Eqs. A.7c and A.7d the maximum allowed mass flow rate is assumed to be the 95$^{\text{th}}$ percentile of the available data, to avoid taking into account outliers which might be associated to measuring errors, while the coefficient $\alpha = (UA)_s / \mathrm{P}_{95}(\widetilde{\dot{m}}_{st}) / c_p$.

A.3 Results of the building thermal models

Tables A.1 to A.3 report for each substation the errors resulting from the calibration of the thermal models on respectively hourly, monthly and annual data. Errors are calculated both a) between the estimated yearly profile by applying the model to the clustered attributes and the original measurements (the error includes the one committed by using the model and the one by representing the reference year through a series of typical operating periods), and b) between the yearly profile estimated by applying the models directly to the yearly profiles of the attributes and the original measurements.

A.3.1 Substations with outliers in monthly measurements

Figures A.2 to A.5 show the results of the piece-wise interpolation used to calibrate the thermal model based on monthly measurements, for substations presenting outliers. The monthly data is estimated by re-sampling the available hourly heat loads.

Table A.1: Errors of thermal model based on hourly measurements.

SUBSTATION	MAPE 1[a] [%]	MAPE 2[b] [%]	APE 1[a] [%]	APE 2[b] [%]
SS1	27.3	27.01	0.7	3.7
SS2	38.8	13.26	0.7	1.7
SS3	28.8	17.75	1.6	4.0
SS4	33.3	20.40	4.0	4.5
SS5	27.9	13.75	0.4	2.6
SS6	35.6	20.61	38.7	3.7
SS7	37.0	20.43	38.9	1.3
SS8	30.4	17.73	0.9	4.1
SS9	27.8	18.96	2.0	0.9
SS10	34.0	21.39	3.9	0.5
SS11	34.7	24.75	3.6	0.3
SS12	30.9	22.67	3.3	5.1
SS13	27.6	14.01	2.7	1.4
SS14	31.0	14.66	27.1	0.1
SS15	29.5	18.98	2.7	0.2
SS16	27.0	19.07	1.9	0.1
SS17	27.9	18.19	4.3	1.6
SS18	28.5	18.99	0.7	1.7

[a] Calculated between the hourly profile reconstructed by applying the model to the aggregated attributes and the original one (the error takes into account the clustering procedure).
[b] Calculated between the hourly profile reconstructed by applying the model to the hourly attributes and the original one (the error does not take into account the clustering procedure).

Table A.2: Thermal model based on monthly measurements: errors and estimated threshold temperature.

SUBSTATION	$T^{tr,H}$ [°C]	MAPE [%][a]	APE 1[%][b]	APE 2[%][a]
SS19	18.2	19.8	4.3	7.3
SS20	17	13.6	2.9	7.5
SS21	16.1	17	1.4	8.4

[a] Calculated between the monthly/annual energy estimated by applying the model to the hourly profile of the ambient temperature and the measurements (the error does not take into account the clustering procedure).
[b] Calculated between the annual energy estimated by applying the model to the clustered ambient temperature and the original one (the error takes into account the clustering procedure).

A.4 Definition of the typical and extreme periods of operation

The typical periods of operation are identified by applying the k-medoids clustering approach presented in [54]. The optimum number of clusters is chosen by comparison taking into account not only the performance of the clustering approach, but also the error of the thermal model on reproducing the yearly profile, as reported in Section 1.4.1. With this procedure seven days of the year, listed in Table A.4, are chosen as representative of the system operation.

Table A.3: Errors of thermal model based on yearly measurements.

SUBSTATION	APE [%]
SS22	5.52
SS23	5.52
SS24	5.52
SS25	5.52
SS26	7.08

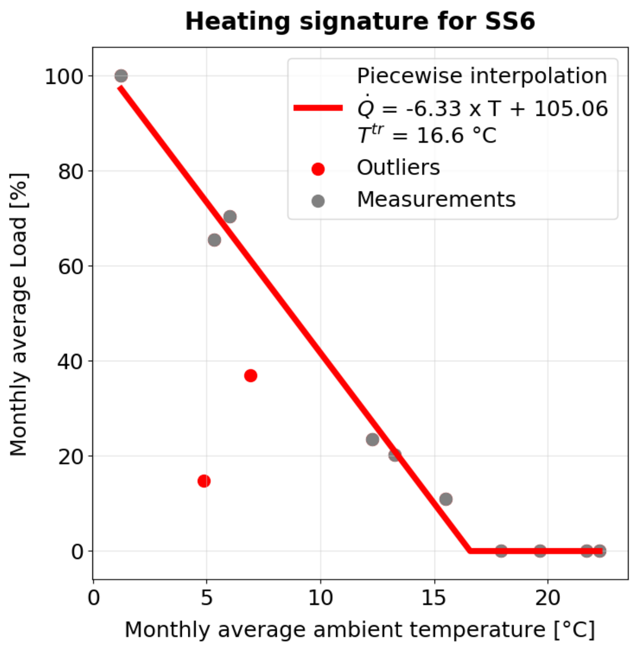

Figure A.2: Piecewise linear interpolation of normalized monthly data to estimate the threshold temperature and coefficients of the heating curve for substation SS6.

Cluster #	k-medoid
1	05th of September
2	14th of April
3	28th of April
4	12th of January
5	09th of January
6	28th of January
7	20th of August

Table A.4: Representative days of the typical operating periods of operation

With the final aim of designing the energy system, beyond the typical operating periods, the extreme conditions must be defined, to make sure that the sizing of the equipment is able to sustain the most critical operation. Therefore, two additional operating time steps are

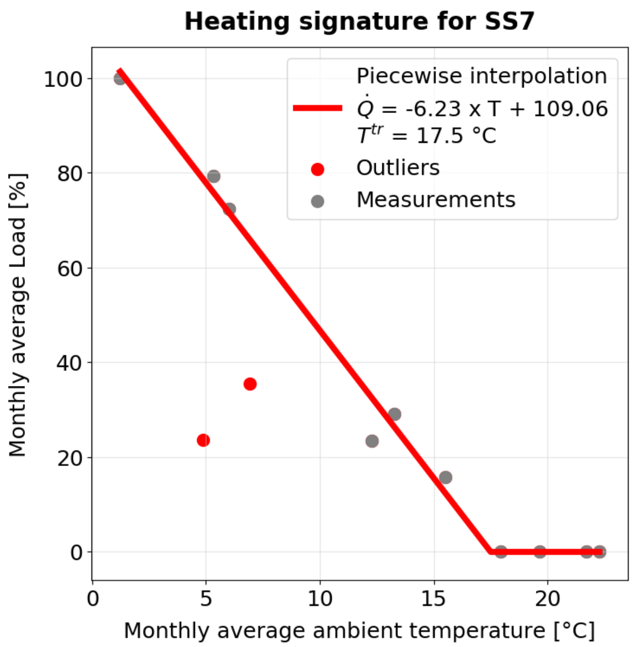

Figure A.3: Piecewise linear interpolation of normalized monthly data to estimate the threshold temperature and coefficients of the heating curve for substation SS7.

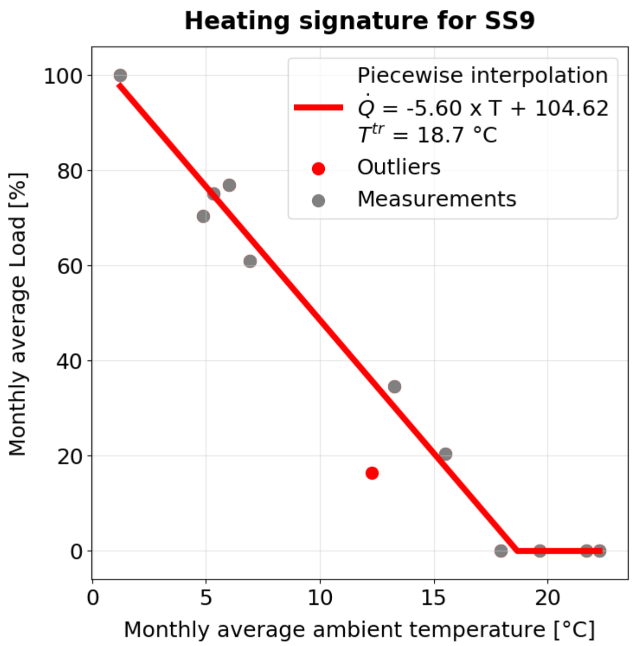

Figure A.4: Piecewise linear interpolation of normalized monthly data to estimate the threshold temperature and coefficients of the heating curve for substation SS9.

introduced representing extreme heating and cooling conditions. In the case of the substations for which hourly measurements are available the extreme conditions are defined based on the

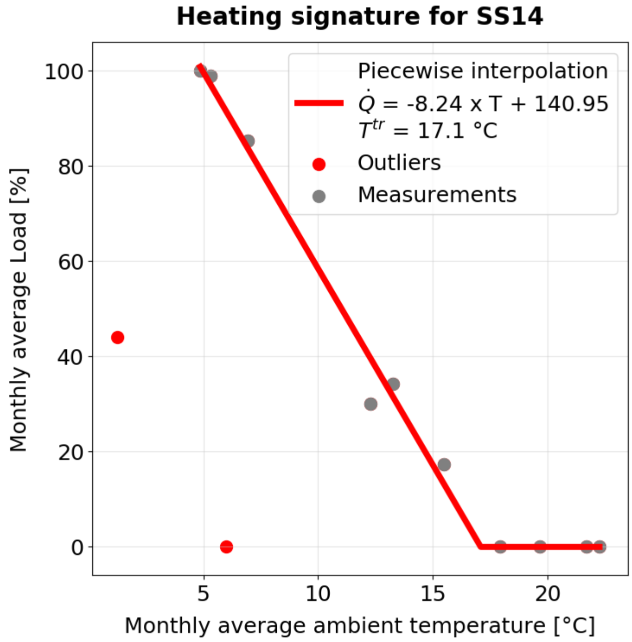

Figure A.5: Piecewise linear interpolation of normalized monthly data to estimate the threshold temperature and coefficients of the heating curve for substation SS14.

estimated split between the static and ventilation appliances and the most critical conditions modeled or measured, as reported in Eqs. A.8a to A.8d:

$$r_s^H = \frac{\sum_t \dot{Q}_{t,s}^{H,vent}}{\sum_t \dot{Q}_{t,s}^H} \qquad \forall s \in \mathbf{SS} \quad \text{(A.8a)}$$

$$\dot{Q}_{s,max}^{H,vent} = \max(\dot{Q}_{t,s}^H, \widetilde{\dot{Q}}_{t,s}^H) \cdot r_s^H \qquad \forall s \in \mathbf{SS} \quad \text{(A.8b)}$$

$$\dot{Q}_{s,max}^{H,rad} = \max(\dot{Q}_{t,s}^H, \widetilde{\dot{Q}}_{t,s}^H) \cdot (1 - r_s^H) \qquad \forall s \in \mathbf{SS} \quad \text{(A.8c)}$$

$$\dot{Q}_{s,max}^H = \dot{Q}_{s,max}^{H,rad} + \dot{Q}_{s,max}^{H,vent} \qquad \forall s \in \mathbf{SS} \quad \text{(A.8d)}$$

where:

- r_s^H is the ratio defining the portion of heat load supplied by the ventilation units over the total assigned to the substation, estimated by the model in case of hourly measurements or assumed otherwise;
- $\dot{Q}_{t,s}^{H,[-/vent/rad]}$ represents the result of the thermal model applied to the typical periods of operation;
- $\widetilde{\dot{Q}}_{t,s}^H$ stands for the original measured profile for the substation s;
- $\dot{Q}_{s,max}^{H,[-/vent/rad]}$ is the power associated to the substation and to each type of user for the extreme operating period;

A similar approach is followed for the cooling requirements. In this case final end-users are supposed to be ventilation units and radiant panels. To the extreme operating periods, the maximum demand estimated by the model for the reference year 2018 is taken, as reported in Eqs. A.9a to A.9c:

$$\dot{Q}^{C}_{s,max} = \max(\dot{Q}^{C}_{t,s}) \qquad \forall s \in \mathbf{SS} \quad \text{(A.9a)}$$
$$\dot{Q}^{C,vent}_{s,max} = \dot{Q}^{C}_{s,max} \cdot r^{C}_{s} \qquad \forall s \in \mathbf{SS} \quad \text{(A.9b)}$$
$$\dot{Q}^{C,rad}_{s,max} = \dot{Q}^{C}_{s,max} \cdot (1 - r^{C}_{s}) \qquad \forall s \in \mathbf{SS} \quad \text{(A.9c)}$$

where:

- r^{C}_{s} is the ratio defining the portion of cooling load supplied by the ventilation units over the total assigned to the substation on an hourly basis;
- $\dot{Q}^{C}_{t,s}$ represents the result of the thermal model to estimate the hourly cooling demand during the reference year;
- $\dot{Q}^{C}_{s,max}$ is the cooling demand assigned to the substation during the extreme operating condition (cooling mode);
- $\dot{Q}^{C,vent}_{s,max}$ is the cooling demand assigned to the ventilation units of the substation during the extreme operating condition (cooling mode);
- $\dot{Q}^{C,rad}_{s,max}$ is the cooling demand assigned to the radiant panels of the substation during the extreme operating condition (cooling mode);

The value of the ratio r^{C}_{s} is assumed based on discussions with experts in the field.

A.5 Estimation of the users installed heating capacity

The installed capacity of the heat exchangers $\widetilde{\dot{Q}}_{0,s}$ is available only for a limited number of substations. In this case its value is compared with the power associated to the extreme period of operation (defined in the section above). In case the given capacity results lower than the maximum assigned power then the latter is taken, while if greater the given capacity is considered. If not available, the substation installed capacity is estimated through the maximum assigned power and an over-sizing factor γ_0. Equation A.10 summarizes all the possibilities.

$$\dot{Q}_{0,s} = \begin{cases} \tilde{\dot{Q}}_{0,s} & \text{if } \exists\, \widetilde{\dot{Q}}_{0,s} \text{ and } \widetilde{\dot{Q}}_{0,s} \geq \dot{Q}^{H}_{s,max} \\ \dot{Q}^{H}_{s,max} & \text{if } \exists\, \widetilde{\dot{Q}}_{0,s} \text{ and } \widetilde{\dot{Q}}_{0,s} < \dot{Q}^{H}_{s,max} \\ \gamma_0 \cdot \dot{Q}^{H}_{s,max} & \text{if } \nexists\, \widetilde{\dot{Q}}_{0,s} \end{cases} \qquad \forall s \in \mathbf{SS} \quad \text{(A.10)}$$

The over-sizing factor γ_0 is assumed as the median of the available ones ($\gamma_0 = \widetilde{\dot{Q}_{0,s}/\dot{Q}^H_{s,max}}$) after removing the outliers (i.e., values below and above the first and last quartile). Finally, to define the installed capacity of each type of user the same ratio assumed for the energy distribution (r_s) is employed.

In the specific application within each type of user (ventilation and static appliances) two different generations are distinguished[1]:

- **Vantilation:**
  - **I generation:** 3/4 of the power associated to the ventilation units in the substation ($\dot{Q}^{H,vent}_{s,t}$), to which 80/60°C are assigned as design conditions for the supply/return network temperatures;
  - **II generation:** 1/4 of the power associated to the ventilation units in the subsation ($\dot{Q}^{H,vent}_{s,t}$) to which 70/50°C are assigned as design conditions for the supply/return network temperatures.
- **Radiators:**
  - **I generation:** 2/3 of the power associated to the radiators in the substation ($\dot{Q}^{H,rad}_{s,t}$) to which 70/50°C are assigned as design conditions for the supply/return network temperature
  - **II generation:** 1/3 of the power associated to the radiators in the substation ($\dot{Q}^{H,rad}_{s,t}$) to which 50/40 °C are assigned as design conditions for the supply/return network temperature

The assumption above is employed for the estimation of the new operating temperature profile for each type of users and generation, as explained in Section 1.4.4.

A.6 Estimation of the cooling demand

A.6.1 Shifting the profile of the number of passengers to the reference year

The people presence is considered greatly affecting the cooling demand of a building due to the generation of internal gains. Since heating and cooling measurements do not refer to the same year, it is chosen to calibrate a simple linear model for the cooling demand to be able to extrapolate the trends to periods outside the measuring time. One of the attributes chosen to calibrate the model is the daily number of passengers. The latter is available for the year 2018, taken as the reference. On the contrary measurements on the cooling demand refer to the year 2019. For this reason an extrapolation of the passenger profiles for the year 2019 has

[1] All the assumptions are validated by experts of the application and revision of the technical sheets available.

to be made. Therefore, the profile is first investigated to check which are the most influencing parameters.

Figure A.6 show the Pearson coefficients calculated between the number of passengers, the profile of week-days and weekends, holidays, ambient temperature and solar radiation. The latter is meant to represent the seasonal variation over the year.

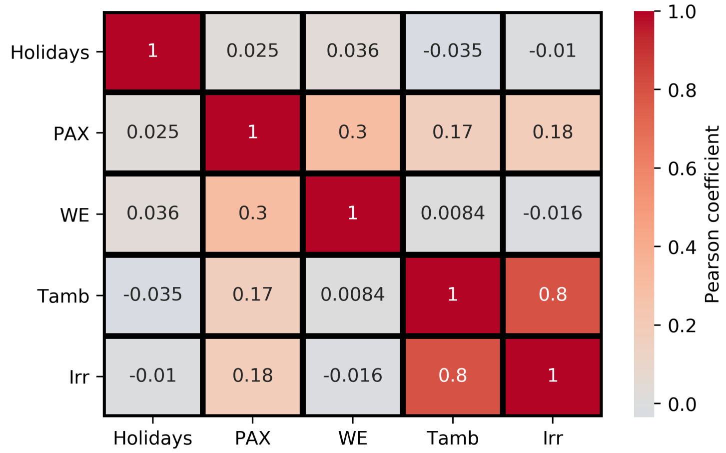

Figure A.6: Pearson coefficient between daily number of passengers (PAX), profile of week-end days (WE), profile of holidays (Holidays), ambient temperature (Tamb) and solar irradiation (Irr).

The highest dependency appears to be between the number of passengers and weather a day is falling during the week or the week-end. The trends of the different parameters together with the normalized dayily number of passengers are plot in Fig. A.7.

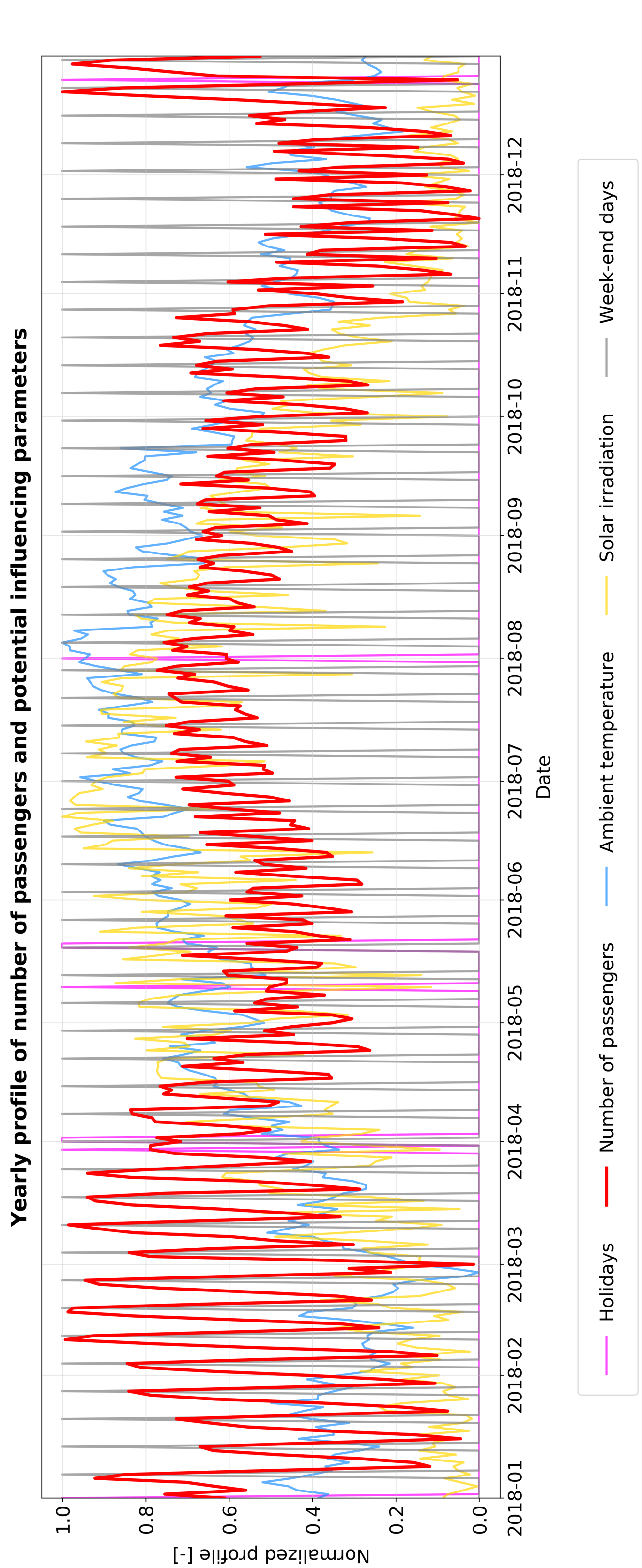

Figure A.7: Normalized profile of daily number of passengers, week-end days, holidays, ambient temperature and solar irradiation.

By checking the trends shown in Fig. A.7 one can notice the highly dependence of the number of passengers to occurrence of week-end days. The same cannot be claim for the holidays. A seasonal trend can be noticed mostly with difference between the winter and summer seasons. In light of all the consideration to extrapolate the trend to the following year it is chosen to simply shift it of one day. The resulting profile would be able to catch the presence of the week-ends as well as the seasonal variation.

A.6.2 Cooling thermal building model error

Table A.5: Errors in cooling demand estimation

SUBSTATION	MAPE [%][a]	APE [%][a]
SS8	23.45	1.2
SS4	27.13	0.0
SS14	34.12	2.25
SS20	23.47	0.0

[a] Calculated between the yearly profile estimated by applying the model and the original one (the error does not take into account the clustering procedure).

Figures A.8 to A.10 show the average daily cooling power supplied by respectively substation SS14, SS4, SS20 and the results of the relative calibrated models. The original profiles are based on the estimation of the coefficient of performance (COP) for the different cooling machines following the procedures reported in Section 1.5.2.

A.6.3 Operating temperatures

The cooling requirements in each substation are supposed to be delivered partially by the ventilation units and the remaining by radiant panels. To the two technologies different operating temperature are assigned based on discussions with experts in the field and of the particular application. Ventilation units are supposed to require temperature of 13/18°C, while radiant panels 16/19°C. In newly constructed buildings only radiant panels are supposed to be delivering cooling demand.

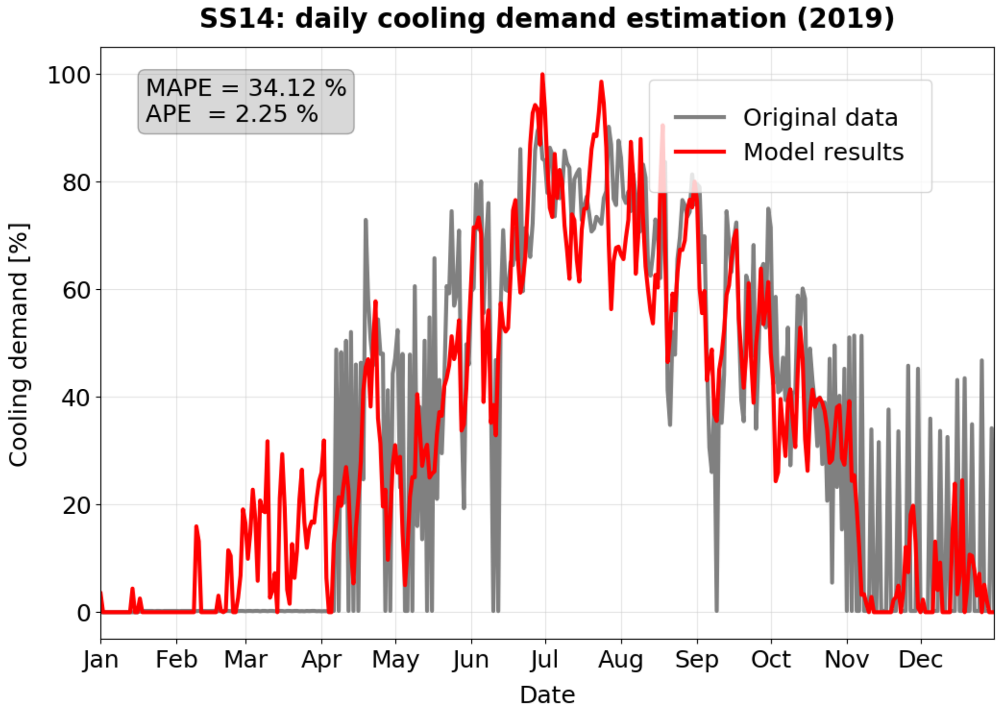

Figure A.8: Normalized profile of daily average cooling power supplied by substation SS14 and results of the calibrated model

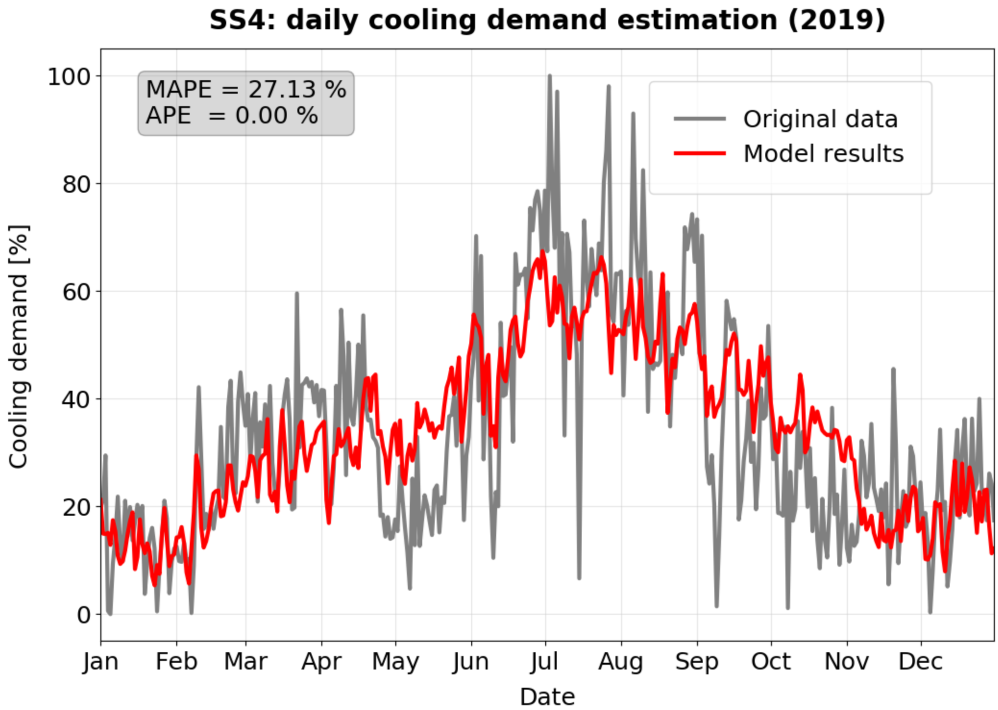

Figure A.9: Normalized profile of average daily cooling power supplied by substation SS4 and results of the calibrated model.

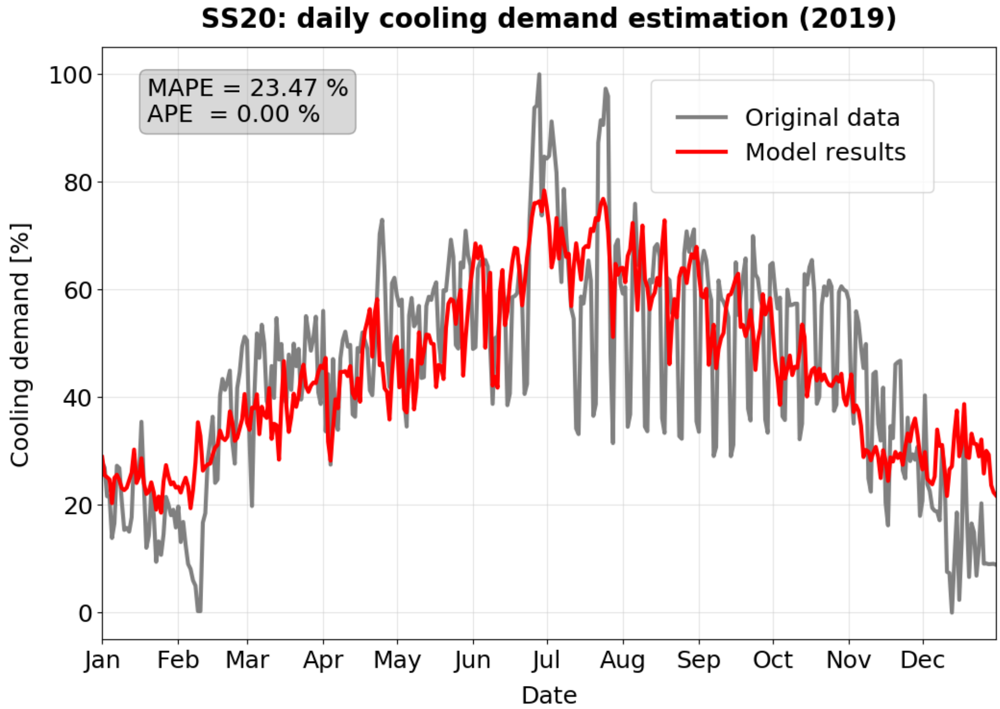

Figure A.10: Normalized profile of average daily cooling power supplied by substation SS20 and results of the calibrated model.

B Chapter 2: Optimal DES design additional information

B.1 Modelling assumptions and parameters

B.1.1 Water-water heat pump

Estimating the isentropic efficiency of the reference compressor

The compressor taken as reference is the following:

- Manufacturer: Bitzer Kuhlmaschinenbau GmbH [100]
- Type: Twin screw semi-hermetic
- Model: CSH8573-140Y-40P
- Refrigerant: HFC R134a

The manufacturer discloses the results of standardized tests (EN12900) publishing the refrigerant mass flow rate, heat evacuated and electric power as polynomial functions of the evaporating and condensing temperatures, as shown in Eq. B.1:

$$y = c_1 + c_2 \cdot T_e + c_3 \cdot T_c + c_4 \cdot T_e^2 + c_5 \cdot T_e \cdot T_c + c_6 \cdot T_c^2 + c_7 \cdot T_e^3 + c_8 \cdot T_c \cdot T_e^2 + c_9 \cdot T_e \cdot T_c^2 + c_{10} \cdot T_c^3 \tag{B.1}$$

where T_e and T_c are the refrigerant evaporating and condensing temperatures, respectively. Table B.1 reports the coefficients of the polynomials in Eq. B.1 for estimating the heat absorbed at the evaporator $\dot{Q}^e$, the compressor electric power $\dot{E}^{el}$ and the refrigerant mass flow rate $\dot{m}$.

The evaporating and condensing pressure levels can be calculated from the corresponding temperature at saturation conditions:

$$p_e = f(T_e, x = 0) \tag{B.2a}$$

$$p_c = f(T_e, x = 0) \tag{B.2b}$$

Table B.1: Coefficients of Eq. B.1 with validity range $T_e \in [-20;25]$ and $T_c \in [20;70]$

	c_1	c_2	c_3	c_4	c_5	c_6	c_7	c_8	c_9	c_{10}
$\dot{Q}^e$ **[W]**	313910,89	12170,23	-1733,45	199,12	-60,92	-13,20	1,20	-1,34	-0,36	0,00
$\dot{P}^{el}$ **[W]**	31630,71	765,97	343,16	17,03	-18,38	2,55	0,16	-0,26	0,19	0,11
$\dot{m}$ **[kg/h]**	5283,33	172,21	18,96	2,22	1,32	-0,45	0,01	0,01	-0,02	0,00

From Table B.1 the compressor electric power and mass flow can be estimated and therefore the enthalpy change:

$$\Delta \mathrm{h}(\mathrm{T}_c, \mathrm{T}_e) = \frac{\dot{\mathrm{P}}(\mathrm{T}_c, \mathrm{T}_e)}{\dot{\mathrm{m}}(\mathrm{T}_c, \mathrm{T}_e)} \cdot 3600 \tag{B.3}$$

The thermodynamic properties at the sucking point of the compressor can also be estimated, based on the evaporating condition and the temperature increase due to the superheating $\Delta \mathrm{T}_{SH}$ (10°C according to the norm EN12900):

$$\mathrm{s}_{in} = f(\mathrm{T}_e + \Delta \mathrm{T}_{SH},\ \mathrm{p}_e) \tag{B.4a}$$

$$\mathrm{h}_{in} = f(\mathrm{s}_{in},\ \mathrm{p}_e) \tag{B.4b}$$

The enthalpy change of the isentropic compression is given by:

$$\Delta \mathrm{h}_{is} = f(\mathrm{p}_c,\ \mathrm{s}_{in}) - \mathrm{h}_{in} \tag{B.5}$$

And therefore the isentropic efficiency of the compressor can be calculated as $\eta_{is} = \Delta \mathrm{h}_{is}/\Delta \mathrm{h}$.

The results of the isentropic efficiency for the whole operating range of the machine are shown in Fig. 2.1.

Water-water heat pump model: additional parameters

Table B.2 reports the main assumptions of the water-water heat pump model.

Table B.2: Water-water heat pump modelling parameters.

Description	**Symbol**	**Value**	**Unit**
Superheating after evaporation	$\Delta \mathrm{T}^{SH}$	≥ 2	K
Minimum ΔT at the evaporator	$\Delta \mathrm{T}_e^{min}$	2	K
Minimum ΔT at the condenser*	$\Delta \mathrm{T}_c^{min}$	0	K
ΔT between inlet and outlet at the source side	-	4	K
Minimum temperature increase	$\Delta \mathrm{T}_{min}^{lift}$	10	K

$\star$ The minimum temperature difference in the condenser is neglected because of the presence of the superheating which would normally create a temperature difference.

Deviation between simple and advanced COP calculations

Figures B.1 and B.2 show the cumulative number of hours of occurrence for different values of deviation between the advanced and simple COP calculation within the reference year of operation, for a potential central and decentralized HP, respectively. A point (X,Y) on the plot means that for Y% of the hours during the heating season, the deviation is less or equal than X%.

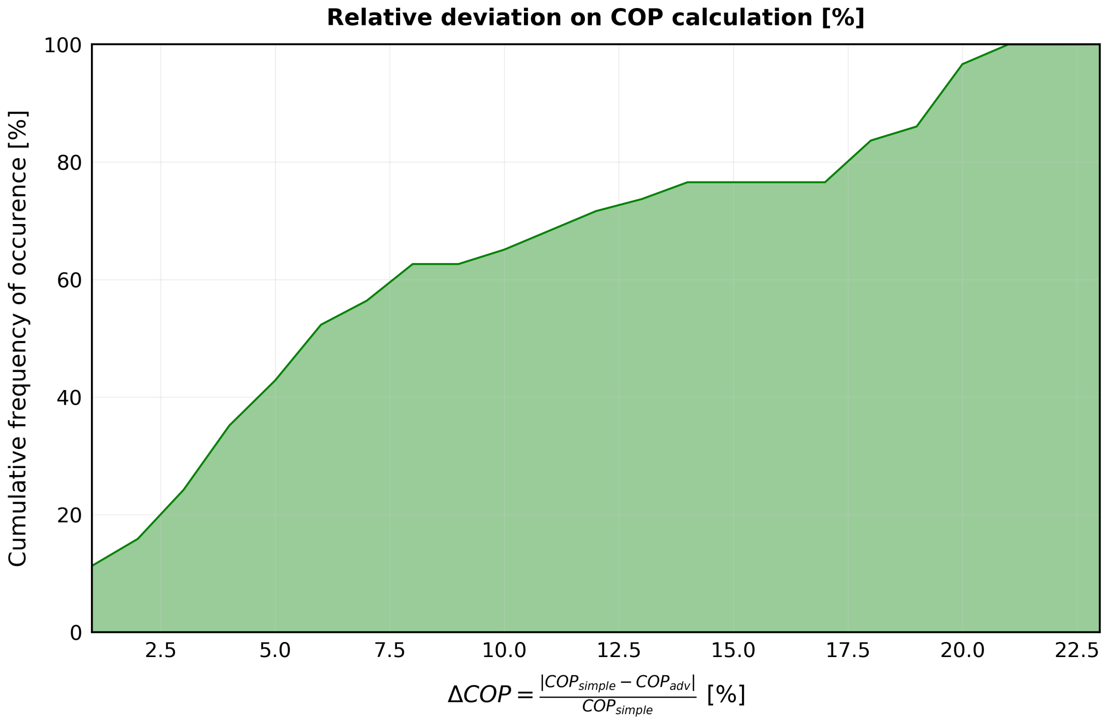

Figure B.1: Deviation of simple and advance COP calculation and cumulative frequency of occurrence over the reference year for a potential central plant.

B.1.2 Air-water heat pump

Air-water HPs are modelled in a simpler way with respect to the water-water configuration, assuming a constant Carnot efficiency during the operation. Table B.3 lists the main assumptions used for modelling this technology.

B.1.3 Chillers

The Carnot efficiency of the CHIs is supposed constant and equal to 0.2. Indeed, as reported in Fig. B.3 the variation of this efficiency with respect to variation of the source and sink temperatures is only marginal and therefore neglected in this study.

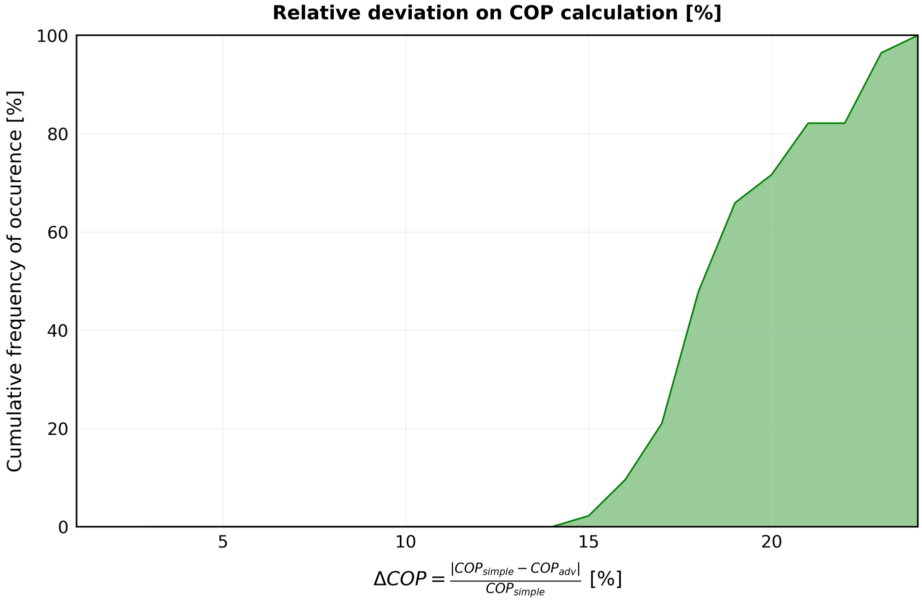

Figure B.2: Deviation of simple and advance COP calculation and cumulative frequency of occurrence over the reference year for a potential decentralized heat pump.

Table B.3: Air-water heat pump modelling parameters.

Description	**Symbol**	**Value**	**Unit**
Minimum ΔT at the evaporator	ΔT^{e}_{min}	3	K
Minimum ΔT at the condenser	ΔT^{c}_{min}	1.5	K
Carnot efficiency	η_{II}	0.5	-
ΔT between inlet and outlet at the sink side	-	10	K

Moreover, to avoid very high unrealistic values of the COP at the decrease of the ambient temperature, a maximum value of 5 is taken. This value is chosen based on the maximum value registered within the range of the operating temperature reported in Fig. B.3 and showed in Fig. B.4

Table B.4 lists the main assumptions of the model for chillers

B.1.4 Electrical heaters

ELHs are simply modelled with two streams: a resource stream linked to the electricity layer and a hot thermal stream, representing the heat delivered. The two are linked through the device efficiency, as reported in Eq. B.6.

$$\Delta\dot{H}_{s,t} = \eta_{ELH} \cdot \dot{M}^{+,ref}_{ELH,el,t} \cdot f_{ELH,t} \qquad \forall\ t \in \mathbf{T}, \forall\ s \in \mathbf{HS}_{elh}, \forall elh \in \mathbf{ELH} \quad \text{(B.6)}$$

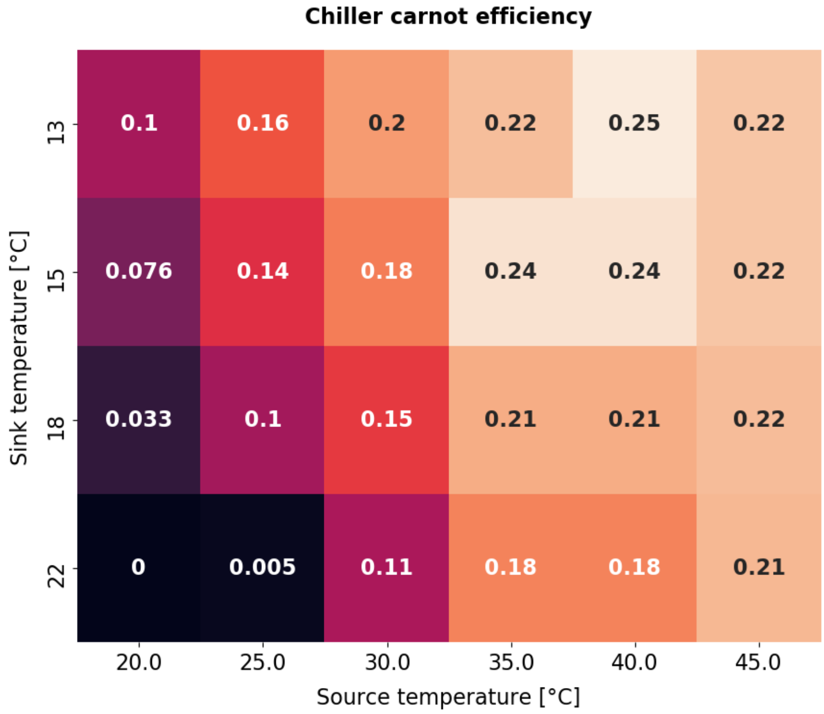

Figure B.3: Chillers Carnot efficiency at varying source and sink temperatures (source: [54]).

Table B.4: Chiller modelling parameters.

Description	Symbol	Value	Unit
Minimum ΔT at the evaporator	ΔT_e^{min}	2	K
Minimum ΔT at the condenser	ΔT_c^{min}	1.5	K
Carnot efficiency	η_{II}	0.2	-
Maximum COP	COP^{max}	5	-

The device electric efficiency is assumed equal to 0.99 [54].

B.1.5 Natural gas boilers

The model of natural gas BOIs includes two streams: a thermal stream defining the useful heat released by the boiler and the resource stream of natural gas representing the input to the unit. As reported in Eq. B.7 the two streams are correlated by the efficiency of the boiler η_{BOI} assumed equal to 0.85.

$$\Delta\dot{H}_{s,t} = \eta_{BOI} \cdot \dot{M}^{+,ref}_{BOI,NG,t} \cdot f_{BOI,t} \qquad \forall\ t \in \mathbf{T}, \forall\ s \in \mathbf{HS}_{boi}, \forall boi \in \mathbf{BOI} \quad (B.7)$$

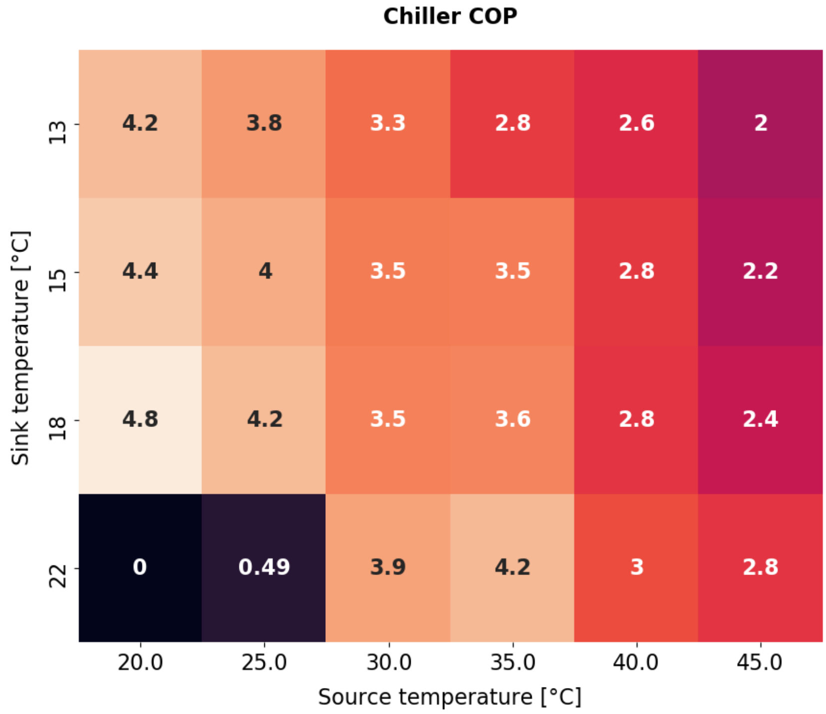

Figure B.4: Chillers COP at varying source and sink temperatures (source: computed from [54]).

B.1.6 Photovoltaic panels

Photovoltaic (PV) panels are included as a simple model with a constant efficiency. The sizing dimension is the installed square meters, linked to the unit electricity production through the modules efficiency and the solar global irradiation as reported in Eq. B.8.

$$\dot{M}^{-}_{PV,el,t} = \eta_{PV} \cdot \mathrm{GHI}_t \cdot f_{PV} \qquad \forall\ t \in \mathbf{T}, \forall\ PV \in \mathbf{PV} \quad \text{(B.8)}$$

The modules efficiency is assumed equal to 0.2. Unlike all other units that could be used at partial load (by means of Eq. 2.2), PV, if installed, always produce electricity according to the solar irradiation and the module efficiency, rather than varying with the partial load. Therefore, for these units Eq. 2.2 is replaced by Eq. B.9.

$$f_{u,t} = f_u \qquad \forall\ t \in \mathbf{T}, \forall\ u \in \mathbf{PV} \quad \text{(B.9)}$$

The maximum bound of the unit multiplication factor $\mathrm{F}^{\max}_{PV}$ is chosen for each building depending on the building's available roof surface.

B.1.7 Cost functions coefficients

The interest rate and life-time in Eq. 2.44 are chosen as:

- i is the interest rate, assumed as 0.06;
- n_u is the machines life time assumed as 20 years for all technologies;
- n_n is the network life time assumed as 40 years.

Table B.5 lists the parameters for the cost functions of the different technologies and resources.

Table B.5: Cost function coefficients.

	Ref. size	$\mathbf{C^{inv,1}}$ **[kCHF]**	$\mathbf{C^{inv,2}}$ **[CHF/size]**	$\mathbf{C^{op}}$ **[CHF/size/h]**
Technology				
HP CT*	kW_{el}	43.02	891	0
HP*	kW_{el}	1.93	8826	0
CH*	kW_{el}	1.93/43.02	8826/891	0
HEX*	kW_{th}	2.35	71	0
PV†	m^2	17.78	253.76	0
ELH‡	kW_{th}	968	13	0
BOI‡	kW_{th}	3800	105	0
Pipe DN50§	m	0	520	0
Pipe DN100§	m	0	656	0
Pipe DN125§	m	0	751	0
Pipe DN200§	m	0	924	0
Pipe DN250§	m	0	1023	0
Pipe DN300§	m	0	1096	0
Resources				
Ground source water	kW_{th}			0.02
Electricity buying	kW_{el}			0.20
Electricity selling	kW_{el}			-0.06
Natural gas	kW_{NG}			0.10

* Source: adjusted from [83]
† Source: [101]
‡ Source: adjusted from [54]
§ Source: [102] (extrapolated if needed)

B.2 Linearization of product among binaries

The product between two generic binaries y_1 and y_2 is linearized by introducing a new binary variable z. The product $y_1 \cdot y_2$ can only be non-zero if both of them equal one, thus $y_1 = 0$

and/or $y_2 = 0$ implies that $z = 0$, which is enforced by Eqs. B.10a and B.10b.

$$z \leq y_1 \tag{B.10a}$$

$$z \leq y_2 \tag{B.10b}$$

Finally, Equation B.11 states that z equals one if the product between y_1 and y_2 equals one, which happens only if both of them equal one:

$$z \geq y_1 + y_2 - 1 \tag{B.11}$$

B.2.1 Definition of network temperatures

For each network, one or more operating temperature can be defined as couples of supply and return temperatures. The temperature of the anergy and cooling network is not subject to optimization and linked to the temperature of the available LTH. This temperature is assumed to remain constant at 10°C and a fixed ΔT of 2 K between the supply and return is imposed. For the heating network (HN), temperatures can be defined as linear functions of the ambient temperature, as previously shown in Fig. 2.12 or modified to supply DHW. These profiles follow an heating curve until the temperature reaches that demanded by the DHW and remain constant at higher ambient temperatures. In this case the return temperature is constructed such that a ΔT of 10°C is respected at design conditions. Potential network profiles able to cover DHW demand are reported in Fig. B.5.

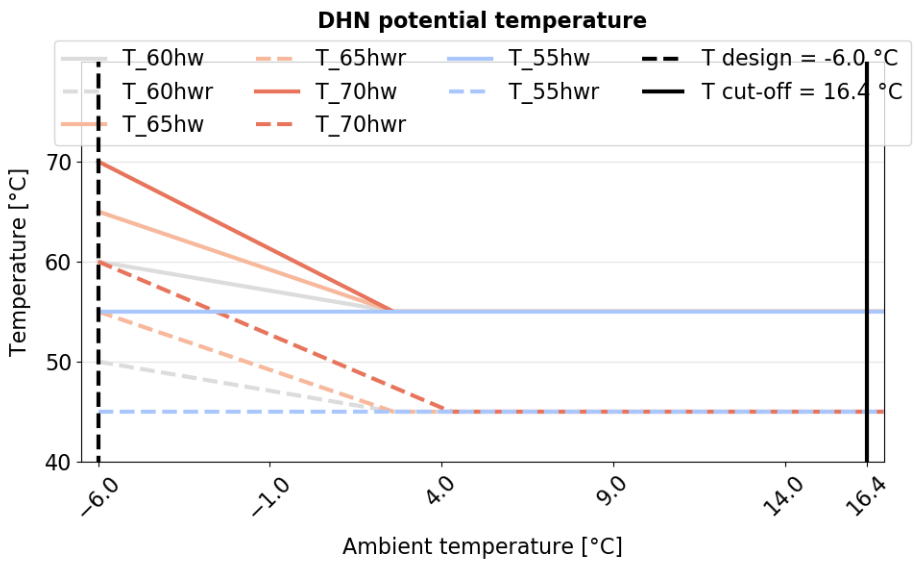

Figure B.5: Example of heating network temperature profiles for the coverage of DHW demand. Profiles denoted with "hw" are assigned to the feeding line, while the ones denotes with "hwr" are for the corresponding return line.

B.3 Definition of thermal losses

For each network diameter and operating temperature a loss factor coefficient q_{dn}^{loss}, expressed in [kW/K/m], is defined. This coefficient is used in Eq. 2.24 to estimate the heat losses associated to the operation of the HN. Table B.6 reports the piping information and assumed maximum velocity for different pipes diameters.

Table B.6: Pipe details. Sources: adapted by extrapolation if needed from [22, 102].

D_i	D_p	D_e	v
50	60.3	140	1
65	76.1	160	1.12
80	88.9	180	1.24
100	114.3	225	1.4
125	139.7	250	1.5
200	219.1	355	2.1
250	272	425	2.3
300	324	495	2.5
600	624	915	3

D_i represents the internal pipe diameter, D_p includes the pipe thickness, D_e the layer of insulation and v is the maximum flow velocity associated to each pipe. For all the pipes the conductive thermal coefficient of the insulation layer and pipe wall are assumed as $k_s = 0.025$ [W/m^2/K] and $k_p = 0.21$ [W/m^2/K], respectively. It is assumed that losses are covered by the central plant and no losses are assigned to the anergy and cooling networks. Losses are estimated considering piping installed both above the ground and buried. The former is employed in the case that pipes are installed in technical rooms, as common in non-residential building blocks, such as commercial buildings or university campuses.

B.3.1 Above ground piping

Given a mass flowing at temperature T_i inside a pipe of length L and surrounded by the environment at temperature $T_\infty < T_i$, due to the second principle of thermodynamics heat is naturally transferred from the fluid to the surroundings. The mechanisms governing such a transfer are: forced convection inside the pipes, conduction through the pipe walls and the insulation and finally natural convection and radiation with the surrounding. Losses due to natural convection and radiation with the surrounding are neglected due to their lower contribution with respect to the other mechanisms. Losses can be expressed considering the pipe as a HEX: water at inlet temperature T_i exchanges the heat $\dot{Q}_{loss}$ with the environment, supposed at a constant temperature T_∞. As a result, the water temperature decreases by a ΔT_{loss}. The exchange occurs through the pipe walls characterized by an overall heat transfer coefficient U and exchange surface A.

$$\dot{Q}_{loss} = UA \log \frac{(T_i - T_\infty) - (T_i - \Delta T_{loss} - T_\infty)}{(T_i - T_\infty)/(T_i - \Delta T_{loss} - T_\infty)} \tag{B.12}$$

The overall heat transfer coefficient U can be estimated through the analogy with an electric circuit, where all the resistances due to the different heat transfer mechanisms are in series.

$$U^{-1} = R_{tot} = R_i + R_c \tag{B.13}$$

R_i refers to the forced convection inside the pipe and R_c gathers the conductive heat transfer through the pipe walls and the insulation thickness. Finally to estimate the overall losses the ones of the feeding and returning lines have to be summed up.

The resistance associated to the heat transferred by forced convection can be expressed in the case of a circular pipe as follows:

$$R_i = \frac{1}{h_i 2\pi r_i L} \tag{B.14}$$

where r_i is the internal pipe diameter, L the pipe length, and h_i the convective heat transfer coefficient, which can be estimated from the Nusselt number as reported in Eq. B.15.

$$h_i = \mathrm{Nu_D} \frac{k}{D_i} \tag{B.15}$$

k is the thermal conductivity in []W/m^2/K] and D_i the pipe internal diameter. The Nusselt number for turbulent flow can be estimated thorough the Gnielinski's relation, as follows:

$$\mathrm{Nu_D} = \frac{(f/8)(\mathrm{Re_D} - 1000)\mathrm{Pr}}{1 + 12.7\sqrt{f/8}(\mathrm{Pr}^{2/3} - 1)} \tag{B.16}$$

The correlation is valid in the interval $2300 \leq \mathrm{Re_D} \leq 5 \cdot 10^6$ and $0.6 \leq \mathrm{Pr} \leq 10^5$, where $\mathrm{Re_D} = \frac{vD\rho}{\nu}$ is the Reynolds number and $\mathrm{Pr} = \frac{\xi}{\alpha} = \frac{\mu}{\rho\alpha}$ is the Prandtl number.
The friction factor f for smooth pipes may be computed from Filonenko's equation:

$$f = \frac{1}{(1.82 \log_{10} \mathrm{Re_D} - 1.64)^2} \tag{B.17}$$

The resistance opposed to the heat flux by the pipes walls and the insulation thickness can be calculated by summing up the two contributions:

$$R_c = \frac{\ln(r_p/r_i)}{k_p 2\pi L} + \frac{\ln(r_e/r_p)}{k_s 2\pi L} \tag{B.18}$$

where k_p is thermal conductivity of the pipe walls and k_s is the one of the insulation material.

The estimated losses for the supply and return pipes are consequently summed up and referred to the nominal heat delivered, as reported in B.19:

$$\dot{Q}_{loss,rel} = \frac{\dot{Q}_{loss,f} + \dot{Q}_{loss,r}}{\dot{m}c_p(T^f - T^r)} \tag{B.19}$$

where T^f and T^r are respectively the temperature in the feeding and returning pipe inlet, while mass flow rate and heat capacity are computed at a mean temperature $(T^f + T^r)/2$. Losses computed over different distances and at multiple temperatures are reported in Fig. B.6. The difference between supply and return temperatures is always assumed equal to 10°C. The temperature loss on the graphs refers to the feeding pipe.

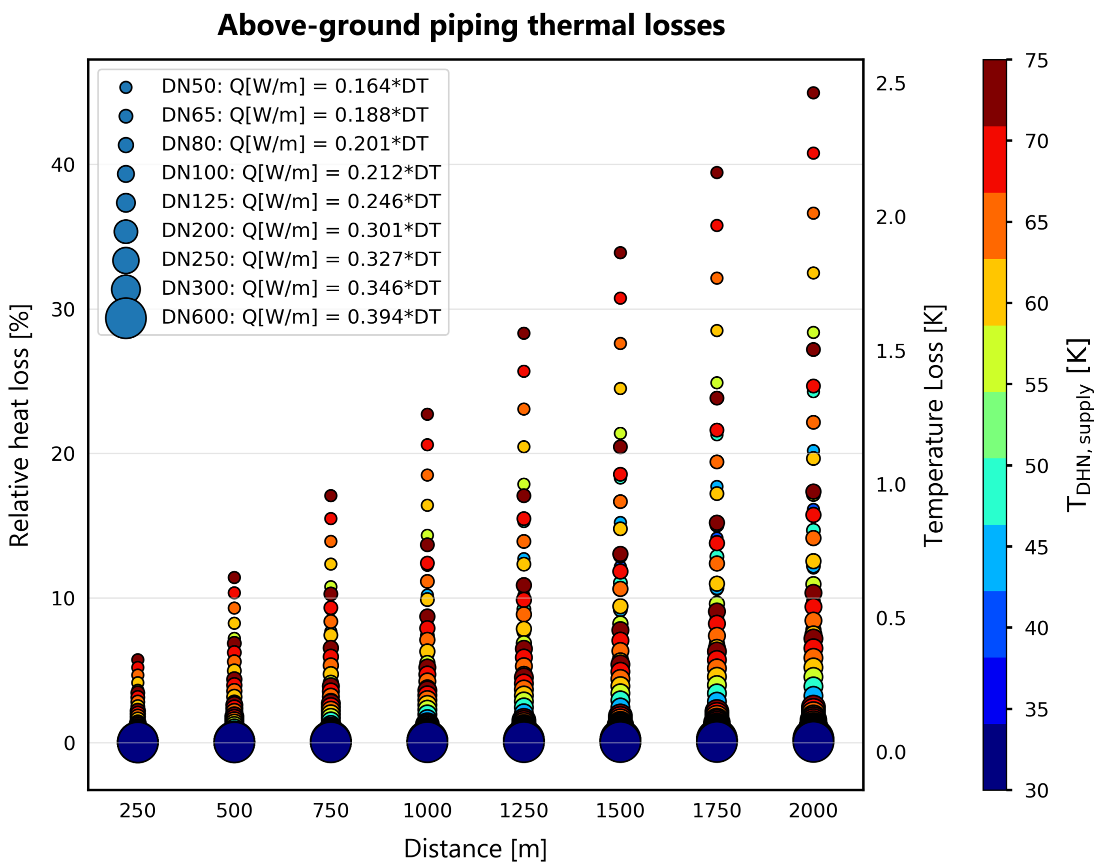

Figure B.6: Thermal losses calculation. In the legend: expression for thermal losses of a single pipe of indicated diameter and with a temperature difference ΔT with the surrounding.

The effect of the mass flow rate is investigated by computing the losses for two pipe diameters (respectively DN50 and DN200) under different reduction in flow velocity. Results are reported in Fig. B.7, which shows that the influence of the flow velocity is greater for smaller tubes, but the overestimation made by assuming the flow at a constant maximum speed is minor.

Similarly the effect of the temperature on thermal losses is investigated by computing the

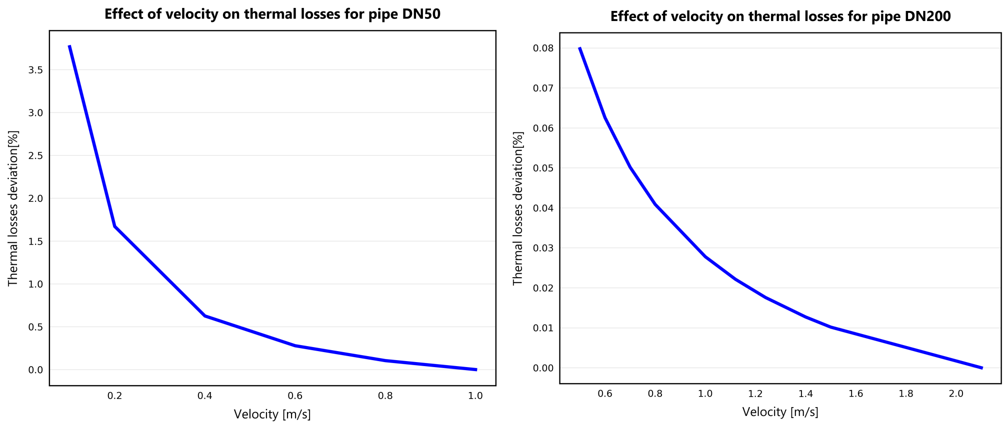

(a) Thermal losses for DN50 at different flow velocity.

(b) Thermal losses for DN200 at different flow velocity.

Figure B.7: Effect of flow velocity on thermal losses.

losses at different flow temperatures. Figure B.8 shows the results respectively for DN50 and DN200, highlighting a linear relation between the losses and the flow temperature and the satisfying quality of the estimation based on the parameters reported in Fig. B.6.

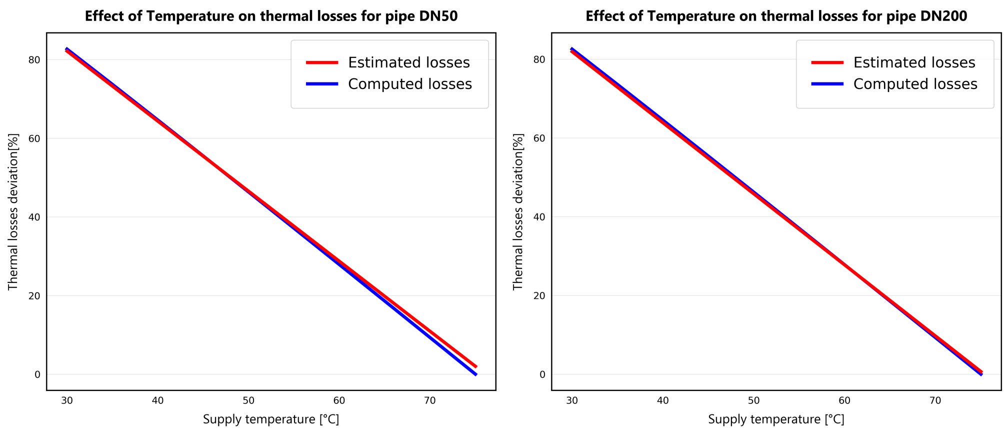

(a) Thermal losses for DN50 at flow temperatures.

(b) Thermal losses for DN200 at different flow temperature.

Figure B.8: Effect of flow temperature on thermal losses.

B.3.2 Under-ground piping

For pipes placed underground, the mechanism of natural convection is replaced with conduction through the ground, that cannot be anymore neglected as in the previous case. Moreover, the mutual interaction of the nearby feeding and returning pipe must be taken into account as well as the resistance at the surface of the ground. The latter mechanisms are implemented following the formulation reported in [103].

Equation B.12 holds also in case of under-ground pipelines, with the proper estimation of the overall heat transfer coefficient. Therefore, the same approach to compute the temperature drop across the pipes can be applied.
The resistance at the ground is converted to an equivalent layer of soil with a corrected pipe depth calculated according to:

$$H = H' + \frac{k_g r}{h_{gs}} \tag{B.20}$$

where the heat transfer coefficient at the ground surface can be assumed equal to 14.6 [W/m^2/K], as reported in [104]. With the corrected pipe depth the ground resistance is computed as:

$$R_g = \frac{\ln(2H/(r_e))}{k_g r 2\pi L} \tag{B.21}$$

The mutual interaction of the feeding and returning lines is taken into account by the resistance expressed as follows:

$$R_m = \frac{\ln(1 + (2H/E)^2)}{k_g 4\pi L} \tag{B.22}$$

where E is the distance between the centers of the feeding and returning pipelines. In case of symmetrical pipes the heat loss coefficients can be calculated as reported in Eqs. B.23a and B.23b.

$$U_1 = \frac{R_i + R_c + R_g}{(R_i + R_c + R_g r)^2 - R_m^2} \tag{B.23a}$$

$$U_2 = \frac{R_m}{(R_i + R_c + R_g r)^2 - R_m^2} \tag{B.23b}$$

Consequently, the heat losses in the feeding line can be estimated through Eq. B.24a, while those in the return by Eq. B.24b.

$$\dot{Q}_{loss,f} = (U_1 - U_2)(T^f - T_g r) + U_2(T^f - T^r) \tag{B.24a}$$

$$\dot{Q}_{loss,r} = (U_1 - U_2)(T^r - T_g r) - U_2(T^f - T^r) \tag{B.24b}$$

$T_g r$ is the ground temperature. Losses computed for different diameters, distances, and at multiple temperatures for buried pipes are reported in Fig. B.9. The difference between supply and return temperatures is always assumed equal to 10°C. The temperature loss on the graphs refers to the supply pipeline.

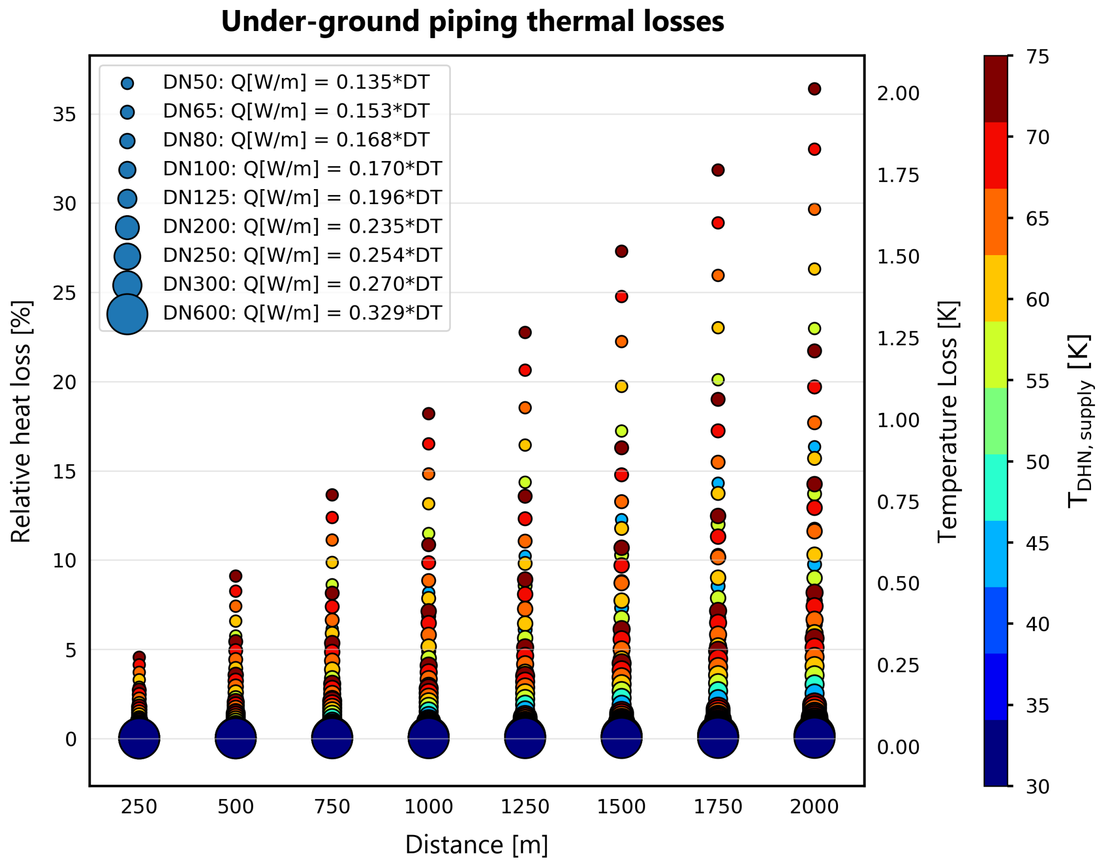

Figure B.9: Thermal losses calculation. In the legend: expression for thermal losses of a single pipe of indicated diameter and with a temperature difference ΔT with the surrounding.

Given the linearity of the thermal losses with respect to changes in temperatures and the marginal effect of the flow rate the expression in Eq. 2.24 is considered as a good approximation. Moreover, due to the marginal difference of temperature in the fluid, as visible in Figs. B.6 and B.9, this effect is neglected during the optimization.

B.4 Additional results

Figures B.10 to B.13 show the heating and cooling signatures with corresponding supply and return temperatures of the distribution system assigned to the buildings according to the different usage, construction period and eventually renovation.

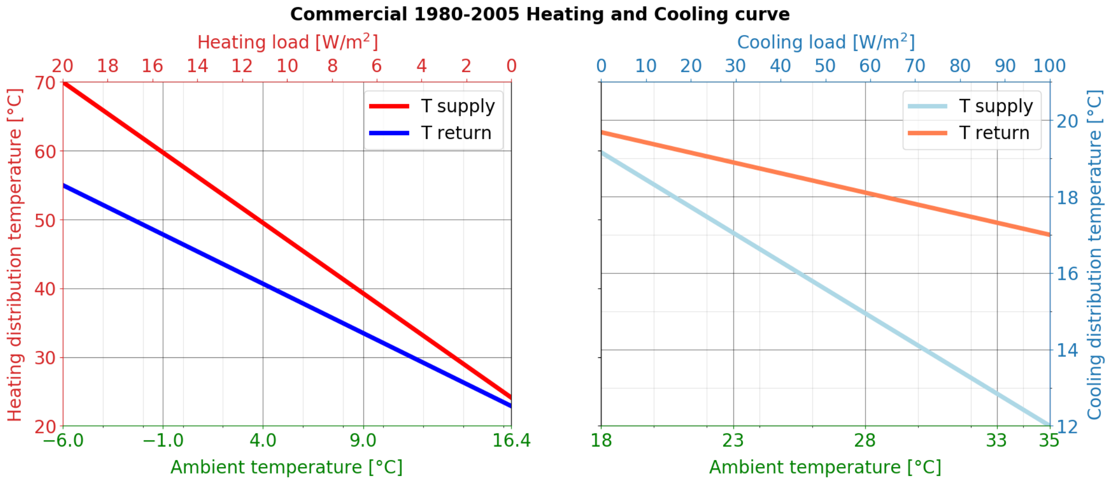

Figure B.10: Heating and cooling signature for a building of commercial usage, constructed in the period 1980-2005.

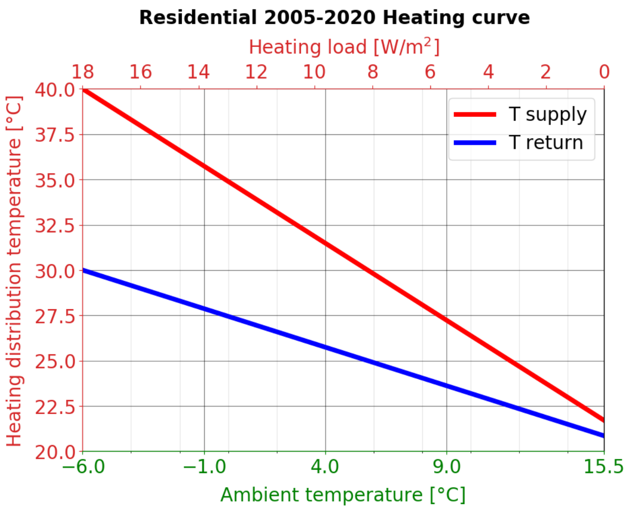

Figure B.11: Heating and cooling signature for a building of residential usage, constructed in the period 2005-2020.

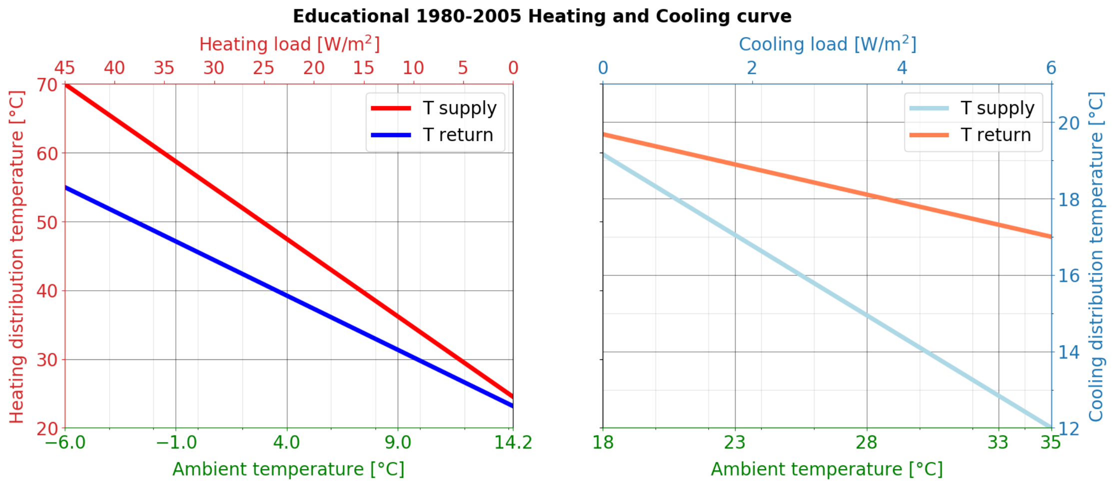

Figure B.12: Heating and cooling signature for a building of educational usage, constructed in the period 1980-2005

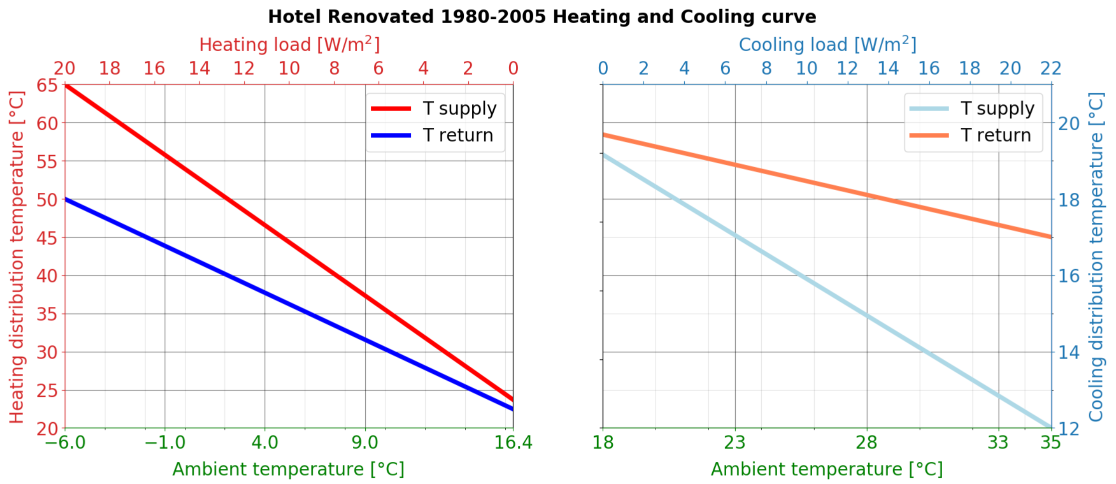

Figure B.13: Heating and cooling signature for an hotel building, constructed in the period 1980-2005 and renovated.

B.4.1 Pareto frontiers for network temperatures enabling DHW supply

Figures B.14 to B.16 show the Pareto frontiers (and corresponding fully centralized solutions[1]) for HN temperature profiles defined to cover DHW and the anergy network (AN) configuration, in the CAPEX-OPEX, CAPEX-KPI^{env} and CAPEX-Ex_{loss} domains, respectively.

[1]Design obtained by constraining the use of standalone units to the only CHIs for the coverage of refrigeration needs.

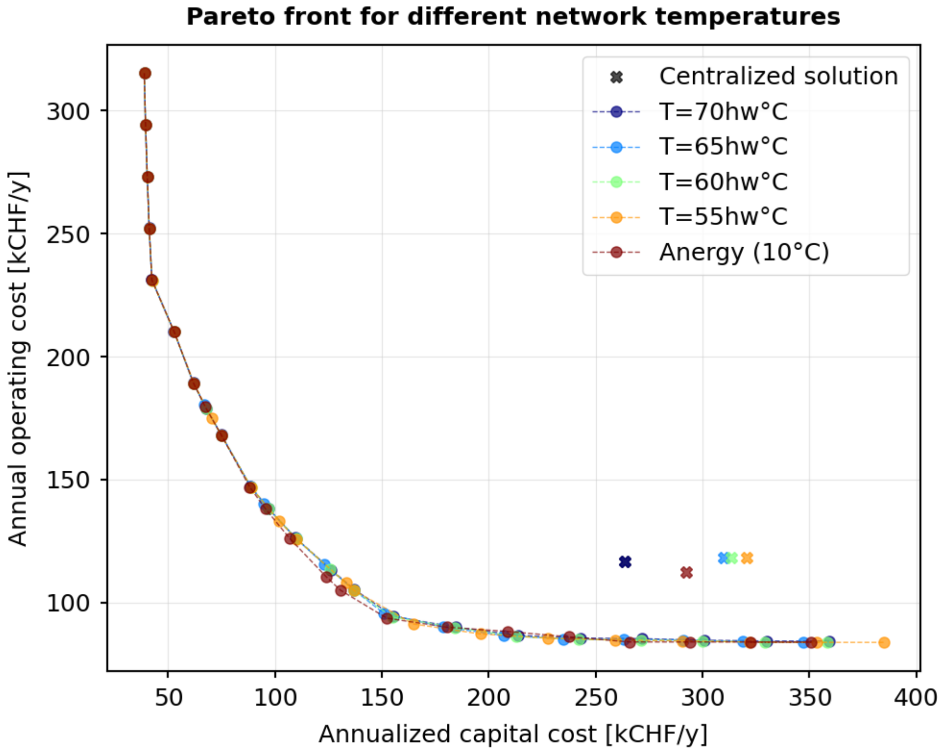

Figure B.14: Pareto-optimal solutions for different HN temperatures including DHW coverage and the AN. Centralized solutions represent designs excluding standalone units.

B.4.2 Results for the configuration equipped with the anergy network

For the Pareto-optimal solutions and the fully centralized one related to the configuration with the AN, Figs. B.17 to B.20 show respectively: the capacity of technologies installed and equivalent operating hours at full load, the breakdown of the capital cost, the way how heating and cooling requirements are satisfied and finally the network expansion at increasing capital investment allowance.

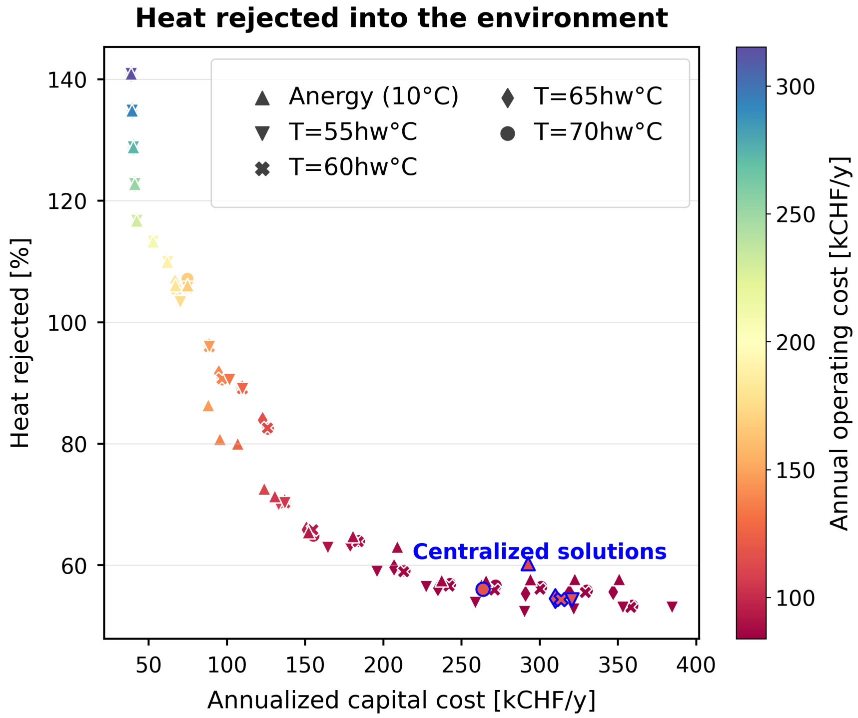

Figure B.15: Pareto optimal solutions for different HN temperatures including DHW coverage and the AN plotted in the CAPEX-KPI^{env} domain. Centralized solutions represent designs excluding standalone units.

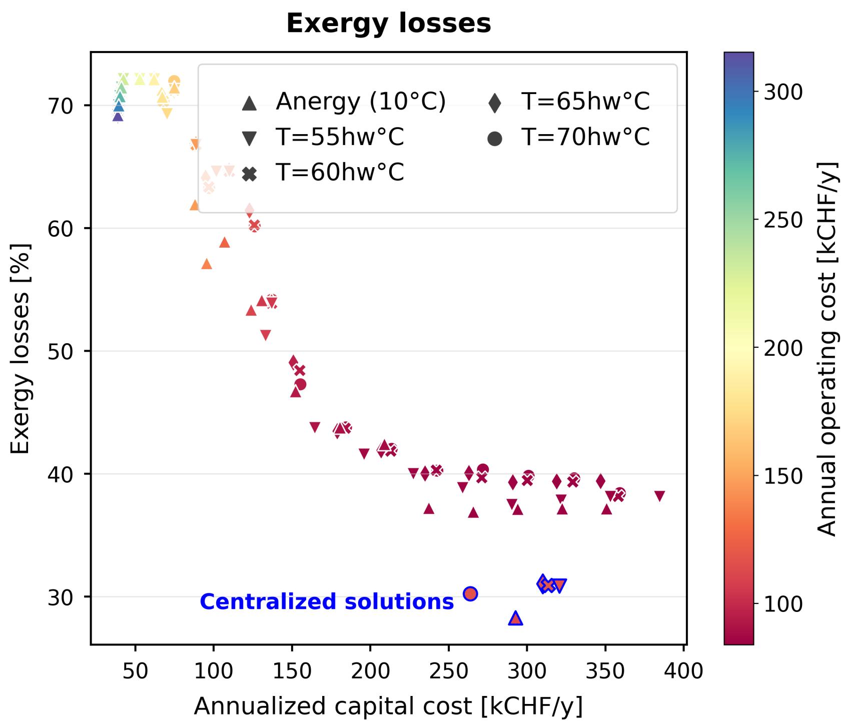

Figure B.16: Pareto optimal solutions for different HN temperatures including DHW coverage and the AN plotted in the CAPEX-Ex_{loss} domain. Centralized solutions represent designs excluding standalone units.

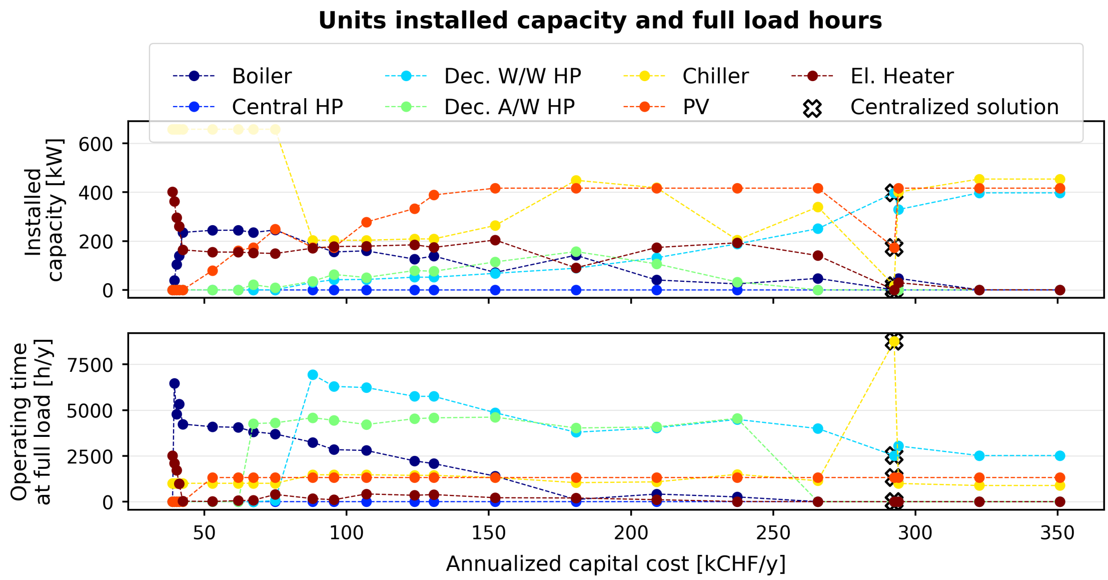

Figure B.17: Units installed capacity and equivalent full load operating hours for the Pareto-optimal configurations (and fully centralized one) related to the AN. Capacity expressed as KW_{el} for PV and ELH, as kW_{th} at the condenser for the HP, as kW_{th} at the evaporator for the CHI and as kW_{th} of heat delivered for the BOI.

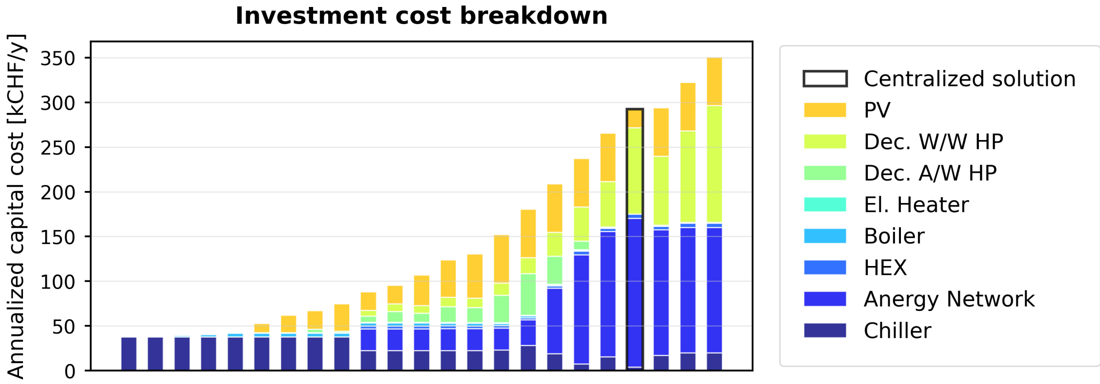

Figure B.18: Annualized investment cost breakdown for the Pareto-optimal configurations (and the fully centralized one) related to the AN.

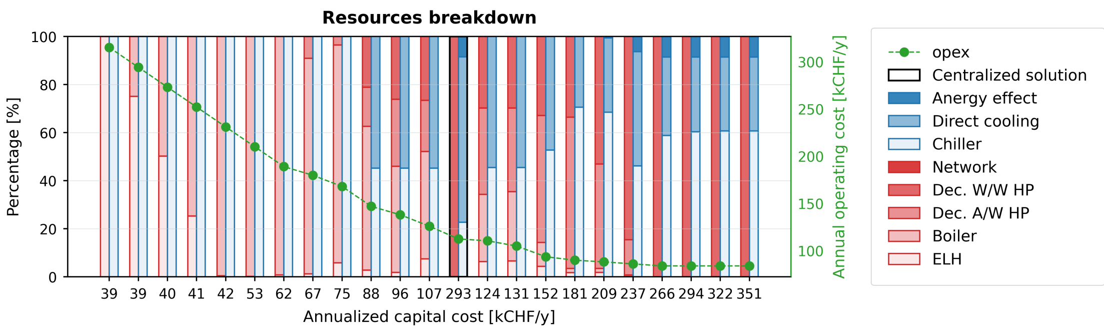

Figure B.19: Breakdown of heating and cooling demand coverage and capital and operating expenses for the Pareto-optimal configurations (and the fully centralized one) related to the AN.

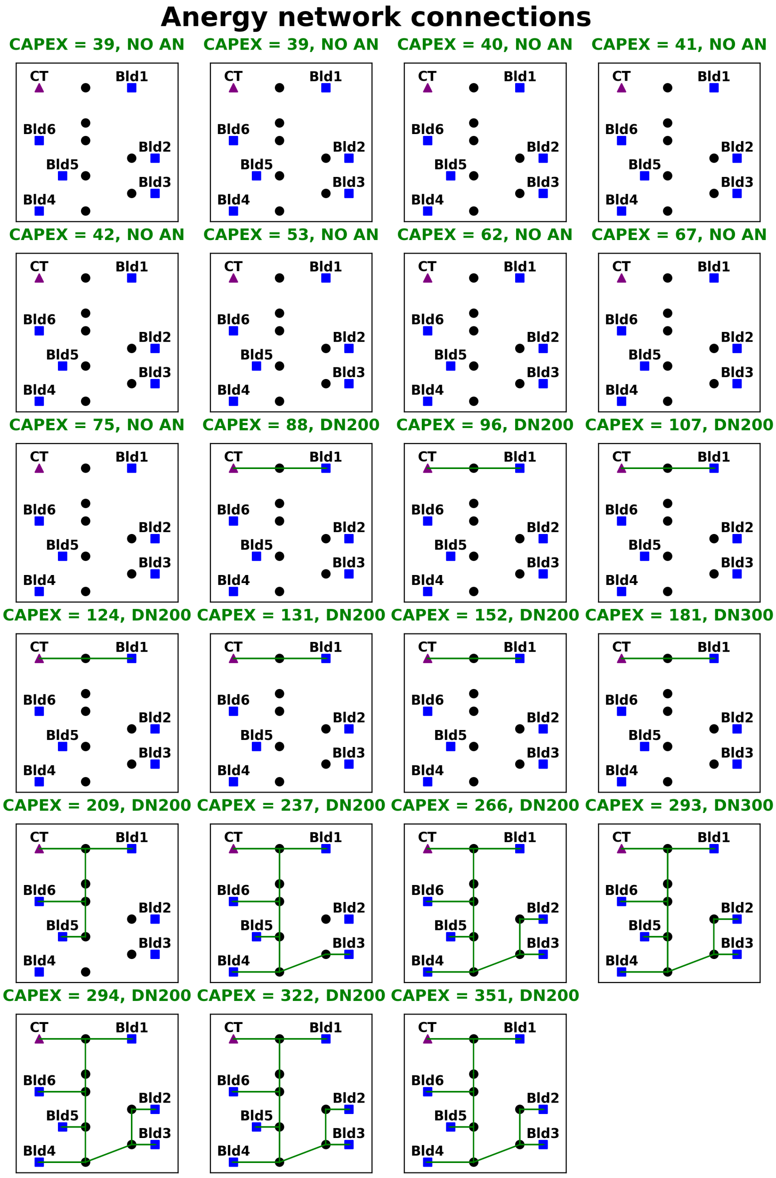

Figure B.20: Layout of the distribution network for configurations with the AN. Capital cost expressed in kCHF/y.

C Chapter 3: Optimal DES retrofit additional information

C.1 Modelling assumptions and parameters

C.1.1 Definition of network temperatures

For the two HNs, the existing and the potentially newly installed one, the operating temperatures are defined through the optimization process. On the contrary, the temperature of the AN is not subjected to any optimization and considered linked to the temperature of the lake water. Three level of temperatures are defined:

- Winter operation (4^{th}, 5^{th} and 6^{th} typical operating periods + extreme heating condition): $T_{AN}^{f/r} = 5/3$°C
- Summer operation (1^{st} and 7^{th} typical operating periods + extreme cooling condition): $T_{AN}^{f/r} = 15/17$°C
- Mid-season operation (2^{nd} and 3^{rd} operating periods): $T_{AN}^{f/r} = 11/9$°C

C.1.2 Chillers

The potential working conditions of the CHIs are listed in table Table C.1. A maximum condensing temperature T_c^{max} of 50°C is assumed.

Beyond the existing machines, in each location the possibility of installing new chillers is given. The latter are modelled as the existing machines, except for an increase Carnot efficiency for all operating modes involving both source and sink at liquid state from 0.4 to 0.6.

Table C.1: Chillers operating modes.

Mode	**T^e [°C]**	**T^c [°C]**	
Cooling	12	$T^{amb} + 1.5$	
Cooling + Heating	T^r_{AN}	T_c^{max*}	
Cooling + Heating	T^r_{AN}	T^f_{HN1} *	if $T^f_{HN1} < T_c^{max}$
Cooling + Heating	T^r_{AN}	T^f_{HN2} *	if $T^f_{HN2} < T_c^{max}$
Cooling + Heating + DHW	T^f_{AN}	T_c^{max**}	

* The temperature profile follows a heat curve.
** To supply DHW the temperature profile is kept constant at 50°C instead of following an heat curve.

C.1.3 Thermal storage

As mentioned in the chapter the storage model is included only to take into account the thermal capacity of the network and overcoming the uncertainty on the definition of the heating and cooling profiles. The latter is particularly important to investigate synergies between the two requirements. Moreover, considering that the the water is stored at the temperature of the LTH, close to the ambient conditions, losses for self discharge are neglected, as well charging and discharging efficiency. The maximum storage volume is assumed equal to 565 l, which is the volume of water contained in a potential AN which would connect the furthest user needing cooling demand. Table C.2 lists the model parameters and values.

Table C.2: Thermal storage model coefficients.

Description	**Symbol**	**Value**	**Unit**
Self discharging loss coefficient	σ_s	1	[-]
Charging efficiency	η_s^+	1	[-]
Discharging efficiency	η_s^-	1	[-]
Maximum storage volume	V_s^{max}	565	l

Eventual changes of the storage capacity due to a different AN layout are neglected.

C.2 Additional results

Figure C.1a shows the breakdown of the total cost for the Pareto-optimal solutions listed in Table 3.6, relative to the advanced solving strategy which includes the upper bound of the network investment cost among the variables optimized at the master level. Figure C.1b shows for the same configurations how the heating and cooling demand are supplied.

Figure C.1: Results of the Pareto optimal solutions listed in Table 3.6.

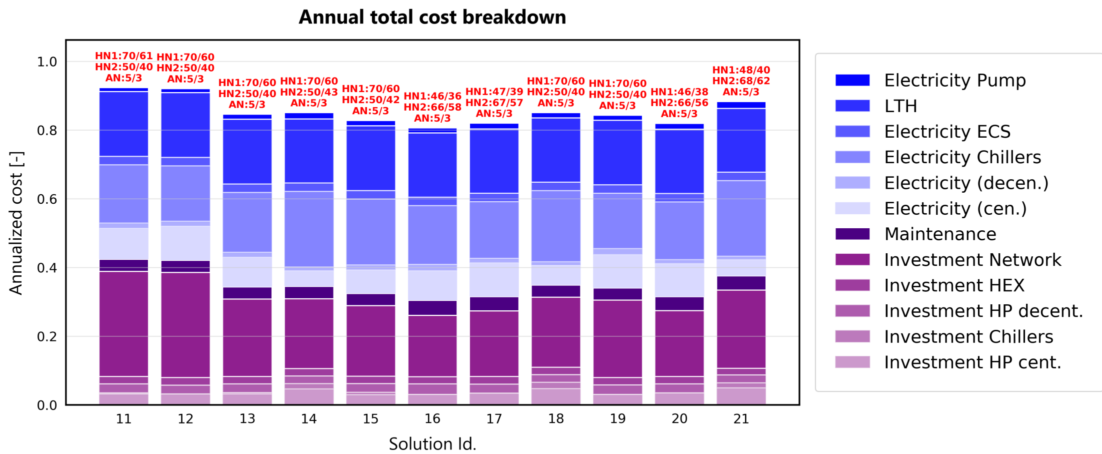

(a) Annual total cost breakdown. Values normalized with respect to the total cost of the reference configuration.

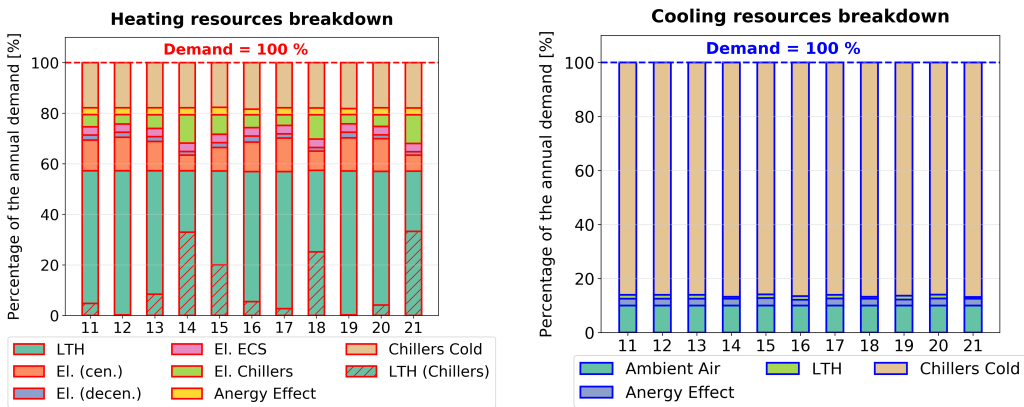

(b) Energy breakdown of resources employed to supply the heating (on the left) and the cooling (on the right) demand.

Figure C.2 shows for the same set of solutions the installed capacity of the conversion technologies. Values are expressed in terms of heating power at the condenser, normalized with respect to the heating peak demand.

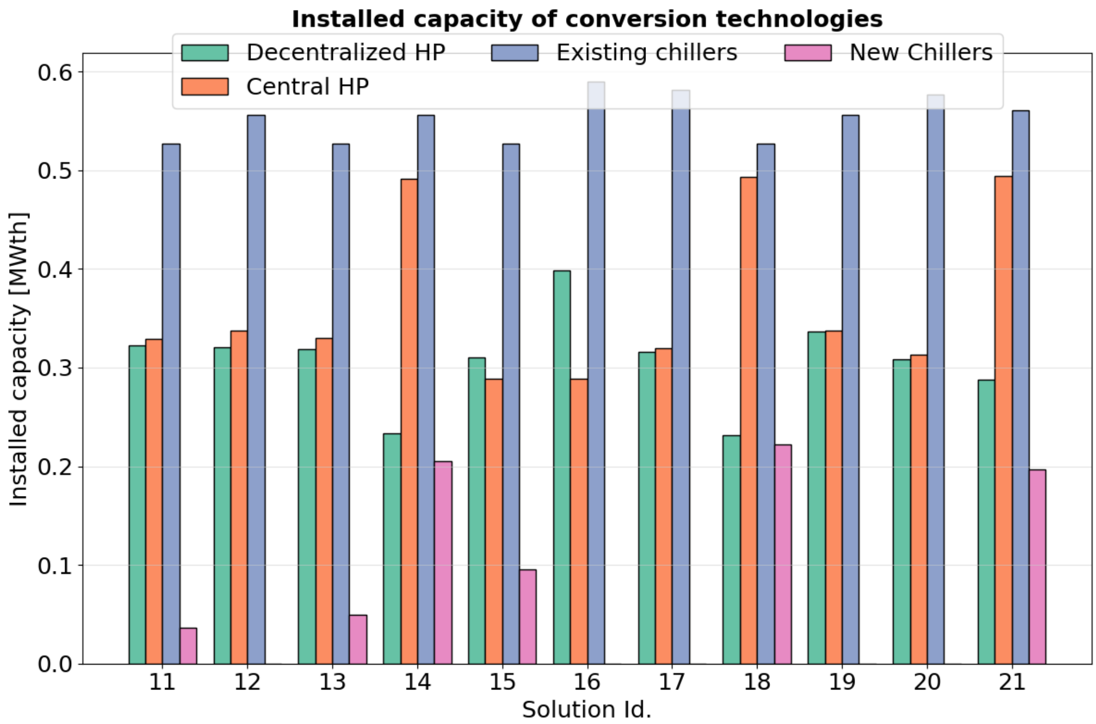

Figure C.2: Installed capacity of conversion technologies for Pareto optimal solutions listed in Table 3.6. Values normalized with respect to the heating peak demand. Capacity referred to the heat rejected at the condenser.

Bibliography

[1] IEA. *Global Energy Review 2020. The impacts of the Covid-19 crisis on global energy demand and CO2 emissions*. Tech. rep. 2020, p. 55.

[2] Alkiv, Sverre and Irvine, Mark. *Impact of COVID on energy transition*. Tech. rep. DNK, June 2020. URL: (visited on 05/18/2021).

[3] Le Quéré, Corinne et al. "Temporary reduction in daily global CO 2 emissions during the COVID-19 forced confinement". *Nature Climate Change* 10.7 (July 2020). Number: 7 Publisher: Nature Publishing Group, pp. 647–653. ISSN: 1758-6798. DOI: 10.1038/s41558-020-0797-x. URL: (visited on 05/18/2021).

[4] (IRENA), International Renewable Energy Agency et al. *Renewable energy policies in a time of transition: Heating and cooling*. Tech. rep. 2020, p. 150. URL: .

[5] Society, National Geographic. *Village*. Aug. 2013. URL: (visited on 05/22/2021).

[6] United Nations et al. *World urbanization prospects: 2018 : highlights*. OCLC: 1128882042. 2019. ISBN: 978-92-1-148318-5.

[7] IEA. *Global Status Report for Buildings and Construction 2019*. Tech. rep. Paris, France: International Energy Agency (IEA), 2019. URL: (visited on 04/24/2021).

[8] Programme, 2020 United Nations Environment. *United Nations Environment Programme (2020). 2020 Global Status Report for Buildings and Construction: Towards a Zero-emission, Efficient and Resilient Buildings and Construction Sector*. Tech. rep. Nairobi: 2020 United Nations Environment Programme, 2020. URL: (visited on 04/24/2021).

[9] (IEA), International Energy Agency. *Perspectives for the Clean Energy Transition – Analysis*. Tech. rep. International Energy Agency (IEA). URL: (visited on 04/24/2021).

[10] (IEA), International Energy Agency. *Market Report Series: Renewables 2019*. Tech. rep. 2019. URL: (visited on 03/29/2021).

[11] Nowak, Thomas. *Heat pumps. Integrating technologies to decarbonise heating and cooling*. Tech. rep. European Copper Institute, 2018.

[12] Mathiesen, B. V. et al. *Towards a decarbonised heating and cooling sector in Europe: Unlocking the potential of energy efficiency and district energy*. Tech. rep. Aalborg Universitet, 2019. URL: (visited on 05/19/2021).

[13] Paardekooper, S. et al. *Heat Roadmap Europe 4: Quantifying the Impact of Low-Carbon Heating and Cooling Roadmaps.* Tech. rep. Denkmark: Aalborg Universitetsforlag, 2018. URL: (visited on 05/19/2021).

[14] *Digital Roadmap for District Heating & Cooling.* Tech. rep. DHC+ Technology Platform c/o Euroheat & Power, July 2019. URL: (visited on 05/19/2021).

[15] Werner, S. "District Heating and Cooling". *Reference Module in Earth Systems and Environmental Sciences.* Elsevier, Jan. 2013. ISBN: 978-0-12-409548-9. DOI: 10.1016/B978-0-12-409548-9.01094-0. URL: (visited on 05/19/2021).

[16] Gadd, Henrik and Werner, Sven. "Heat load patterns in district heating substations". *Applied Energy* 108 (Aug. 2013), pp. 176–183. ISSN: 0306-2619. DOI: 10.1016/j.apenergy.2013.02.062. URL: (visited on 05/19/2021).

[17] Lund, Henrik et al. "4th Generation District Heating (4GDH): Integrating smart thermal grids into future sustainable energy systems". *Energy* 68.Supplement C (Apr. 2014), pp. 1–11. ISSN: 0360-5442. DOI: 10.1016/j.energy.2014.02.089. URL: .

[18] Schmidt, Dietrich et al. "Low Temperature District Heating for Future Energy Systems". *Energy Procedia.* 15th International Symposium on District Heating and Cooling, DHC15-2016, 4-7 September 2016, Seoul, South Korea 116.Supplement C (June 2017), pp. 26–38. ISSN: 1876-6102. DOI: 10.1016/j.egypro.2017.05.052. URL: .

[19] Imran, Muhammad et al. "The feasibility analysis for the concept of low temperature district heating network with cascade utilization of heat between networks". *Energy Procedia.* 15th International Symposium on District Heating and Cooling, DHC15-2016, 4-7 September 2016, Seoul, South Korea 116.Supplement C (June 2017), pp. 4–12. ISSN: 1876-6102. DOI: 10.1016/j.egypro.2017.05.050. URL: .

[20] Rämä, Miika and Sipilä, Kari. "Transition to low temperature distribution in existing systems". *Energy Procedia.* 15th International Symposium on District Heating and Cooling, DHC15-2016, 4-7 September 2016, Seoul, South Korea 116.Supplement C (June 2017), pp. 58–68. ISSN: 1876-6102. DOI: 10.1016/j.egypro.2017.05.055. URL: .

[21] Nord, Natasa et al. "Necessary Measures to Include more Distributed Renewable Energy Sources into District Heating System". *Energy Procedia.* 15th International Symposium on District Heating and Cooling, DHC15-2016, 4-7 September 2016, Seoul, South Korea 116 (June 2017), pp. 48–57. ISSN: 1876-6102. DOI: 10.1016/j.egypro.2017.05.054. URL: (visited on 05/23/2021).

[22] Henchoz, Samuel. "Potential of refrigerant based district heating and cooling networks". PhD thesis. Lausanne, Switzerland: École Polytechnique Fédérale de Lausanne, 2016. DOI: 10.5075/epfl-thesis-6935. URL: (visited on 01/13/2020).

[23] Suciu, Raluca-Ancuta. "Fifth generation district energy systems for low carbon cities". PhD thesis. Lausanne, Switzerland: École Polytechnique Fédérale de Lausanne, 2019. DOI: 10.5075/epfl-thesis-7332. URL: (visited on 12/18/2019).

[24] (IRENA), International Renewable Energy Agency. *Global Renewables Outlook: Energy transformation 2050*. Tech. rep. 2020. URL: (visited on 03/29/2021).

[25] *EU Primary Energy Factor for Electricity: key to ensure well-informed choices, achieve real energy savings and reduce consumer energy bills*. Tech. rep. Brussels, Belgium: COGEN Europe, 2017. URL: .

[26] Amblard, Frédéric Louis-Pierre Raphaël Marie. *Reliability and Performance of Model Predictive Control for Demand Response with Residential Heat Pumps*. Number: THESIS Publisher: EPFL. 2020. DOI: 10.5075/epfl-thesis-7926. URL: (visited on 05/18/2021).

[27] *EHPA Stats*. URL: (visited on 05/18/2021).

[28] Page, Jessen et al. "Aggregating building energy demand simulation to support urban energy design". *SUSTAINABLE HABITAT FOR DEVELOPING SOCIETIES – Choosing The Way Forward*. Vol. 1. Ahmedabad, India: CEPT UNIVERSITY PRESS, Centre for Documentation & Publications CEPT University, Kasturbhai Lalbhai Campus, University Road, Navrangpura, Ahmedabad 380009, Gujarat, India, Dec. 2014, pp. 378–385. URL: (visited on 05/07/2021).

[29] Choudhary, R. "A probalistic model for assessing energy consumption of the non-domestic building stock". *Build. Simul.* (2011), pp. 14–16.

[30] Parker, J. et al. "A calibrated whole building simulation approach to assessing retrofit options for Birmingham Airport" (Sept. 2012). URL: (visited on 01/06/2018).

[31] Robinson, Caleb et al. "Machine learning approaches for estimating commercial building energy consumption". *Applied Energy* 208 (Dec. 2017), pp. 889–904. ISSN: 0306-2619. DOI: 10.1016/j.apenergy.2017.09.060. URL: (visited on 02/04/2018).

[32] Rahman, Aowabin et al. "Predicting electricity consumption for commercial and residential buildings using deep recurrent neural networks". *Applied Energy* 212 (Feb. 2018), pp. 372–385. ISSN: 0306-2619. DOI: 10.1016/j.apenergy.2017.12.051. URL: (visited on 02/04/2018).

[33] Girardin, Luc. "A GIS-based Methodology for the Evaluation of Integrated Energy Systems in Urban Area". PhD thesis. École Polytechnique Fédérale de Lausanne, 2012. DOI: 10.5075/epfl-thesis-5287. URL: (visited on 01/28/2020).

[34] Fazlollahi, Samira et al. "Multi-objectives, multi-period optimization of district energy systems: III. Distribution networks". *Computers & Chemical Engineering*. Selected papers from ESCAPE-23 (European Symposium on Computer Aided Process Engineering - 23), 9-12 June 2013, Lappeenranta, Finland 66 (July 2014), pp. 82–97. ISSN: 0098-1354. DOI: 10.1016/j.compchemeng.2014.02.018. URL: (visited on 06/03/2019).

[35] Andrić, I. et al. "Assessing the feasibility of using the heat demand-outdoor temperature function for a long-term district heat demand forecast". *Energy Procedia*. 15th International Symposium on District Heating and Cooling, DHC15-2016, 4-7 September 2016, Seoul, South Korea 116.Supplement C (June 2017), pp. 460–469. ISSN: 1876-6102. DOI: 10.1016/j.egypro.2017.05.093. URL: (visited on 01/02/2018).

[36] Frayssinet, Loïc et al. “Modeling the heating and cooling energy demand of urban buildings at city scale”. *Renewable and Sustainable Energy Reviews* 81.Part 2 (Jan. 2018), pp. 2318–2327. ISSN: 1364-0321. DOI: 10.1016/j.rser.2017.06.040. URL: (visited on 01/02/2018).

[37] Kazas, Georgios et al. “Energy Demand Profiles Assessment at District Scale: A Stochastic Approach for a Block of Buildings Demand Profiles Generation”. *Energy Procedia*. 6th International Building Physics Conference, IBPC 2015 78.Supplement C (Nov. 2015), pp. 3410–3415. ISSN: 1876-6102. DOI: 10.1016/j.egypro.2015.11.610. URL: (visited on 01/02/2018).

[38] Swan, Lukas G. and Ugursal, V. Ismet. “Modeling of end-use energy consumption in the residential sector: A review of modeling techniques”. *Renewable and Sustainable Energy Reviews* 13.8 (Oct. 2009), pp. 1819–1835. ISSN: 1364-0321. DOI: 10.1016/j.rser.2008.09.033. URL: (visited on 01/02/2018).

[39] Kavgic, M. et al. “A review of bottom-up building stock models for energy consumption in the residential sector”. *Building and Environment* 45.7 (July 2010), pp. 1683–1697. ISSN: 0360-1323. DOI: 10.1016/j.buildenv.2010.01.021. URL: (visited on 01/02/2018).

[40] Lim, Hyunwoo and Zhai, Zhiqiang John. “Review on stochastic modeling methods for building stock energy prediction”. *Build. Simul.* 10.5 (Oct. 2017), pp. 607–624. ISSN: 1996-3599, 1996-8744. DOI: 10.1007/s12273-017-0383-y. URL: (visited on 01/02/2018).

[41] Koulamas, C. et al. “Suitability analysis of modeling and assessment approaches in energy efficiency in buildings”. *Energy and Buildings* 158 (Jan. 2018), pp. 1662–1682. ISSN: 0378-7788. DOI: 10.1016/j.enbuild.2017.12.002. URL: (visited on 01/03/2018).

[42] Borgstein, E. H. et al. “Evaluating energy performance in non-domestic buildings: A review”. *Energy and Buildings* 128.Supplement C (Sept. 2016), pp. 734–755. ISSN: 0378-7788. DOI: 10.1016/j.enbuild.2016.07.018. URL: (visited on 01/03/2018).

[43] Heo, Y. et al. “Calibration of building energy models for retrofit analysis under uncertainty”. *Energy and Buildings* 47 (Apr. 2012), pp. 550–560. ISSN: 0378-7788. DOI: 10.1016/j.enbuild.2011.12.029. URL: (visited on 01/10/2018).

[44] Legorburu, Gabriel and Smith, Amanda D. “Incorporating observed data into early design energy models for life cycle cost and carbon emissions analysis of campus buildings”. *Energy and Buildings* 224 (Oct. 2020), p. 110279. ISSN: 0378-7788. DOI: 10.1016/j.enbuild.2020.110279. URL: (visited on 05/12/2021).

[45] Foucquier, Aurélie et al. “State of the art in building modelling and energy performances prediction: A review”. *Renewable and Sustainable Energy Reviews* 23.Supplement C (July 2013), pp. 272–288. ISSN: 1364-0321. DOI: 10.1016/j.rser.2013.03.004. URL: (visited on 01/02/2018).

[46] Bornand, Bastien Maxence et al. "Investment Planning Methodology for Complex Urban Energy Systems Applied to a Hospital Site". *Frontiers in Energy Research* 8 (Dec. 2020). Number: ARTICLE. DOI: 10.3389/fenrg.2020.537973. URL: (visited on 04/30/2021).

[47] Wen, Qingmei et al. "Genetic algorithm-based operation strategy optimization and multi-criteria evaluation of distributed energy system for commercial buildings". *Energy Conversion and Management* 226 (Dec. 2020), p. 113529. ISSN: 0196-8904. DOI: 10.1016/j.enconman.2020.113529. URL: (visited on 05/12/2021).

[48] Pagliarini, Giorgio and Rainieri, Sara. "Modeling of a thermal energy storage system coupled with combined heat and power generation for the heating requirements of a University Campus". *Applied Thermal Engineering* 30.10 (July 2010), pp. 1255–1261. ISSN: 1359-4311. DOI: 10.1016/j.applthermaleng.2010.02.008. URL: (visited on 05/12/2021).

[49] Safaei, Amir et al. "A model for optimal energy planning of a commercial building integrating solar and cogeneration systems". *Energy* 61 (Nov. 2013), pp. 211–223. ISSN: 0360-5442. DOI: 10.1016/j.energy.2013.08.048. URL: (visited on 05/12/2021).

[50] Beccali, Marco et al. "Artificial neural network decision support tool for assessment of the energy performance and the refurbishment actions for the non-residential building stock in Southern Italy". *Energy* 137 (Oct. 2017), pp. 1201–1218. ISSN: 0360-5442. DOI: 10.1016/j.energy.2017.05.200. URL: (visited on 05/13/2021).

[51] Tukey, John W. *Exploratory Data Analysis*. Vol. 23. Reading (Massachusetts), Menlo Park (California), London, Amsterdam, Don Mills (Ontario), Sydney: Addison-Wesley, 1977. URL: (visited on 06/03/2021).

[52] SIA-2024:2015. *Données d'utilisation des locaux pour l'énergie et les installations du bâtiment*. Tech. rep. Zuirch, Switzerland: Société suisse des ingénieurs et des architectes (SIA), 2015. URL: .

[53] Page, J. et al. "A generalised stochastic model for the simulation of occupant presence". *Energy and Buildings* 40.2 (Jan. 2008), pp. 83–98. ISSN: 0378-7788. DOI: 10.1016/j.enbuild.2007.01.018. URL: (visited on 05/17/2021).

[54] Stadler, Paul Michael. "Model-based sizing of building energy systems with renewable sources". PhD thesis. Lausanne, Switzerland: École Polytechnique Fédérale de Lausanne, 2019. DOI: 10.5075/epfl-thesis-9560. URL: (visited on 12/20/2019).

[55] Kotzur, Leander et al. "Impact of different time series aggregation methods on optimal energy system design". *Renewable Energy* 117 (Mar. 2018), pp. 474–487. ISSN: 0960-1481. DOI: 10.1016/j.renene.2017.10.017. URL: (visited on 05/17/2021).

[56] Bahl, Björn et al. "Time-series aggregation for synthesis problems by bounding error in the objective function". *Energy* 135 (Sept. 2017), pp. 900–912. ISSN: 0360-5442. DOI: 10.1016/j.energy.2017.06.082. URL: (visited on 05/17/2021).

[57] Hoffmann, Maximilian et al. "A Review on Time Series Aggregation Methods for Energy System Models". *Energies* 13 (Feb. 2020), p. 641. DOI: 10.3390/en13030641.

[58] Ma, Zhenjun et al. "A variation focused cluster analysis strategy to identify typical daily heating load profiles of higher education buildings". *Energy* 134 (Sept. 2017), pp. 90–102. ISSN: 0360-5442. DOI: 10.1016/j.energy.2017.05.191. URL: (visited on 05/23/2021).

[59] Belfiore, Francesca et al. "Optimization based approach to assist the transition of large energy users to low temperature networks". *Proceedings of the 33rd International Conference on Efficiency, Cost, Optimization, Simulation and Environmental Impact of Energy Systems (ECOS 2020)*. Vol. 4. Number: CONF. Curran Associates, Inc., Sept. 2020. ISBN: 978-1-71381-406-1. URL: (visited on 04/15/2021).

[60] Belfiore, Francesca et al. "MILP based approach for the preliminary investigation of thermal networks in urban areas". *To be presented at the 17th International Building Performance Simulation Association Conference (IBPSA 2021)*. Sept. 2021.

[61] Power, Euroheat &. *Euroheat & Power: Country by Country 2017*. Tech. rep. Section: CBC. Brussels, 2017. URL: (visited on 03/29/2021).

[62] Platform, DHC+ Technology. *District Heating and Cooling - A Vision towards 2020-2030-2050*. Tech. rep. Section: Brochures. Brussels, 2012. URL: (visited on 03/29/2021).

[63] Werner, Sven. "International review of district heating and cooling". *Energy* 137.Supplement C (Oct. 2017), pp. 617–631. ISSN: 0360-5442. DOI: 10.1016/j.energy.2017.04.045. URL: .

[64] Rismanchi, B. "District energy network (DEN), current global status and future development". *Renewable and Sustainable Energy Reviews* 75.Supplement C (Aug. 2017), pp. 571–579. ISSN: 1364-0321. DOI: 10.1016/j.rser.2016.11.025. URL: (visited on 01/04/2018).

[65] Buffa, Simone et al. "5th generation district heating and cooling systems: A review of existing cases in Europe". *Renewable and Sustainable Energy Reviews* 104 (Apr. 2019), pp. 504–522. ISSN: 1364-0321. DOI: 10.1016/j.rser.2018.12.059. URL: (visited on 06/06/2019).

[66] Aunedi, Marko et al. "Modelling of national and local interactions between heat and electricity networks in low-carbon energy systems". *Applied Energy* 276 (Oct. 2020), p. 115522. ISSN: 0306-2619. DOI: 10.1016/j.apenergy.2020.115522. URL: (visited on 08/03/2020).

[67] (IRENA), International Renewable Energy Agency. *Green hydrogen cost reduction*. Tech. rep. 2020. URL: (visited on 03/29/2021).

[68] Harb, Hassan et al. "MIP approach for designing heating systems in residential buildings and neighbourhoods". *Journal of Building Performance Simulation* 9.3 (May 2016), pp. 316–330. ISSN: 1940-1493. DOI: 10.1080/19401493.2015.1051113. URL: (visited on 01/30/2020).

[69] Bordin, Chiara et al. "An optimization approach for district heating strategic network design". *European Journal of Operational Research* 252.1 (July 2016), pp. 296–307. ISSN: 0377-2217. DOI: 10.1016/j.ejor.2015.12.049. URL: (visited on 08/08/2020).

[70] Kuriyan, K. and Shah, N. "A combined spatial and technological model for the planning of district energy systems". *International Journal of Sustainable Energy Planning and Management* 21 (2019), pp. 111–131. DOI: 10.5278/ijsepm.2019.21.8.

[71] Marquant, Julien F. et al. "A holarchic approach for multi-scale distributed energy system optimisation". *Applied Energy* 208.Supplement C (Dec. 2017), pp. 935–953. ISSN: 0306-2619. DOI: 10.1016/j.apenergy.2017.09.057. URL: .

[72] Stadler, Paul et al. "Model-based optimization of distributed and renewable energy systems in buildings". *Energy and Buildings* 120 (May 2016), pp. 103–113. ISSN: 0378-7788. DOI: 10.1016/j.enbuild.2016.03.051. URL: (visited on 01/30/2020).

[73] Pieper, H. et al. "Modelling framework for integration of large-scale heat pumps in district heating using low-temperature heat sources: A case study of Tallinn, Estonia". *International Journal of Sustainable Energy Planning and Management* 20 (2019), pp. 67–86. DOI: 10.5278/ijsepm.2019.20.6.

[74] Jing, Rui et al. "Distributed or centralized? Designing district-level urban energy systems by a hierarchical approach considering demand uncertainties". *Applied Energy* 252 (Oct. 2019), p. 113424. ISSN: 0306-2619. DOI: 10.1016/j.apenergy.2019.113424. URL: (visited on 07/31/2020).

[75] Papoulias, Soterios A. and Grossmann, Ignacio E. "A structural optimization approach in process synthesis—I: Utility systems". *Computers & Chemical Engineering* 7.6 (Jan. 1983), pp. 695–706. ISSN: 0098-1354. DOI: 10.1016/0098-1354(83)85022-4. URL: (visited on 02/10/2020).

[76] Papoulias, Soterios A. and Grossmann, Ignacio E. "A structural optimization approach in process synthesis—II: Heat recovery networks". *Computers & Chemical Engineering* 7.6 (Jan. 1983), pp. 707–721. ISSN: 0098-1354. DOI: 10.1016/0098-1354(83)85023-6. URL: (visited on 12/21/2020).

[77] Gasser, Lukas et al. "High efficiency heat pumps for low temperature lift applications" (2017), p. 10.

[78] Mavrotas, George. "Effective implementation of the ε-constraint method in Multi-Objective Mathematical Programming problems". *Applied Mathematics and Computation* 213.2 (July 2009), pp. 455–465. ISSN: 0096-3003. DOI: 10.1016/j.amc.2009.03.037. URL: (visited on 03/11/2021).

[79] Fourer, Robert et al. *AMPL: A Modeling Language for Mathematical Programming*. Second. 2003.

[80] *CPLEX Optimizer*. Dec. 2020. URL: (visited on 12/28/2020).

[81] SIA-385/2:2015. *Installations d'eau chaude sanitaire dans les bâtiments - Besoins en eau chaude, exigences globales et dimensionnement*. Tech. rep. Zuirch, Switzerland: Société suisse des ingénieurs et des architectes (SIA), 2015. URL: .

[82] Portmann, Markus et al. *Sonnendach.ch und Sonnenfassade.ch: Berechnung von Potenzialen in Gemeinden*. Tech. rep. Bern: Bundesamt für Energie BFE, Mar. 2019. URL: (visited on 04/15/2021).

[83] Henchoz, Samuel et al. "Performance and profitability perspectives of a CO2 based district energy network in Geneva's City Centre". *Energy* 85 (June 2015), pp. 221–235. ISSN: 0360-5442. DOI: 10.1016/j.energy.2015.03.079. URL: (visited on 02/08/2018).

[84] *Energy use in buildings*. Text. URL: (visited on 01/02/2020).

[85] Sandberg, Nina Holck et al. "Dynamic building stock modelling: Application to 11 European countries to support the energy efficiency and retrofit ambitions of the EU". *Energy and Buildings*. Towards an energy efficient European housing stock: monitoring, mapping and modelling retrofitting processes 132 (Nov. 2016), pp. 26–38. ISSN: 0378-7788. DOI: 10.1016/j.enbuild.2016.05.100. URL: (visited on 12/18/2019).

[86] Li, Haoran and Nord, Natasa. "Transition to the 4th generation district heating - possibilities, bottlenecks, and challenges". *Energy Procedia* 149 (Sept. 2018), pp. 483–498. ISSN: 18766102. DOI: 10.1016/j.egypro.2018.08.213. URL: (visited on 06/06/2019).

[87] Neirotti, Francesco et al. "Analysis of Different Strategies for Lowering the Operation Temperature in Existing District Heating Networks". *Energies* 12.2 (Jan. 2019). Number: 2 Publisher: Multidisciplinary Digital Publishing Institute, p. 321. DOI: 10.3390/en12020321. URL: (visited on 04/20/2021).

[88] Rowlings, Andrew and Walker, Arron. "Sustainable Energy Options for the Future Airport Metropolis". *Proceedings 4th IASME/WSEAS international conference (EEESD'08), Algarve, Portugal* (Jan. 2008).

[89] Delangle, Axelle et al. "Modelling and optimising the marginal expansion of an existing district heating network". *Energy* 140 (Dec. 2017), pp. 209–223. ISSN: 0360-5442. DOI: 10.1016/j.energy.2017.08.066. URL: (visited on 08/03/2020).

[90] Popovski, Eftim et al. "The role and costs of large-scale heat pumps in decarbonising existing district heating networks – A case study for the city of Herten in Germany". *Energy* 180 (Aug. 2019), pp. 918–933. ISSN: 0360-5442. DOI: 10.1016/j.energy.2019.05.122. URL: (visited on 04/20/2021).

[91] Guelpa, Elisa et al. "Reduction of CO2 emissions in urban areas through optimal expansion of existing district heating networks". *Journal of Cleaner Production* 204 (Dec. 2018), pp. 117–129. ISSN: 0959-6526. DOI: 10.1016/j.jclepro.2018.08.272. URL: (visited on 04/20/2021).

[92] Rämä, Miika and Wahlroos, Mikko. "Introduction of new decentralised renewable heat supply in an existing district heating system". *Energy* 154 (July 2018), pp. 68–79. ISSN: 0360-5442. DOI: 10.1016/j.energy.2018.03.105. URL: (visited on 04/20/2021).

[93] Dominković, Dominik Franjo et al. "Technical, economic and environmental optimization of district heating expansion in an urban agglomeration". *Energy* 197 (Apr. 2020), p. 117243. ISSN: 0360-5442. DOI: 10.1016/j.energy.2020.117243. URL: (visited on 04/23/2021).

[94] Qaeini, Saeed et al. "Combined heat and power units and network expansion planning considering distributed energy resources and demand response programs". *Energy Conversion and Management* 211 (May 2020), p. 112776. ISSN: 0196-8904. DOI: 10.1016/j.enconman.2020.112776. URL: (visited on 04/23/2021).

[95] Hou, Jin et al. "Implementation of expansion planning in existing district energy system: A case study in China". *Applied Energy* 211 (Feb. 2018), pp. 269–281. ISSN: 0306-2619. DOI: 10.1016/j.apenergy.2017.10.118. URL: (visited on 04/23/2021).

[96] *Dakota Reference Manual: moga.* URL: (visited on 12/28/2020).

[97] Cajot, Sébastien et al. "Interactive Optimization With Parallel Coordinates: Exploring Multidimensional Spaces for Decision Support". *Frontiers in ICT* 5.32 (Jan. 2019). Number: ARTICLE. DOI: 10.3389/fict.2018.00032. URL: (visited on 04/28/2021).

[98] Schüler, Nils Christian. *Computational methods for multi-criteria decision support in urban planning.* Number: THESIS Publisher: EPFL. 2018. DOI: 10.5075/epfl-thesis-8877. URL: (visited on 04/28/2021).

[99] Wallerand, Anna Sophia. *Integration of solar energy with industrial processes.* Number: THESIS Publisher: EPFL. 2018. DOI: 10.5075/epfl-thesis-8635. URL: (visited on 04/28/2021).

[100] *Bienvenue à BITZER.* URL: (visited on 01/13/2020).

[101] OFEN. *Simulation de systèmes d'énergie.* Tech. rep. Bern: SuisseEnergie, Office fédéral de l'énergie (OFEN), Feb. 2020. URL: (visited on 05/10/2021).

[102] Lund, Rasmus and Mohammadi, Soma. "Choice of insulation standard for pipe networks in 4th generation district heating systems". *Applied Thermal Engineering* 98 (Apr. 2016), pp. 256–264. ISSN: 1359-4311. DOI: 10.1016/j.applthermaleng.2015.12.015. URL: (visited on 10/21/2020).

[103] Bøhm, Benny. "On transient heat losses from buried district heating pipes". *International Journal of Energy Research* 24 (Dec. 2000), pp. 1311–1334. DOI: 10.1002/1099-114X(200012)24:15<1311::AID-ER648>3.0.CO;2-Q.

[104] Kvisgaard, B. and Hadvig, S. *Varmetab fra fjernvarmeledninger (Heat Loss from Pipelines in District Heating Systems).* Tech. rep. Copenhagen, Denmark, 1980.

Francesca **Belfiore**

Rue du Panorama 14, CH-1800 Vevey, Switzerland

francesca.belfiore89@gmail.com | francesca-belfiore

Education

Doctor of philosophy (PhD), Energy *Sion, Switzerland*

École Polytechnique Fédérale de Lausanne (EPFL) *2021*

- Thesis title: « District heating and cooling systems to integrate renewable energy in urban areas »
- Supervisors: Prof. François Maréchal (EPFL), Prof. Jessen Page (HES-SO)

Master of Science, Energy Engineering *Milano, Italy*

Politecnico di Milano *2016*

- Thesis title: « Techno-economic optimization of a regenerative combined cycle gas turbine power plant »
- Supervisors: Prof. Emanuele Martelli (POLIMI), Dr. Sevket Baykal (GE Power), Dr. Raffaele Bolliger (GE Power)
- Grade: 110 cum laude/110

Bachelor of Science, Mechanical Engineering *L'Aquila, Italy*

Università degli studi dell'Aquila *2013*

- Thesis title: «Integration of trigeneration and solar energy with multiobjective optimization»
- Supervisor: Prof. Michele Anatone
- Grade: 110/110

Experience

Research and teaching assistant *Sion, Switzerland*

École Polytechnique Fédérale de Lausanne (EPFL) · HES-SO Valais-Wallis *2017 - 2021*

- **Modeling and optimization** of urban energy systems (conversion technologies and distribution networks)
- Collaboration with an international airport to assist its transition towards a fossil-free energy system
- Organization of objectives, tasks and deliverable in a multi-disciplinary project
- Assistance to **teaching** activities and students supervision

Systems engineer trainee *Baden, Switzerland*

General Electric Power *2015 - 2016*

- Modeling and thermo-economic optimization of energy systems to assess the feasibility of **advanced technologies**
- Development and maintenance of **engineering software tools**: presentation, training, engineering and technical support to users

Competencies

Project management

Structuring and organization of project tasks; communication with client; results presentation and documentation; time management

Soft skills
Results-oriented attitude; team spirit; adaptability; holistic vision; organization; discipline; open-mindedness

Energy engineering
Modeling and optimization of integrated energy systems; sustainable energy systems; building physics; data analysis

Operations research
Mathematical programming techniques (LP/MILP/NLP); multi-objective optimization; problem decomposition techniques.

Software & Programming
Python; AMPL (mathematical programming); MatLab; Belsim Vali; QGIS; Git; MS Office; Latex

Languages

Italian	Mother tongue
English	Fluent spoken and written (C1)
French	Intermediate (B2)

Publications

Journals

2020	B.Bornand, L. Girardin, **F. Belfiore**, J. L. S. Robineau, S. Bottallo, F. Maréchal. *Investment Planning Methodology for Complex Urban Energy Systems Applied to an Hospital Site*	*Frontiers in Energy Research*

Conference proceedings

2018	**F. Belfiore**, F. Baldi, F. Maréchal. *Exergy Recovery During Liquefied Natural Gas Regasification Using Methane as Working Fluid*	*PRES, Prague (Czech)*
2020	**F. Belfiore**, A. Mian, J. Page, F. Maréchal. *Optimization based approach to assist the transition of large energy users to low temperature networks*	*ECOS, Osaka (Japan)*
2021	**F. Belfiore**, R. Tristan, J. Page, F. Maréchal. *MILP based approach for the preliminary investigation of thermal networks in urban areas*	*IBPSA, Bruge (Belgium)*